Design and synthesis of new copper complexes bearing *N,N* – heterocyclic derivatives ligands – Potential active photoredox catalyst for organic transformations

Dissertation

Zur Erlangung des Doktorgrades der Naturwissenschaften
Dr. rer. nat.
Der Fakultät für Chemie und Pharmazie
der Universität Regensburg

vorgelegt von

Marco Antonio Henríquez Toro

aus Chile

im Jahr 2023

Pontificia Universidad Católica de Chile
Facultad de Química y de Farmacia
Dirección de Investigación y Postgrado
Regensburg University

Thesis manuscript: Marco Antonio Henríquez Toro; to obtain the Academic Degree of Doctor in Chemistry.

Approved by:

Dr. Alan Raúl Cabrera Caballero
Pontificia Universidad Católica de Chile
Prof. Dr. Oliver Reiser
Regensburg University

Thesis committee

Dr. Luis Lemus
Universidad Santiago de Chile

Dr. Denis Fuentealba
Pontificia Universidad de Chile

Dr. Claudio Saitz
Universidad de Chile

2023

A mi madre y mi padre

Closing time, every new beginning
Comes from some other beginning's end

Acknowledgements

In this scientific journey, many people contributed to my training and supported me with suggestions for my projects or positively encouraged me to continue researching. In a few words, I thank each one of them.

I express my gratitude to my two supervisors, Dr Alan Cabrera, for admitting me to his group and giving me the opportunity to work in his laboratory, in addition to giving me the tools regarding copper complexes chemistry and supporting me in my doctoral project during these five years. I thank Prof. Dr Oliver Reiser for opening the doors of his laboratories, giving me the freedom to investigate and showing me the excellent field of photochemistry. Many thanks to both of you for your support and for your feedback to continuously improve the manner of doing research.

I would also like to thank the thesis committee: Dr Denis Fuentes Alba, Dr Luis Lemus, and Dr Claudio Saitz, for correcting my work, providing their criticism in a constructive way and active participation in this process.

I appreciate the help of Dr Mirko Natali (Ferrara University) and Dr Pablo Jaque (Universidad de Chile), for their scientific help in my first project. Without them, I would not have been able to publish my work. In addition, with your information, I was able to understand the photophysical properties of copper complexes better and support what was done experimentally with a theoretical point of view. Also, Dr Sebastian Engl, who guided me in my first internship, patiently teaching me the techniques in photocatalysis and helping me in the construction of my first manuscript.

I happily acknowledge the help of the members of SyTeCCO laboratory, who gave me good times in the years that I carried out this project in Chile. I must

also mention the undergraduate students who were under my supervision: Max Bayas, Diego González, Francisco Fuentes, and Elizabeth Duran, who taught me to deliver my knowledge to them.

I acknowledge the members of Prof Reiser's group for their support during my time in Germany. A special mention to Youssef Abderrazak, Dr Onnicha Khaikate, Magdalena Koch, Elcin Ulus, Ruben Veronesi, Dr Tobias Babl, Dr Tomislav Krolo, Viktor Klopfer, Eva Plut, Sebastian Fisher, Andreas Ratzenböck, Nikolai Wurzer and Dr Aditya Bhattacharyya, all of them for incorporating me into their work team and day-to-day, whether in small talk in the hallway or drinking a beer in the kitchen.

Probably a paragraph is too short to mention the help of Anurag Chinchole, who accompanied me throughout my research process in Germany, more than a collaborator he became a brother. In addition, we overcame numerous day-to-day problems, supporting our research, and carrying out a couple of projects.

I must also highlight the help of Camilo Verdugo; thanks for sharing your motivation and skill in chemistry and for your commitment to collaborate in my projects. In the same way, I show gratitude to Prithwa Das, who trusted me at the beginning of her studies, taking the last project I found.

As well, I must underline the help of Alejandra Acuña, who accompanied me these five years. I was lucky to meet you in the program's first year, then do the work together and continue with this friendship.

I take advantage of thanking my parents and friends from the “Bandita” group for their love and being there, even from a distance. Also, I must recognize the enormous support that Michela Marcon gave me in the last stage of this

manuscript; writing this work has not been easy, but she always encouraged me with motivational words to finish this process.

On the other hand, I must thank the analysis departments of both universities that allowed me to characterize and complete this work. I distinguish the excellent work carried out by the technical team of Dr Reiser's group and their availability to assist my research. Also, the NMR team of the Pontificia Universidad Católica de Chile were always willing to receive my samples.

This work would not have been possible without funding. The ANID N21180705 scholarship allowed me to study during these five years. Additionally, the *IPUR* program permitted me to stay for three months in the group of Prof. Dr Oliver Reiser. Once again, I mention the ANID institution, which allowed me to participate in a photochemistry course in Italy and national and international conferences. Finally, I acknowledge both universities for their facilities and the internal supervisor’s projects.

Abbreviations

°C	Degree Celsius	L	Ligand
4CzIPN	1,2,3,5-Tetrakis(carbazol-9-yl)-4,6-dicyanobenzene	LC	Ligand-centred
Å	Ángstrom	LED	Light emitting diode
acac	Acetylacetone	LEEC	Light-emitting electrochemical cells
AIDS	acquired immunodeficiency syndrome	LLCT	Ligand-to-ligand charge transfer
Ar	Aromatic ring	LMCT	Ligand-to-metal charge transfer
Ar-BIAN	bis(arylamino)-acenaphthene	LUMO	Lowest Unoccupied Molecular Orbital
ATRA	Atom Transfer Radical Addition	m	mili
BDE	Bond-dissociation energy	Me	Methyl
BDMA	*N*-(Phenylmethyl)dimethylamine	mg	milligram
BINAP	(2,2′-bis(diphenyl phosphino)-1,1′-binaphthyl)	MHz	Mega hertz
binc	bis(2-isocyanophenyl) phenylphosphonate	MLCT	Metal to ligand charge transfer
boc	tert-Butyloxycarbonyl	mM	miliMolar
bphen	4,7-Diphenyl-1,10-phenanthroline	mol %	mole percent
bpy	2,2′-Bipyridine	Mw	Microwave
bpy*	6-methyl-4-(2,4,5-trimethylphenyl)-2,2'-bipyridine	n.d.	No detected

BTMG	2-tert-Butyl-1,1,3,3-tetramethylguanidine	n.r.	No reaction
BTPP	tert-Butylimino-tri(pyrrolidino)phosphorane	N_2	nitrogen
Bu	Butyl	NHC	N-Heterocyclic Carbene
cf.	Compare (latín, *confer*)	NIR	Near infrared
CV	Cyclic voltammetry	nm	nanometre
dap	2,9-bis(para-anisyl)-1,10-phenanthroline	NMR	Nuclear magnetic resonance
dba	Dibenzylideneacetone	ns	nanosecond
DBU	1,8-diazabicyclo (5.4.0)undec-7-ene	Nu	nucleophile
DCP	Dicumyl Peroxide	OAc	acetate
dd	doublet	OLED	organic light-emitting diodes
deg	degree	PC	photocatalyst
DIPEA	N,N-Diisopropylethylamine	PC*	Photocatalyst in excited state
DMA	Dimethylacetamide	PCET	proton-coupled electron transfer
DME	Dimethoxyethane	PET	photoinduced electron transfer
DMF	Dimethylformamide	Ph	phenyl
dmp	2,9-Dimethyl-1,10-phenanthroline	phen	phenanthroline
DMSO	Dimethyl sulfoxide	pKa	negative base-10 logarithm of the acid dissociation constant (K_a) of a solution.
dpa	dipyridylamine	POP	Bis[(2-diphenylphosphino)phenyl] ether

dpbz	1,2-Bis(diphenylphosphino)benzene	ppm	parts per million
dpp	2,9-diphenyl-1,10-phenanthroline	ppy	2-phenylpyridine
dppf	1,1′-Ferrocenediyl-bis(diphenylphosphine)	pypzs	5- (4-fluorosulfonyl) amino-3- (2-pyridyl)-pyrazole
dq	2,2'-biquinoline	r.t.	Room temperature
dtbbpy	4,4′-Di-tert-butyl-2,2′-dipyridyl	redox	Redox- oxidation
DTBP	Di-tert-butyl peroxide	R_f	retardation factor
E	Energy	s	Singlet, seconds
$E_{1/2}$	Half wave potential	S-BINAP	(S)-(-)-2,2’-Bis(diphenylphosphino)-1,1’-binaphthalene
EDA	Electron Donor-Acceptor	SCE	saturated calomel electrode
EPR	Electron paramagnetic resonance	SET	single electron transfer
equiv	equivalents	t	time or triplet
E_{red}	Reduction potential	TBHP	tert-Butyl hydroperoxide
ESI	Electronspray ionization	TD-DFT	Time-dependent density-functional theory
ET	Energy transfer	Tf	triflyl (= trifluoro methane sulfonyl)
et al.	et alia (Latin: and others)	THF	tetrahydrofuran
Et_3N	Triethylamine	TLC	Thin layer chromatography
EtOAc	Ethyl acetate	TMEDA	Tetramethyl ethylenediamine
eV	electronvolt	TMG	1,1,3,3-tetramethylguanidine

EWG	Electron-withdrawing group	tmp	3,4,7,8-tetramethyl-1,10-phenanthroline
f	oscillator strength	TMS	trimethylsilyl
h	hour	Ts	tosyl (= 4-toluenesulfonyl)
HAT	Hydrogen atom transfer	UV	ultraviolet
HeH	Hantzsch Ester	VIS	Visible
Het	heteroatom	W	Watts
HIV	human immunodeficiency virus	X	Halogen
HOMO	Highest Occupied Molecular Orbital	XantPhos	4,5-Bis(diphenylphosphino)-9,9-dimethylxanthene
HP	High power	XRD	X-ray diffraction
HRMS	High resolution mass spectrometry	δ	parts per million
Hz	Hertz	λ	wavelength
iPr	*iso*-propyl	µs	Microseconds
^{i}PrEtN	*N,N*-Diisopropylethylamine	Φ	quantum yield
ISC	Inter system crossing		
J	coupling constant		
K	Kelvin		
kg	kilogram		

INDEX

INDEX OF TABLE

INDEX OF FIGURES

INDEX OF SCHEMES

SUMMARY

In this work, five new heteroleptic Cu^{I} complexes (**C1-5**) of the type [Cu(dpa)(*P,P*)]BF_4 based on dipyridylamine (dpa) as *N*,*N* ligand and commercial diphosphines ligands have been synthesised through a simple methodology with high yields. All complexes were thoroughly characterised by spectroscopic and spectrometric techniques, as well by theoretical calculations. These showed MLCT absorptions in the 300–370 nm region and emission in the 450–520 nm region with quantum yields and lifetimes that depend on the nature of the *P,P* ligand. The photocatalytic performance of Cu^{I} complexes **C1-5** were evaluated for their use as photoredox catalysts in ATRA reactions, decarboxylative coupling and an Appel-type reaction. The use of readily available dpa as *N*,*N* ligand constitutes an attractive alternative to the well-established phenanthroline ligands typically used in photocatalysis. Additionally, modifications of the dpa ligand were explored without good positive results. On the other hand, six Cu^{II} complexes (**C6-12**) were synthesized and evaluated in two reactions. Unfortunately, the results did not exceed the yields reported by Cu(dap)Cl_2 and [Cu(dmp)$_2$Cl]Cl.

Csp^3-sp coupling by copper and light was explored using two strategies. (1) Using the Cu^{I}-phenylacetylide species and *N*-alkoxyphtalimides or alkyl Katryzky salt as a radical source. In this case, the coupling product was obtained in 52 % of yield. However, we decided to explore a more challenging route, (2) Using HAT as a way to generate alkane radicals, using a mixture of Cu(OAc)$_2$ and oxidant as reaction initiators. Unfortunately, in this last strategy, the performance did not exceed the 26 % yield.

Finally, preliminary studies for the multicomponent aminosulfonylation of styrene reaction were developed; the reaction optimization was done, and 83 % yield of the product was obtained using tosyl chloride, carbazole and styrene.

ZUSAMMENFASSUNG

In dieser Arbeit werden über eine einfache Methodik in hoher Ausbeute fünf neue, heteroleptische Cu^{I}-Komplexe (**C1-5**) des Typs [Cu(dpa)(*P,P*)]BF_4 mit Dipyridylamin (dpa) als *N*,*N*-Liganden sowie kommerziell verfügbaren Diphosphinliganden erhalten. Alle Komplexe wurden durch spektroskopische, spektrometrische sowie quantenchemische Rechnungen charakterisiert. Die Produkte zeigen MLCT Absorptionen im Bereich von 300-370 nm und Emissionen im Bereich von 450-520 nm, die Quantenausbeuten und Lebenszeiten hängen dabei von der Art der *P,P*- Liganden ab. Untersucht wurde die photokatalytische Aktivität der Cu^{I} -Komplexe **C1-5** für die Anwendung als Photokatalysator in ATRA Reaktionen, decarboxylierenden Kreuzkupplungen sowie Appel-Reaktionen. Die Verwendung von leicht zugänglichen *N*,*N*-Liganden stellt eine attraktive Alternative zu den oft in Photokatalysen verwendeten Phenanthrolinliganden dar. Zusätzlich untersucht wurden Modifikationen der dpa-Liganden, mit positiven Ergebnissen. Weiterhin wurden sechs Cu^{II}-Komplexe (**C6-12**) hergestellt und in zwei Reaktionen eingesetzt. Die Ausbeuten lagen dabei unter denen, die für $Cu(dap)Cl_2$ und $[Cu(dmp)_2Cl]Cl$ berichtet wurden.

Csp^3-sp-Kupplungen durch Kupfer und Licht wurden anhand von zwei Strategien untersucht: (1) mit Cu^{I}-phenylacetylid-spezies und *N*-alkoxyphtalimid oder Alkyl-Katryzkysalz als Radikalquelle wurden 52 % Ausbeute an Kupplungsprodukt erzielt. (2) mit HAT als Radikalquelle wurden durch Verwendung einer Mischung von $Cu(OAc)_2$ und eines Oxidationsmittels als Initiator lediglich Ausbeuten von 26 % erreicht.
Schließlich wurde die Multikomponenten-Aminosulfonylierung von Styrol experimentell beleuchtet; es wurde eine Reaktionsoptimierung durchgeführt mit 83 % Ausbeute an Zielprodukt bei Verwendung von Tosylchlorid, Carbazol und Styrol.

Resumen

En este trabajo se han sintetizado cinco nuevos complejos heterolépticos Cu^{I} (**C1-5**) del tipo [Cu(dpa)(*P,P*)]BF_4 utilizando dipiridilamina (dpa) como ligando *N,N* y ligandos comerciales de difosfinas mediante una simple metodología obteniendo altos rendimientos. Todos los complejos se caracterizaron minuciosamente mediante técnicas espectroscópicas y espectrométricas, y cálculos teóricos. Estos mostraron absorciones (MLCT) en la región de 300 a 370 nm y emisiones en la región de 450 a 520 nm con rendimientos cuánticos y tiempos de vida que dependen de la naturaleza del ligando *P,P*. Se evaluó la actividad de los complejos **C1-5** para su uso como catalizadores fotoredox en reacciones ATRA, acoplamiento descarboxilativo y una reacción tipo Appel. El uso de dpa como ligando *N,N* propone una alternativa atractiva a los ligandos de fenantrolina utilizados típicamente en fotocatálisis. Además, se exploraron modificaciones del ligando dpa sin buenos resultados positivos. Por otro lado, seis complejos Cu^{II} (**C6-12**) fueron sintetizados y evaluados en dos reacciones fotocatalíticas. Desafortunadamente, los resultados no superaron los rendimientos reportados por $Cu(dap)Cl_2$ y $[Cu(dmp)_2Cl]Cl$.

El acoplamiento Csp^3-sp por cobre y luz se exploró utilizando dos estrategias. (1) Uso del complejo Cu^{I}-fenilacetileno y los sustratos *N*-alcoxiftalimidas o sal de alquilo Katryzky como fuentes de radicales. En este caso, el producto de acoplamiento se obtuvo con un rendimiento del 52 %. Sin embargo, decidimos explorar una ruta más desafiante, (2) Utilizando HAT como una forma de generar radicales alcanos, usando una mezcla de $Cu(OAc)_2$ y oxidante como iniciadores de la reacción. Desafortunadamente, en esta última estrategia, el rendimiento no superó el rendimiento de 26 %.

Finalmente, se desarrollaron estudios preliminares para la reacción multicomponente de aminosulfonilación de estireno; se realizó la optimización de la reacción y se obtuvo un rendimiento del 83 % del producto utilizando cloruro de tosilo, carbazol y estireno como sustratos.

GENERAL INTRODUCTION

1. INTRODUCTION

1.1 Photochemistry and photocatalysis

One of the essential goals in modern chemical research is the development of new methodologies for organic synthesis in terms of selectivity, efficiency, safety, and sustainability. Classical synthetic methods involve multiple steps and use toxic and explosive reagents, generally lacking in selectivity. Even strong reaction conditions such as high pressure and temperature.[1] To access these, non-renewable energy sources are required, which emit CO_2, and this is the main responsible for global warming.[2]

In order to change this, a century ago, an Italian photochemist from the university of Bologna, Giacomo Ciamician, established a new alternative for organic synthesis. He identified the use of sunlight as a renewable and safer energy supplier for organic transformation.[3] On the other hand, currently, many industries use light for chemical changes. An example is a pharmaceutical company SANOFI that uses light (UV-light) in macro-reactors for photooxidation reactions to obtain products of commercial interest. An example is the photooxidation of dihydroartemisinic acid to semi-synthetic artemisinic; they generated this process on a scale of 370 kg. (Figure 1). [4]

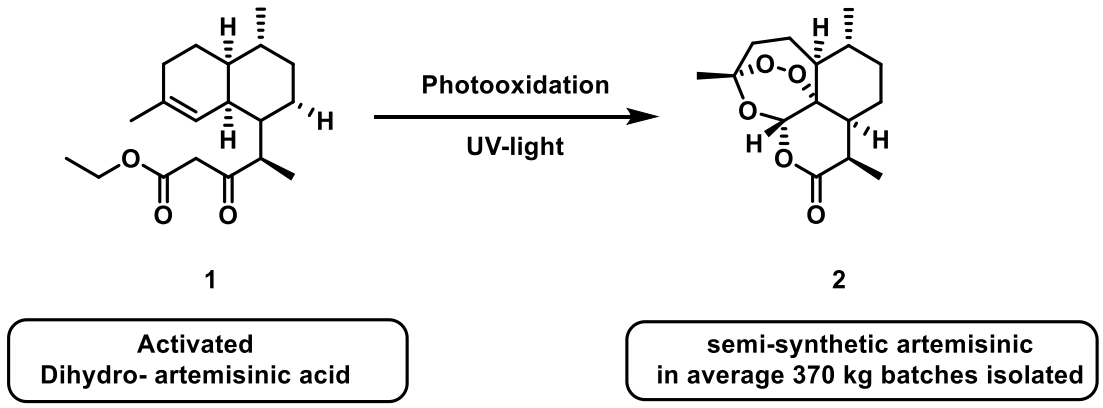

Figure 1. General representation for photooxidation of dihydroartemisinic acid

developed by SANOFI company.

The meaning of photochemistry is a chemical transformation among atoms or molecules originating by absorption of light in the range of ultraviolet and visible light (UV-visible), from100 nm to 800 nm. Moreover, photochemistry suggests many advantages such as atom economy, eco-friendliness, reactions in a few steps, mild conditions, selectivity, and generally high purity of the desired product in contrast to classical chemical reactions.[5] One of its inconveniences is that most organic molecules are not able to absorb in the visible range. An alternative is the use of a photosensitiser capable of absorbing visible light in a particular wavelength and then transferring the energy to a substrate, thus promoting the desired product obtention. This advance in organic synthetic chemistry has improved traditional synthetic chemistry through the development of innovative routes using light.[5]

The most commonly employed photocatalysts are poly-pyridyl or phenanthroline derivatives, including transition metal complexes with low spin ($4d^6$ and $5d^6$) electron configurations. Particularly, complexes of ruthenium ($[Ru(bpy)_3]^{2+}$) or iridium (*fac*-$Ir(ppy)_3$) (Figure 2). These features light absorption in the visible region, long-lived electronic excited state, intense luminescence, and tuneable electrochemical behaviour. These attributes are interesting in other fields involving light as an energy source like dye-sensitised solar cells, light-emitting diodes, visible light water splitting, among others. However, Ru and Ir are scarce and toxic metals, which is a disadvantage in industrial processes in terms of eco-friendly and upscaling experiments. [6]

The need to replace these precious metals and generate more sustainable processes has developed new lines of research focused on metals of low cost and high abundance in the earth, such as Cu, Co, Zn and Cr, belonging to the first-row transition metals, [7] for example $[Cu(dap)_2]Cl$. [8] On the other hand,

many research groups have aimed their studies on organic dyes, such as Eosin Y.[9]

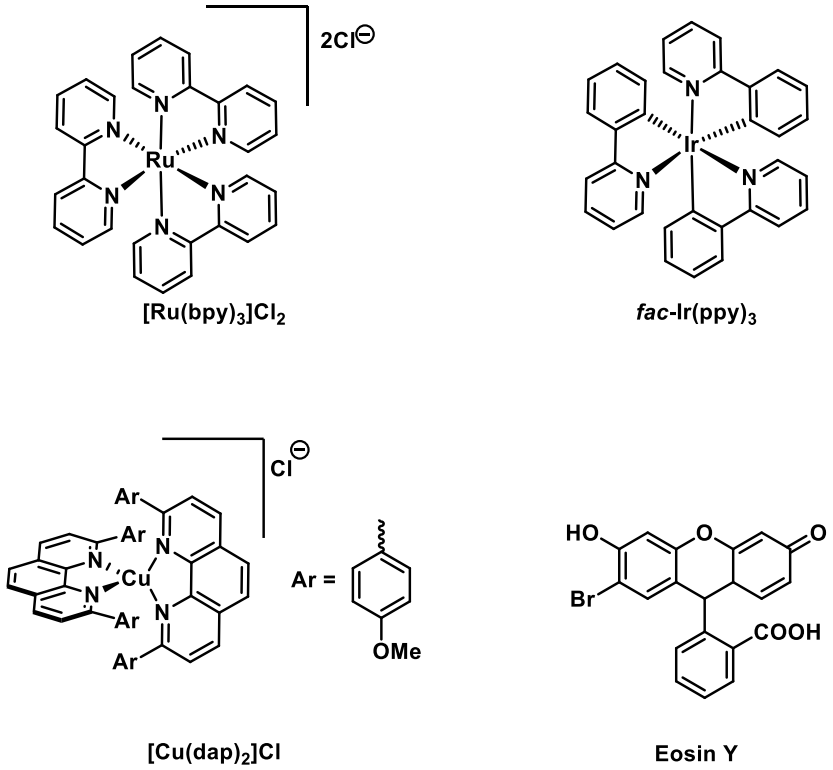

Figure 2. The most common employed catalysts in photochemistry

A photocatalyst (PC) absorbs light to generate a high-energy excited singlet state (PC*). In the case of metal-based photocatalyst, this is through a metal-to-ligand charge transfer (MLCT). Then, this singlet's excited state undergoes a fast intersystem crossing (ISC) to give the lowest energy triplet MLCT state, which usually has a longer lifetime and is able to perform an energy transfer (ET) or photoinduced electron transfer (PET) process more efficiently as compared to their ground states. [10,11]

The redox transformations of PC* could follow two different pathways as oxidative or reductive quenching cycles. PC* acts as a reductant in the oxidative quenching cycle, reducing an electron acceptor by a single electron

transfer (SET) process. The products of this are the radical anion and the oxidised form of the employed photocatalyst. Most of the time, this oxidised species is a strong oxidant and may accept an electron from some donor (typically from a substrate itself) to form the radical cation and regenerate the photocatalytic cycle. A compound that gains an electron from PC* is said to be a sacrificial oxidative quencher of the photocatalyst.

On the contrary, in the reductive quenching cycle, PC* functions as an oxidant, receiving an electron from sacrificial electron donors to give a reduced form of PC. This intermediate is a suitable reductant and can donate an electron to return the ground-state species of PC. (Figure 3). [11]

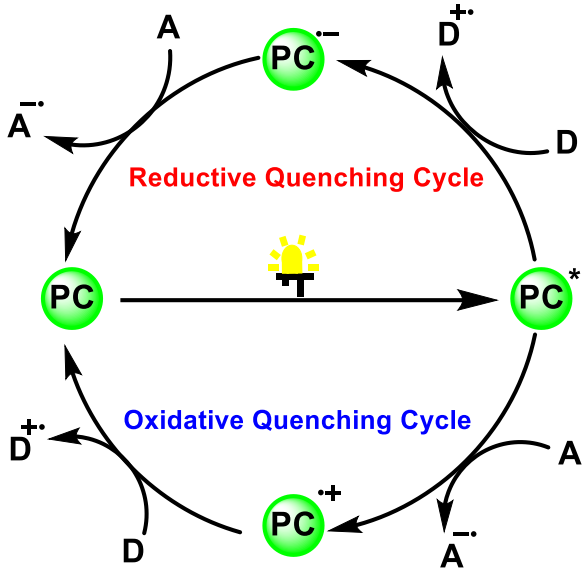

Figure 3. General representation of electron transfer process in a Latimer-diagram, (PC = photocatalyst; A = acceptor; D = donor, blue: oxidative quenching cycle; red: reductive quenching cycle).

As mentioned above, copper has become a new alternative against rare metals due to their similar properties and cheapest cost. The valuable role of copper as a widely available source for light-induced processes has also been recognised, featuring strong reducing power, sufficient excited-state lifetime, and high luminescence in the excited state. Copper complexes have been applied in photocatalytic hydrogen production from water, biological process, or active components in organic light-emitting diodes (OLED) and light-emitting electrochemical cells (LEEC). [12]

Reports in the literature about copper in photocatalysis have been increasing in the last five years.[8] Several publications show the use of copper in new reactions. However, there is still a lack in terms of the structural design of the catalyst and the reactivity, which could help understand the electronic transfer process.

1.2 Electrochemical and photophysical properties of Cu^{I} complexes

Homoleptic copper (I) complexes with phenanthroline derivatives ligand exhibit a MLCT band (λ MLCT) close to 450 nm, strong reducting potential ($E_{1/2}$= -1.43 V), and an excited-state lifetime (τ) close to 270 ns in CH_2Cl_2, lower than the τ exhibited by ruthenium complexes (2300 ns). In order to overcome this gap, ligands derived from phosphines (*P,P*) have been introduced in Cu^{I} heteroleptic complexes, reaching τ values in the order of 16,000 ns. However, this kind of complexes show a blue shift of the MLCT band, displacing from 450 to 380 nm approximately. In order to approach the VIS region, adding electron donor groups in the *N,N* ligand and/ or in the *P,P* ligand is necessary.[13]

From the structural point of view, the complex $[Cu(phen)^2]^+$ possesses tetrahedral ground state geometry (D_{2d} symmetry). Once it reaches the excited state, the intersystem crossing occurs from the singlet excited state (^{1}MLCT) to the triplet excited state (^{3}MLCT). At this point, the complex can perform a bimolecular electron transfer and is susceptible to oxidation ($d^{10} \Rightarrow d^9$). The oxidation of the complex promotes a pseudo-Jahn-Teller distortion, changing its spatial conformation towards a flat square geometry (D_2 symmetry). This phenomenon is known as flattening, and thus the complex can be easily attacked by nucleophiles at its fifth axial coordination sites, such as a water or solvent molecule. If the ligands do not sterically prevent the nucleophilic attack, the fifth coordination site will be occupied. This stabilise the excited complex, preventing the metal reduction from Cu^{II} to Cu^{I} and, therefore, without returning to its original tetrahedral geometry, interrupting the photocatalytic cycle. On the contrary, if the ligands sterically prevent the nucleophilic attack by an axial flank, the complex can be reduced, allowing it to return to its original spatial arrangement and continue the catalytic cycle. On the other hand, the complexes in the flattened state can undergo a non-radiative deactivation pathway (Figure 4). [14]

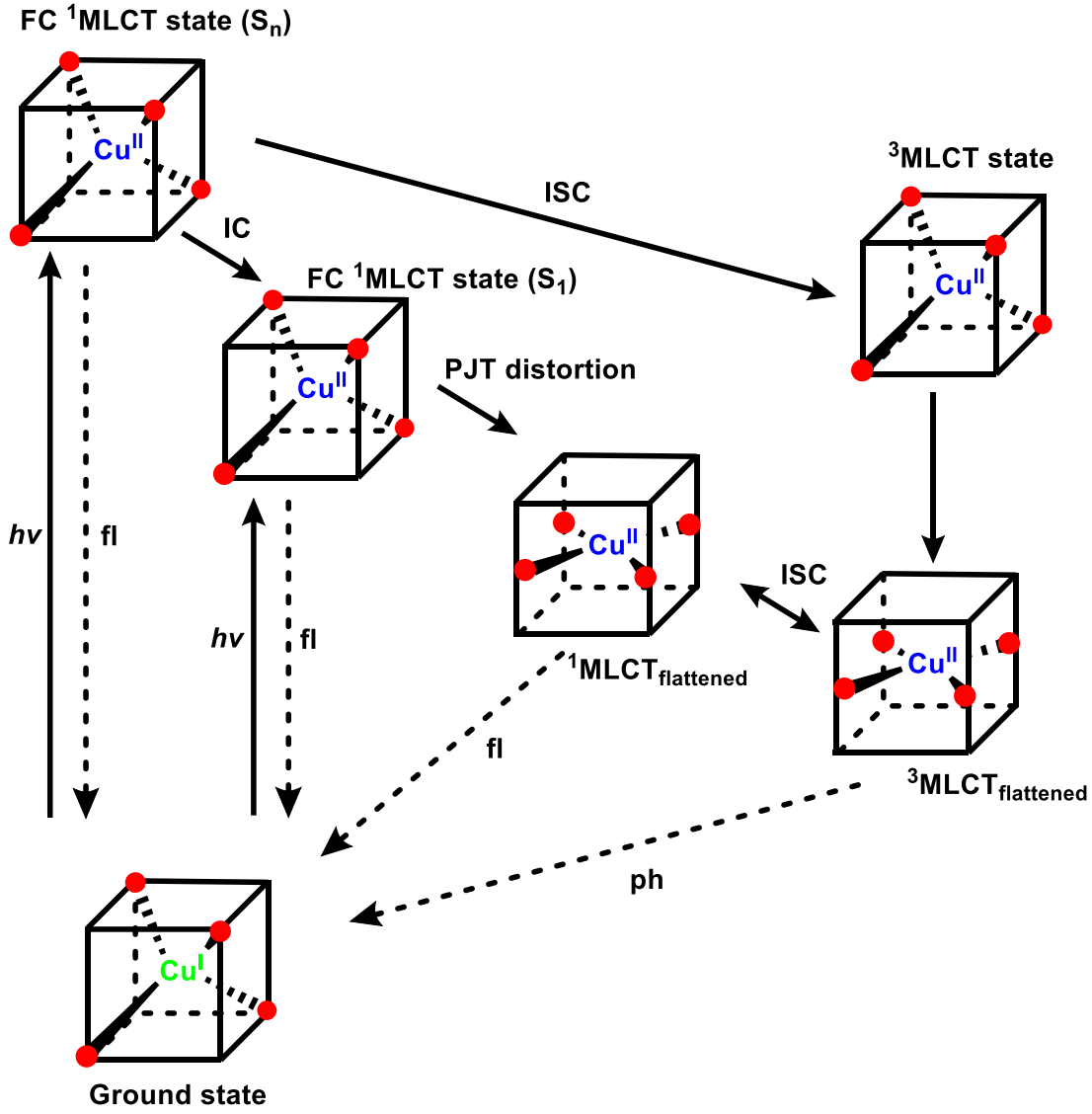

Figure 4. A general Jablonski diagram of photoinduced electronic transition for homoleptic copper complexes

1.3 Cu^{I} complexes in organic reactions mediated by light.

1.3.1. Cu^{I} in ATRA reactions

Atom transfer radical addition (ATRA) reaction allows the di-functionalisation of olefins. The traditional way of initiating this reaction is using a radical reagent or thermal activation.[8] However, in 2012 Oliver Reiser's group showed the activation of several olefins with different halogenated reagents using $[Cu(dap)_2]Cl$ as photocatalyst through irradiation of green light. One of the examples reported was the activation of styrene with CBr_4. The ATRA product **5** has a great synthetic utility, because can be attacked with a nucleophile and in the presence of a base, such as 1,8-diazabicyclo(5.4.0)undec-7-ene (DBU), obtain valuable intermediates (**6**) for the synthesis of pyrazoles (Scheme 1).[15]

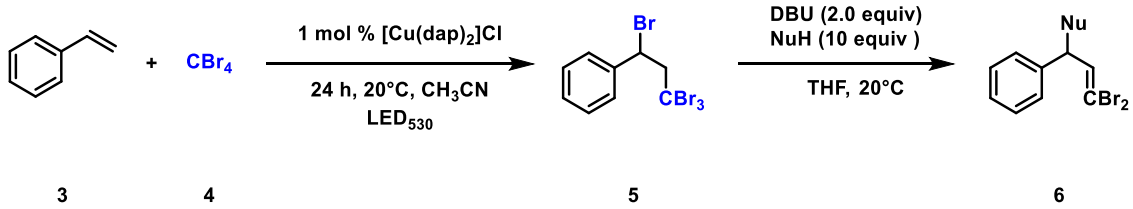

Scheme 1. ATRA test reaction and synthetic utility of the ATRA product.

1.4. Understanding the design-reactivity relation of copper complexes in photoredox catalysis

1.4.1 $[Cu(dap)_2]Cl$ – ATRA reactions

The copper photocatalyst most used in ATRA reactions is $[Cu(dap)_2]Cl$.[8] It is a homoleptic copper complex with robust optoelectronic properties such as: 437 nm absorption, 270 ns lifetime in the excited state, and -1.43 V reduction potential, which allows for activation of different substrates.[16] Furthermore, this complex uses bulky aryl substituents at positions 2,9 of the phenanthroline ligand. This permits the complex to carry out the catalytic cycle shown since it does not allow the complex to stabilise copper(II) or form an exciplete; these protect the metal centre. Additionally, this complex is not sensitive to air. Several publications showed that $[Cu(dap)_2]Cl$ allows to access to new synthetic methodologies such as: allylation of α-haloketones, chlorosulfonylation, chlorotrifluoromethylation, haloperfluoroalkylation and difunctionalization of alkenes with iodoform, and oxo-azidation of styrene derivatives, among others (Scheme 2).[15,17–24]

Allylation of α-haloketones

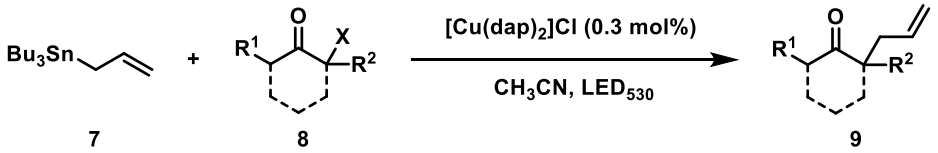

7 8 9

Chlorosulfonylation and chlorotrifluoromethylation of alkenes

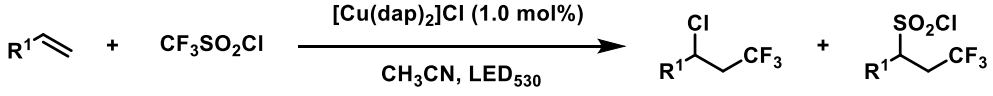

10 11 12 13

(i)	R = electron-withdrawing group	major	minor
(ii)	R = electron donor group	minor	major

Haloperfluoroalkylation of alkenes and alkynes

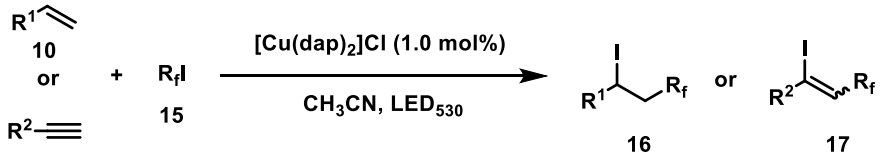

16 17

Chlorosulfonylation of alkenes

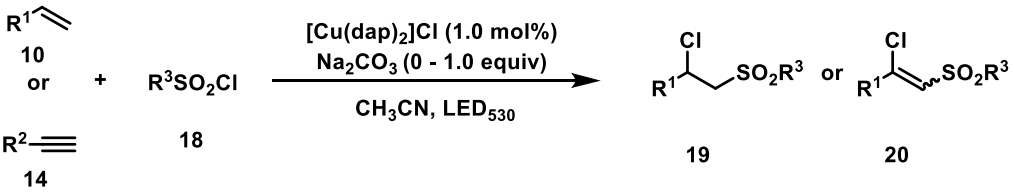

19 20

ATRA reaction of Iodoform with olefins

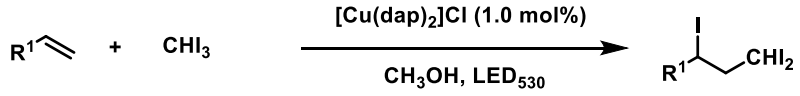

10 21 22

Oxoazidation of styrene derivatives

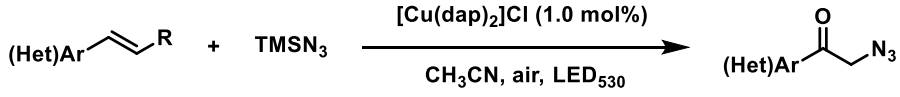

23 24 25

Scheme 2. Examples of new synthetics methodologies achieved by [Cu(dap)2]Cl.

The general catalytic cycle for ATRA reactions is exemplified based on Scheme 1 (Figure 5). The first step of the reaction mechanism is the activation of the complex initiated by the absorption of light; the MLCT process occurs, which generates the change in the oxidation state of Cu^{I} to Cu^{II} and the reduction of the ligand, as already mentioned this undergo a pseudo-Jahn teller distortion and a change in the spatial conformation. Furthermore, it is thought to involve oxidative excited-state quenching by the organohalogen compound, followed by adding the resulting organic radical to the alkene. The neutral addition product is then oxidised by Cu^{II} to close the photocatalytic cycle resulting in a cation that can be attacked in a nucleophilic manner by the halide anion (X^{-}) from the early photoinduced reaction step, thereby forming the final product. These ATRA reactions are redox neutral; therefore, no sacrificial reagent is required.

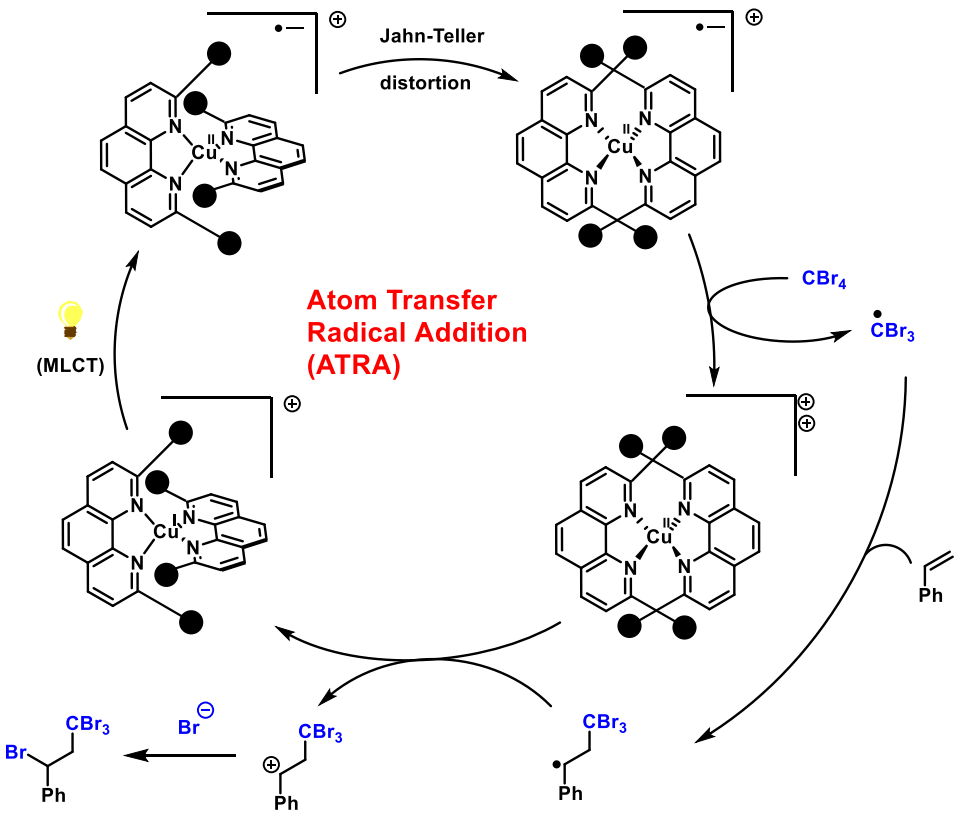

Figure 5. General catalytic cycle for ATRA reactions.[25]

1.4.2 New homoleptic Cu^{I} complexes.

Several homoleptic copper (I) complexes have been reported for different applications; generally, these are based on bidentate *N,N* ligands such as bipyridine and phenanthroline, the latter being more studied in photocatalysis. Various groups have used the reaction previously shown as an ATRA test type reaction. In 2018, Mayer et al. studied the pattern of substitution of the aryl group contained in phenanthroline with donor groups and studied the effect of the photocatalyst counterion. In more detail, this group synthesised a series of novel homoleptic phenanthroline-containing Cu^{I} complexes featuring sterically- and electronically varied 2,9-diaryl-1,10-phenanthroline ligands in order to understand the influence of substituent effects on the photoredox capacity. [25]

In the same year, the Han See Soon group studied the behaviour of bis(arylamino)-acenaphthene (Ar-BIAN) ligands. This is recognised as versatile, redox-noninnocent π-acceptors that are easily synthesised by condensation reactions between acenaphthenequinone and commercial anilines. The advantage of these ligands has been previously demonstrated since they avoid unwanted thermal relaxation due to their low-lying non-emissive triplet excited states. [26]

In 2019, Novak et al. reported a battery of Cu^{I} complexes using the type α-diimine ligand and studied their properties over ATRA reactions. These kinds of ligands are attractive since their synthesis comes from commercially available starting materials such as ethylenediamine and benzaldehydes, using ethanol as solvent at room temperature in one step. Moreover, ligands are obtained in high yield. Furthermore, in these ligands, the steric and electronic effects can be managed using different anilines, allowing easier access to photoredox catalysts. This class of copper complexes are activated under irradiation with green light.[27] (Figure 6).

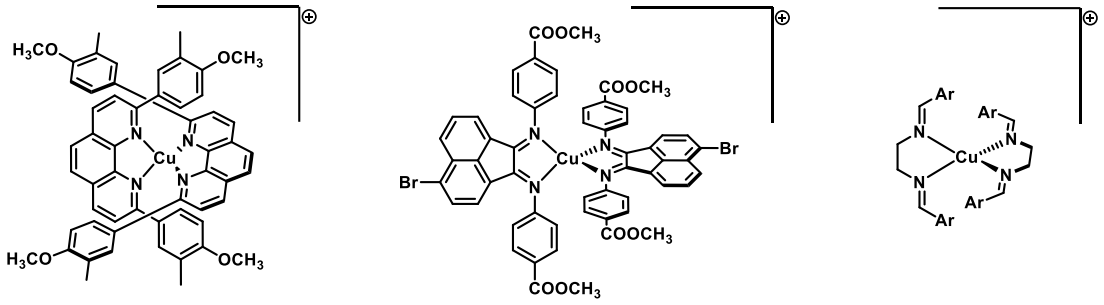

Figure 6. Homoleptic $[Cu(N,N)_2]^+$ used in ATRA test reaction.

1.5 Heteroleptic copper complexes in photocatalysis.

Heteroleptic complexes have taken interest from the academy because they are generally easy to prepare, and in addition, these can be synthesised from ligands that have atoms such as C, S, and P. In heteroleptic complexes, due to the pseudo-tetrahedral geometry that the complex can adopt having two different ligands, the spacial arrangement can reduce the flattening effect over the Cu^I metal centre and lower the non-radiative radiation.[28,29]

Generally, the ligands used in heteroleptic complexes are *N,N* and *P,P* coordinating bidentate ligands. Phosphine ligands stabilise the Highest Occupied Molecular Orbital (HOMO) of the complexes and modify the optoelectronic properties, usually increasing the triplet state population. Consequently, an increase in the quantum yield and the lifetime in the excited state. This modification based on the use of different auxiliary ligands in terms of rise the energy has been attractive in the field of photocatalysis because the excited state energy processes are more likely to occur SET.[14,16]

In the year 2012, Collin's group reported the first use of heteroleptic copper complexes in photoredox catalysis. They demonstrated the role of $[Cu(dmp)(POP)]^+$ and $[Cu(dmp)(XantPhos)]^+$ (dmp = 2,9-Dimethyl-1,10-phenanthroline) using 25 mol% of the photocatalysts in the synthesis of [5]Helicene with moderate results (57 % Yield).[16]

One of the first heteroleptic copper complexes used in ATRA reactions was reported by Oliver Reiser's group in 2015, using a phenanthroline-derived and bisisonitrile ligands, type $[Cu^{I}(dpp)(binc)]BF_4$ (dpp = 2,9-diphenyl-1,10-phenanthroline; binc = bis(2-isocyanophenyl) phenylphosphonate). The main characteristics of this are the easy preparation of the binc ligand and the high lifetime in the excited state (17 μs). This complex is active in the ATRA reactions previously reported by the same group and has been used among Boc-Allylamine (**28**) and Diethyl-Bromomalonate (**29**) substrates to obtain the desired allylated products in good yields (over 90%) (Scheme 3), using a lower photocatalyst loading (0.5 mol%), shorter reaction time (7.5 h) better than reported for $[Cu(dap)_2]Cl$ complex (75% yield, 1.0 % mol, 24 h). Furthermore, $[Cu^{I}(dpp)(binc)]BF_4$ could be utilised for allylation reactions with trimethylallylsilane under mild visible-light photoredox conditions.[30]

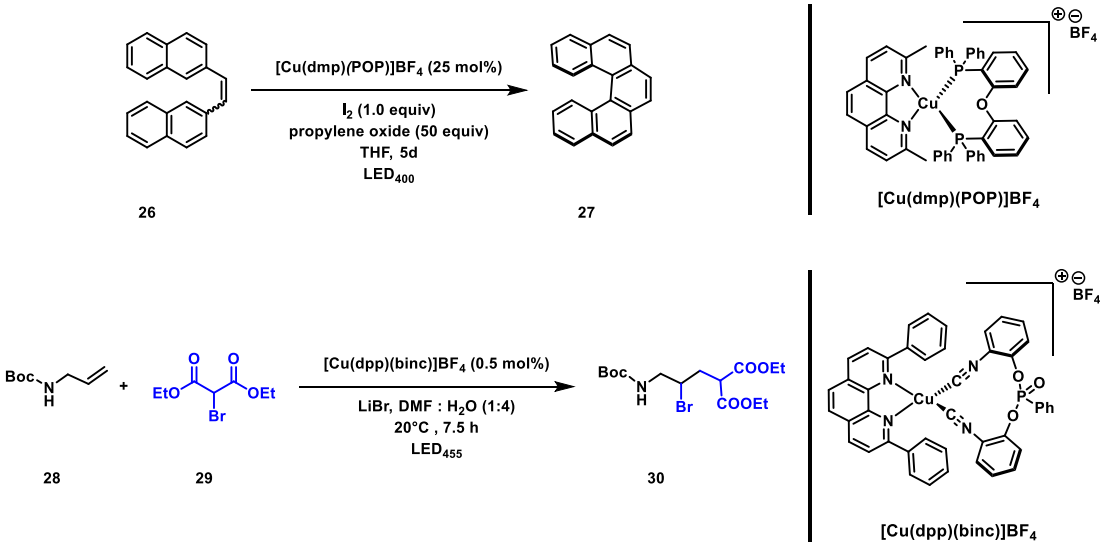

Scheme 3. Synthesis of [5]Helicene by $[Cu(dmp)(POP)]BF_4$ and synthesis of $[Cu(dpp)(binc)]BF_4$

Collins and co-workers demonstrated the use of $[Cu(tmp)(BINAP)]BF_4$ (tmp = 3,4,7,8-tetramethyl-1,10-phenanthroline; BINAP = (2,2′-bis(diphenylphosphino)-1,1′-binaphthyl)) as an efficient catalyst for Appel reaction; this reaction has been realised in bach and flow set-up using purple LED, obtaining the product in good yields, nearly to previously reported by ruthenium catalyst.[31] Later, they reported fifty homo- and heteroleptic -copper complexes based on different possibilities of mixing several *N,N* and *P,P* chelating ligands. The role of the phosphine BINAP predominates in the decarboxylative reaction between *N*-(acyloxy)phthalimide (**33**) and bromoalkyne (**34**) to form the coupling product Csp^3-Csp (**35**). The second reaction explored was a proton-coupled electron transfer (PCET) process. They investigated the homolytic activation of ketones (**36**) to produce neutral ketyl radicals. Among the fifty Cu^I complexes, $[Cu(dq)(BINAP)]BF_4$ (dq = 2,2'-biquinoline) was the most active, generating 71 % yield of the product. Finally, the last study was the energy transfer process, and they showed the use of heteroleptic copper complexes over the visible-light sensitisation of vinyl azides (**38**) to aim pyrrole synthesis (**39**). In this experiment, almost all the copper complexes exhibited good yields, over 95 %, and $[Cu(dmp)(BINAP)]BF_4$ obtained the product in quantitative amount. [32](Scheme 4)

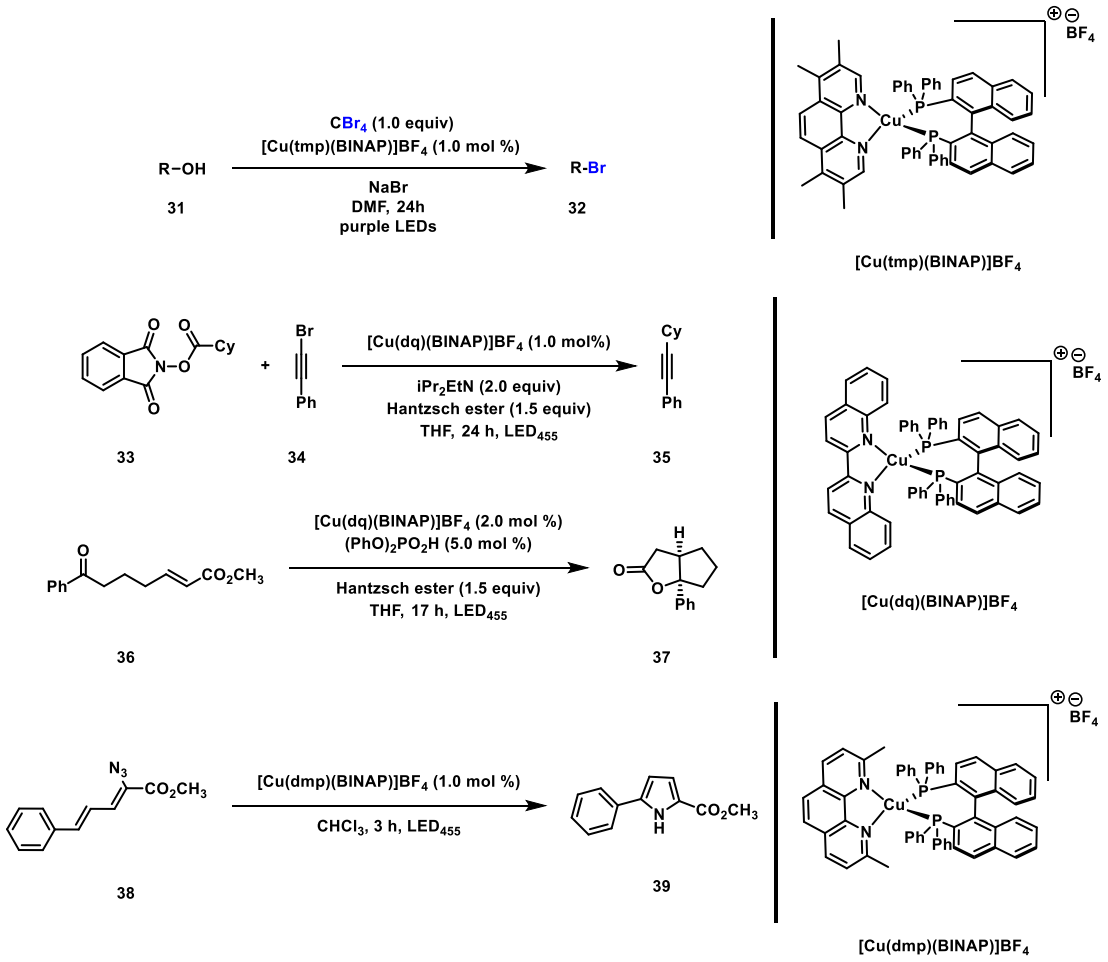

Scheme 4. Summary of reactions developed by Collin's group.

As mentioned above, Reiser's group reported the ability of $[Cu(dap)_2]Cl$ in the chlorosulfonylation reaction. This reaction promoted the coupling between styrene or phenylacetylene with several tosyl chloride derivatives. In the case of phenylacetylene, the isomeric mixture *E* and *Z* are obtained in good yields.[21]

In contrast to this result, Xile Hu and co-workers reported a heteroleptic copper complex based on bipyridine derivative and bidentate phosphine ligands, type $[Cu(bpy^*)(XantPhos)]BF_4$ (bpy* = 6-methyl-4-(2,4,5-trimethylphenyl)-2,2'-bipyridine),[33] effective in the formation of the chlorosulfonylation product **42**. One of the most remarkable results is the exclusive obtaining of the *E* isomer

from the chlorosulfonylation reaction over alkynes, being a highly selective reaction under blue light irradiation (Scheme 5).[34] They argued that this phenomenon is due to an outer sphere mechanism. This photocatalyst unlocks the research window towards the selectivity of catalysts, even more in this reaction that incorporates a functional group such as sulfones in various substrates. This moiety can be found in many drugs and natural products. This functional group has been recognised as a neuroprotective agent towards Parkinson's Disease Therapy and inhibits many types of cysteine proteases.[35,36]

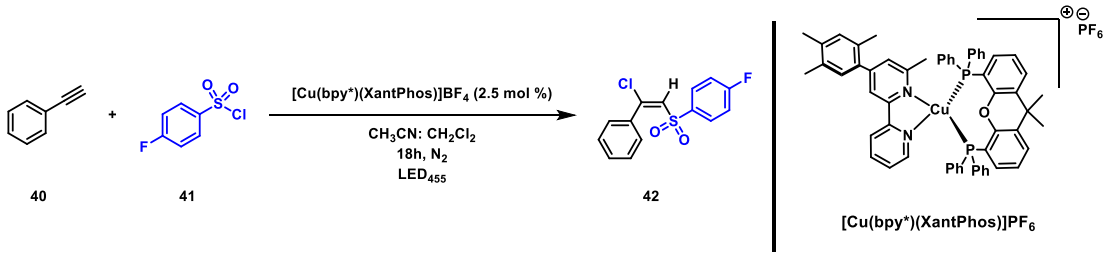

Scheme 5. Chlorosulfonylation reaction developed by Xile Hu' group.

Three years later, Collins group again demonstrated the ability of heteroleptic copper complex type [Cu(bphen)(XantPhos]BF_4 (bphen = 4,7-Diphenyl-1,10-phenanthroline; XantPhos = 4,5-Bis(diphenylphosphino) - 9,9 - dimethylxanthene) in two energy transfer process. They reported that bphen ligand lengthened the excited state lifetime, which is crucial for this kind of process. The first case of study is a series of 25 di and trisubstituted alkenes in a photoisomerisation reaction *E* to *Z*, including macrocycles and 1,3- enynes. Furthermore, the photocatalyst is used in a tandem ATRA/photoisomerisation process, as an example is the reaction mentioned before between aryl sulfonyl chlorides and phenylacetylene derivatives, that means the first step is the obtention of the mixture of *E/Z* ATRA product and then is the photoisomerisation which give *E* isomer product. [37]

In the same year, Luo and co-workers explored the structure-activity of heteroleptic copper complexes in [2+2] photodimerisation of chalcones (Scheme 6), cinnamates and cinnamamides. They found that the phenanthroline ligand with substituents at the 2,9-positions and the 4,7-positions showed high activity in the photodimerisation via an energy transfer pathway.[38]

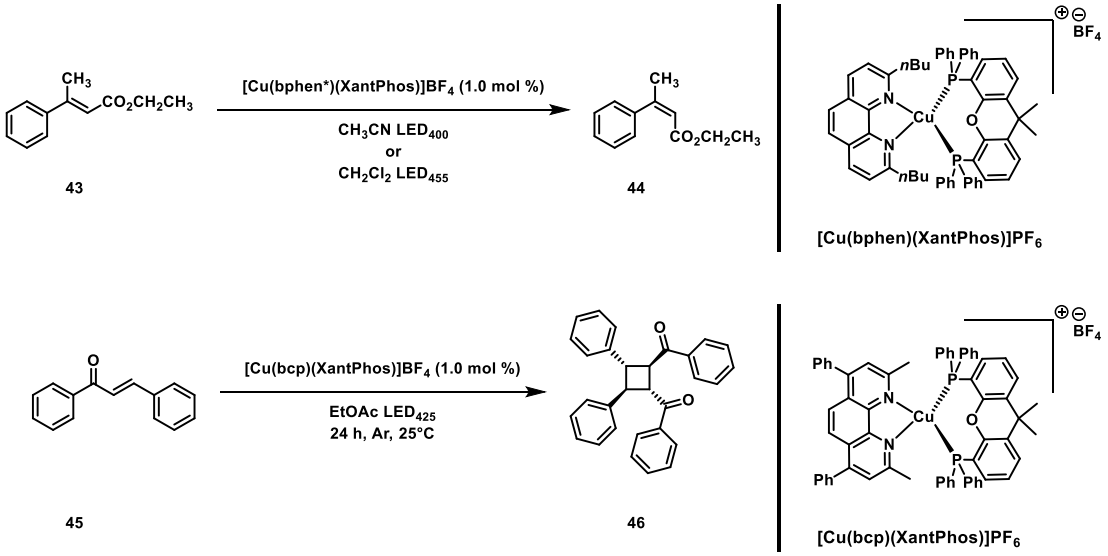

Scheme 6. Photoisomerisation reaction *E* to *Z* developed by Collin's group and [2+2] photodimerisation settled by Luo.

1.5.2 Heteroleptic copper complexes in photocatalysis- The importance of the ligand design.

In recent years, an effort has been made to study in depth the relationship that ligands may have with activity in photocatalytic reactions. Regarding heteroleptic complexes, the structure of phenanthroline has been studied. The extension in the π system has been modified from one to three aromatic rings (ddpq, ddppz, or dbdppz), see Figure 7. This group of complexes was studied in three different types of reactions (SET, PCET, ET). However, this π extension is not particularly active as the complexes carrying the original dmp ligand. They even concluded that future development of photocatalysis via reductive quenching should avoid using such diimine ligands.[39]

On the other hand, the same group demonstrated that a good design in the *N,N* ligand could help a particular reaction. They reported a bifunctional copper-based photocatalyst type [Cu(pypzs)(BINAP)]BF_4 (pypzs = 5- (4-fluorosulfonyl) amino-3- (2-pyridyl)-pyrazole) supported on pyrazole-pyridine (*N,N*) ligand combining a sulfonamide moiety that functions as an intramolecular hydrogen-bond donor for a photochemical PCET process. A good performance employing redox properties and pKa are required for the PCET process, especially when the photocatalyst contains an H-bond donor. To afford valuable diols, they achieved a reductive pinacol-type coupling (**48**) from readily available aldehydes and ketones (**47**). [40]

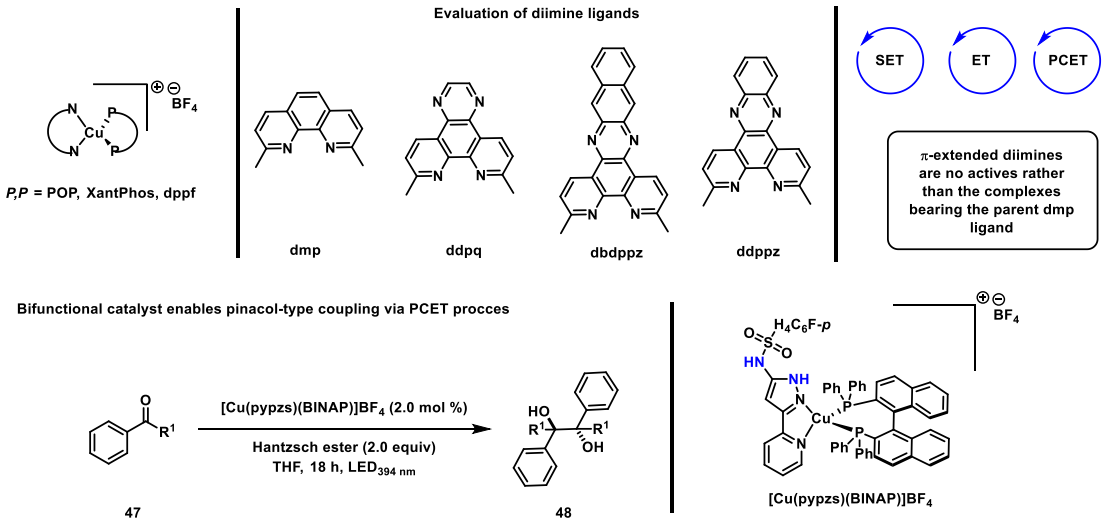

Figure 7. Examples of design and evaluation of heteroleptic copper complexes applied in photoredox reactions.

1.6 Introducing Cu^{II} complexes in photocatalysis

Currently, well-established copper complexes in photo-ATRA processes are based in the +1 oxidation state of the metal. However, in the 2018, Reiser's group introduced $Cu(dap)Cl_2$ in oxo-azidation and chlorosulfonylation of styrenes.[21,23] The advantage of this kind of catalyst, with +2 as oxidation state, is that it can be synthesised without the need for an inert atmosphere or dry solvents, presents red-shift absorption bands (over 450 nm) and are more stable than copper (I) complexes under O_2 or water. However, copper (I) is still an active species by reduction of copper two; copper (I) specie is stabilised by another dap ligand or acetonitrile from the solvent. Later, the same group reported a new copper (II) complex, using dmp as a ligand, type $[Cu(dmp)_2Cl]Cl$. This photocatalyst has been considered efficient, considerably more cost-effective than previously reported copper (I) photocatalyst, and active in several reactions.[41] It is possible to observe that a similar synthesis can generate two complexes with different geometries, a flat square with a four-coordinate metal and a square-based pyramid with a five-coordinate metal

centre (Scheme 7).

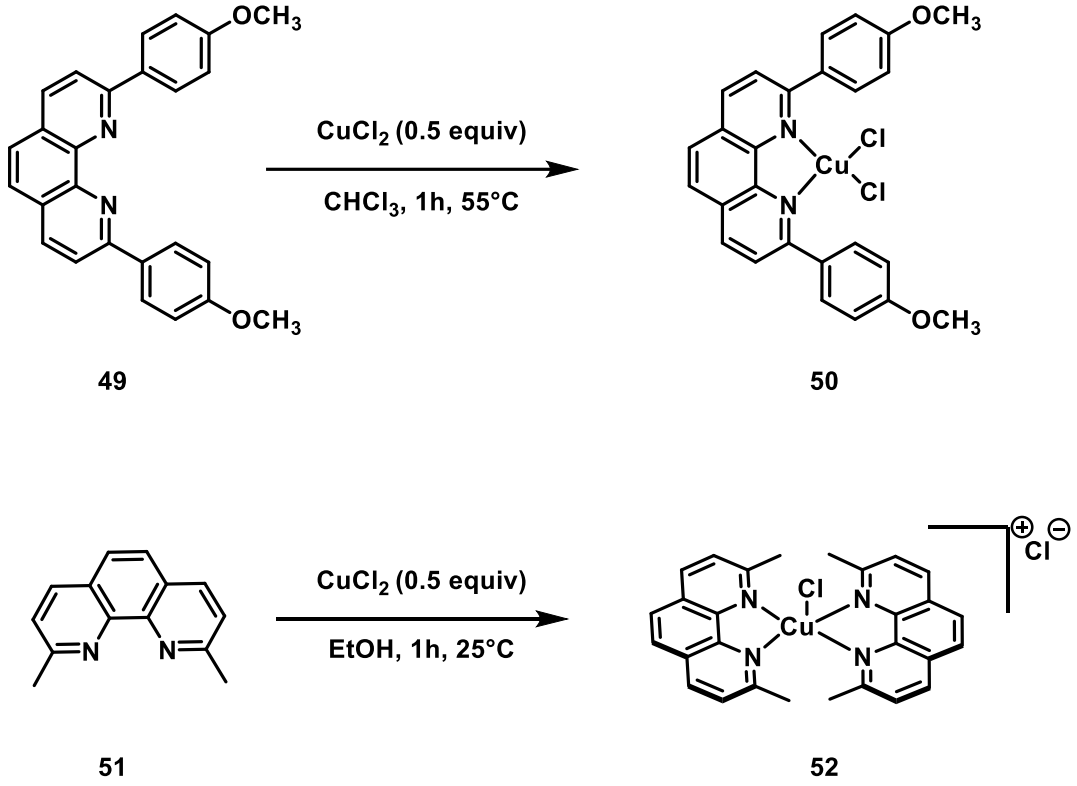

Scheme 7. Synthesis of $Cu(dap)Cl_2$ and $[Cu(dmp)_2Cl]Cl$

Nevertheless, from the ligand perspective of the study, photophysical and electrochemical properties of the group substitutions and positions on *N,N* environment in photochemistry it is still scarce. It is barely possible to find reports based on phenanthroline or bipyridine ligands.[32] This is evidence that the field of copper photocatalyst is still in research; it is open research from the point of view of the design of the catalyst, tuning of their optoelectronic properties and unexpected reactions that copper could reach in the nearly future.

1.7 Project proposal

Because of the relevance of organic transformations using light as green and traceless reagent, this project proposes the development of a new family of copper complexes as photoredox catalysts, having higher conversion efficiencies, selectivity, easier modulation of the redox-optical properties, lower synthesis costs and lower toxicity. In this new family of copper photocatalysis, *N,N* ligand corresponds to symmetric *N,N*-heterocyclic derivative and *P,P* represents commercially available biphosphines: POP, BINAP, XantPhos, dpbz and dppf.

The proposed ligand structure is based on the need to: stabilise the D_{2d} complex symmetry in the excited state, thereby preventing non-radiative relaxation via structural complex change (flattening), solvent quenching, and promotion of as much red-light absorption as possible. To achieve this, ligands must possess a conjugated π extended structure that stabilises their structural reorganisation and must also have a high degree of a steric hindrance (phenyl extension), which by repulsion of substituents maintains their basal state symmetry. Besides, the *P,P* auxiliary ligand is destined to produce both high steric congestion, providing a restriction on the degrees of *N,N* ligand freedom, forcing the complex to maintain its tetrahedral geometry, and electronic modulation of the HOMO of the complexes, thereby increasing the redox-optical properties efficiency of the complexes and their stability as well.

HYPOTHESIS AND GOALS

2. HYPOTHESIS

A novel series of Cu^{I} and Cu^{II} salts and complexes bearing *N,N*-heterocyclic polypiridinic derivative ligand will allow access to a new series of compounds with the photophysical and electrochemical properties that will enable their use as active catalysts in photoredox reactions

3. GOALS

3.1 MAIN GOALS

Synthesise, characterise and evaluate electrochemical and photophysical properties of new series of Cu^{I} and Cu^{II} complexes bearing *N,N*-heterocyclic polypyridinic derivative ligands as an active catalyst in photoredox reactions.

3.2 SPECIFIC GOALS

1. To develop the synthesis and characterisation of Cu^{I} complexes type $[Cu^{I}(N,N)(P,P)]BF_4$. Where *N,N* correspond to the dpa ligand with the most straightforward substitution pattern and *P,P* are commercial phosphines ligands .
2. To develop the synthesis and characterisation of dpa derivatives ligands substituted in positions 2, 3 or 4 with electron donor or electron-withdrawing aryl functional groups.
3. To develop the synthesis and characterisation of Cu^{II} complexes type $Cu^{II}(N,N)Cl_2$; $[Cu^{II}(N,N)_2Cl]Cl$. Where *N,N* correspond to several *N,N*-heterocyclic polypyridinic ligands.
4. To evaluate the electrochemical and optoelectronic properties (λ_{abs}, λ_{emi}, τ, ϕ) of the synthesised copper complexes.
5. To evaluate the new battery of copper salts and complexes, with optimal redox-optical properties, as an active photocatalyst for functional group transformations in different reported organic reactions, mediated by visible light.
6. To explore new photoredox reactions using the synthetised copper complexes.

CHAPTER I - COPPER COMPLEXES WITH NITROGENATED LIGANDS AS PHOTOCATALYSIS

RESULTS AND DISCUSSION

4.1 Ligand aim

As mentioned above in the general introduction, $[Cu(dap)_2]Cl$ copper complex has managed to meet the three essential keys for photocatalysis, which are: absorption in the visible light range to reach the active species in the excited state, enough lifetime in the excited state to generate energy transfer processes and / or electronics. In addition, robust redox potentials for chemical transformations of different organic substrates. However, the synthesis of the dap ligand uses a 4-step linear synthesis (Scheme 8). In addition to the possible variations on dap ligand using different electronic functional groups as substituents in different positions on the phenanthroline moiety have already been studied by Thomas Rawner [42], and the effect on photocatalysis reactions. These results of an optimised system and knowledge of the limitations of phenanthroline derivatives ligands has opened the window to search for new ligands that are easily accessible and with potential in photocatalysis.

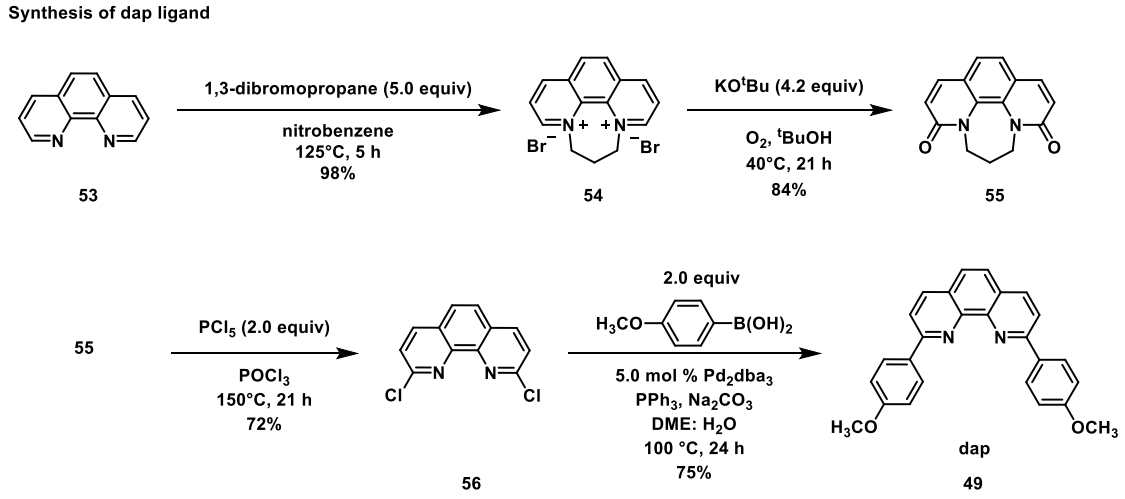

Scheme 8. Dap synthesis by Thomas Rawner.

The proposal of this work is based on the dpa ligand, which has been studied with different metals (Pd, Pt, and Al) and has been used in applications ranging from drug precursors to catalyst support.[43–47] One of the most remarkable studies of the dpa ligand is in copper complexes type [Cu(NHC)(dpa)]BF_4 towards the light-emitting electrochemical cells application reported by Costa's groups. They published the effect of modulation on the optoelectronics properties of these complexes using different donor and acceptor groups on dpa ligand. Besides being one of the most efficient among others *N,N* bidentate centres [48]

This ligand was chosen as the basis for this work because it is a ligand that is easy to synthesise (one step). In addition, the plausible modifications in this *N,N* heterocycle, that originates from two pyridines, could allow the studies of their properties according to different modifications separately. In order to carry out an initial study, and evaluate the auxiliary ligand *P,P* towards photocatalysis, we have selected several commercial phosphines, to study the steric effect and protection of the metal centre, the effect of a second metal and the effect of a chiral phosphine in photocatalysis reactions.

4.1.1 Synthesis of Cu^{I} complexes type [Cu(I)(*dpa*)(*P,P*)]BF_4

Five new heteroleptic copper (I) complexes of the type [Cu(dpa)(*P,P*)]BF_4 were synthesised in two steps following methodologies reported in the literature[28,29] (Scheme 9). Equimolar amounts of dpa ligand and $[Cu(CH_3CN)_4]BF_4$ were stirred in CH_2Cl_2 under N_2 atmosphere at 20 °C, followed by the addition of the *P,P* ancillary ligand. The resulting complexes were isolated by crystallisation from CH_2Cl_2/toluene mixtures in 85–95% yield, showing high air and thermal stability both in the solid-state as well as in solution for several days.

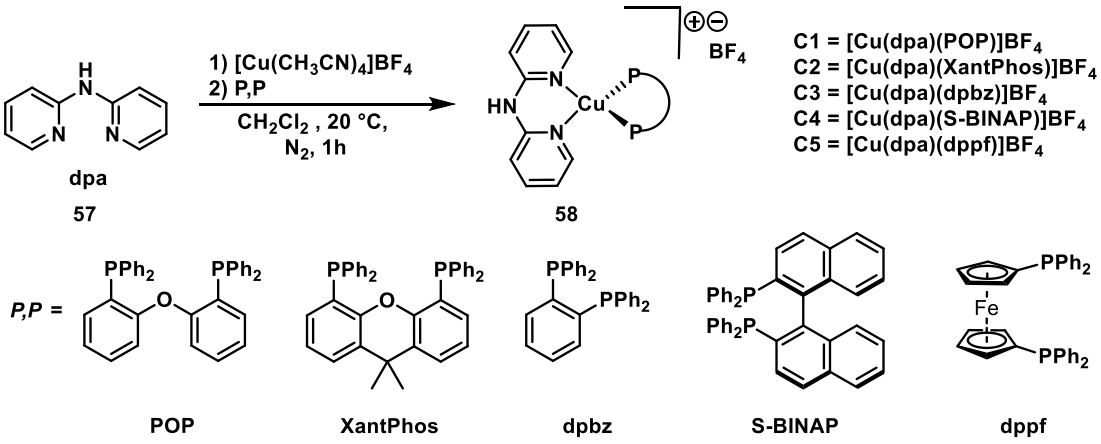

Scheme 9. Synthetic route to obtain heteroleptic Cu^{I} complexes **C1-5**.

4.1.2 Structural characterization of Cu^{I} complexes type $[Cu^{I}(dpa)(P,P)]BF_4$

4.1.2.1 NMR characterisation of C1-5.

NMR characterisation of **C1-5** shows the successful coordination of the ligands to the metal centre as judged by the chemical shift in the ^{1}H spectra of N-H (close to 9.0 ppm) in all complexes compared to the dpa-free ligand (close to 8.0 ppm). The phosphine signals in the ^{31}P NMR of all complexes exhibit a chemical shift compared to the free ligands and are observed from 0 ppm to -14 ppm (see the Appendix for the detailed characterisation).

4.1.2.2 X-ray characterisation of C1-5.

The molecular structures of the complexes **C1-5** were obtained by XRD (Figure 8, Table 1). These complexes exhibit pseudo-tetrahedral coordination around the copper(I) mononuclear centre, surrounded by one dpa ligand and one bidentate phosphine ligand. The dpa ligand showed small bite angles in the range of 91° – 94°, whereas the bidentate *P,P* ligands displayed larger bite angles in the range of 100° -115°. The larger bite angle observed for XantPhos (**C2**) than for POP (**C1**) ligand can be attributed to the higher rigidity of the former due to the methylated cycloalkane. In general, the difference between the bite angles of the *N,N*, and *P,P* ligands induce the distortion observed to the tetrahedral geometry likely reflects the rigidity of the *P,P* ligand, where all values are similar to those reported in the literature for analogue complexes of the type $[Cu(N,N)(P,P)]^{+}$. Regarding the bond distances, these are very similar among each complex. Small distances are observed between the nitrogen and the copper atoms (ca 2.05 Å), while longer lengths are seen for the Cu-P bond (in the range 2.24 Å – 2.29 Å), in agreement with values already reported.[49] On the other hand, according to the literature, [50] τ_4 was determined, the value that is closest to a perfect tetrahedron is for **C2** and the greatest distortion is for **C3**.

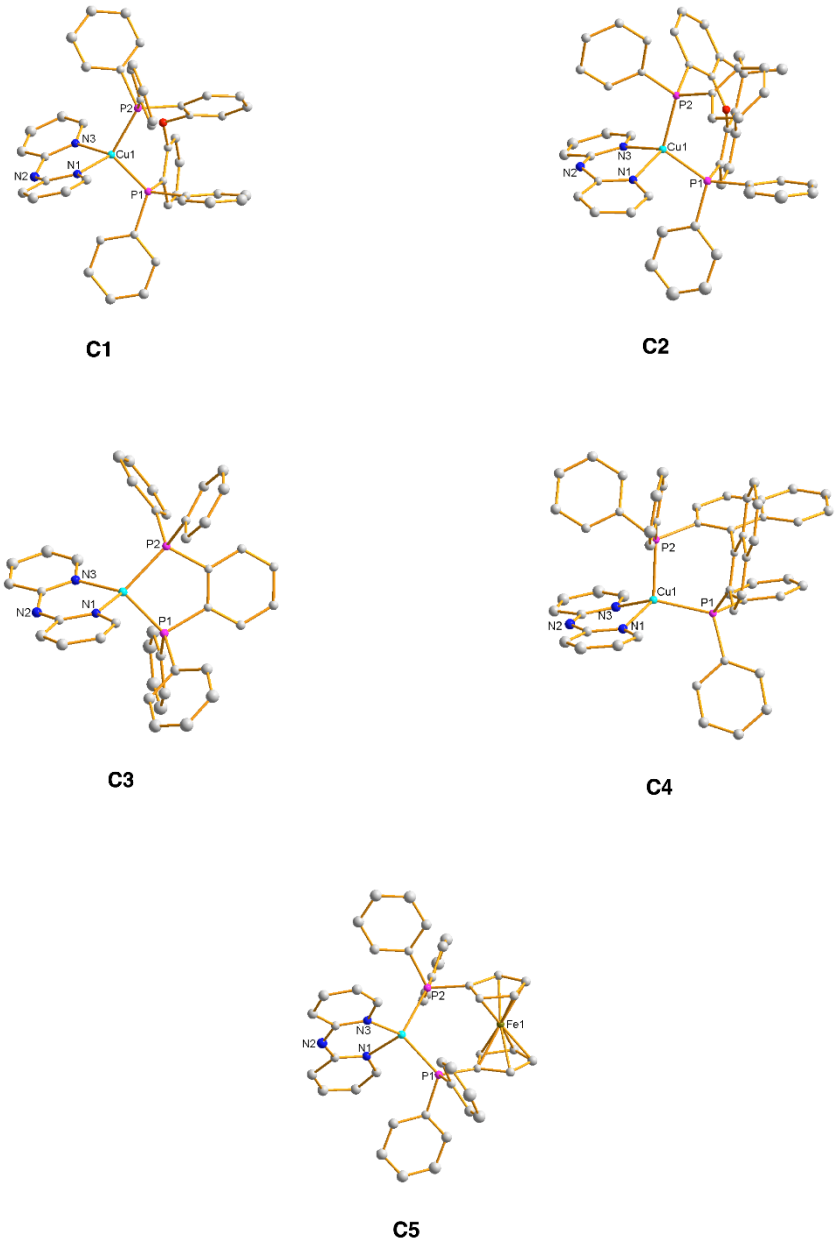

Figure 8. ORTEP plot of complexes **C1-5**, with partial numeration scheme. Hydrogen atoms and counter ion were removed for clarity. Thermal ellipsoids were drawn with 30 % probability.

Table 1. Selected X-Ray analysis data for **C1-5**.

	C1	**C2**	**C3**	**C4**	**C5**
Bond Angle [deg]					
N1–Cu–N3	92.24	92.03	94.04	91.82	92.40
P1–Cu–P2	110.58	115.77	90.93	100.1	110.76
Dihedral Angle [deg]					
N1–Cu–N3/ P1–Cu–P2	89.47	88.69	80.57	82.50	78.38
Bond Length [Å]					
Cu–N1	2.039	2.051	2.018	2.059	2.061
Cu–N3	2.069	2.068	2.025	2.065	2.061
Cu–P1	2.270	2.254	2.249	2.265	2.279
Cu–P2	2.261	2.267	2.249	2.299	2.279
simple geometry index for four-coordinate complexes					
τ_4	1.11	1.08	1.24	1.19	1.11

4.1.3 Electrochemical, photophysical and TD-DFT characterisation

4.1.3.1 Cyclic voltammetry experiments for C1-5

The electrochemical properties of the complexes **C1-5** were measured by cyclic voltammetry (CV) in CH_2Cl_2 as solvent (Table 2, Figure A30). Complexes **C1**, **C2**, and **C4** exhibit one quasi-reversible oxidation process with a half-wave potential at ca 0.60 V vs SCE, attributable to the Cu^{I}/Cu^{II} transition. For **C3**, this process occurs at less positive potentials (0.293 V vs SCE) and is followed by an additional irreversible wave. The lower value for the Cu^{I}/Cu^{II} oxidation can be related to the reduced electron-withdrawing character of the diphosphine dpbz ligand as a consequence of the reduced bite angle imposed by the steric constraints of the ligand (Table 1). In the case of **C5**, a reversible oxidation process is observed at $E_{1/2}$ = 0.88 V vs SCE, followed by an intense and

irreversible wave with a peak potential at 1.57 V vs SCE. As observed for analogous Cu^{I} complexes featuring a dppf ligand,[51] the first process can be assigned to oxidation of the ferrocenyl moiety. In contrast, the irreversible process at more positive potentials can be attributed to the oxidation of the copper metal centre, reflecting the electrostatic repulsion from the charged ferrocenyl moiety.[51] A comparison of the oxidation potentials of **C1-4** with those measured for the complexes reported by Hu and co-workers featuring a phenanthroline-based *N,N* ligand shows that the Cu^{I} oxidation occurs at less positive values.[33] This can be explained considering the influence of the dpa ligand being apparently less electron donating than polypyridine ligands.

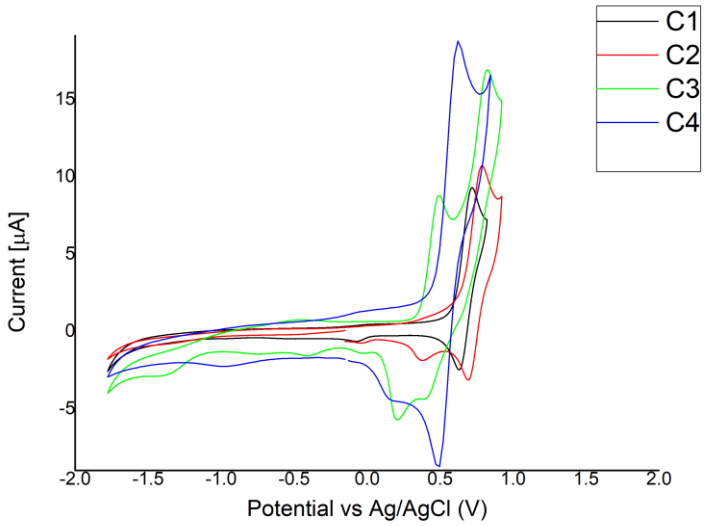

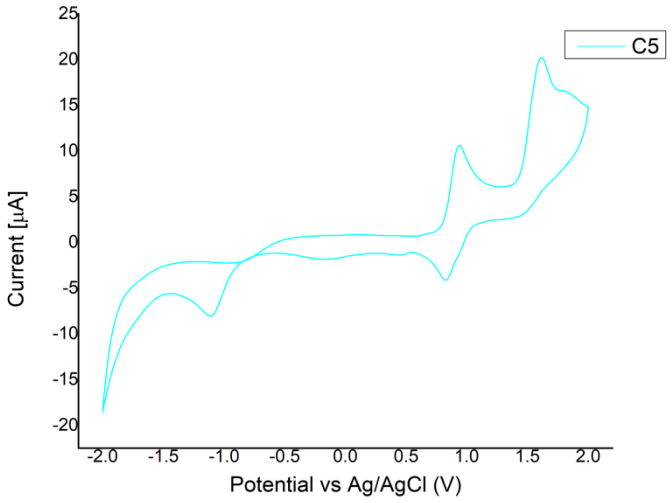

Figure 9. Cyclic voltammogram profiles were recorded in an anhydrous CH_2Cl_2 solution of **C1-5** (1 mM) with 0.1 M $TBAPF_6$ as supporting electrolyte at a scan rate of 0.1 V/s. Three-electrode cell configuration (Pt disc working electrode, saturated Ag/AgCl reference electrode and Pt wire counter electrode). Above **C1-4** and below **C5.**

4.1.3.2 UV-visible experiments for C1-5.

The UV-Visible normalised spectra of the five heteroleptic Cu^{I} complexes in CH_3CN as solvent are depicted in Figure 11. All the complexes showed intense absorption bands in the 200–300 nm region, plausibly attributable to spin-allowed π-π* ligand-centred transitions. Additionally, weak and energetically lowest absorption bands between 300–370 nm are assignable to spin allowed $d_{(Cu)}$-$\pi^*_{(N,N)}$ MLCT transitions involving the dpa ligand. Similar spectral patterns were observed in copper(I) complexes of the type $[Cu(NHC)(dpa)]^+$ reported by Costa's group.[48] Furthermore, **C5** exhibits a weak broader absorption band with a maximum at 440 nm, which can be assigned to Laporte forbidden d-d transitions involving the iron(II) centre of the dppf ligand.

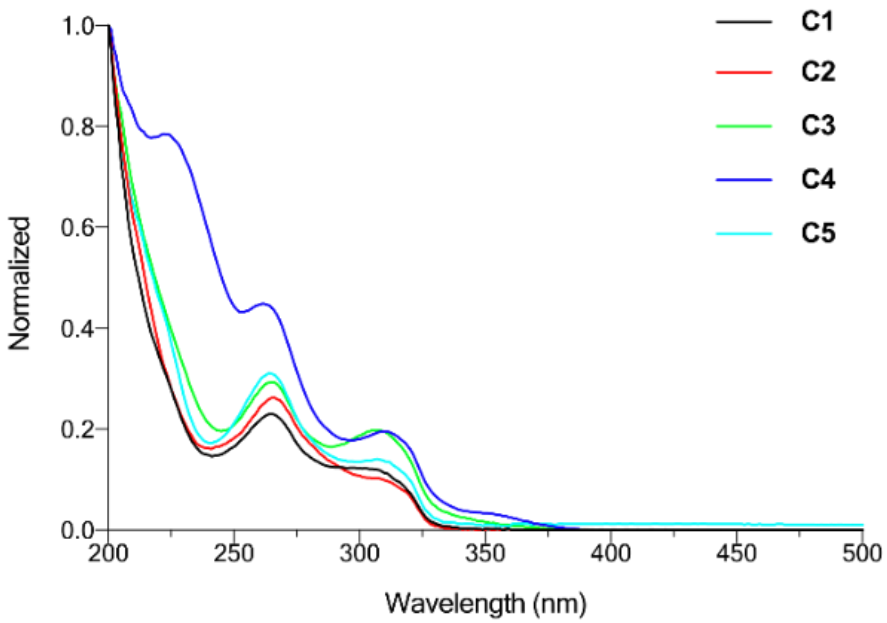

Figure 10. Normalised UV-Visible spectra for **C1-5** in CH_3CN at room temperature.

4.1.3.3 DFT studies for C1-5.

The vertical excited-states properties computed using the TD-DFT framework unveil the origin and the underlying electronic transitions in the complexes **C1-5**. The electronic transitions for **C1**, provided by TD-DFT calculations, are depicted in Figure 11 as a representative example, and the data for complexes **C1-5** are summarised in Table 2 and Table A6. Overall, it can be noted that the highest energy band is mainly dominated by the ligand-centred (LC) π-π* transition of the dpa ligand mixed, to a minor extent, with a ligand-to-ligand charge transfer (LLCT) transition involving the dpa and *P,P* moieties. The weak band at lower energy is mainly characterised by metal-to-ligand charge transfer (MLCT) transition from Cu^{I} to dpa ligand (*cf.* Table 2). However, one exception to this general behaviour is found, specifically, in **C4**. In this case, an additional MLCT band at lower energy is observed, where its character involves a charge transfer from the dpa-Cu^{I} fragment to the *P,P* ligand.

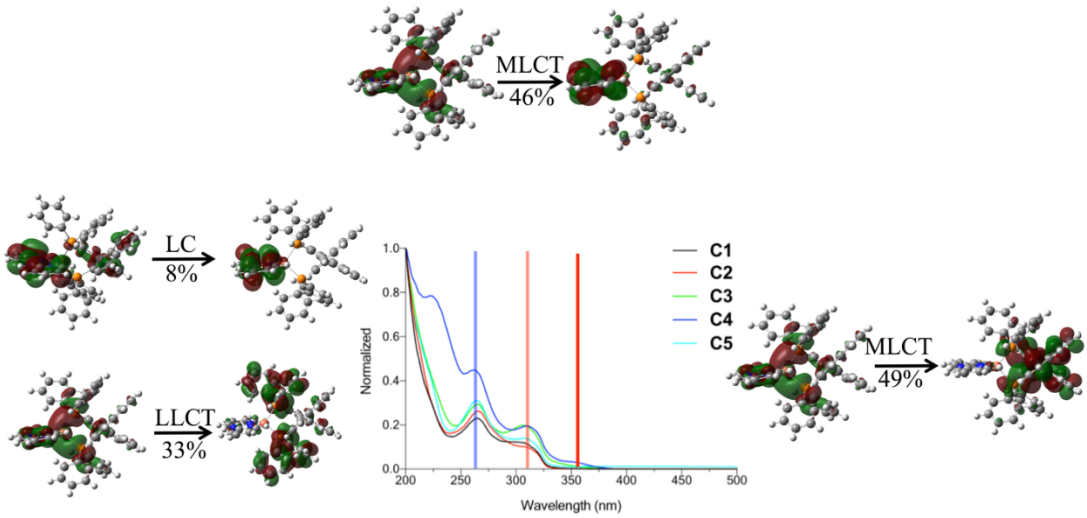

Figure 11. Electronic transitions character for **C4**, obtained by TD-DFT calculations.

Table 2. Summary of CV measurements[a] and TD-DFT data of **C1-5**

Complex	$E_{1/2}$ [V][a]	E [eV]	λ [nm] (Character)	*f*
C1	0.630	4.28 3.46	290 (LC+LLCT) 358 (MLCT, Cu→dpa)	0.0793 0.0526
C2	0.690	4.37 3.50	284 (LLCT) 354 (MLCT, Cu→dpa)	0.0789 0.0509
C3	0.293 0.785 [b]	4.24 3.28	293 (LC) 378 (MLCT, Cu→dpa)	0.1611 0.0456
C4	0.550	4.35 3.56 2.99	285 (LLCT) 348 (MLCT, Cu→dpa) 415 (MLCT, dpaCu→P,P)	0.0912 0.0528 0.0308
C5	0.881 1.575 [b]	4.36 3.58 2.41	284 (LC+LLCT) 354 (MLCT, Cu^{I}→dpa) 513 (d-dπ*)	0.0798 0.0233 0.0005

[a] Cyclic voltammogram profiles recorded in anhydrous CH_2Cl_2 solution of **C1-5** (1 mM) with 0.1 M $TBAPF_6$ as supporting electrolyte at a scan rate of 0.1 V/s. Three-electrode cell configuration (Pt disc working electrode, saturated Ag/AgCl reference electrode and Pt wire counter electrode). $E_{1/2}$ values

referred to SCE. [b] Irreversible wave, peak potential given. E = Electronic transition energy, λ = wavelength, *f* = oscillator strength.

4.1.3.4 Emission experiments for C1-5.

The photoluminescence properties of all complexes were studied in degassed CH_2Cl_2 solution at room temperature and 77 K in a 4:1 ethanol/methanol glassy matrix (Table 3, Figure 12). All complexes **C1-5** exhibit emission in CH_2Cl_2 at room temperature (Figure 12a). Quantum yields of 3.1 % and 1.9 % were measured for **C1** and **C2**, respectively, whereas quantum yields <0.1 % were recorded for the remaining complexes (see Table 3). Lifetimes of 8.6, 7.9, and 20.8 μs were measured for **C1**, **C2**, and **C4**, respectively, while for the other complexes, the lifetimes were below the instrumental resolution (<10 ns). The nature of the emissive state can be discussed in relation to the luminescence spectra measured at 77 K (Figure 12b). Complexes **C1**, **C2**, **C3**, and **C5** show an emission which undergoes a substantial blue shift when recorded in the glassy matrix at 77 K. This can be attributed to the rigidochromic effect exerted by the solid-state matrix and is characteristic of excited states of charge transfer nature. Accordingly, the corresponding luminescence can be attributed to phosphorescence from a triplet MLCT involving a formal Cu^{II} centre and a reduced dpa ligand. However, the appreciably long lifetime observed in **C1-3** at 77 K (hundreds μs, Table 3) strongly suggests that the contribution of a triplet LLCT state cannot be completely ruled out.[52] This attribution agrees with the trend in the energy of the luminescence maxima that reflects the observed trend in the oxidation potential of the Cu^{I} centre. Furthermore, these considerations well comply with the quantum yield and lifetime data measured at room temperature for complexes **C1** and **C2** and the corresponding radiative constants (~$3x10^4$ s^{-1}), whose values are in the order of those found for similar copper(I) complexes.[12] On the other hand, both reduced quantum yields and lifetimes for complexes **C3** and **C5** seem to be characteristic of these types of

complexes and thus correlate with the nature of the *P,P* ligand. For **C3**, the small P–Cu–P angle (~90°) and smaller dihedral angle (see Table 1) very likely promote efficient flattening distortion within the excited state, thus improving non-radiative deactivation routes. On the other hand, in **C5**, the ferrocenyl moiety within the dppf ligand is expected to quench the triplet MLCT excited state via energy transfer.[49,53] This quenching process maintains its intrinsic efficiency in the glassy matrix at 77 K, thus explaining the short lifetime measured for **C5** also under these latter conditions.

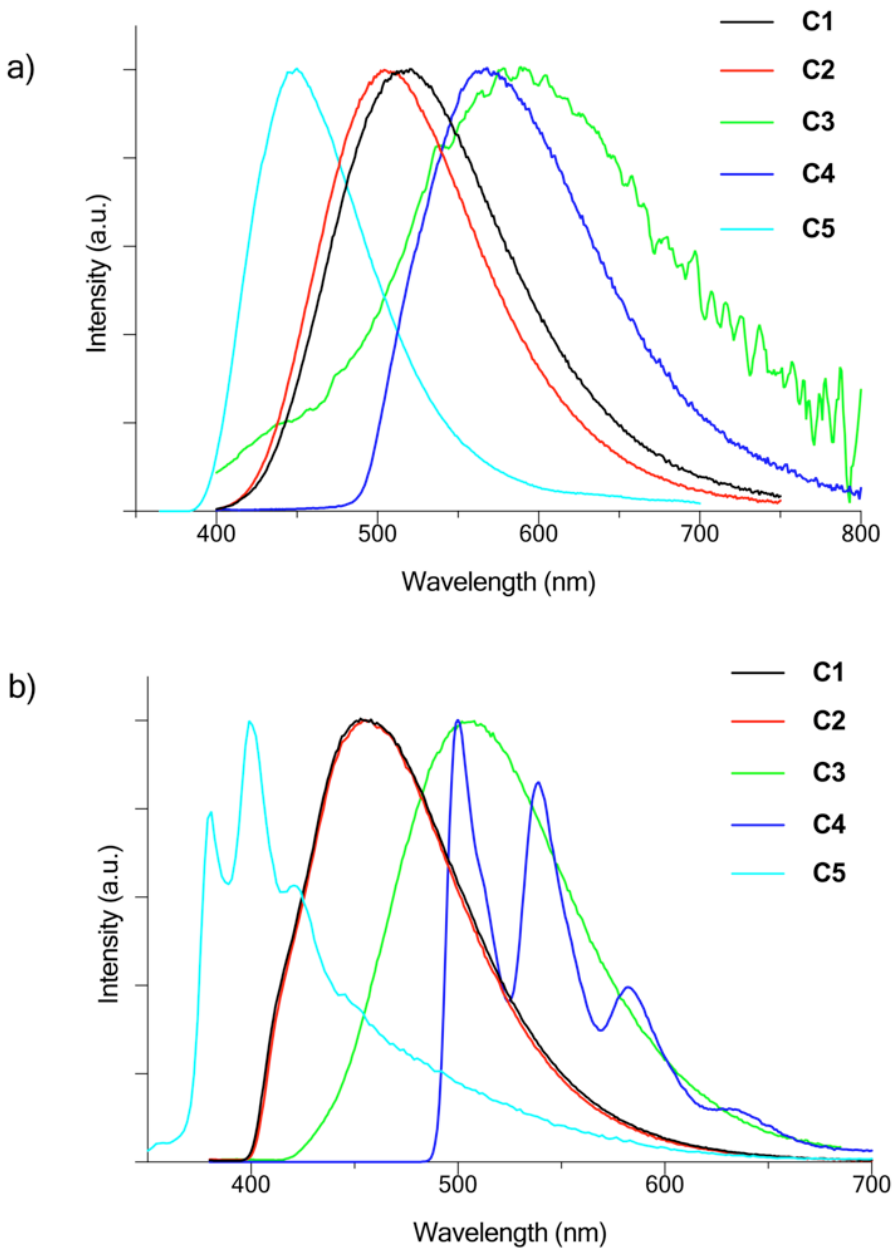

Figure 12. Emission spectra of **C1-5** in a) N_2-purged CH_2Cl_2 at room temperature and b) 4:1 ethanol/methanol glassy matrix at 77 K

The emission of complex **C4** at 77 K occurs at similar energies as observed at room temperature. It displays a structured profile with three distinct maxima suggesting a different character of the emitting excited state with respect to the other Cu^{I} complexes of the series. Interestingly, this phosphorescence is similar to that found for a related $Cu(BINAP)_2^+$ complex[54] and can be assigned to a triplet LC involving the binaphthyl group of the *P*,*P* ligand. The observed long lifetime (15.1 μs), characteristic of spin-forbidden deactivation from LC excited states, is entirely consistent with this attribution. An emitting state of LC character even in CH_2Cl_2 at room temperature well explains the small quantum yield experimentally measured. The latter, combined with the lifetime of 20.8 μs, indeed provides a radiative constant of 43 s^{-1}, which is considerably smaller than that calculated for the triplet MLCT state in complexes **C1** and **C2** (see above) and thus consistent with the different nature of the excited state in **C4** responsible for the observed luminescence.

Table 3. Summary of emissions properties of **C1-5**

	CH_2Cl_2			77 K	
	λ (nm)	Φ (%)	τ (μs)	λ (nm)	τ (μs)
C1	520	3.1 [a]	8.6	453	0.46
C2	504	1.9 [a]	7.9	455	0.41
C3	590	0.08 [b]	- [d]	507	1.6
C4	567	0.09 [b]	20.8	500,539,581,634	15.1
C5	449	0.02 [c]	- [d]	380, 399, 420	- [d]

[a] using fluoresceine in 0.1 M NaOH (Φ = 0.94) as the standard. [b] using $Ru(bpy)_3^{2+}$ in H_2O (air-equilibrated, Φ = 0.028) as the standard. [c] using quinine sulfate in 0.05 M H_2SO_4 (Φ = 0.53) as the standard. [d] below the detection limit of the laser flash photolysis (ca 10 ns).

4.1.4. Photocatalytic studies for C1-5

4.1.4.1 Test reaction for C1-5

ATRA test reaction between styrene and CBr_4 was chosen as the model reaction to study the photocatalytic activity of the synthesised complexes (Table 4). Notably, the desired product is not obtained by omitting the catalyst (Table 4, entry 1). Established Cu-photocatalysts like $[Cu(dap)_2]Cl$ or $[Cu(dmp)(rac\text{-}BINAP)]PF_6$ are capable of delivering **5** in good to excellent yields (Table 4, entries 2-3).[15,55] Hence, we subjected the complexes **C1-5** to the reaction (entries 4-8), which revealed that **C4** was indeed a competent catalyst in the title reaction, giving rise to **5** in an excellent yield of 99 % (Table 4, entry 7). In line with the observed electrochemical and photophysical properties (Tables 2 and 3), the improved activity of complex **C4** is associated with S-BINAP as the *P,P* ancillary ligand, which confers rigidity to the complex. As a consequence, a long excited-state lifetime arises, which seems to be pivotal in favouring enhanced photocatalytic activity via bimolecular routes. No asymmetric induction in **5** was observed, suggesting that the introduction of the CBr_3 group into the product does not benefit from the chiral nature of catalyst **C4**.

Table 4. ATRA test reaction evaluation using **C1-5**[a]

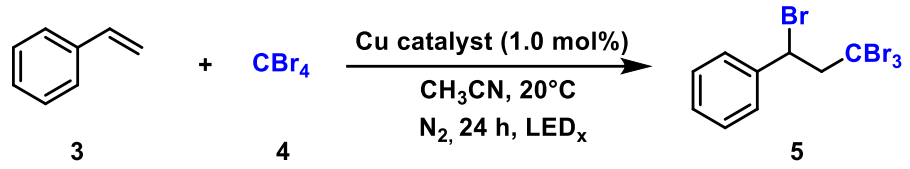

3 4 5

Entry	Catalyst	LED_x	Yield % [b]
1	without	455	n.r
2	$[Cu(dap)_2]Cl$	530	99
3	$[Cu(cup)(rac\text{-}BINAP)]PF_6$	455	71
4	$[Cu(dpa)(POP)]BF_4$ (**C1**)	455	37
5	$[Cu(dpa)(XantPhos)]BF_4$ (**C2**)	455	15
6	$[Cu(dpa)(dpbz)]BF_4$ (**C3**)	455	51
7	$[Cu(dpa)(S\text{-}BINAP)]BF_4$ (**C4**)	455	99
8	$[Cu(dpa)(dppf)]BF_4$ (**C5**)	455	15

[a] styrene (0.5 mmol, 1.0 equiv), CBr_4 (0.5 mmol, 1.0 equiv), catalyst (1.0 mol%) in CH_3CN (dry, degassed, 3 mL); Irradiation at X nm (LED) under N_2 atmosphere for 24 h at 20 °C. [b] ^{1}H-NMR Yield was determined using 1,3,5-trimethoxybenzene as an internal standard.

4.1.4.2 Substrate scope for C4 using test reaction.

Several olefin derivatives were used to study and expand the scope of products obtained by the **C4** complex

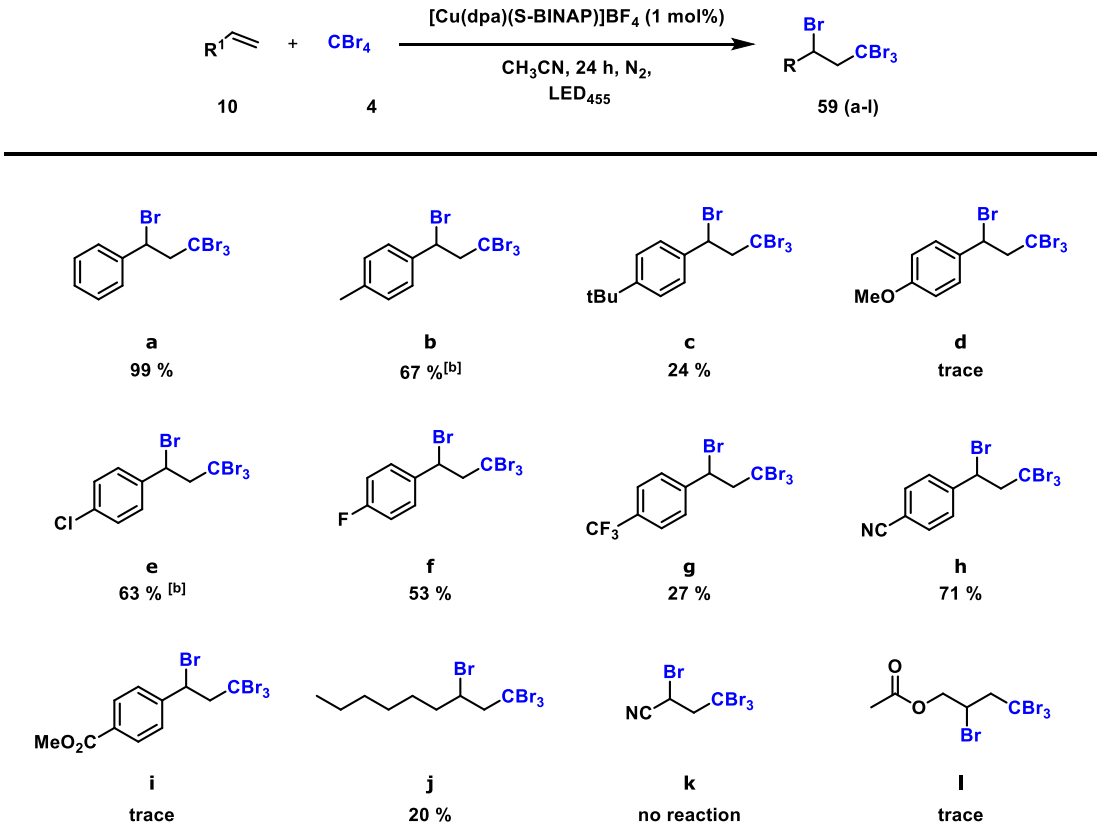

Scheme 10. Scope of the reaction ATRA test using [Cu(dpa)(S-BINAP)]BF_4 [a]. [a] styrene (0.5 mmol, 1.0 equiv), CBr_4 (0.5 mmol, 1.0 equiv), catalyst (1.0 mol%) in CH_3CN (dry, degassed, 3 mL); Irradiation at 455 nm (LED) under N_2 atmosphere for 24 h at 20 °C. [b] 1.0 equivalent of pyridine 2,6-lutidine was used.

[Cu(dpa)(S-BINAP)]BF_4 can achieve the desired product in different olefins with yields ranging from 20 % - 99 %, and electron donor and electro-withdrawing functional groups were used. When the aromatic ring is substituted

with an alkyl group in the *para* position, the yield drops from 99 % (**59a**) to 67 % and 24 % (**59b-c**). On the other hand, for a system substituted with a donor group such as OMe, traces of **d** were observed, and the polymerisation product was found, similar to that reported by Itoh's group.[55] Otherwise, when the system is substituted with halogens such as Cl or F (**59e-f**), the product is obtained in good yield, 71 % and 68 %, respectively. On the other hand, when the system is substituted with a deficient group of electrons like CF_3 (**59g**), and CN (**59h**), the product can be obtained in 34 % and 71 %. However, when a $COOCH_3$ (**59i**) group is used, only traces of the product are observed, in addition to the starting material. For unactivated olefins, such as 1-octene, the desired product was obtained in a low yield of 20 %. Moreover, in order to study the tolerance to functional groups, acrylonitrile and allyl acetate were used; unfortunately, the desired products were not obtained; the reaction crude show starting material and traces for **59k** and **59l**, respectively.

4.1.4.3 Chlorosulfonylation reaction of styrene evaluation using C1-5.

The reported chlorosulfonylation reaction was evaluated using **C1-5** (Table 4). Significantly, the desired product **61** is not obtained by skipping the catalyst (entry 1). The complexes **C1-5** were evaluated, and the results are showed from entries 2 to 6**. C4** exhibits a significant difference among the other photocatalyst giving the product **61** in 93 % yield (entry 5). The catalyst loading was evaluated (entries 5, 7-8), and the yield decreases slightly when the load is reduced by 0.5, but when it goes to 1.0 mol %, the yield falls by 30 %, being 2.5 mol% the optimal load. Additionally, it is observed that each ligand separately (dpa and S-BINAP) and the copper precursor do not give the desired product (entries 10-12).

Table 5. Control parameters of **C1-5** in chlorosulfonylation reaction of styrene.[a]

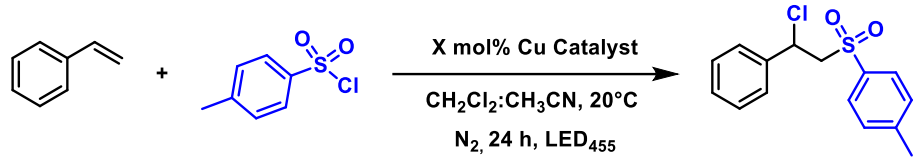

3 60 61

Entry	Catalyst	X	Yield % [b]
1	without	-	n.r
2	[Cu(dpa)(POP)]BF_4 (**C1**)	2.5	10
3	[Cu(dpa)(XantPhos)]BF_4 (**C2**)	2.5	n.r.
4	[Cu(dpa)(dpbz)]BF_4 (**C3**)	2.5	n.r.
5	[Cu(dpa)(S-BINAP)]BF_4 (**C4**)	2.5	93[c]
6	[Cu(dpa)(dppf)]BF_4 (**C5**)	2.5	32
7	[Cu(dpa)(S-BINAP)]BF_4 (**C4**)	2.0	90
8	[Cu(dpa)(S-BINAP)]BF_4 (**C4**)	1.0	60
10	dpa	2.5	n.r.
11	S-BINAP	2.5	n.r.
12	[Cu(CH_3CN)$_4$]BF_4	2.5	n.r.

[a] styrene (0.5 mmol, 1.0 equiv), TsCl (0.5 mmol, 1.0 equiv), catalyst (X mol%) in CH_3CN (dry, degassed, 3 mL); Irradiation at 455 nm (LED) under N_2 atmosphere for 24 h at 20 °C. [b] ^{1}H-NMR Yield was determined using 1,3,5-trimethoxybenzene as an internal standard. [c] isolated yield.

4.1.4.4 Chlorosulfonylation reaction over alkynes using C4.

Remarkably, , the selective formation of the *E* isomer is observed in good yields for chlorosulfonylation reaction over alkynes, contrasting $[Cu(dap)_2]Cl$ which produces *E/Z* mixtures of products.[21] It is assumed that Cu(*N,N*)(*P,P*)$^+$ complexes are able to promote an additional energy transfer pathway to convert the *Z* product to the corresponding *E* isomer in a photoisomerization process, which is in accordance to a recent report by Collin *et al*.[37] It is possible to observe moderate yields when the tosyl contains donor or electron-withdrawing group as substituent.

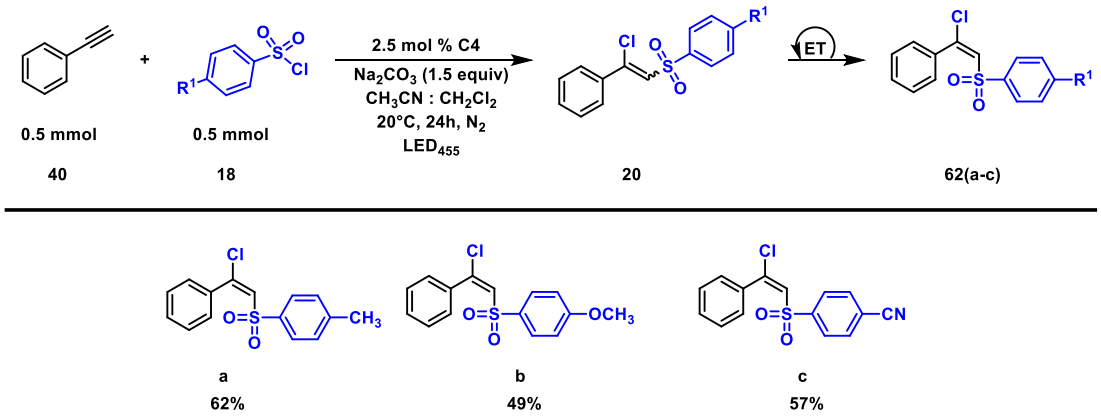

Scheme 11. Examples of tandem ATRA/photoisomerization using **C4**.

4.1.4.4 Gram scale experiments of C4 in ATRA reactions.

ATRA–test and chlorosulfonylation reaction were scaled by a factor of 10, $[Cu(dpa)(S\text{-}BINAP)]BF_4$ complex showed high viability to scaling processes with only a slight decrease in reaction yield.

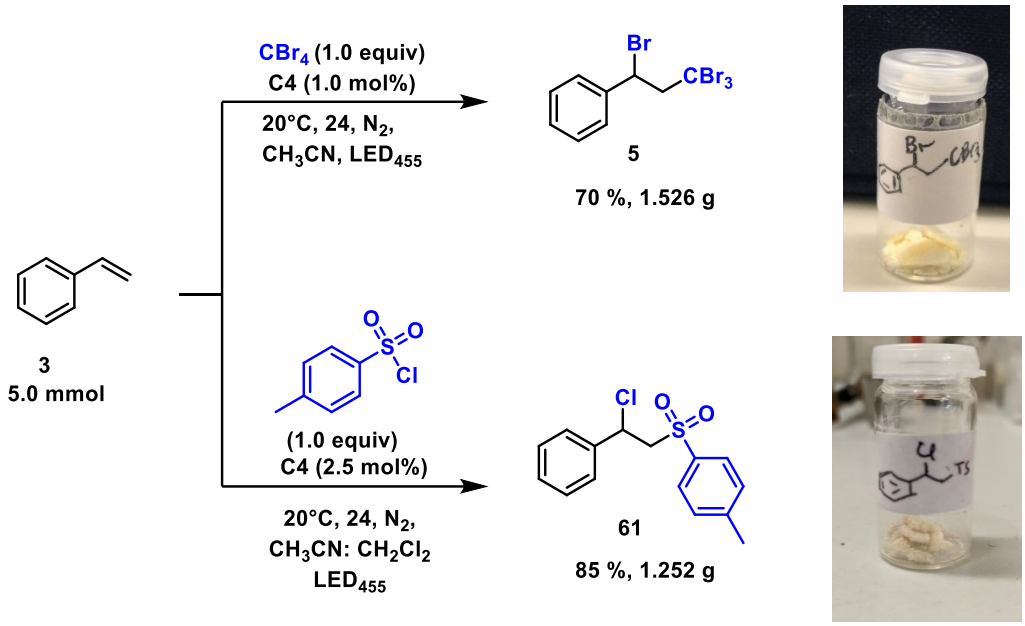

Scheme 12. Gram scale experiments for ATRA-test and chlorosulfonylation reaction over styrene.

4.1.4.5 C4 in other photoreactions.

4.1.4.5.1 Appel-type reaction mediated by light.

Visible-light Appel-type reaction was chosen as an example of a SET process. **C4** was moderately effective in this reaction yielding the desired product in 56 %, which constituted a higher yield compared to $[Cu(dap)_2]Cl$ (40%).[41]

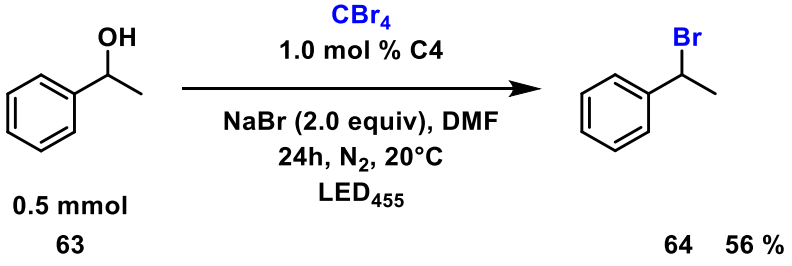

Scheme 13. Appel-type reaction using **C4**

4.1.4.5.2 Decarboxylative coupling reaction.

Several groups have used *N*-(acyloxy)phthalimide derivatives as a radical source in carbon-carbon bond-forming processes.[56] Indeed, **C4** achieved the decarboxylative fragmentation of **33** and subsequent coupling with **34** to access C_{sp3}-C_{sp} coupling product **35** in 52 % compared to other heteroleptic Cu^{I} photocatalysts reported by Collins in 2018.[32]

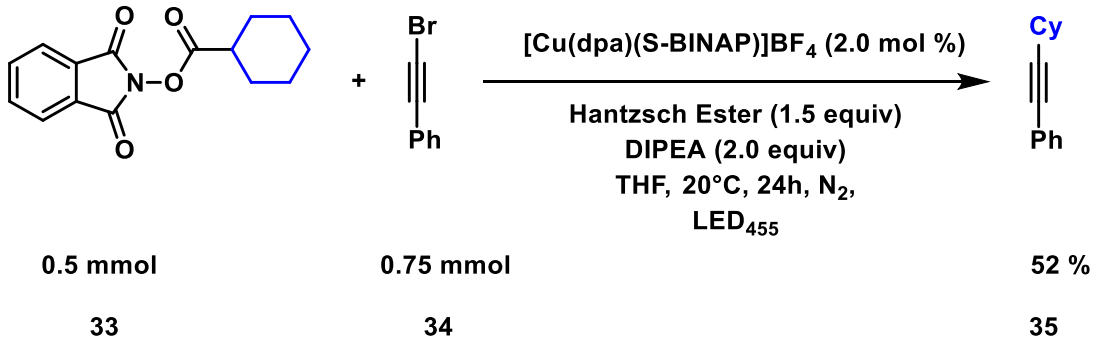

Scheme 14. Decarboxylative coupling reaction using **C4**.

4.1.4.5.3 Photochemical pinacol type coupling reaction.

To study **C4** photocatalyst in PCET-type reactions, we have used the photochemical pinacol type coupling reaction reported by Collins; the authors report a 92 % yield for the [Cu(dq)(S-BINAP)]BF_4 complex when dppa is used as an additive. They also mentioned the importance of N-H free bonds to modulate the pka.[40] As our dpa ligand has a free N-H bond, we thought it could be effective in this reaction. However, the expected product was not observed (Scheme 15).

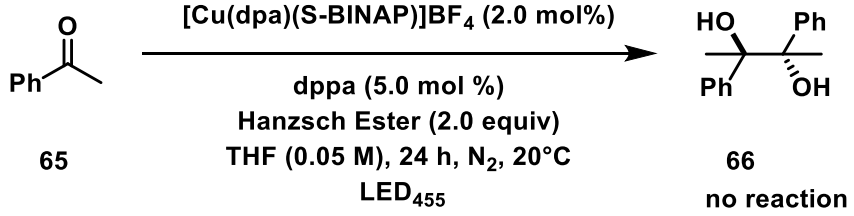

Scheme 15. Pinacol coupling reaction using **C4**.

4.2 Modifications in dpa ligand

Dpa ligand can be synthesised from cheap and available starting materials such as bromine pyridine and amino pyridine. It is possible to find different synthetic routes, for example, via the Buchwald-Hartwig reaction using a palladium catalyst ($Pd(dba)_3$) heating in DMF (i, Scheme 16)[57]. Alternatively, dpa synthesis has been reported by a one-pot aromatic nucleophilic substitution reaction under reflux for 24 hours, obtaining the desired product in 51 % yield.[58] To generate cheap synthetic pathways, we decided to remove the palladium catalyst and improve the second condition (ii, Scheme 16). Dpa ligand was obtained in 81 % yield, using 2-fluoropyridine instead of 2-bromopyridine. The first step is the deprotonation of 2-aminopyridine with NaH followed by addition of 2-fluorine pyridine; this small change allows the reaction to proceed in 4 hours without heating (iii, Scheme 16).

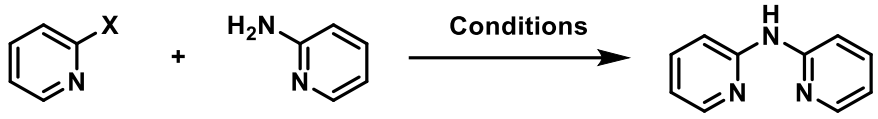

67 **68** **57**

Conditions

i) $Pd(dba)_3$, S-BINAP, DMF, reflux (Buchwald-Hartwig reaction) 90 % Yield
ii) NaH, Toluene, 24 h, reflux; X = Br 51 % Yield
iii) Our conditions; 4 h, NaH, X = F, 25°C, 81 % Yield

Scheme 16. Summary of synthetic routes to obtain dpa ligand.

4.2.1 Nucleophilic aromatic substitution pathway.

In order to obtain a symmetrically substituted dpa derivative, the reaction condition optimisation was carried out using 2-aminopyridine and 2-

fluoropyridine derivatives, positions 5 or 6 of pyridine ring contain a phenyl group substituted in position *para* with a donor and electron-withdrawing group such as OCH_3 and CF_3, respectively.

Table 6. Summary of experiments to obtain dpa derivatives. [a]

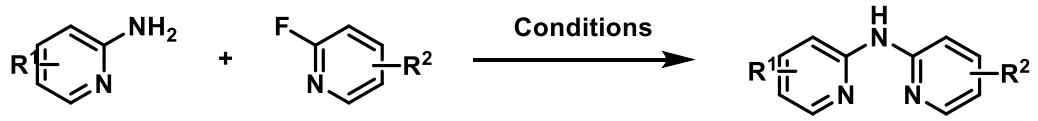

69 **70** **71**

Entry	Pyridine position	R_1	R_2	Heating mode	Base	Solvent	Time (h)	Yield (%)
1	5	*p*-Ar-OMe	*p*-Ar-OMe	r.t	NaH	Toluene	24	n.r.
2	5	*p*-Ar-OMe	*p*-Ar-OMe	r.t to reflux	NaH	Toluene	24	n.r.
3	5	*p*-Ar-OMe	*p*-Ar-CF_3	r.t to reflux	NaH	Toluene	144 h	n.r.
4	5	*p*-Ar-OMe	*p*-Ar-OMe	r.t to reflux	n-Buli	DMF	24	n.r.
5	5	*p*-Ar-OMe	*p*-Ar-OMe	r.t to reflux	KH	THF	24	n.r.
6	5	*p*-Ar-CF_3	*p*-Ar-CF_3	r.t. to reflux	n-Buli	DMF	24	n.r.
7	5	*p*-Ar-CF_3	*p*-Ar-CF_3	Mw	K_2CO_3	DMF	1	n.r.
8	5	*p*-Ar-CF_3	*p*-Ar-CF_3	Mw	K_2CO_3	DMF	2	n.r.
9	6	*p*-Ar-OMe	*p*-Ar-OMe	Mw	K_2CO_3	DMF	1	n.r.

10	6	*p*-Ar-CF_3	*p*-Ar-CF_3	Mw	NaH	DMF	1	n.r

[a] See methodology section for more details about experimental procedures.

Table 6 summarises the conditions used to synthesise the dpa ligand derivatives using the coupling partners: **69** and **70**. The reaction conditions for obtaining the dpa ligand were used at room temperature and under reflux, but the coupling product was not observed (entries 1-2). To favour the aromatic nucleophilic substitution reaction, the coupling partners were different. The nucleophilic reagent (amino pyridine) was used with the donor group (OMe), and the electrophilic ring (fluoropyridine) was with the CF_3 group, but the asymmetric ligand was not observed (entry 3). Different parameters were changed, such as solvent, bases and substitution position in the phenyl ring. Nevertheless, none of these modifications allowed the obtention of the ligand derivative (entries 4-6). Additionally, microwave-assisted (Mw) reactions were attempted, changing variables such as the ring's substitution, time, and different bases. Despite all attempts, it was not possible to obtain the expected derivatives.

4.2.2 Buchwald Hartwig coupling

Costa´s group has used the Buchwald Hartwig reaction conditions to generate different modifications in the dpa ligand, reporting yields from 31 % to 99 % [48,59]. The yield strongly depends on the substitution in the pyridine ring; this is a reaction based on the cross-coupling between an alkyl halide and an amino group using a palladium catalyst. Based on this report, we use similar conditions for our purpose. However, the reaction of our 5- and 6-substituted pyridine derivatives with phenyl groups with donor groups were not successful (Scheme 17). Due to the extensive studies carried out and the lack of success, we decided not to pursue the synthesis of these ligands.

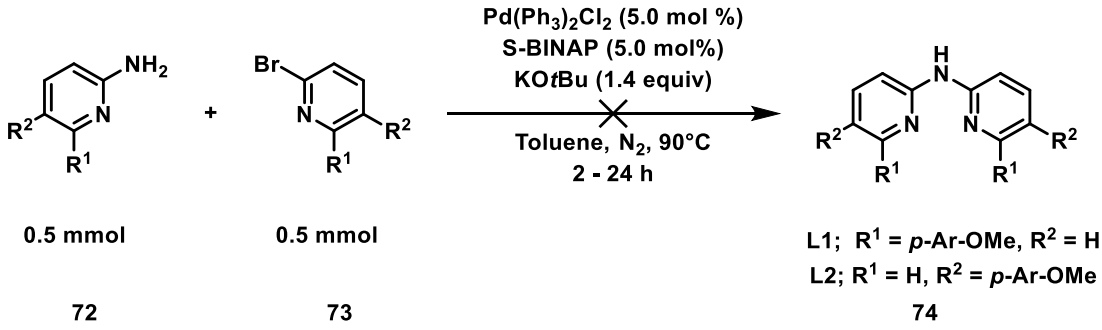

Scheme 17. Synthetic route to obtain dpa derivative ligands using Buchwald Hartwig conditions.

5.2 Copper (II) complexes in photocatalysis – Structure & reactivity relationship.

5.2.1 Synthesis and characterisation of C6-12

Seven Cu^{II} complexes of the type $[Cu(N,N)_2Cl]Cl$ were synthesised in one step following a methodology reported in the literature (Scheme 18). The structure of the copper (II) complexes is versatile, depending on the reaction conditions. We performed the synthesis using a 2:1 ratio of ligand and $CuCl_2$ in ethanol. The synthetic route led to a pentacoordinated complex, coordinated by two bipyridine derivatives and chloride ligands. Due to the paramagnetic nature of the complexes, the first characterisation analysis was by mass spectroscopy.

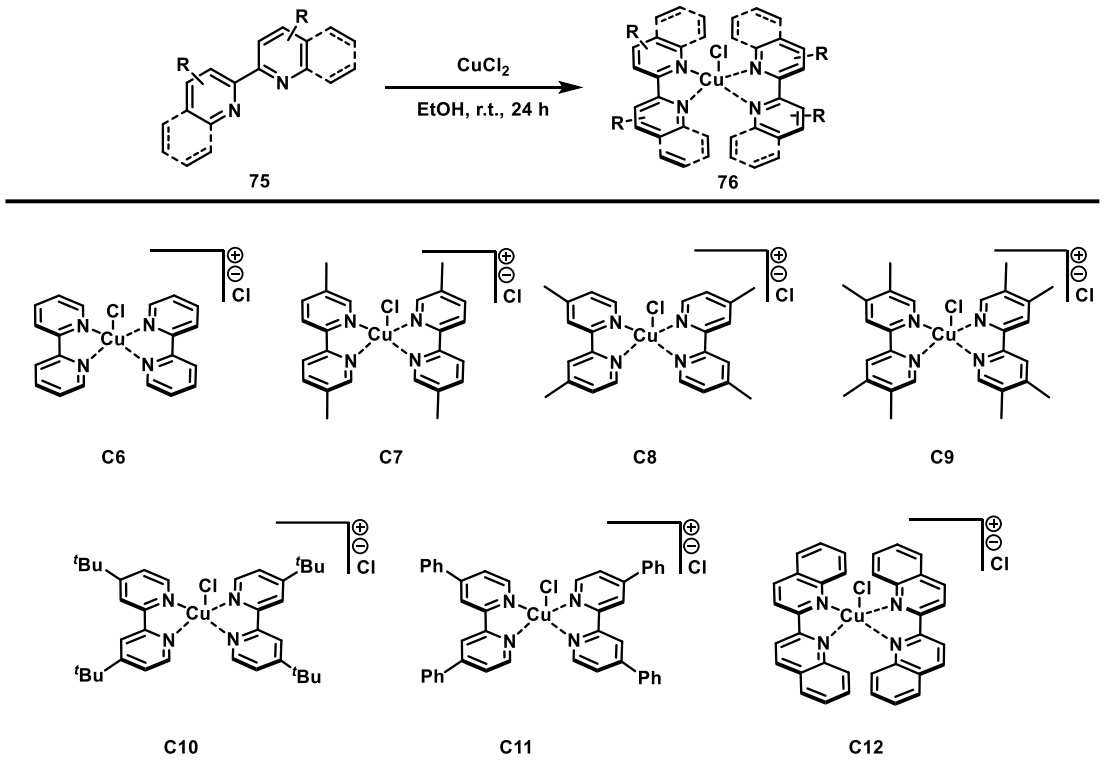

Scheme 18. Synthetic route to obtain Cu^{II} complexes **C6-12** using bypirdine derivatives ligands.

5.2.2 Uv-visible for C6-12

The UV-Visible normalised spectra of the seven Cu^{II} complexes in CH_3CN as solvent are depicted in Figure 13. All the complexes showed strong absorption bands in the 200–350 nm region, attributable to spin-allowed π-π* ligand-centred transitions of the N heterocyclic rings. Concerning the d-d band, it is a forbidden band of low absorbency, and it cannot be appreciated due to the low concentration of the sample.

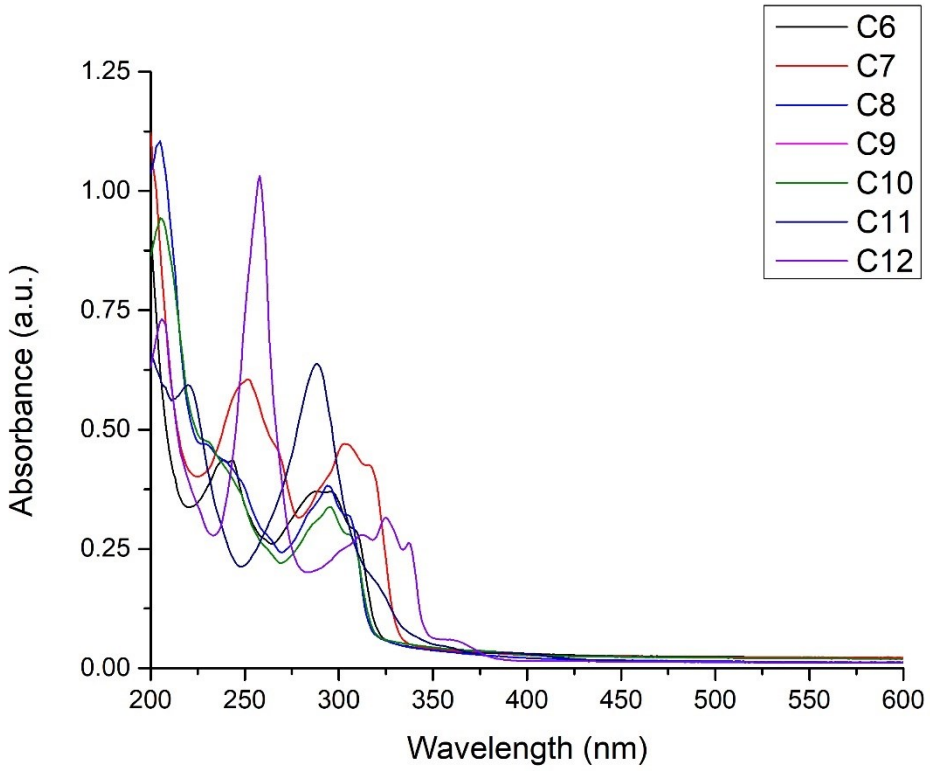

Figure 13. UV-Visible normalised spectra for **C6-12**

5.2.3 Photocatalytic studies for C6-12

The reported oxo-azidation reaction was evaluated using **C6-12** (Table 7) to compare the structure-reactivity relationship of copper two complexes with ligands derived from bipyridine. We exposed our complexes to the same reaction conditions used for the Cu(dap)Cl_2 complex, which delivered the expected product in 72 % yield and benzaldehyde as a byproduct in 21 % yield (entry 1). Overall, **C6-12** does not overcome this performance; the **C7-10** complexes obtained the product with an average of 55 % yield (entry 3-6). The copper (II) complex with bipyridine ligand substituted with phenyl groups (**C11**) does not work for this reaction (entry 7). On the other hand, the complex with the bisisoquinoline ligand (**C12**) gives a more significant proportion of the by-product, and it is possible to see in the crude NMR remaining styrene (entry 8).

Table 7. Oxo-azidation reaction evaluation using **C6-12**[a].

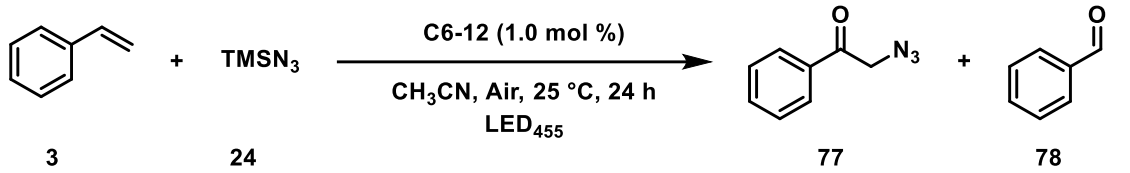

Entry	Photocatalyst	**77**[b]	**78**[b]
1	$Cu(dap)Cl_2$[23]	72 %	21 %
2	**C6**	34 %	15 %
3	**C7**	54 %	3 %
4	**C8**	53 %	20 %
5	**C9**	55 %	4 %
6	**C10**	56 %	4 %
7	**C11**	n.r.	n.r.
8	**C12**	8 %	16 %

[a] styrene (0.5 mmol, 1.0 equiv), $TMSN_3$ (1.0 mmol, 2.0 equiv), catalyst (1.0 mol %) in CH_3CN (2.0 mL); Irradiation at 455 nm (LED) under air atmosphere for 24 h at 25 °C. [b] ^{1}H-NMR Yield was determined using 1,1,2,2-tetrachloroethane as an internal standard.

We again used the reported chlorosulfonalytion reaction over styrene to evaluate **C6-12** complexes (Table 8). To compare, we have taken $[Cu(dmp)_2Cl]Cl$, which has excellent results in ATRA-type reactions and has served as an alternative to the $[Cu(dap)_2]Cl$ complex in terms of low cost. Bipyridine derivatives ligands in copper two complexes are not a good alternative in terms of efficiency. **C6-12** complexes do not exceed the reported yield of 92 % (entry 1). The highest yield is obtained for **C9** with 45 % (entry 5), when the bipyridine ligand is substituted with two methyl groups. All the reactions were carried out for 24 h, and in the crude NMR it is possible to find styrene, which indicates that **C6-12** required a longer reaction time.

Table 8. Control parameters of **C6-12** in chlorosulfonalytion reaction of styrene.[a]

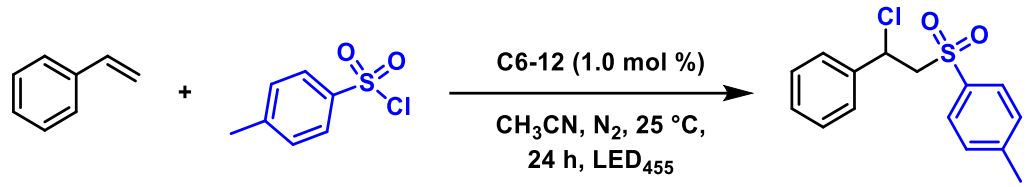

3 **60** **61**

Entry	Photocatalysts	Yield % [b]
1	$[Cu(dmp)_2Cl]Cl$[41]	92 %
2	**C6**	30 %
3	**C7**	36 %
4	**C8**	23 %
5	**C9**	45 %
6	**C10**	17 %.
7	**C11**	n.r.
8	**C12**	6 %

[a] styrene (0.5 mmol, 1.0 equiv), TsCl (0.5 mmol, 1.0 equiv), catalyst (1.0 mol %) in CH_3CN (dry, degassed, 3 mL); Irradiation at 455 nm (LED) under N_2 atmosphere for 24 h at 25 °C. [b] ^{1}H-NMR Yield was determined using 1,1,2,2-tetrachloroethane as an internal standard.

CHAPTER II – COPPER-PHOTOCATALYSED C_{SP^3}-C_{SP} COUPLING

6. INTRODUCTION – CHAPTER II

6.1 Alkynyl-containing drugs

Alkynes are common structural motifs in a wide range of natural products, bioactive molecules, and organic materials. The use of a carbon-carbon triple bond in a drug molecule has been explored in terms of benefits such as biological activity, improved solubility and bioavailability properties, and metabolic stability. These characteristics have been demonstrated in molecules such as ethinylestradiol (hormone drug for estrogen medication), efavirenz (an antiretroviral drug for HIV/AIDS), dynemicin A (an antitumor drug for cancer) and alfaprostol (a veterinary drug for breeding control) (Figure 13).[60] In addition, this group is considered versatile as an intermediate because it can be synthetically modified through different chemical transformations.

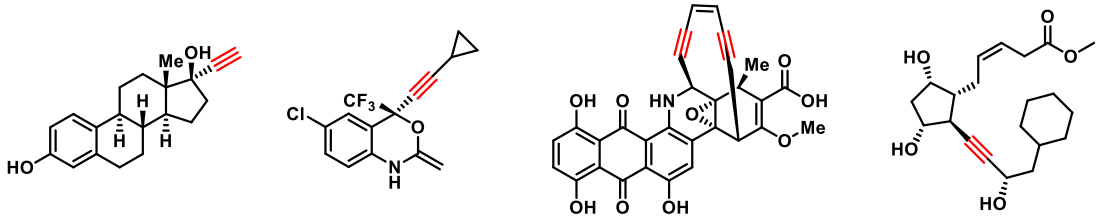

ethynylestradiol 79 | **efavirenz** 80 | **dynemicin A** 81 | **alfaprostol** 82

Figure 14. Representative alkynyl-containing drugs.

Sonogashira coupling has been best known for Csp^3-Csp bond formation. This kind of bond construction has drawn academic attention to contribute to the development of alkyne synthesis to increase the organic toolbox. Numerous methodologies have been designed generally based on the use of metal-dependent reactions, from reactions using organometallic reagents to transition metals such as Pd, Cu, Co, Ni, Fe, Ru, Ir, and Ag. On the other hand,

non-dependent metal methods have been developed quite successfully, using thermal conditions, oxidising agents, or light-induced reactions. [61]

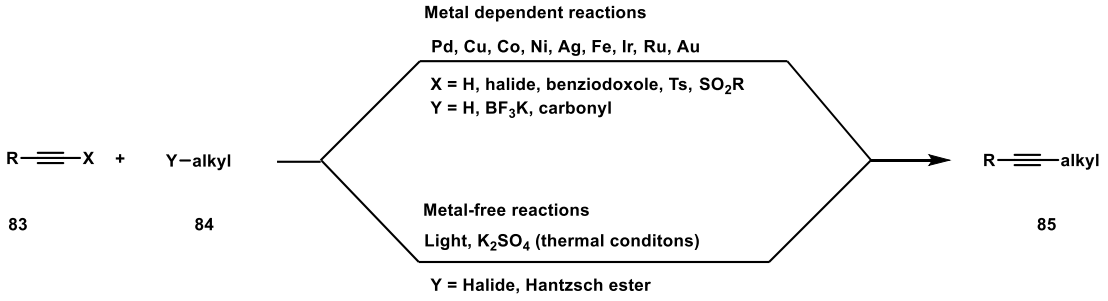

Figure 15. Summary for C-C coupling through metal-dependent and metal-free reactions.

6.2 Photoinduced C-C coupling reaction mediated by copper catalysis

N-phthalimides ester derivatives as precursors of alkyl radicals have shown significant advantages for the formation of the C-C bond.[56] Yi Pan's group describes a decarboxylative cross-coupling method to produce substituted alkynes from various carboxylic acids using a mixture of CuCl and $Cu(acac)_2$ (acac = acetylacetonate) copper catalysts via photoexcitation. Furthermore, the use of DFT calculations revealed that the favourable reaction pathway is via the bidentate acetylacetonate ligand and copper coordination; these intermediate plays an essential role in the inhibition of homo-coupling of the alkyne (Figure 16A).[62] On the other hand, (bromoethynyl)benzene has served as model substrate for photocoupling reaction to evaluate heteroleptic copper(I) complexes and copper (II) complexes,[32,41,63] in these cases, it has not been demonstrated in detail the mechanism, but apparently, it should be similar to the one described previously.

Hwang's group has contributed to the literature with reactions using the Cu^{II}-acetylide complex under an oxygen atmosphere and blue irradiation.[64–70] Moreover, he has recognised the Cu^{I}-acetylide complex as an effective photoreductant (E_{red} = 2.05 V vs SCE, for copper Cu^{I}-phenylacetylene in acetonitrile). In 2012, they achieved a photoinitiated Sonogashira reaction using aryl halides (bromides and iodides) and aryl- or alkylacetylenes. Using CuCl, Cu^{I}-acetylide is formed in situ, and an intermediate is formed through a charge interaction between the aryl halide group and the photoactive copper complex (Figure 16B).[71] Six years later, Lalic's group modified this methodology and expanded it to alkyl iodides and terminal alkynes; the authors identified the essential use of the terpyridine-derived ligand to avoid the homocoupling product and polymerisation of the starting material. Successfully, they achieved the desired coupling product with yields up to 90 % (Figure 16C).[72]

In the year 2022, Yang and co-workers synthesised a new heteroleptic copper type [Cu(BINAP)(tpy)]Cl ($E_{1/2}$ (Cu^{II}/Cu^{I*})= -3.14 V vs AgCl) and used it as a photocatalyst in Sonogashira coupling reactions mediated by blue light. They introduced a new strategy in the synthesis to form triple bonds; as a radical supplier, they use a wide range of sulfonium salts which can be easily prepared from commercially available and inexpensive thiols, alcohols, and alkyl halides. They obtained the expected coupling product through a desulphurisation process, and they proposed that the radical is generated after reduction using [Cu(BINAP)(tpy)]Cl, which is satisfactorily powerful in reducing the sulfonium salt (E_p = −2.23 V vs Ag/AgCl) depicted in Figure 16D. Nevertheless, the mechanism proposed by Yang shows that the photoactive specie is the complex CuL1L2-phenylacetylene, L1= BINAP and L2 = tpy, formed in situ. [73]

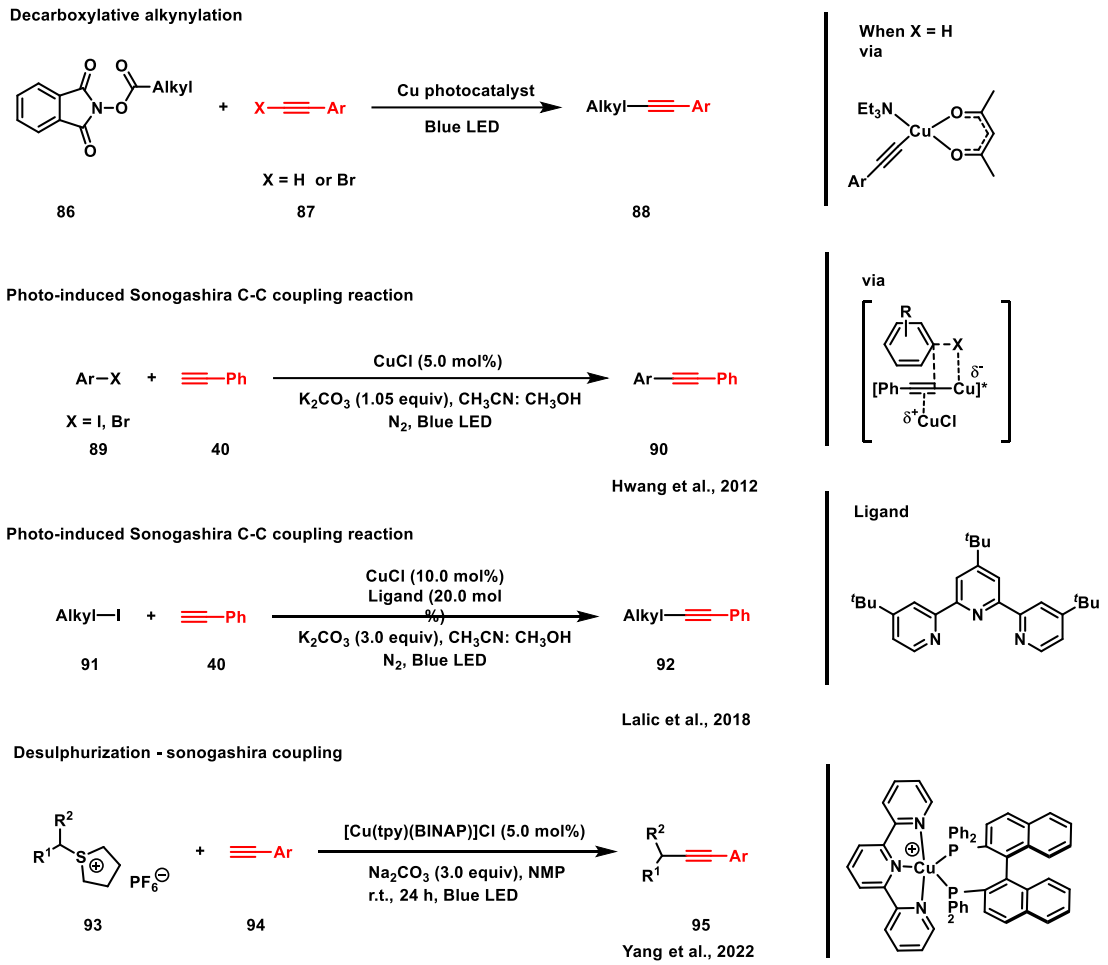

Figure 16. Selected examples for photoinduced C-C coupling reaction mediated by copper catalysis.

6.3 Photoinduced Csp^3-Csp coupling multicomponent reactions mediated by copper catalysis

Xiao and co-workers developed a procedure to catalysed a three-component radical cross-coupling of cycloketone oxime esters, alkenes, and terminal alkynes to obtain cyanoalkyl-containing propargyl compounds. Single electron transfer reduction of an oxime ester can be challenging due to its reduction potential (E_{red} = −2.18 V vs SCE in DMF). The authors explain that dtbbpy ligand can improve the reaction due to the boost in the reduction potential of

Cu^{I}-phenylacetylene from E_{red} = -0.89 V vs SCE to E_{red} = -2.82 V vs SCE, demonstrating that the reaction is thermodynamically favourable (Figure 17A).[74]

Zhang and co-workers established a photoinduced copper-catalysed carbon alkylation of styrene derivatives. Once more, Cu^{I}-acetylide plus tpy ligand act as photoredox catalysts under blue irradiation to generate alkyl radicals trapped by styrene, and then the photoactive specie built a Csp^3-sp bond through the reduction elimination step.[75] At the same time, the same group introduced a single chiral copper complex utilising the same model reaction, obtaining a highly enantioselective chiral multicomponent product (Figure 17B).[76]

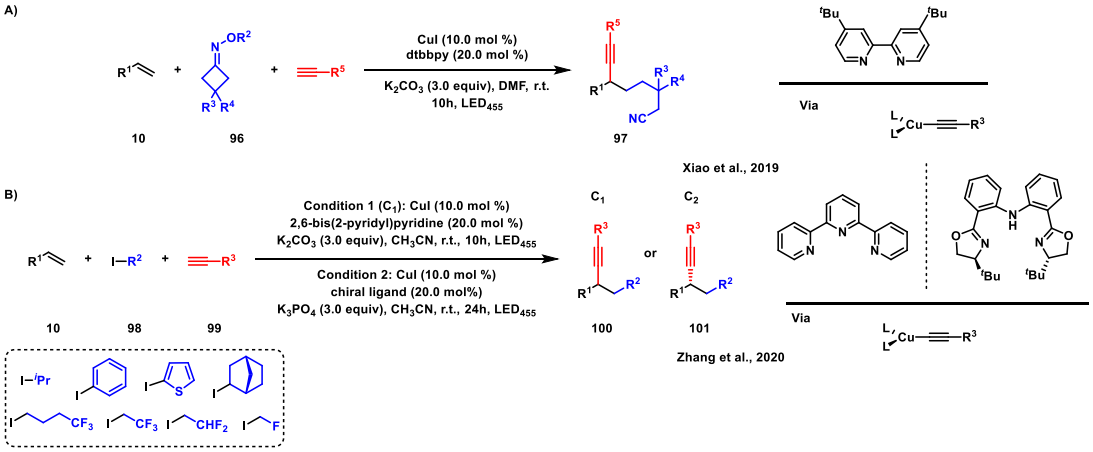

Figure 17. Photoredox-catalysed difunctionalization of alkenes through Cu^{I}-acetylide.

6.4 Katryzky salt as a radical source

Amines functional group are abundant in the chemical architecture of many natural products, drug moieties and agrochemicals. Moreover, the amine moiety is a significant functionality in amino acids, constituting fundamental building blocks for peptide construction. Several strategies have been explored

to develop C-N bonds, but complementary strategies for deaminative reactions have been studied in parallel. Katrizky was one of the pioneers in this field in the 70', and he introduced a new type of electrophile for substitutions reactions: bulky pyridium salts synthesised from pyrilium salts and primary amines, synthesised in one-step. Generally, these methods use ethanol as solvent, and the product is purified using recrystallisation techniques. Ten years later, the redox properties of these molecules were investigated and applied to generate carbon centre radicals for C-C coupling.[77] The first methodologies using this starting material are based on expensive catalysts like ruthenium or iridium; these strategies exhibit similar behaviour of Katryzky salt and *N*-(acyloxy)phthalimide derivatives. In order to avoid these metals, Dorota Gryko and co-workers founded a metal-free photoredox strategy for forming Csp^3–Csp bonds using as coupling partners 2,4,6-triphenylpyridinium salts derivatives and alkynyl *p*-tolylsulfones and Eosin Y under green light as the irradiation source.[78]

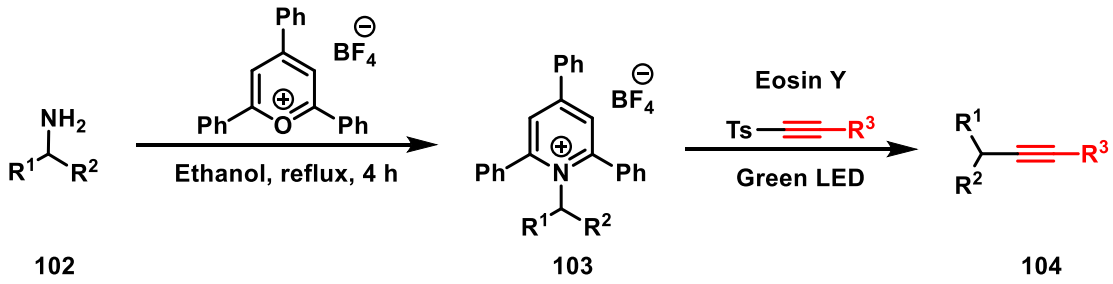

102 103 104

Scheme 19. General synthetic route for Katryzky salts and methodology reported by Dorota Gryko and co-workers.

6.5 Hydrogen Atom Transfer (HAT) as opportunities for new synthetic routes

Alkenes and cycloalkenes merged as a new alternative for new radical sources. They are attractive as low-cost raw materials because they can be obtained from abundant natural gas or petroleum resources. These starting materials

are challenging for synthetic chemists due to their high Csp^3-H bond dissociation energy (BDE, 96-105 Kcal/mol), low polarity and solubility. In recent decades, numerous methodologies have been reported for their activation using extreme reaction conditions, high temperature, oxidants, and/ or non-catalysed methodologies. On the other hand, hydrogen atom transfer (HAT) has gained interest in activating C-H bonds using light and transition metal catalysis (e.g. Cu, Ni, Co, Ce, Cr, Mn) to convert abundant material into valuable products.[79]

6.6 Photocatalyzed Hydrogen Atom Transfer mediated by copper photocatalysis

In the last five years, copper has attracted the attention of various groups to be used in HAT processes due to its nature and the ability to interact with organic substrates by internal sphere mechanisms. Wu and co-workers develop a photocatalysed strategy for the synthesis of 2-vinyl heterocycles derivatives via activation of oxo-Csp^3-H and Csp-H using the nature of Cu^I-phenylacetylide under visible light irradiation a room temperature. This intermediate in the excited state delivers an electron to tert-butyl hydroperoxide (TBHP) for the generation of the ^{t}BuO radical, which activates the α-Csp^3-H bond of the heterocycle for the subsequent addition to the metal.[80]

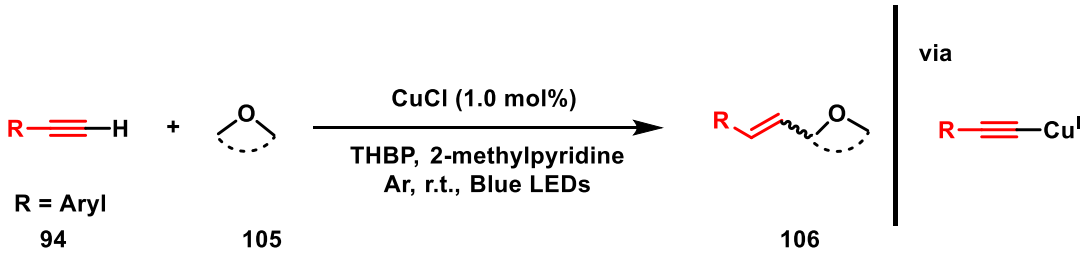

Scheme 20. Photoredox Oxo-Csp^3-H bond functionalisation via Cu^I-phenylacetylide catalysis

The HAT formation process has been carried out in different ways, and one is through ligand to metal charge transfer (LMCT). Rovis and co-workers use this pathway to form Csp^3-Csp bonds, working with unactivated alkanes and electron-deficient alkenes. The authors exhibit an innovative catalytic system using a mixture of $CuCl_2$ (20.0 mol%) and LiCl (50.0 mol%) under light (390 nm) at 60 °C. This proportion makes that $CuCl_2$ coordinate a solvent molecule and a chlorine atom from LiCl. This photoactive species $[(CH_3CN)Cu^{II}Cl_3]^-$ undergoes a LMCT process to form chlorine radicals. Consequently, this begins the HAT with the alkane, which is summarised in Figure 18. The production of chlorine radicals by $CuCl_2$/LiCl and reduction through LMCT offers new opportunities for C-H bond activation using a practical and simple protocol.[81]

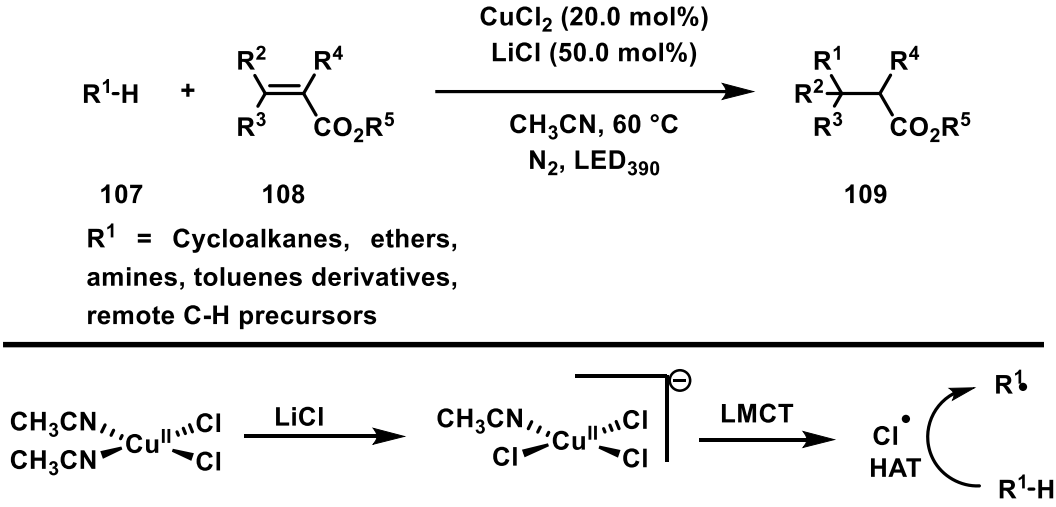

Figure 18. Synthetic route for Csp^3-H bond alkylation via photoinduced LMCT mediated by copper and summary of LMCT mechanism by $[(CH_3CN)Cu^{II}Cl_3]^-$

In 2020, König's group reported a method for the alkylation of substrates containing N−H bonds using $Cu(OAc)_2$ as catalyst and peroxide as reaction initiator. In this case, and on the contrary to the example mentioned above (Figure 19), upon light irradiation at room temperature, the peroxide reagent

works as a HAT reagent to activate Csp^3-H bonds and Cu^{II} works as the catalyst. The mechanism proposed by the authors is depicted in Figure 18. Starting with the interaction of peroxide and light delivering the $Cu^{II}(NR^2R^3)(OAc)$ complex from $Cu(OAc)_2$ and the amide derivatives. Simultaneously, the photolysis of DTBP (**112**) forms ^tBuO radical (**113**), which made a HAT step to the alkane generating a radical (R^1), which is trapped by $Cu^{II}(NR^2R^3)(OAc)$, leading to the formation of $R^1Cu^{III}(NR^2R^3)(OAc)$ intermediate complex. Followed by the reductive elimination step, which forms the expected coupling product **111**.[82]

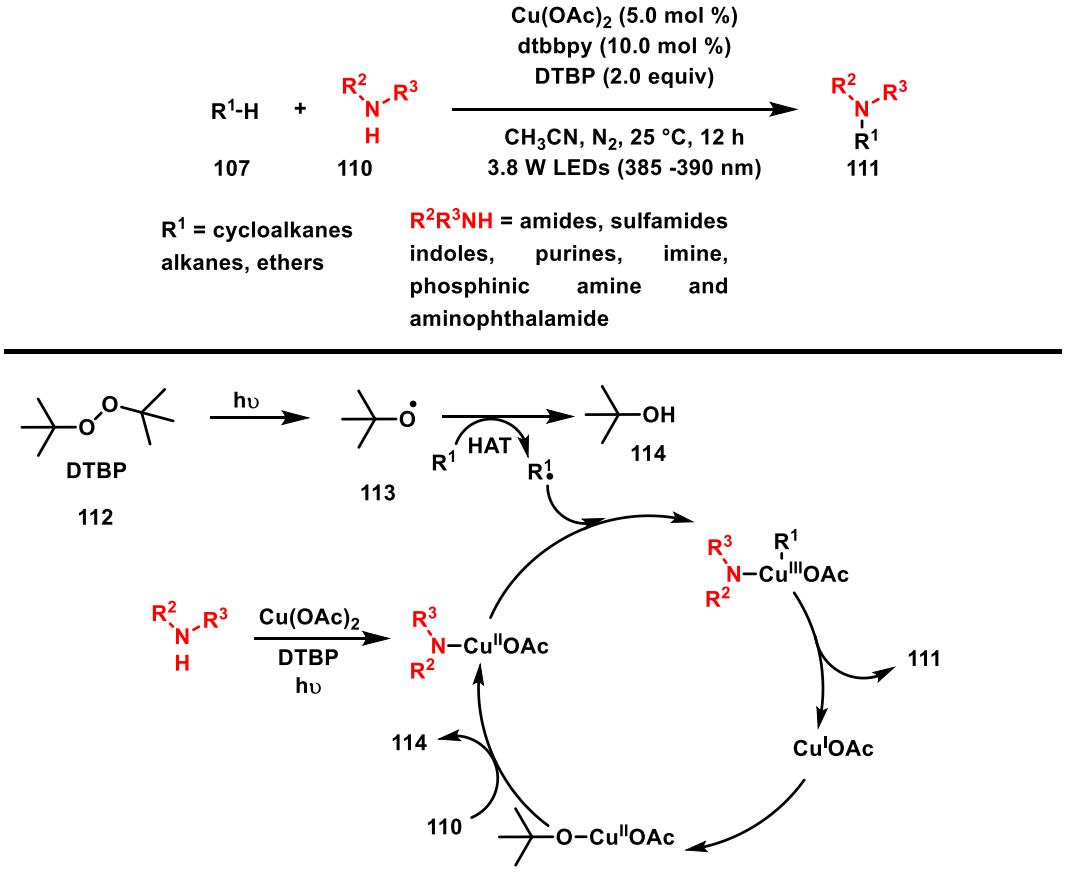

Figure 19. Koning's group general route proposed and mechanism for Cu^{II}-photocatalyzed N-H alkylation with alkanes.

6.7 Project Proposal

Based on the literature shown above, the approaches to generate the Csp^3-sp bonds have not been fully explored. In order to find simple and environmentally friendly methods, it is interesting to explore new radical sources type N-OR or Katryzky salts using copper and light (Scheme 21A). On the other hand, it is a challenge to explore the reactivity of alkanes as starting material for radical generation through HAT and subsequent coupling with terminal alkynes via the Cu^I-phenylacetylide (Scheme 21B).

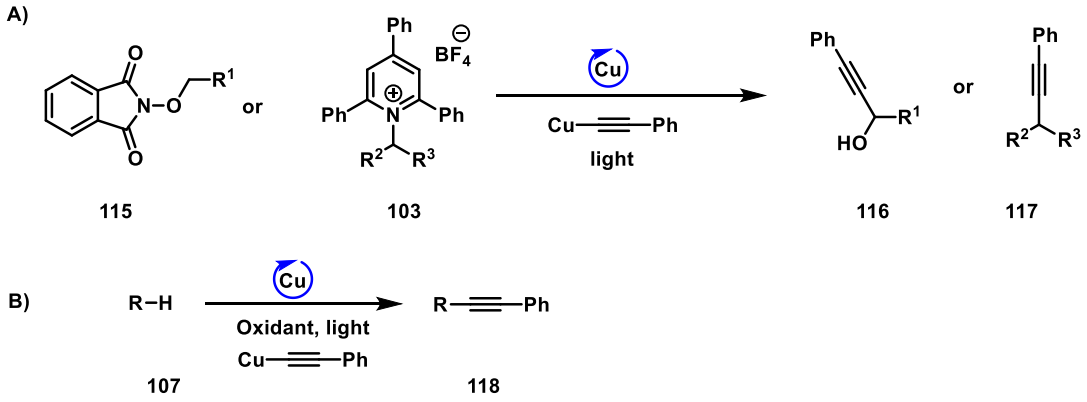

Scheme 21. General proposal to obtain Csp^3-sp coupling via A) *N*-alkoxyphtalimides derivatives or Katryzky salt as radical source B) Direct HAT using oxidant and copper as a catalyst

7 RESULTS AND DISCUSSION

We have selected the 2-butoxyisoindoline-1,3-dione as a model substrate because it has been activated using [Cu(dmp)(XantPhos)]BF_4 in the activation of several *N*-alkoxyphtalimides derivatives.[83] In this reaction, the coupling partners were phenylacetylene or (bromoethynyl)benzene, using similar conditions reported in the literature.[83] The reaction mixture was exposed at 455 nm under a nitrogen atmosphere using anhydrous DMF as a solvent (Table 9). The reported photocatalyst [Cu(dmp)(XantPhos)]BF_4 did not deliver the expected product; when X = Br (entry 1), the same result was observed for the mixture of CuCl or CuBr and terpyridine (entry 2-3). After 24 hours, in all cases, just starting material was observed.

Table 9. Control experiments for propargyl reaction[a].

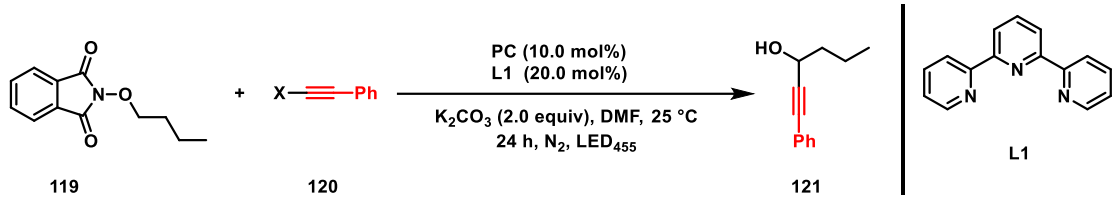

Entry	X	PC	Yield % [b]
1	Br	[Cu(dmp)(XantPhos)]BF_4[c]	n.r.
2	H	CuCl	n.r.
3	H	CuBr	n.r.

[a] 2-butoxyisoindoline-1,3-dione (0.25 mmol, 1.0 equiv), X (0.25 mmol, 1.0 equiv), photocatalyst (10.0 mol%), L1 (20.0 mol%), K_2CO_3 (2.0 equiv) in DMF (dry, degassed, 3 mL); Irradiation at 455 nm (LED) under N_2 atmosphere for 24 h at 25 °C. [b] ^{1}H-NMR Yield was determined using 1,3,5-trimethoxybenzene as an internal standard. [c] no ligand.

As the product derived from propargyl was not observed. We use the reported conditions for activation of *N*-(acyloxy)phthalimide,[32,41,63] and we used three

photocatalysts in the presence of DIPEA and Hanszch ester, using THF as solvent (Table 10). Unfortunately, the copper complexes failed to generate the α-oxy carbon-centred radical under these conditions.

Table 10. Control experiments for propargyl reaction using Cu^{I} photocatalyst. [a].

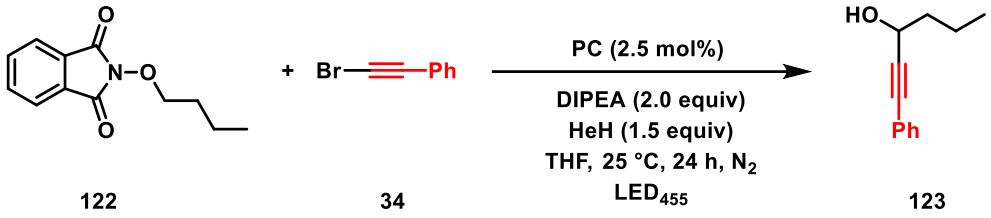

122 34 123

Entry	Catalyst	Yield % [b]
1	$[Cu(dpa)(S\text{-}BINAP)]BF_4$	n.r
2	$[Cu(dmp)_2]Cl$	n.r.
3	$[Cu(dmp)(XantPhos)]PF_6$	n.r.

[a] 2-butoxyisoindoline-1,3-dione (0.25 mmol, 1.0 equiv), (bromoethynyl)benzene (0.25 mmol, 1.0 equiv), photocatalyst (2.5 mol %), HeH (1.5 equiv), DIPEA (2.0 equiv) in THF (dry, degassed, 3 mL); Irradiation at 455 nm (LED) under N_2 atmosphere for 24 h at 25 °C. [b] ^{1}H-NMR Yield was determined using 1,3,5-trimethoxybenzene as an internal standard. n.r. = no reaction

Since *N*-alkoxyphtalimides derivatives did not work as a radical source, we decided to explore cyclohexyl Katryzky salt reactivity, due to this compound has served as a model substrate for several groups.[77] Our first attempts are summarized in Table 11. We decided to use copper salts as CuCl or CuBr (entry 1-2) to generate the species (*N,N,N*)Cu^{I}-phenylacetylene to reduce the Katryzky salt. However, only starting material was observed in after 24 h. The same result was detected when [Cu(dmp)(XantPhos)] was generated in-situ (entry 3).

Table 11. Control experiments for Csp^3-Csp coupling reaction using Cu^I photocatalyst.[a].

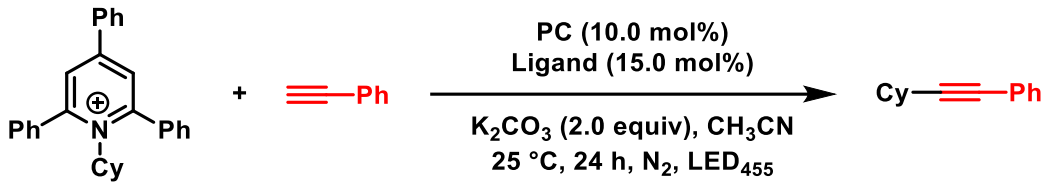

124 40 35

Entry	PC	Ligand	Yield % [b]
1	CuCl	terpyridine	n.r
2	CuBr	terpyridine	n.r.
3	$[Cu(CH_3CN)_4]BF_4$	dmp and XantPhos	n.r.

[a] cyclohexyl Katritzky salt (0.4 mmol, 2.0 equiv), phenylacetylene (0.2 mmol, 1.0 equiv), photocatalyst (10.0 mol %), ligand (15.0 mol %), K_2CO_3 (2.0 equiv) in CH_3CN (dry, degassed, 3 mL); Irradiation at 455 nm (LED) under N_2 atmosphere for 24 h at 20 °C. [b] ^{1}H-NMR Yield was determined using 1,3,5-trimethoxybenzene as an internal standard. n.r. = no reaction.

Katrizky salts derivatives have shown similar chemical behaviour with *N*-(acyloxy)phthalimide when iridium is used as photocatalyst. We decided to continue with the conditions from Table 11, using as coupling partner (bromoethynyl)benzene. Pleasantly, the expected product was obtained when heteroleptic copper complexes were used (Table 12, entry 1-3), and our highest yield was 52 % when 2.0 mol% of $[Cu(dq)(S\text{-}BINAP)]BF_4$ was used. Surprisingly, the homoleptic copper complexes $[Cu(dap)_2]Cl$ at 530 nm did not provide any product, and catalysts like *fac*-$[Ir(ppy)_3]$ and $[Ru(bpy)_3]Cl_2$ do not work under these conditions (entry 5-6). Besides, the control experiments suggest that the reaction needs an heteroleptic photocatalyst and other essential parameters such as DIPEA, Hantzsch Ester, light and nitrogen atmosphere (entry 7-11). The literature gives us the information to explain why cyclohexyl Katryzky salt is working under these conditions, compared to *N*-

alkoxyphtalimides. One possibility is that an EDA complex is generated from the interaction between cyclohexyl Katryzky salt and DIPEA or Hantzsch Ester; this collaboration favours the formation of the carbon-centred radical in the presence of a photocatalyst.

Table 12. Catalysts screening and control experiments for Csp^3-Csp coupling reaction[a].

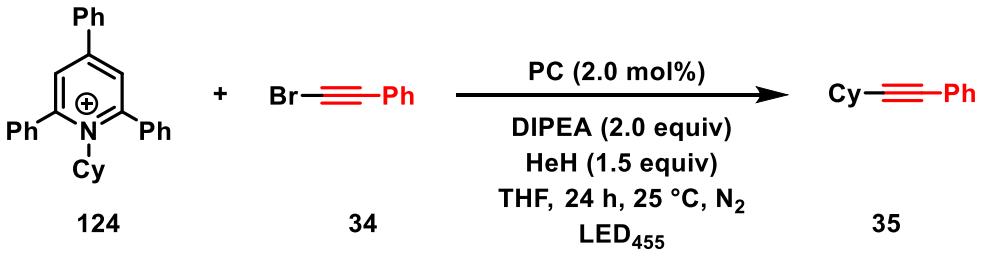

124 34 35

Entry	Conditions	Yield % [b]
1	$[Cu(dq)(S\text{-}BINAP)]PF_6$	52
2	$[Cu(dmp)(S\text{-}BINAP)]PF_6$	32
3	$[Cu(dq)(XantPhos)]PF_6$	10
4	$[Cu(dap)_2]Cl$ at 530 nm	n.r.
5	*fac*-$[Ir(ppy)_3]$	n.r.
6	$[Ru(bpy)_3]Cl_2$	n.r.
7	Without PC	n.r.
8	$[Cu(dq)(S\text{-}BINAP)]PF_6$ without light	n.r.
9	$[Cu(dq)(S\text{-}BINAP)]PF_6$ without DIPEA	n.r.
10	$[Cu(dq)(S\text{-}BINAP)]PF_6$ without HeH	n.r.
11	$[Cu(dq)(S\text{-}BINAP)]PF_6$ (air)	n.r.

[a] cyclohexyl Katritzky salt (0.4 mmol, 2.0 equiv), phenylacetylene (0.2 mmol, 1.0 equiv), photocatalyst (2.0 mol%), HeH (1.5 equiv), DIPEA (2.0 equiv) in THF (dry, degassed, 3 mL); Irradiation at 455 nm (LED) under N_2 atmosphere for 24 h at 25 °C. [b] ^{1}H-NMR Yield was determined using 1,3,5-trimethoxybenzene as an internal standard. n.r. = no reaction.

In the year 2022, Liu et al. published a methodology based on the deaminative Sonogashira coupling of alkyl pyridinium salts using nickel catalysis.[60] They reported this coupling using a mixture of catalytic amounts of $NiCl_2$ x $6H_2O$ (15.0 mol%) and ligand (10.0 mol%), an inexpensive catalyst system. They have introduced a reachable and bench-stable amide-type pincer ligand, which coordinates the metal forming the active specie (*N,N,N*)Ni^{II}-phenylacetylene giving the coupling product in good yields. Although this protocol is based on thermal conditions (reaction at 80 °C), is an attractive one-pot synthetic route from abundant alkylamines (Scheme 22). Due to the similarity between the project that we were doing using copper and this recent publication, we decided to modify the goals towards generating a Csp^3-sp coupling using unsubstituted starting materials.

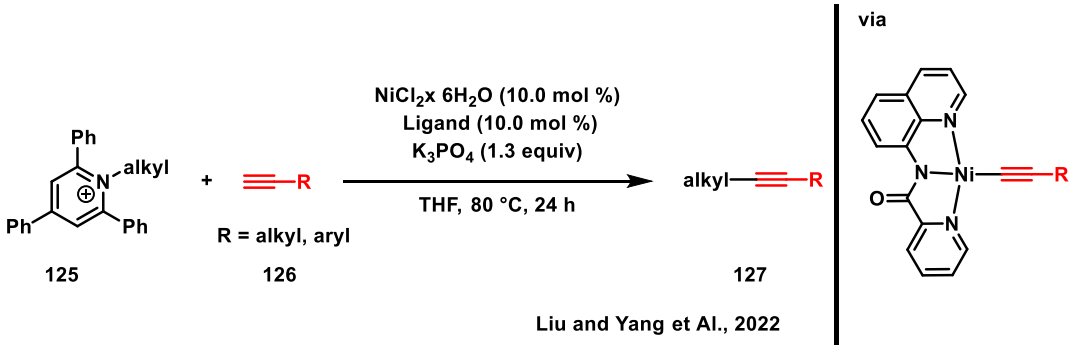

Scheme 22. Nickel-catalysed deaminative Sonogashira coupling of alkylpyrdinium salts via *N,N,N* pincer ligand.

The König's group strategy to generate radicals from cycloalkanes was the use of an oxidant such as DTBP and the nature of copper to generate the Cu-phenylacetylide species. Accordingly, we irradiated our reaction mixture at different wavelengths using 0.2 mmol of phenylacetylene and ten equivalents of cyclohexane, 10.0 mol% of $Cu(OAc)_2$, 20.0 mol% terpyridine ligand with 2.0 equiv DTBP, obtaining the expected coupling product in 26 % at 385 nm. At longer wavelengths, the yield decreases considerably, at 455 nm just traces

are obtained. It is possible to observe in the TLC the homocoupling product of phenylacetylene. Furthermore, the control experiments suggest that the explored components are necessary to obtain the product. At the beginning of the reaction, a yellow colour is observed in the reaction mixture, which is characteristic of the Cu^{I}-phenylacetylene species.

Table 13. Control parameters experiments for Csp^3-Csp coupling reaction using HAT pathway. [a]

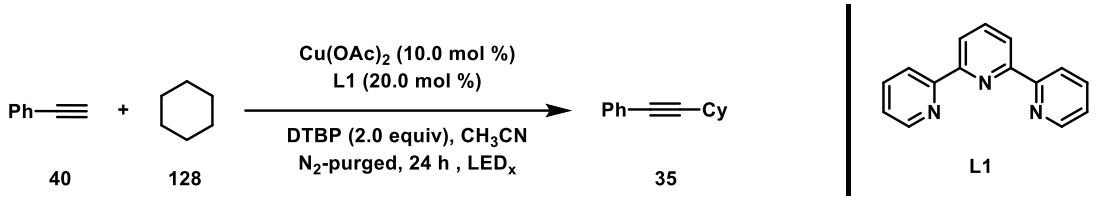

Entry	Conditions	Yield % [b]
1	365 nm	20
2	385 nm	26
3	400 nm	6
4	455 nm	traces
5	Without Cu and L1	n.r.
6	Without DTBP	n.d.
7	Without Light	n.r.
8	In Air	n.d.

[a] phenylacetylene (0.2 mmol, 1.0 equiv), cyclohexane (2.0 mmol, 10.0 equiv), catalyst (10.0 mol%), ligand (20.0 mol %), DTBP (0.4 mmol, 2.0 equiv) in CH_3CN (dry, degassed, 3 mL); Irradiation at X nm (LED) under N_2 atmosphere for 24 h at 20 °C. [b] ^{1}H-NMR Yield was determined using 1,1,2,2-

tetrachloroethane as an internal standard. n.r. = no reaction, n.d. = not detected.

In the first attempts, the presence of the phenylacetylene coupling product was observed in TLC and crude NMR, corresponding to the reaction that can occur in parallel. There are various reports explaining the Glaser coupling mechanism. For example, Aiwen lei and co-workers studied the mechanism through X-ray absorption spectroscopy and in situ EPR for the reduction of Cu^{II} to Cu^{I} species, by alkynes in the presence of tetramethylethylenediamine (TMEDA). In this case, TMEDA plays a dual function as ligand and base. They reported that the homocoupling mechanism goes through the coordination of the phenylacetylene to the copper complex, followed by its deprotonation, and giving the formation of a bimetallic copper intermediate linked by two phenylacetylene. This specie induce a C-C coupling concerted step and the consequent coordination of the anions chlorines, producing the homocoupling compound **130** and the dimer complex **131** $[(TMEDA)CuCl]_2$.[84,85] The TMEDA ligand does not offer protection to the metallic centre to avoid homocoupling products. Therefore, sterically hindered ligands must be used to go for other products. As an example of this, Laleh Tahsini has reported a Pincer Cu-NHC complexes employed in the Sonogashira cross-coupling reaction. They demonstrate that the homo-coupling product is avoided if the ligand possesses bulky substituents. They obtained the best results for the model reaction when the NHC ligand was with a *tert*-butyl group (**133**), and the homocoupling product was appreciated in trace amounts (Figure 20).[86]

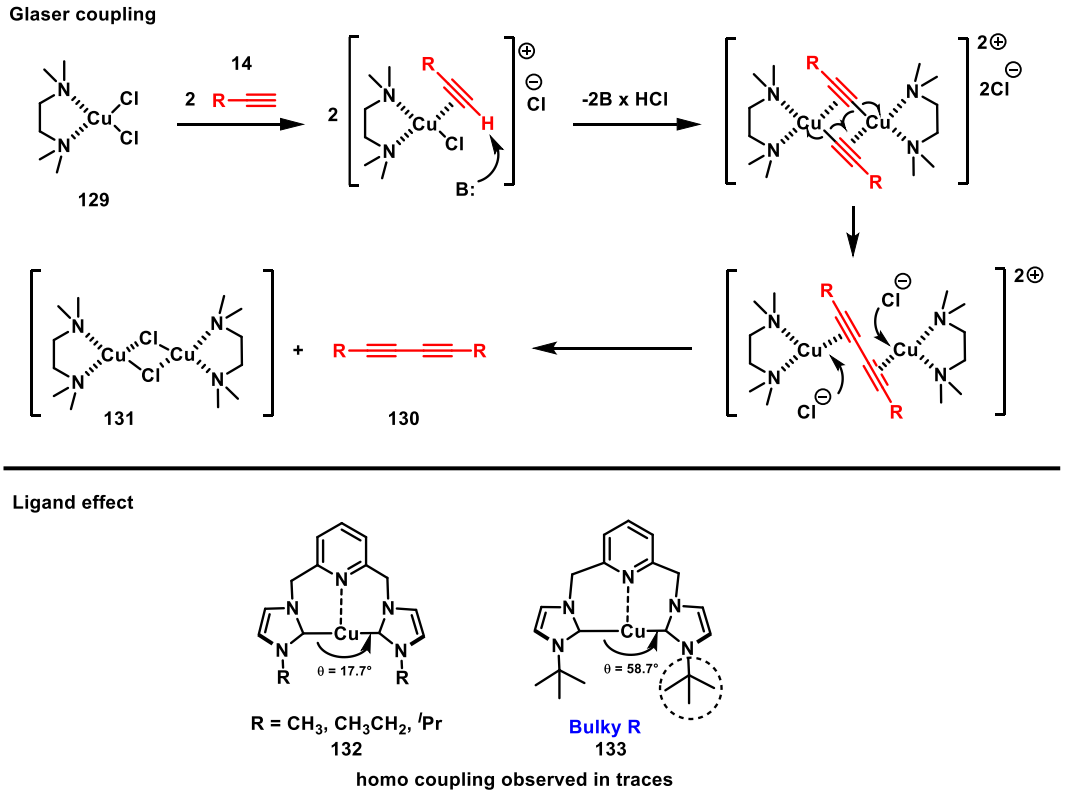

Figure 20. The mechanism proposed by Aiwen and co-workers for Glaser coupling and ligand effect study to avoid homocoupling by Tashini.

In the year 2019, Liu and co-workers published a Sonogashira coupling reaction for Csp^3-Csp bond formation mediated by copper catalyst, and they demonstrated a general stereoconvergent reaction using a broad range of terminal alkynes and racemic alkyl halides; this reaction was possible by a chiral cinchona alkaloid – based *P,N* ligand. Remarkably, the role of the ligand was crucial in this reaction to avoid the homocoupling product. They proved that one ligand could make a big difference. The authors showed that ligand L*4 (Scheme 23), within a series of 14 ligands, drastically changed the yield of and selectivity of the reaction, from traces to 90 % of yield of the expected product (**135**). Surprisingly, ligand L*2 is not giving the expected product; in other reports has been used successfully in alkylation reactions using copper as a catalyst under these conditions.[87]

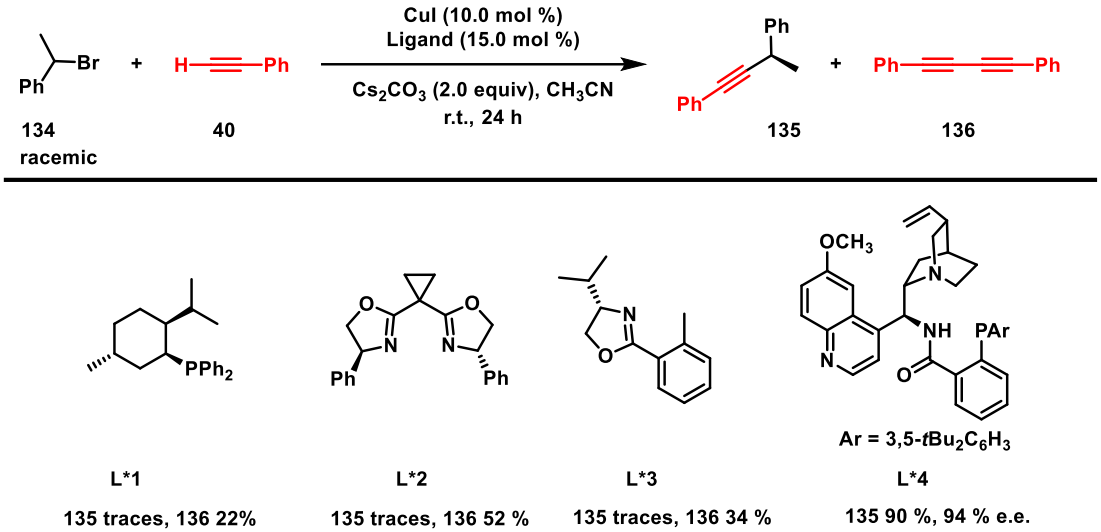

Scheme 23. The effect of different ligands in the model reaction and the optimal results

Based on the mentioned reports and the importance of the ligands, we have decided to explore 11 ligands commonly used in copper-catalysed reactions. For this, the conditions of Table 13 were used for our reaction mixture as the basis of the study. The terpyridine derivate with tert-butyl groups as substituents decreases the yield to half. Ligands type *N*-heterocycle are ineffective, and the expected product is obtained in traces. Identical results were observed for bidentate phosphine ligands. A tripodal ligand is not practical for the coupling reaction. Surprisingly, chiral cinchona alkaloid–based *P,N* ligand developed by Liu does not show the desired product under our conditions.

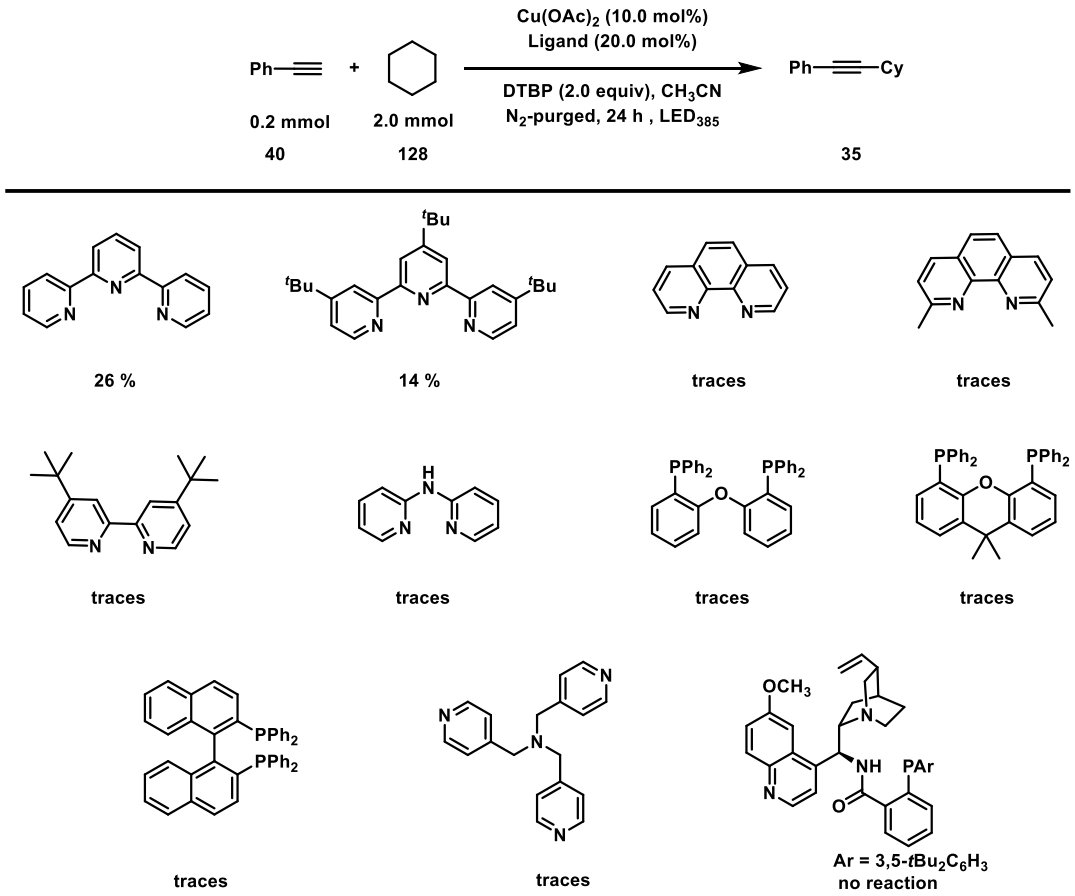

Scheme 24. Ligand screening. ^{1}H-NMR Yield was determined using 1,1,2,2-tetrachloroethane as an internal standard.

As mentioned in the introduction, the oxidizing agent plays a central role in starting the reaction. That is why, we have explored the nature of the oxidizing reagent (Table 14) and screened the most commonly used one in HAT-type reactions. However, the yield decreased for organic oxidants like *t*-BuOOH and DCP (entry 2-3), and for inorganic oxidants like $K_2S_2O_8$ and H_2O_2, the coupling product was not observed.

Table 14. Evaluation of oxidants for Csp^3-Csp coupling reaction using HAT pathway. [a]

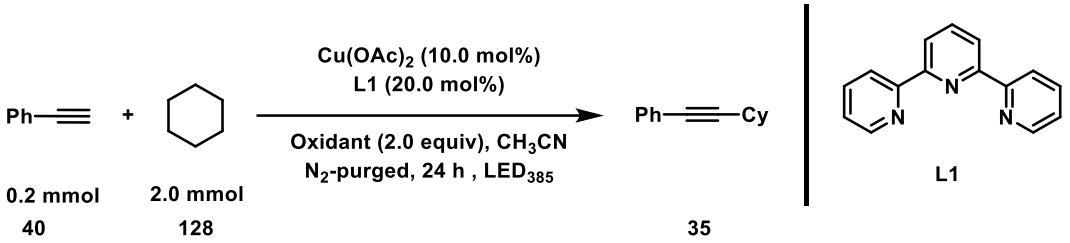

Entry	Oxidant	Yield % [b]
1	DTBP	26
2	^{t}BuOOH	20
3	DCP	13
4	$K_2S_2O_8$	n.r.
5	H_2O_2	n.r.

[a] phenylacetylene (0.2 mmol, 1.0 equiv), cyclohexane (2.0 mmol, 10.0 equiv), $Cu(OAc)_2$ (10.0 mol%), ligand (20.0 mol%), Oxidant (0.4 mmol, 2.0 equiv) in CH_3CN (dry, degassed, 3 mL); Irradiation at X nm (LED) under N_2 atmosphere for 24 h at 20 °C. [b] ^{1}H-NMR Yield was determined using 1,1,2,2-tetrachloroethane as an internal standard. n.r. = no reaction.

In order to increase our reaction yields, a set of copper salts were studied (Table 15). It is possible to see that the yield is reduced by more than half when the monohydrated form of $Cu^{II}(OAc)_2$ catalyst was used. For other salts such $Cu^{II}(OTf)_2$, $CuCl_2$, $CuSO_4$, and CuF_2 x H_2O, the yield is almost negligible, and the product is observed in trace amounts. By changing the oxidation state from +2 to +1 (CuOAc, CuBr and CuCl), the product is obtained in a overate of 8 % (entry 7). On the other hand, the characteristic colour of the Cu^{I}-phenylacetylide species is yellow, which was not appreciated for $CuSO_4$.

Table 15. Evaluation of copper salts for Csp^3-Csp coupling reaction using HAT pathway. [a]

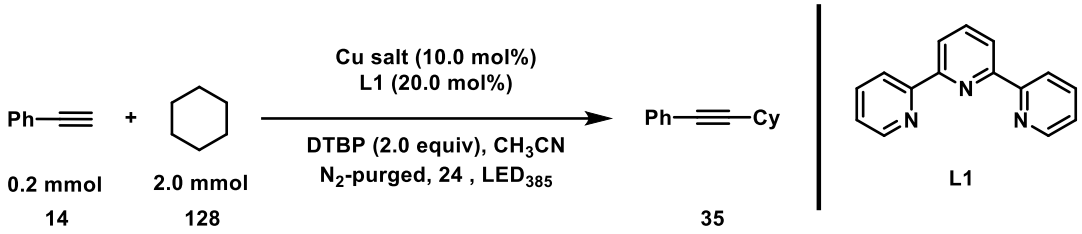

Entry	Cu salt	Yield % [b]
1	$Cu^{II}(OAc)_2$	26
2	$Cu^{II}(OAc)_2$ x H_2O	10
3	$Cu^{II}(OTf)_2$	6
4	$CuCl_2$	7
5	$CuSO_4$	n.r.
6	CuF_2 x H_2O	4
7	$Cu^{I}OAc$	8
8	CuCl	6
9	CuBr	8
10	CuI	7

[a] phenylacetylene (0.2 mmol, 1.0 equiv), cyclohexane (2.0 mmol, 10.0 equiv), catalyst (10.0 mol%), ligand (20.0 mol %), DTBP (0.4 mmol, 2.0 equiv) in CH_3CN (dry, degassed, 3 mL); Irradiation at X nm (LED) under N_2 atmosphere for 24 h at 20 °C. [b] ^{1}H-NMR Yield was determined using 1,1,2,2-tetrachloroethane as an internal standard.

Many photocatalyzed reactions are solvent-dependent, and the components' solubility determines the reaction's success. In our initial conditions, using CH_3CN (entry 1), once all the components were added to the reaction mixture, it is possible to observe tiny droplets corresponding to cyclohexane and a few amount of a solid, corresponding to $Cu(OAc)_2$. Although this has not been a problem for previous methods using the mixture of cyclohexane and $Cu(OAc)_2$, we decided to screen the solvent to improve the solubility of the components. Using only dry solvents (Table 16), and chlorinated solvents like CH_2Cl_2, the yield is reduced by 10 % (entry 2). When we used a solvent such as a chlorobenzene, neither the expected product or the phenylacetylene homocoupling product were observed. Surprisingly, we were able to detect the Cy-Cy coupling product by ^{1}H-NMR (entry 3). For polar solvents like DMF, DMSO, DMA or acetone, the reaction does not occur (entry 4-7).

Table 16. Evaluation of solvents for Csp^3-Csp coupling reaction using HAT pathway. [a]

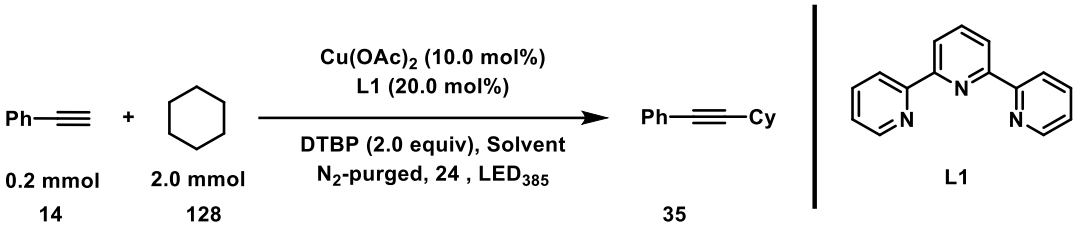

Entry	Solvent	Yield % [b]
1	CH_3CN	26
2	CH_2Cl_2	16
3	PhCl	n.d.
4	DMF	n.r.
5	DMSO	n.r.

6	DMA	n.r.
7	$(CH_3)_2CO$	n.r.

[a] phenylacetylene (0.2 mmol, 1.0 equiv), cyclohexane (2.0 mmol, 10.0 equiv), $Cu(OAc)_2$ (10.0 mol%), ligand (20.0 mol%), DTBP (0.4 mmol, 2.0 equiv) in X Solvent (dry, degassed, 3 mL); Irradiation at 385 nm (LED) under N_2 atmosphere for 24 h at 20 °C. [b] ^{1}H-NMR Yield was determined using 1,1,2,2-tetrachloroethane as an internal standard.

Sometimes a third component could increase the reaction yield. With the purpose of favour the formation of the Cu-phenylacetylene complex, we have exposed our reaction conditions to different inorganic bases such as ^{t}BuOK, KOH, $KHCO_3$ and NaH_2PO_4 (entry 2-5, Table 17) and organic bases such as DIPEA, Et_3N and 2-methylpyridine (entry 6-8, Table 17). The general outcome for base screening as an additive is undesirable, decreasing the reaction yield. Subsequently, we tested the reverse effect by adding an acid additive to the reaction mixture, such as NH_4Cl and AcOH. Sadly, these additive quenches the reaction, and the yield decreased (entry 9-10). Intending to enhance the solubility of both components, we tried: (i) for cyclohexane, we have evaluated TBAI as a phase exchange agent (entry 11) and (ii) for $Cu(OAc)_2$, we tested the addition of water to increase the copper salt solubility (entry 12). Nevertheless, in both cases, the product expected was not observed. Mixing light and thermal conditions, using the Schenk set-up and an oil bath, the reaction mixture was heated up to 50 °C, comparable to the parameters used by Rovis,[81] but under our conditions, the yield dropped to 10 % (entry 13).

Table 17. Evaluation of additives for Csp^3-Csp coupling reaction using HAT pathway. [a]

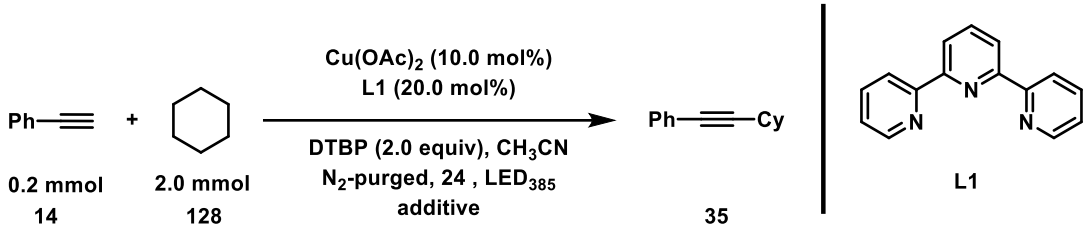

Entry	Additive	Yield % [b]
1	Without	26
2	^{t}BuOK	n.r.
3	KOH	5
4	$KHCO_3$	4
5	NaH_2PO_4	6
6	DIPEA	traces
7	Et_3N	traces
8	2-methylpyridine	7
9	NH_4Cl	8
10	AcOH	7
11	TBAI	n.r.
12	H_2O	n.r.
13	50°C [c]	10

[a] phenylacetylene (0.2 mmol, 1.0 equiv), cyclohexane (2.0 mmol, 10.0 equiv), catalyst (10.0 mol%), ligand (20.0 mol%), DTBP (0.4 mmol, 2.0 equiv) and additive (1.0 equiv) in CH_3CN (dry, degassed, 3 mL); Irradiation at 385 nm (LED) under N_2 atmosphere for 24 h at 20 °C. [b] ^{1}H-NMR Yield was determined using 1,1,2,2-tetrachloroethane as an internal standard. [c] Schlenk set-up

Additionally, we have explored the stoichiometry of three components: copper, ligand, and oxidant (Table 18). When the amount of the oxidant reagent is increased by a factor of five, the reaction yield remains constant (entry 2). Raising the amounts of copper and ligand to double and then to 50 % in a ratio of 1:1, it is possible to observe copper as a solid, and the solubility decreases drastically, obtaining the desired product in negligible quantities (entry 3-4).

Table 18. Stochiometric control for Csp^3-Csp coupling reaction using HAT pathway. [a]

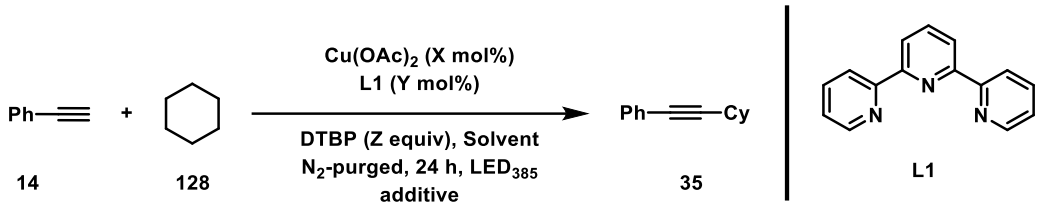

Entry	X	Y	Z	Yield % [b]
1	10	20	2	26
2	10	20	10	28
3	20	40	2	4
4	50	50	2	4

[a] phenylacetylene (0.2 mmol, 1.0 equiv), cyclohexane (2.0 mmol, 10.0 equiv), catalyst (X mol%), ligand (Y mol%), DTBP (Z) in CH_3CN (dry, degassed, 3 mL); Irradiation at 385 nm (LED) under N_2 atmosphere for 24 h at 20 °C. [b] ^{1}H-NMR Yield was determined using 1,1,2,2-tetrachloroethane as an internal standard.

As mentioned in the introduction, C-H activation is challenging due to high BDE. We compared the nature of cyclohexane with three different sources: toluene, THF and 1,3-dihydroisobenzofuran (Scheme 25). Nonetheless, we

could not observe a coupling product for any of them, which means that these conditions are not highly efficient in promoting HAT on other substrates. The reaction was only achieved for the substrate cyclohexane, limiting the substrate scope for other molecules.

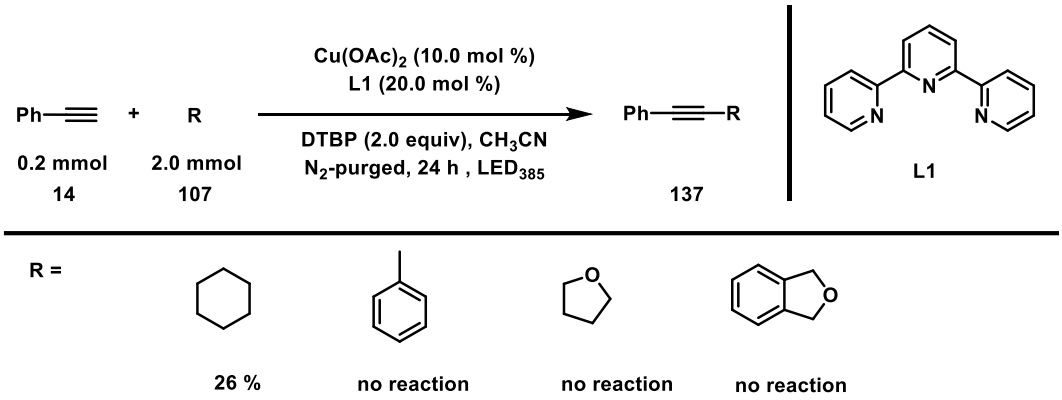

Scheme 25. Evaluation of different HAT sources. ^{1}H-NMR Yield was determined using 1,1,2,2-tetrachloroethane as an internal standard.

Based on the results, we decided to venture into the use of light-mediated dual catalysis (Figure 21). We proposed a system that combines a photocatalyst and copper as a cocatalyst due to its nature and ability to form the Cu-phenylacetylene species. Once the photocatalyst is in its excited state, it will generate the reduction of the oxidizing agent (DTBP), and this will drive the HAT of the alkane. The radical formed will be trapped by the Cu^{II}-phenylacetylene species, passing to a copper three intermediate, forming the desired product through a reductive elimination step. Subsequently, the addition of one equivalent of phenylacetylene to the Cu^{I} species and oxidation of this to Cu^{II} will reduce the photocatalyst and close the catalytic cycle.

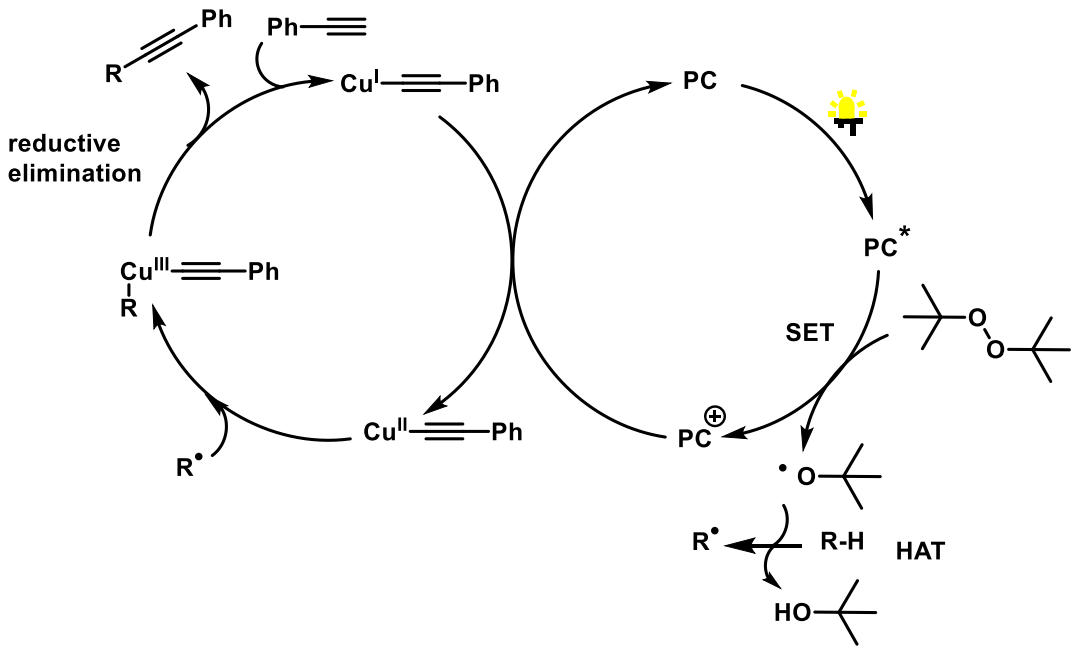

Figure 21. Dual photocatalysis for C-H activation mediated by PC/Cu.

Based on the proposed mechanism depicted in Figure 21, we decided to explore two partners for dual photocatalysis: 4CzIPN or *fac*-[Ir(ppy)$_3$] as photocatalysts and Cu(OTf)$_2$ or Cu(OAc)$_2$ as co-catalysts at 455 nm. The reaction does not show any product when Cu(OTf)$_2$ is used (entry 1-4), and Cu(OAc)$_2$ shows the product in traces. The incorporation of the terpyridine ligand gives the product in 6 % yield when the duo *fac*-[Ir(ppy)$_3$] and Cu(OAc)$_2$ are used (entry 6). Despite a yield of less than 10 %, we decided not to use HAT to pursue carbon-carbon coupling. Up to this point, despite multiple attempts, everything indicates that the proposed conditions are not thermodynamically favourable to generating C-H activation and subsequent coupling with terminal alkynes.

Table 19. Control experiments to evaluate dual photocatalyst conditions.[a]

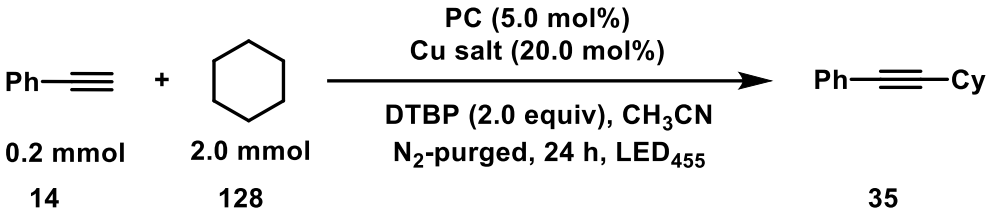

Entry	PC	Cu salt	Yield % [b]
1	4CzIPN	$Cu(OTf)_2$	n.r.
2	4CzIPN	$Cu(OAc)_2$	traces
3	*fac*-[Ir(ppy)$_3$]	$Cu(OTf)_2$	n.r.
4	*fac*-[Ir(ppy)$_3$]	$Cu(OAc)_2$	traces
5	4CzIPN	$Cu(OAc)_2$ + terpyridine	n.r.
6	*fac*-[Ir(ppy)$_3$]	$Cu(OAc)_2$ + terpyridine	6

[a] phenylacetylene (0.2 mmol, 1.0 equiv), cyclohexane (2.0 mmol, 10.0 equiv), photocatalyst (5.0 mol %), copper salt (20.0 mol %), ligand (20.0 mol %), DTBP (0.4 mmol, 2.0 equiv) in CH_3CN (dry, degassed, 3 mL); Irradiation at 455 nm (LED) under N_2 atmosphere for 24 h at 20 °C. [b] ^{1}H-NMR Yield was determined using 1,1,2,2-tetrachloroethane as an internal standard.

CHAPTER III – VISIBLE LIGHT AMINOSULFONYLATION OF STYRENES REACTION MEDIATED BY Cu^{I}

8 INTRODUCTION – CHAPTER III

8.1 Cu^{I} multicomponent reactions mediated by light

Multicomponent reactions have been strategically employed in various synthetic transformations to replace classical methods, which usually involve many steps with tedious procedures or harsh conditions. Therefore, multicomponent reactions reduce time and experimental work. This protocol is attractive for organic chemists, and these have been positioned as helpful tools. The idea of generating products in one step, using several reagents at the same time or catalysts, has allowed access to diverse types of products using green pathways. Copper has been used in multicomponent reactions due to its low cost and its behaviour of directly interacting with starting materials. This has allowed the development of new synthetic strategies for thermal or light conditions. Light-mediated multicomponent copper reactions have been studied by authors such as Greaney, Dilman, Xu, Peter, Fu, Li, and Wang, among others, and this field is still under exploration.[88]

The proposed catalytic mechanism for copper-catalysed three-component reactions is shown in Figure 22. Through a ligand addition process, the $Cu^{I}L$ complex can generate the CuLY species, where Y can be a nucleophile, for example, an amine or phenylacetylene. Upon excitation with light, a suitably ligated $Cu^{I}LY$ complex transfer an electron to an electron-accepting substrate, producing a radical species, which can be caught by an olefin causing a new radical intermediate. At this stage, two possibilities arise: the first option is that $Cu^{II}YL$ oxidizes the radical to generate a carbocation in the substrate, which a third component could nucleophilically attack and at the same time regenerates the initial CuL. The second possibility is that the radical R^2 can rebind to the $Cu^{II}YL$ intermediate to generate a high-valent R-Cu^{III}-YL intermediate, which undergoes a reductive elimination step to deliver the desired multicomponent product and regenerate the initial CuL

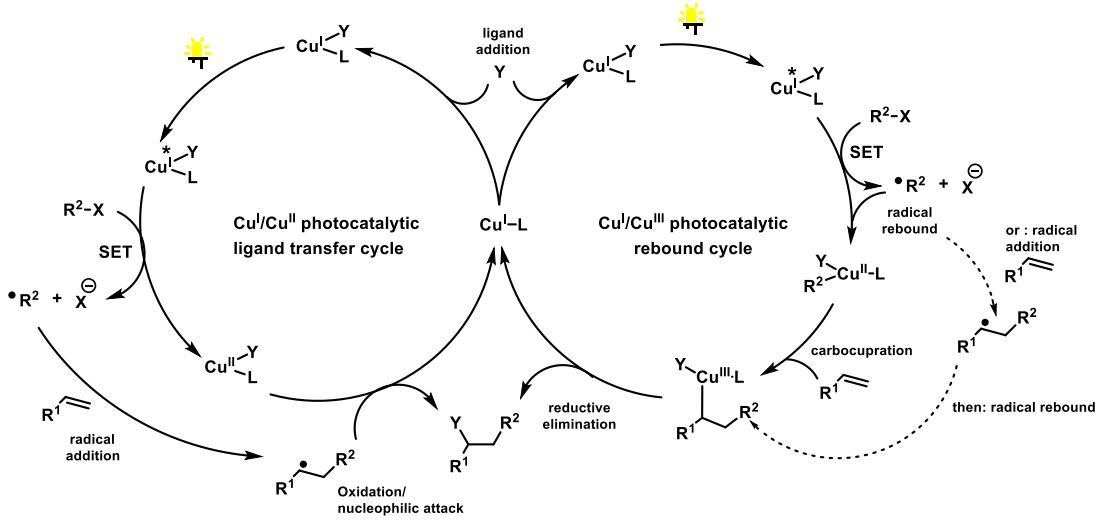

Figure 22. General mechanism cycle of copper-catalysed three-component reactions.

8.2 Multicomponent reaction using a Cu^{I} photocatalysis outer sphere mechanism

Only a few examples have been reported using multicomponent reactions copper-catalysed via an outer sphere mechanism, a pathway that is commonly observed for iridium and ruthenium. Greaney's group introduced the first example, a three-component copper-catalysed ATRA reaction. They used the Zhdankin reagent to generate azide radicals in the difunctionalization of alkenes using [Cu(dap)$_2$]Cl as a photocatalyst under blue light (455 nm). Successfully, they have obtained the azidomethoxylated product using methanol as solvent. In this case, carbocation is formed after oxidation of the radical generated by the capture of N_3 with styrene derivatives. This electrophile is subsequently attacked by a nucleophile (OCH_3), which is the third component of the reaction. They extended the strategy to C-Br/C-N difunctionalization, using acetonitrile instead of methanol, and adding NaBr and NaN_3 as nucleophiles.[89] Three years later, Dilman's group showed a second example of an outer sphere mechanism by copper photocatalyst. The authors

describe the generation of fluorinated radicals from organoboron compounds using the complex [Cu(dap)$_2$]Cl. This process becomes possible owing to the cleavage of the N-O bond within the sacrificial *N*-oxypyridinium ligand. Like Greaney, they propose a similar mechanism, a reduction of the trifluoromethyl borate complex according to a SET with the excited copper(I) complex. As a result, a substituted pyridyl radical eliminated a trifluoromethyl radical, which is trapped by an alkene. Then, the formed benzylic radical is oxidized, making the essential carbocation, and regenerating the photocatalyst. The benzylic carbocation is finally attacked by MeOH, forming the trifluoromethyl methoxylated product.[24]

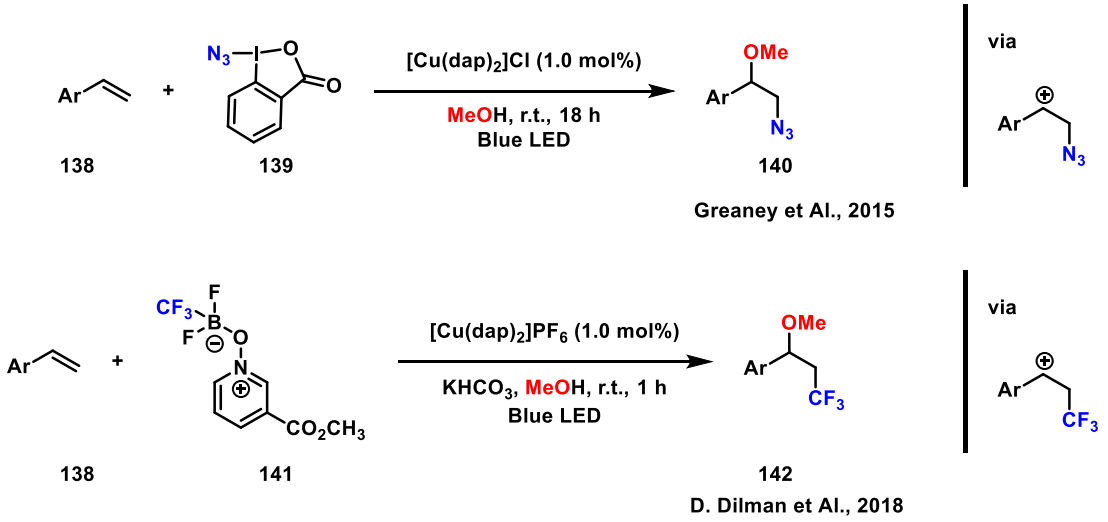

Figure 23. The three-component photo ATRA reaction via an outer-sphere mechanism mediated by [Cu(dap)$_2$]Cl.

8.3 Multicomponent reaction using a Cu(I) photocatalysis inner sphere mechanism.

Xu and co-workers in the year 2018, reported the first example of photoinduced three-component azidofluoroalkylation of alkenes mediated by copper. They generated the Cu^{I}-N$_3$ species in situ from Cu(OAc)$_2$ using a compact fluorescent light bulb (UV-light at 254 nm). Although the author's stated that the

mechanism is unclear, one of the proposed pathways is that the Cu^{I} species in the excited state leads to the formation of R_f radical, which may be trapped by styrene. Subsequently, DIPEA reduces Cu^{II} to Cu^{I} and simultaneously oxidizes $TMSN_3$, giving N_3 radical, followed by a radical coupling process between the radical generated in the first step (Figure 24A).[90]

In the same year, Gregory Fu and his team developed a protocol to construct C-S/C-C bonds using various electrophiles and trifluoromethylthiolate as nucleophiles activating different olefins using a mixture of Cu^{I} and S-BINAP as photocatalyst under blue irradiation. Their mechanistic studies propose L_2Cu-SCF_3 as the active species, which serves as a reducing agent for the formation of alkyl radicals, which react with the olefin, followed by the reduction of Cu^{II}-SCF_3 complex to afford the multicomponent coupling product (Figure 24B).[91] Li and his group contributed with a protocol where copper-catalyzed fluorotrifluoromethylation of unactivated alkenes using CsF as the fluorine source and the Umemoto's reagent as the trifluoromethylating reagent. They irradiated the reaction mixture using thermal and light conditions, like the mechanism described by Xu. The authors indicate that single electron transfer is promoted from L_2Cu^{I} complex to Umemoto's reagent, generating trifluoromethyl radical and a Cu^{II}−F complex. Adding electrophilic trifluoromethyl radical to an alkene gives the nucleophilic alkyl radical, which abstracts a fluorine atom from the Cu^{II}−F tetrahedral complex to provide the fluorotrifluoromethylation product and regenerate the L_2Cu^{I} complex (Figure 24C).[92]

As a last example, Xu and co-workers published a protocol using a chiral copper photocatalyst under blue light to generate cyanofluoroalkylation of alkenes. The photoactive species is $L2Cu^{I}$-CN, which generates R_f radical, which is trapped by styrene and gives the CN that comes from the TMSCN, similarly as the other mechanism, followed by the reductive elimination step to

obtain the desired multicomponent product (Figure 24D).[93]

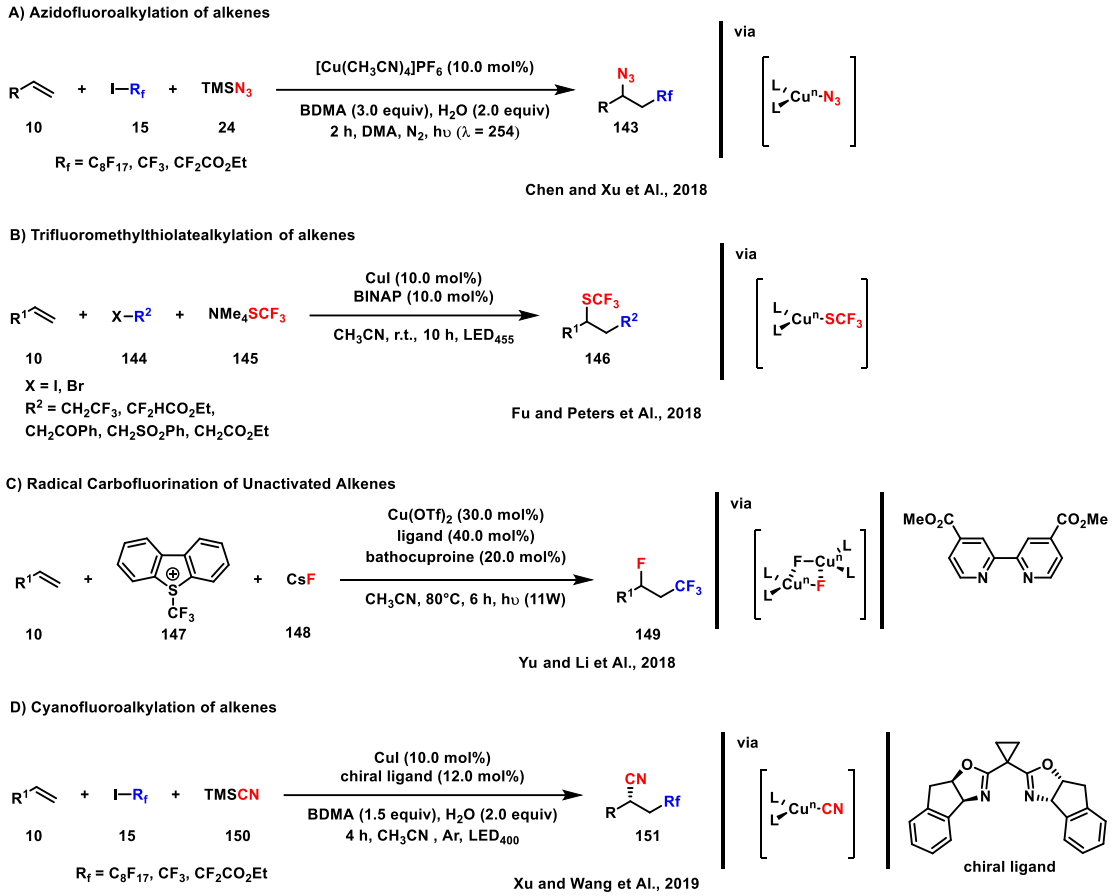

Figure 24. Selected examples for three-component photoreactions via an inner-sphere mechanism mediated by copper catalysis.

8.4 C-N bond formation by Cu^{I} photocatalysis

Nitrogen bonds are highly valued in the architecture of different natural products, pharmaceutical agents, and various materials due to their abundance on the earth. The design of new synthetic routes has called the attention of the academy and the industry to incorporate this atom in different molecular structures owing to the functionalization that nitrogen could deliver to one molecule. A light-induced process has developed several C-N bond formation strategies under mild reaction conditions. These efforts have focused on C–

H/C-X bond activations in the last ten years, including amination of olefins, carbonyl compounds and cross-coupling reactions.[94–96]

Copper has also been used in different C-N bond construction. Fu and Peters are pioneers in the field and delivered the first contribution in 2012. The reported photoinduced Ullmann C-N bond formation protocol via a copper-carbazolide complex (E_{red} = -2.6 V vs SCE) reduce several aryl halides derivatives, using an irradiation of 13 W CFL. They suggest a SET/radical mechanism for Ullmann C-N coupling.[97] Four years later, they published An enantioconvergent cross-coupling of racemic tertiary α-chloroamides with carbazoles and indoles in the presence of a Cu^{I}/Nu/(S)-SITCP complex (Nu = carbazole or indole) that turns both as a photocatalyst and as the source of enantioinduction. The commercially available chiral phosphine ligand (S)-SITCP self-controls the absolute configuration of the product regardless of the initial stereochemistry of the electrophiles.[98]

Another contribution of this group was the intramolecular decarboxylative C–N coupling of *N*-phthalimide esters using an in-situ [Cu(dmp)(XantPhos)]BF_4 heteroleptic copper complex. This protocol is a versatile alternative to the Curtius rearrangement. The authors suggested that excited Cu^{I}* species reduce the *N*-phthalimide esters forming a carboxyl radical and the phthalimide anion, which binds to the Cu^{II} species. Followed by the elimination of CO_2 and the recombination of the alkyl radical with the Cu^{II} species bearing the phthalimide forms the product and regenerates the active Cu^{I} catalyst. However, the participation of the ligands has not been determined. [99]

In 2019, Xiong et al. described a protocol using visible light for copper-catalyzed hydroamination of alkenes. In this catalytic strategy, mechanistic investigations revealed that after excitation of Cu^{I} complex via LCu-Nu (Nu = carbazole, anilines) originated in-situ from a mixture of [Cu(CH_3CN)]BF_4 (10.0

mol%), LiO^tBu (1.5 equiv), and the coordination of the copper centre with the olefin, followed by single electron transfer from the metal to the alkene, with a subsequent proton transfer from the solvent (CH_3CN), leading to Cu^{III} intermediate and releasing the final coupling product by a reductive elimination step. This new methodology gives access to various aryl amines using a Markovnikov regioselective pathway.[100]

This year, Fu's group have successfully synthesised *N*-alkylanilines using a variety of racemic tertiary alkyl electrophiles and different anilines as coupling partners. Like the previous works of this group, they propose that (*P,P*)CuCl acts as a photoreductant and the species [(*P,P*)Cu(NHAr)]Cl is key to the development of the reaction. Furthermore, the authors suggest that using the tert-Butylimino-tri(pyrrolidino)phosphorane base (BTPP) is crucial for trapping the chloride anion. [101]

The same year, Bing Yu's group reported a photocatalytic strategy for the synthesis of 2-aminobenzoxazoles using CuCl as a catalyst. The authors mentioned that the reaction mechanism begins with the coordination of the copper chloride and the nitrogen from the benzoxazole, forming a complex that acts as a photoactive species type $LnCu^I$-benzoxazole, which is crucial to initiate this type of coupling. With this work, they have given a new organic tool to aminate benzoxazoles in one-step synthesis.[102]

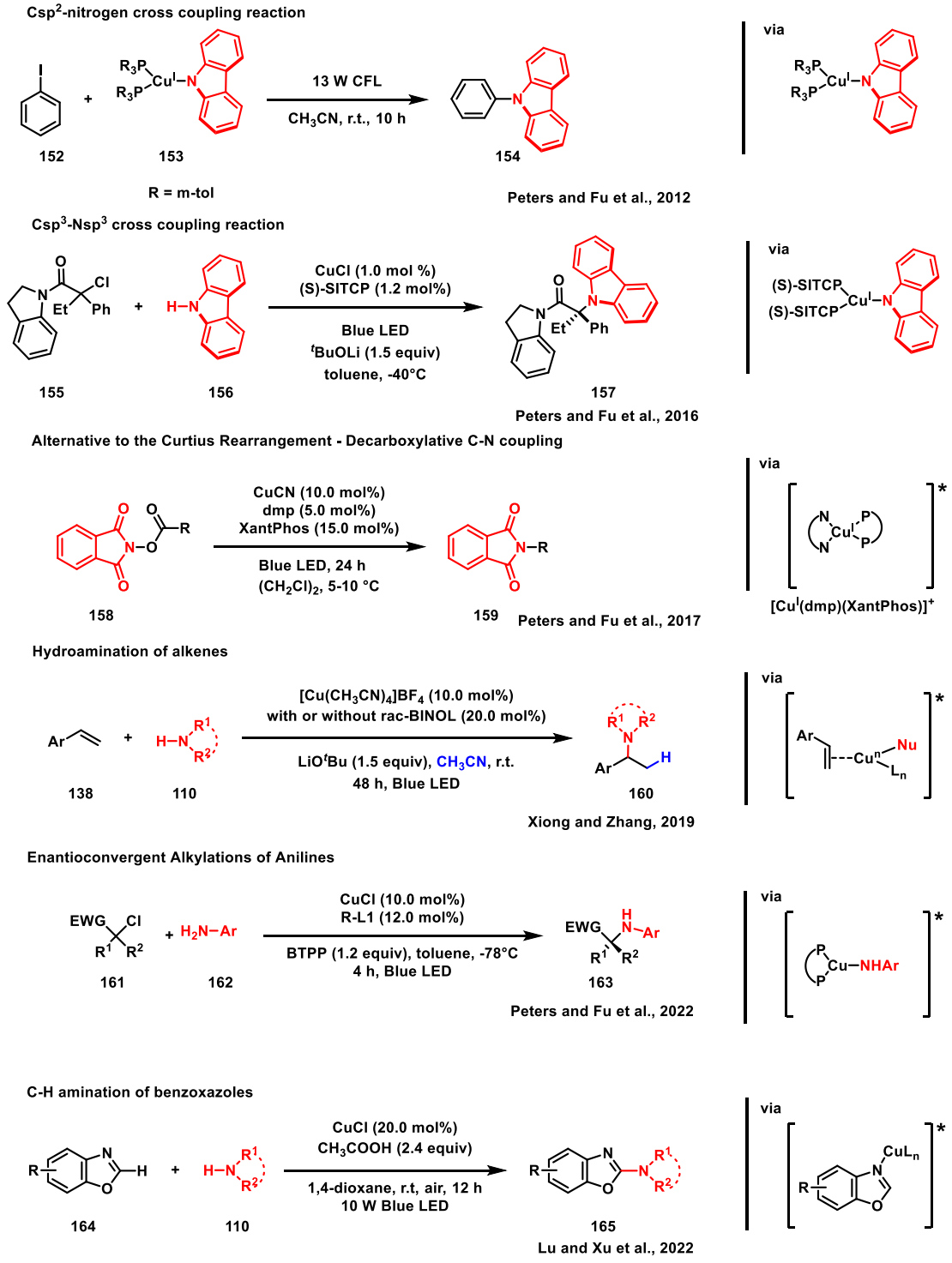

Figure 25. Selected examples for copper photoinduced C-N bond formation

8.5 Photoredox multicomponent reactions by copper-amino complex

Despite the mentioned examples of photoinduced C-N bond formation using copper as a photocatalyst, and other methodologies to access carboamination reaction by multicomponent pathways, there is only one report of carboamination of styrenes derivatives by Cu^{I} acting as photocatalysis. In 2019, Zhang's group published a protocol employing CuCl and S-BINAP for an alkylamination of styrenes derivatives (Scheme 26), using the species Cu^{I}-NR_2R_3 in the excited state as a photoreductant. This activate different alkyl halides, forming alkyl radicals that will be trapped by an alkene. Then, the Cu^{II}-NR_2R_3 species will trap the newly formed radical leading to the formation of the product by a reductive elimination step. Based on this strategy, they have synthesized an efficient method to access various molecules of pharmaceutical interest under mild conditions.[103]

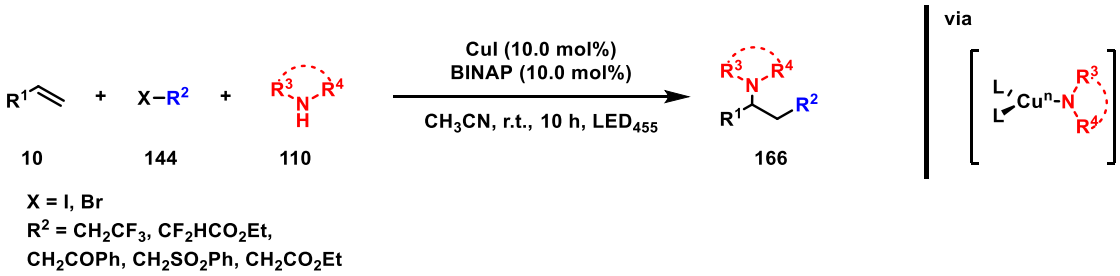

Scheme 26. Copper photoinduced aminoalkylation of styrene derivatives.

8.6 β-amino sulfone derivatives in drugs moieties

β-amino sulfone derivatives are versatile synthons in synthetic chemistry and display a wide range of biological activities as compounds with a medicinal reputation (Figure 26). As a potent matrix metalloproteinase inhibitor, ABT-518 has inhibited cancer cell growth. At the same time, canfosfamide is a nitrogen mustard pro-drug with a potential antineoplastic activity. This pro-drug is in phase 2 of clinical trials to treat several cancer warnings, such as

chemotherapy-resistant ovarian cancer.

Among other drugs, Apremilast has been recognized as an anti-inflammatory drug and used by pharmaceutical companies to cure psoriasis and psoriatic arthritis. Academia and industries have been pursuing several synthetic routes to obtain this target. There are a lot of scientific reports in patent and non-patent literature with different strategies. Although, at the moment, there is no one-pot synthesis route to obtain this pharmaceutical product.

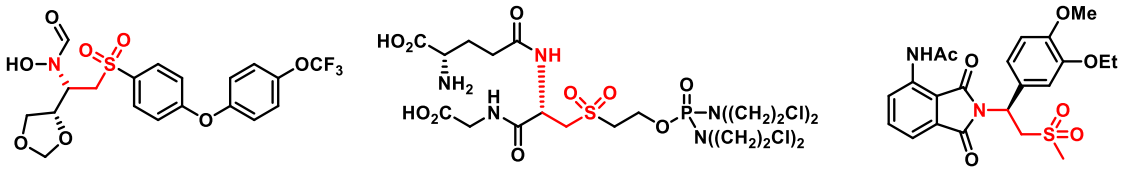

Figure 26. Drug molecules containing β-amino sulfone moieties

More in detail, the synthetic route to obtain Apremilast was developed by the Celgene corporation in the United States (Patent 6,020,358) and is depicted in Scheme 27. This company has described a three-step linear synthesis. In the first step, dimethyl sulfone reacts with *n*-butyllithium to obtain lithium dimethyl sulfone. Then, this is added to a mixture of 3-ethoxy-4-methoxybenzaldehyde, lithium hexamethyldisilazide, and boron trifluoride etherate. After acid hydrolysis, it is obtained the intermediate l-(3-ethoxy-4-methoxyphenyl)-2-(methyl sulfonyl)ethan-1-amine in 39 % yield. Afterwards, this intermediate is condensed with 3-acetamidophthalic anhydride in acetic acid at 110 °C to afford Apremilast in a 59 % total yield. However, there are multiple advances since this report which optimize this reaction and search for different paths.[104]

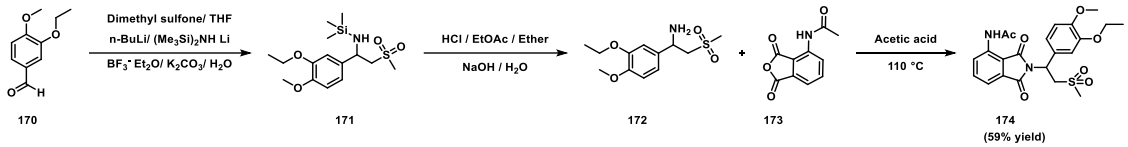

Scheme 27. Synthetic route to obtain Apremilast, developed by the Celgene Corporation.

One of the paths described was published by Wu and co-workers. The authors have described a synthetic pathway that provides access to enantioenriched β-aryl β-phthalimido and *N*-succinimide sulfones. These, can be readily converted to β-amino sulfone derivatives via Rh^{I} catalysed asymmetric addition reaction of arylboronic acids to β-imido vinyl sulfones, using chiral diene as ligand. The reaction mixture uses 5.0 mol% of Rh catalyst and 6.0 mol% of ligand, in the presence of Et_3N and methanol as solvent at 60 °C, to obtain Apremilast analogues. To access the target molecule, they used this methodology and subsequently a protection step where they used Ac_2O at 70 °C for 3 hours.[105]

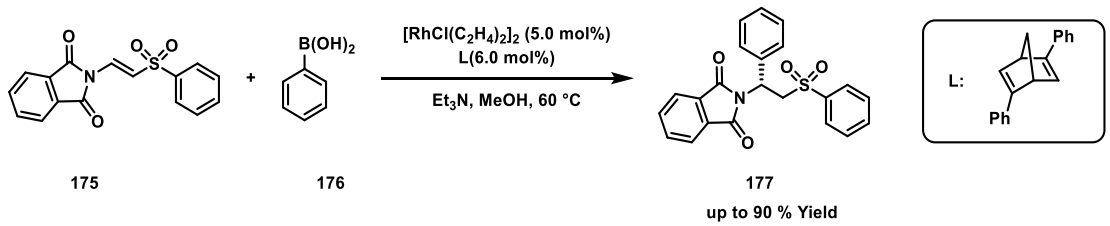

Scheme 28. Synthetic route of Apremilast analogues by rhodium catalyst.

Grela's group has reported the preparation of β-sulfonyl styrenes from diverse vinyl sulfones and/or allylbenzenes using MW-assisted cross-metathesis, ruthenium as a catalyst. These products can be used in medicinal chemistry through classical synthesis to develop different medical targets, as in Apremilast's case. Although they do not obtain the Apremilast directly, they produce the β-sulfonyl styrenes in a gram-scale synthesis. [106]

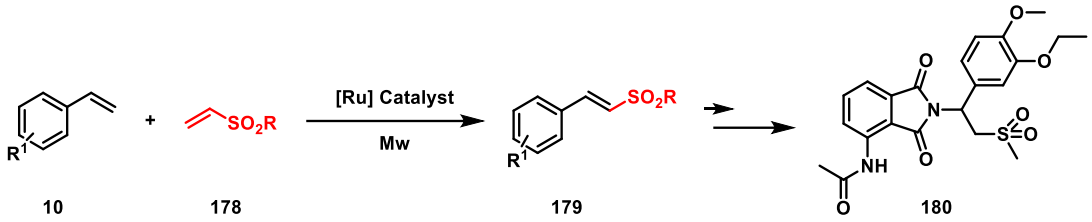

Scheme 29. Synthetic route of β-sulfonyl styrenes derivatives via MW-assisted cross-metathesis Ru-catalysed and Apremilast.

8.7 Proposal

As was stated, copper can interact with amines derivatives forming a photoactive species, type Cu-NR^2R^3 [97,98,101,107–110], which could activate TsCl, generating tosyl radical. Based on this, aminosulfonylation of styrene derivatives is proposed (Scheme 30), due to the nature of the reaction that copper has with the model substrates.

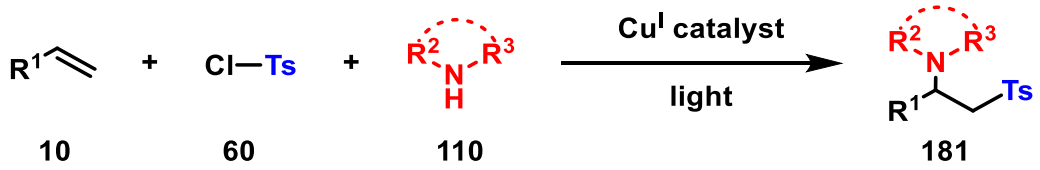

Scheme 30. A proposed synthetic route to obtain aminosulfonylation of styrenes derivatives.

9 RESULTS AND DISCUSSION

To initially test our proposal, we have chosen carbazole as a model substrate, due to its ability to coordinate to copper and form an active complex. In addition, as coupling partner, tosyl chloride was chosen since different copper systems can activate it. We begin using the reaction conditions from the literature:[103] 10.0 mol% CuCl and 1.5 equiv LiO^tBu dissolved in CH_3CN. After being purged with nitrogen, the reaction mixture was exposed to different conditions, summarized in Table 20. The expected product was obtained in 20 % yield by irradiating the mixture at 400 nm using carbazole purified by recrystallization. Surprisingly, when a commercial carbazole (purity over 99%) was used, the yield increased to 32 % Yield (entry 1). The yield remained constant by increasing the light intensity to 2W or switching to the Schlenk set-up system (entry 2-3). The yield decreased by using longer wavelengths (455 nm) (entry 4). On the other hand, we carry out the parameter controls and identify that the model reaction does not generate the product without a catalyst or light. Besides, avoiding oxygen is crucial for achieving the multicomponent product (entry 5-7). Unexpectedly, the absence of base leads to the formation of the chlorosulfonylation product (entry 8), which has been declared a challenge to avoid in multicomponent reactions, where a Cl anion is involved.[111]

Table 20. Control experiments for aminosulfonylation reaction.[a]

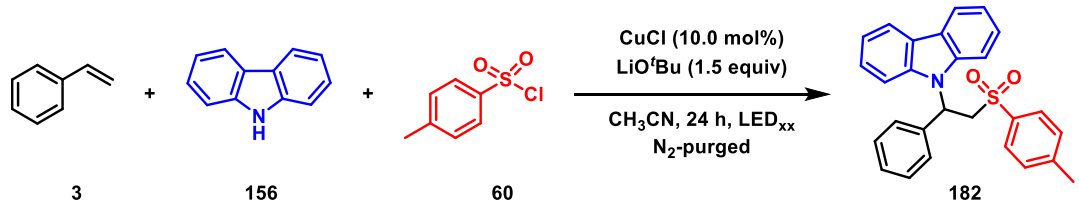

3 156 60 182

Entry	Condition	Yield % [b]
1	400 nm	20 / 32
2	400 nm HP (2 W)	20
3	400 nm Schlenk set-up	18

4	455 nm	13
5	Without Cu	n.r.
6	In Air	n.r
7	Without Light	n.r.
8	Without Base	Chlorosulfonylation product

[a] styrene (0.2 mmol, 1.0 equiv), TsCl (0.3 mmol, 1.5 equiv), carbazole (0.3 mmol, 1.5 equiv), CuCl (10.0 mol %), LiO^{t}Bu (1.5 equiv) in CH_3CN (dry, degassed, 3 mL); N_2 atmosphere for 24 h at 20 °C. [b] ^{1}H-NMR Yield was determined using 1,1,2,2-tetrachloroethane as an internal standard. HP = high intensity.

Intrigued by these results, we decided to explore the nature of different inorganic bases (Table 21). We found our product only using LiO^{t}Bu, KO^{t}Bu, and LiOH as bases (entries 1-3). The undesirable chlorosulfonylation product was observed in good yields, higher than 65% for the rest of the bases (entries 4-8). Surprisingly, NaOH and Li_2CO_3 lead to the formation of this product almost quantitatively.

Table 21. Inorganic base screening for aminosulfonylation reaction[a].

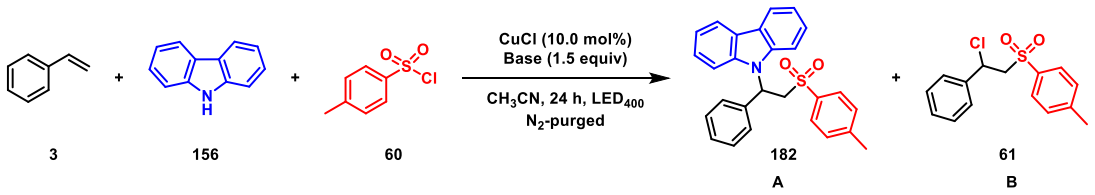

Entry	Base	Product A[b]	Product B[b]
1	LiO^{t}Bu	20 %	n.d.
2	KO^{t}Bu	10 %	n.d.
3	LiOH	20 %	n.d.
4	NaOH	n.d.	95 %
5	KOH	n.d.	83 %
6	Li_2CO_3	n.d.	99 %

7	Na_2CO_3	n.d.	65 %
8	K_2CO_3	n.d.	85 %

[a] styrene (0.2 mmol, 1.0 equiv), TsCl (0.3 mmol, 1.5 equiv), carbazole (0.3 mmol, 1.5 equiv), CuCl (10.0 mol %), Base (1.5 equiv) in CH_3CN (dry, degassed, 3 mL); Irradiation at 400 nm (LED) under N_2 atmosphere for 24 h at 20 °C. [b] ^{1}H-NMR Yield was determined using 1,1,2,2-tetrachloroethane as an internal standard.

After the unexpected behaviour of our model reaction, we varied the copper catalyst (Table 22). First, we studied several copper(I) salts, varying the halogen CuX (entry 1-3). Here, we observed the product A only when CuCl was used (entry 1). Again, we observed the product B quantitatively with CuBr and in 74 % yield for $[Cu(CH_3CN)_4]BF_4$ (entries 3-4). Then, by changing to oxidation state +2, $CuCl_2$ catalyst deliver the chlorosulfonylation product quantitatively. In order to increase the yield of the reaction, we varied the amount of the catalyst to 50 mol% and 100 mol%. Experimentally, it was observed the formation of an insoluble solid; and no reaction product was observed (entries 6-7). Increasing the time to another 24 h does not help the reaction yield (entry 8).

Table 22. Copper salt screening for aminosulfonylation reaction. [a]

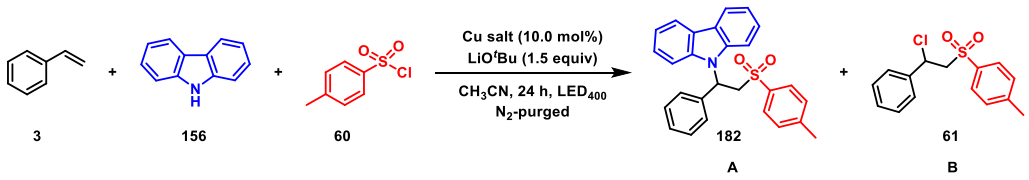

Entry	Cu salt	Product A[b]	Product B[b]
1	CuCl	20 %	n.d.
2	CuI	n.r.	n.r.
3	CuBr	n.d.	99 %
4	$[Cu(CH_3CN)_4]BF_4$	n.d.	74 %

5	$CuCl_2$	n.d.	99 %
6	50 mol % CuCl	n.r.	n.r.
7	100 mol % CuCl	n.r.	n.r.
8	CuCl (48 h)	20 %	n.d.

[a] styrene (0.2 mmol, 1.0 equiv), TsCl (0.3 mmol, 1.5 equiv), carbazole (0.3 mmol, 1.5 equiv), Copper salt (10.0 mol%), LiO^tBu (1.5 equiv) in CH_3CN (dry, degassed, 3 mL); Irradiation at 400 nm (LED) under N_2 atmosphere for 24 h at 20 °C. [b] ^{1}H-NMR Yield was determined using 1,1,2,2-tetrachloroethane as an internal standard.

As mentioned above, Gregory fu and co-workers introduced the alkylation of anilines mediated by copper photocatalysis.[101] They showed that the $CuNR^2R^3$ complex absorbs at 376 nm. On the other hand, they describe the base's importance and crucial role in the reaction, taking the chloride anion from the medium as BTPP x HCl. Based on this work, we explored two new conditions for our model reaction (Table 23). We first exposed our reaction mixture, using 10.0 mol % CuCl and 1.5 mol % of 2-tert-Butyl-1,1,3,3-tetramethylguanidine (BTMG), under irradiation at 365 nm in a nitrogen purged system for 24 hours. Using these conditions, we observed an 83 % yield for our expected product, and we did not detect the chlorosulfonylation product (entry 1). By varying the light intensity to 2W, we observed that the yield decreased to 45 % (entry 2). In the same way, by directing the reaction toward longer wavelengths, the yield remains at 55 % (entry 3-4). Unexpectedly, when we changed the irradiation system from the plate set-up to a commercial Kessil lamp, the yield dropped to traces, showing that the irradiated source is crucial. The reaction cannot be carried out without light (entry 6), and when the reaction time is prolonged until 48 h, the yield drops slightly by 5% (entry 7). We also analysed the nature and behaviour of other organic bases; 1,1,3,3-tetramethylguanidine (TMG) base forms 45 % of the chlorosulfonylation product and inhibits the formation of the multi-component product. DBU or

BTPP do not lead to the formation of any product (entry 9-10). This demonstrates the discrimination of our system for several bases and determines the unique relationship that can be established with copper and BTMG through the formation of a complex. Nevertheless, more studies are required to determine this behaviour.

Table 23. Control experiments for aminosulfonylation reaction using organic base conditions[a].

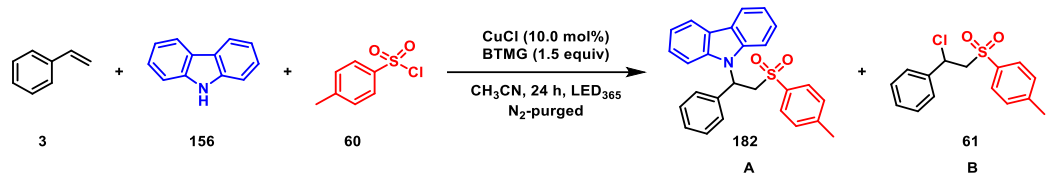

Entry	Variation of condition	Product A[b]	Product B[b]
1	None	83 %	n.d.
2	365 nm (2W)	45 %	n.r.
3	380 nm	56 %	n.d.
4	400 nm	55 %	n.d.
5	Kessil Lamp	traces	n.d.
6	No light	n.r.	n.r.
7	48 h	79 %	n.d.
8	TMG instead of BTMG	traces	45 %
9	DBU instead of BTMG	n.d.	n.d.
10	BTPP instead of BTMG	n.d.	n.d.

[a] styrene (0.2 mmol, 1.0 equiv), TsCl (0.3 mmol, 1.5 equiv), carbazole (0.3 mmol, 1.5 equiv), Copper salt (10.0 mol%), BTMG (1.5 equiv) in CH_3CN (dry, degassed, 3 mL); Irradiation at 400 nm (LED) under N_2 atmosphere for 24 h at 20 °C. [b] ^{1}H-NMR Yield was determined using 1,1,2,2-tetrachloroethane as an internal standard.

To fully understand the mechanism of our reaction, we performed two experiments to rule out that our reaction can be proceeding by nucleophilic aromatic substitution. This, since the literature has shown that copper leads to the formation of the ATRA chlorosulfonylation product.[21,41,63] With this intention, we have mixed carbazole (1.0 equiv) and the chlorosulfonylation product (1.0 equiv) in the presence of 1.5 equivalents of BTMG without copper chloride in two different conditions: at 365 nm and without light. In both cases, we did not observe the formation of our expected product. With this result, we can settle that, using our conditions, the chlorosulfonylation product is not formed in a first step, and the nucleophilic attack of the carbazole anion is not way to replace the chlorine atom.

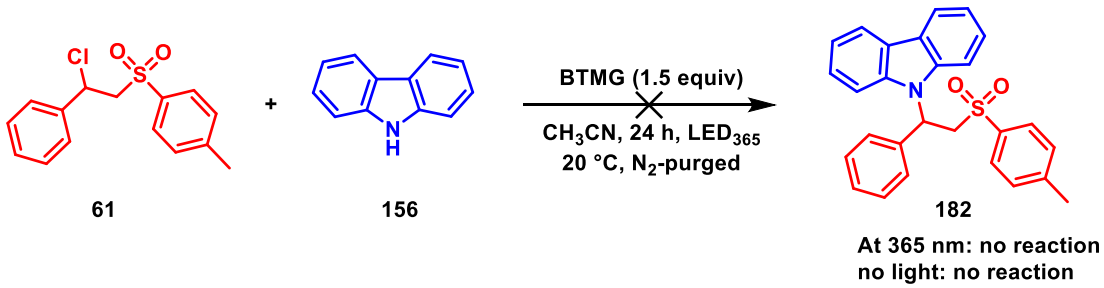

Scheme 31. Nucleophilic substitution experiments

At this point, the proposed mechanism consists of an initial ligand exchange step with the nucleophile, forming the Cu^{I}-NR^2R^3 complex. The nucleophilic site within a π system like carbazole might be a key to the viability of the photoexcitation of the Cu^{I}-amido complex. This intermediate in an excited state would reduce the tosyl chloride derivative to afford a radical Ts and Cu^{II}-NR^2R^3. In this stage, the chlorine anion should be trapped by the BTMG base, forming BTMG x HCl, and avoiding the chlorosulfonylation product. Then, the radical adds to the olefin, generating a new radical intermediate. Lastly, this radical addition product reacts with $Cu^{II}NR^2R^3$, generating the Cu^{III} complexes, which undergo a reductive elimination step to afford the multicomponent product and

the regeneration of the Cu^{I} catalyst. To verify the proposed mechanism, further radical experiments need to be performed.

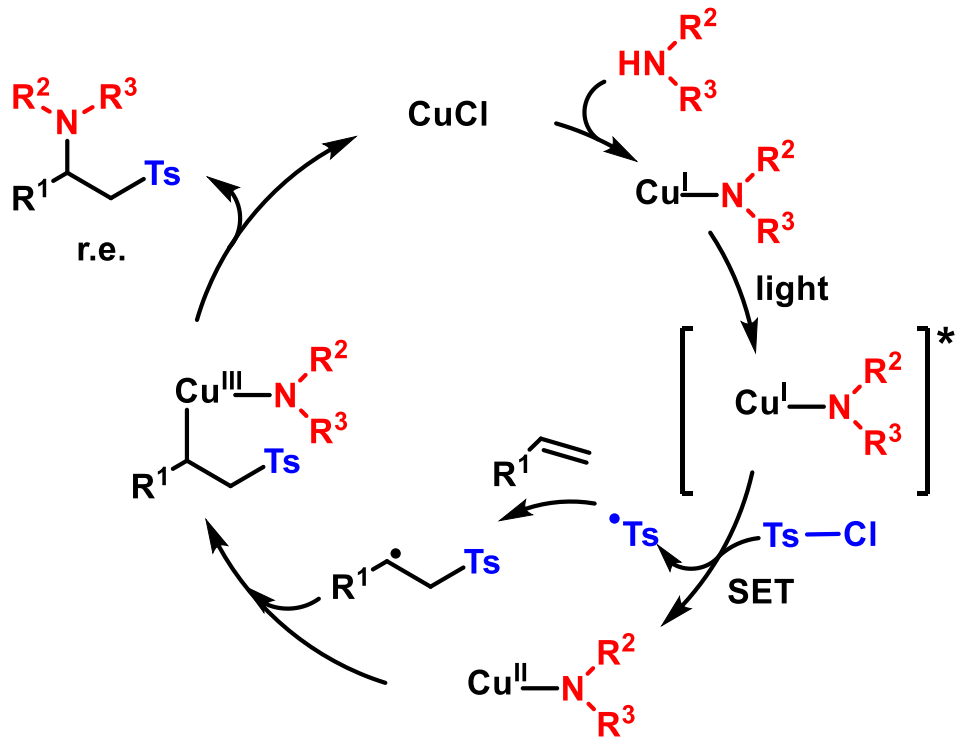

Figure 27. Proposed mechanism for aminosulfonylation of styrene derivatives.

To expand our knowledge in this reaction, we studied the behaviour of styrene derivatives. We used *p*-methoxystyrene and *p*-chlorostyrene, obtaining the multi-component products in 81 % and 52 % yield, respectively. These earliest results allow us to think that the reaction could be expanded to more substrates.

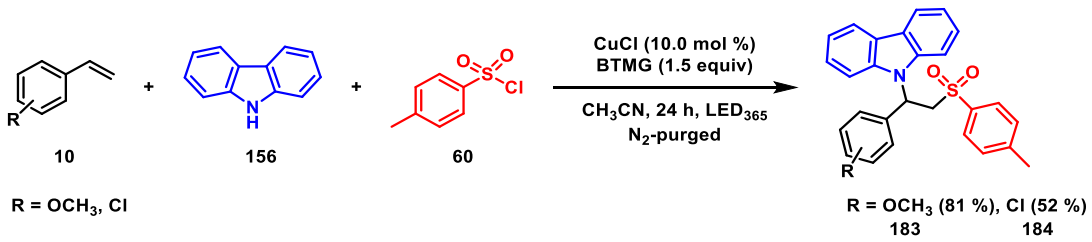

Scheme 32. Preliminary study of aminosulfonylation of styrene derivatives

CONCLUSION

10 CONCLUSIONS

- Five new heteroleptic Cu^{I} complexes containing dpa *N,N* ligand and *P,P* auxiliary ligand (**C1-5**) have been successfully synthesised, with yields between 85–95 %.
- All these complexes were structurally characterised by NMR, FT-IR, HRMS, and XRD. These characterisations are in agreement with the formation of mononuclear heteroleptic complexes.
- The electrochemical and optical characterisation of **C1-5** have been examined, and TD-DFT calculations supported and assigned the character of observed UV-Vis bands. **C1-5** exhibited redox potentials in the range 0.293–1.575 V v/s SCE, MLCT band centred around 300–370 nm, and excited-state lifetimes of 8.6–20.8 μs. The longer lifetime that has been observed for **C4** is pivotal towards profitable photocatalytic applications as demonstrated for five representative transformations, rivalling another homo- and heteroleptic Cu^{I}-photocatalysts with respect to versatility and efficiency.
- Given the facile availability of the dipyridylamine (dpa) on multigram scale, this ligand appears to be an attractive alternative to the more established and used *N,N*-diimine ligand, the 2,9-*p*-anisyl-phenanthroline (dap) ligand.
- The synthesis of dpa derivatives with aryl groups seems challenging due to the difficulty of obtaining the coupling product via nucleophilic aromatic substitution or Buchwald-Hartwig reaction.
- Cu^{II} complexes (**C6-12**) were successfully synthesised and evaluated in chlorosulfonylation and oxo-azidation reactions. Unfortunately, the results did not exceed the yields reported by $Cu(dap)Cl_2$ and $[Cu(dmp)_2Cl]Cl$. Bypirydine ligands do not seem to promise to replace phenanthroline derivatives ligands.
- Under our conditions we could not access propargyl derivatives, the

activation of *N*-alkoxyphtalimides via single electron transfer by Cu^{I}-phenylacetylide it was not successful.

- Csp^3-sp coupling was achieved, the product was obtained in 52 % yield using as model substrates (bromoethynyl)benzene and cyclohexyl Katryzky salt, with DIPEA and HeH in the reaction mixture.
- The generation of radicals in alkanes employing HAT techniques was tricky, and it was impossible to avoid the homocoupling product of phenylacetylene despite utilizing different sterically hindered ligands. For cyclohexane and phenylacetylene, using $Cu(OAc)_2$ and DTBP under irradiation at 385 nm, a maximum yield of 26 % was obtained. The low performance achieved makes this strategy unattractive to incorporate into organic chemical tools.
- Finally, we discovered a multicomponent aminosulfonylation reaction of styrenes, using light and catalyzed by CuCl. The substrates carbazole and tosyl chloride were the model reaction and showed that the BTMG base's role is crucial. This pathway appears to be robust and could activate other substrates.

REFERENCES

[1] D. M. Schultz, T. P. Yoon, *Science (80-.).* **2014**, *343*, DOI 10.1126/science.1239176.
[2] P. E. Brockway, A. Owen, L. I. Brand-Correa, L. Hardt, *Nat. Energy* **2019**, *4*, 612–621.
[3] B. König, *European J. Org. Chem.* **2017**, *2017*, 1979–1981.
[4] S. H. Kung, S. Lund, A. Murarka, D. McPhee, C. J. Paddon, *Front. Plant Sci.* **2018**, *9*.
[5] J. M. R. Narayanam, C. R. J. Stephenson, *Chem. Soc. Rev.* **2011**, *40*, 102–113.
[6] L. Marzo, S. K. Pagire, O. Reiser, B. König, *Angew. Chemie - Int. Ed.* **2018**, *57*, 10034–10072.
[7] A. Rosas-Hernández, C. Steinlechner, H. Junge, M. Beller, *Green Chem.* **2017**, *19*, 2356–2360.
[8] M. Zhong, X. Pannecoucke, P. Jubault, T. Poisson, *Beilstein J. Org. Chem.* **2020**, *16*, 451–481.
[9] V. Srivastava, P. P. Singh, *RSC Adv.* **2017**, *7*, 31377–31392.
[10] C. B. Larsen, O. S. Wenger, *Chem. - A Eur. J.* **2018**, *24*, 2039–2058.
[11] C. K. Prier, D. A. Rankic, D. W. C. MacMillan, *Chem. Rev.* **2013**, *113*, 5322–5363.
[12] Y. Zhang, M. Schulz, M. Wächtler, M. Karnahl, B. Dietzek, *Coord. Chem. Rev.* **2018**, *356*, 127–146.
[13] M. J. Leitl, F. R. Küchle, H. A. Mayer, L. Wesemann, H. Yersin, *J. Phys. Chem. A* **2013**, *117*, 11823–11836.
[14] C. Sandoval-Pauker, G. Molina-Aguirre, B. Pinter, *Polyhedron* **2021**, *199*, 115105.
[15] M. Pirtsch, S. Paria, T. Matsuno, H. Isobe, O. Reiser, *Chem. - A Eur. J.* **2012**, *18*, 7336–7340.
[16] A. C. Hernandez-Perez, S. K. Collins, *Acc. Chem. Res.* **2016**, *49*, 1557–1565.
[17] B. M. Bhanage, O. Reiser, G. Kachkovskyi, D. B. Bagal, M. Knorn, T. Rawner, *Angew. Chemie Int. Ed.* **2015**, *54*, 6999–7002.
[18] X. J. Tang, W. R. Dolbier, *Angew. Chemie - Int. Ed.* **2015**, *54*, 4246–4249.
[19] T. Rawner, M. Knorn, E. Lutsker, A. Hossain, O. Reiser, *J. Org. Chem.* **2016**, *81*, 7139–7147.
[20] T. Rawner, E. Lutsker, C. A. Kaiser, O. Reiser, *ACS Catal.* **2018**, *8*, 3950–3956.
[21] A. Hossain, S. Engl, E. Lutsker, O. Reiser, *ACS Catal.* **2019**, *9*, 1103–1109.
[22] S. Engl, O. Reiser, *ACS Catal.* **2020**, *10*, 9899–9906.
[23] A. Hossain, A. Vidyasagar, C. Eichinger, C. Lankes, J. Phan, J. Rehbein, O. Reiser, *Angew. Chemie - Int. Ed.* **2018**, *57*, 8288–8292.

[24] V. O. Smirnov, A. S. Maslov, V. A. Kokorekin, A. A. Korlyukov, A. D. Dilman, *Chem. Commun.* **2018**, *54*, 2236–2239.
[25] M. M. Cetin, R. T. Hodson, C. R. Hart, D. B. Cordes, M. Findlater, D. J. Casadonte, A. F. Cozzolino, M. F. Mayer, *Dalt. Trans.* **2017**, *46*, 6553–6569.
[26] Y. Y. Ng, L. J. Tan, S. M. Ng, Y. T. Chai, R. Ganguly, Y. Du, E. K. L. Yeow, H. Sen Soo, *ACS Catal.* **2018**, *8*, 11277–11286.
[27] T. Földesi, G. Sipos, R. Adamik, B. Nagy, B. L. Tóth, A. Bényei, K. J. Szekeres, G. G. Láng, A. Demeter, T. J. Peelen, Z. Novák, *Org. Biomol. Chem.* **2019**, *17*, 8343–8347.
[28] A. R. Cabrera, I. A. Gonzalez, D. Cortés-Arriagada, M. Natali, H. Berke, C. G. Daniliuc, M. B. Camarada, A. Toro-Labbé, R. S. Rojas, C. O. Salas, *RSC Adv.* **2016**, *6*, 5141–5153.
[29] I. A. González, M. A. Henríquez, D. Cortés-Arriagada, M. Natali, C. G. Daniliuc, P. Dreyse, J. Maze, R. S. Rojas, C. O. Salas, A. R. Cabrera, *New J. Chem.* **2018**, *42*, 12576–12586.
[30] M. Knorn, T. Rawner, R. Czerwieniec, O. Reiser, *ACS Catal.* **2015**, *5*, 5186–5193.
[31] C. Minozzi, J. C. Grenier-Petel, S. Parisien-Collette, S. K. Collins, *Beilstein J. Org. Chem.* **2018**, *14*, 2730–2736.
[32] C. Minozzi, A. Caron, J. C. Grenier-Petel, J. Santandrea, S. K. Collins, *Angew. Chemie - Int. Ed.* **2018**, *57*, 5477–5481.
[33] M. Alkan-Zambada, X. Hu, *Cu Photoredox Catalysts Supported by a 4,6-Disubstituted 2,2'-Bipyridine Ligand: Application in Chlorotrifluoromethylation of Alkenes*, **2018**.
[34] M. Alkan-Zambada, X. Hu, *Cu-Catalyzed Photoredox Chlorosulfonation of Alkenes and Alkynes*, **2019**.
[35] S. Y. Woo, J. H. Kim, M. K. Moon, S. H. Han, S. K. Yeon, J. W. Choi, B. K. Jang, H. J. Song, Y. G. Kang, J. W. Kim, J. Lee, D. J. Kim, O. Hwang, K. D. Park, *J. Med. Chem.* **2014**, *57*, 1473–1487.
[36] D. C. Meadows, J. Gervay-Hague, *Med. Res. Rev.* **2006**, *26*, 793–814.
[37] C. Cruché, W. Neiderer, S. K. Collins, *ACS Catal.* **2021**, *11*, 8829–8836.
[38] Q. A. Wu, C. C. Ren, F. Chen, T. Q. Wang, Y. Zhang, X. F. Liu, J. Bin Chen, S. P. Luo, *Tetrahedron Lett.* **2021**, *72*, 153091.
[39] J. Sosoe, C. Cruché, É. Morin, S. K. Collins, *Can. J. Chem.* **2020**, *98*, 461–465.
[40] A. Caron, É. Morin, S. K. Collins, *ACS Catal.* **2019**, *9*, 9458–9464.
[41] S. Engl, O. Reiser, *Making Copper Photocatalysis Even More Robust and Economic: Photoredox Catalysis with [CuII(Dmp)2Cl]Cl*, **2019**.
[42] T. Rawner, **2016**.
[43] B. Antonioli, D. J. Bray, J. K. Clegg, K. Gloe, K. Gloe, O. Kataeva, L. F. Lindoy, J. C. McMurtrie, P. J. Steel, C. J. Sumby, M. Wenzel, *J. Chem. Soc. Dalt. Trans.* **2006**, 4783–4794.
[44] S. Fakih, C. T. Wing, D. Eierhoff, C. Mock, B. Krebs, *Zeitschrift fur Anorg. und Allg. Chemie* **2005**, *631*, 1397–1402.

[45] P. Štarha, Z. Dvořák, Z. Trávníček, *J. Organomet. Chem.* **2018**, *872*, 114–122.
[46] S. Wang, C. Bruneau, J.-L. Renaud, S. Gaillard, C. Fischmeister, *Dalt. Trans.* **2019**, DOI 10.1039/c9dt02165e.
[47] M. Vaquero, A. Ruiz-Riaguas, M. Martínez-Alonso, F. A. Jalón, B. R. Manzano, A. M. Rodríguez, G. García-Herbosa, A. Carbayo, B. García, G. Espino, *Chem. - A Eur. J.* **2018**, *24*, 10662–10671.
[48] M. Elie, F. Sguerra, F. Di Meo, M. D. Weber, R. Marion, A. Grimault, J. F. Lohier, A. Stallivieri, A. Brosseau, R. B. Pansu, J. L. Renaud, M. Linares, M. Hamel, R. D. Costa, S. Gaillard, *ACS Appl. Mater. Interfaces* **2016**, *8*, 14678–14691.
[49] A. Kaeser, M. Mohankumar, J. Mohanraj, F. Monti, M. Holler, J.-J. Cid, O. Moudam, I. Nierengaten, L. Karamazin-Berlot, C. Duhayon, B. Delavaux-Nicot, N. Armaroli, J.-F. Nierengarten, *Inorg. Chem.* **2013**, *52*, 12140–12151.
[50] L. Yang, D. R. Powell, R. P. Houser, *J. Chem. Soc. Dalt. Trans.* **2007**, 955–964.
[51] N. Armaroli, G. Accorsi, G. Bergamini, P. Ceroni, M. Holler, O. Moudam, C. Duhayon, B. Delavaux-Nicot, J. F. Nierengarten, *Inorganica Chim. Acta* **2007**, *360*, 1032–1042.
[52] T. M. Cormick, W. Jia, S. Wang, V. Uni, K. L. Canada, **2006**, *45*, 147–155.
[53] A. Listorti, G. Accorsi, Y. Rio, N. Armaroli, O. Moudam, A. Gégout, B. Delavaux-Nicot, M. Holler, J. F. Nierengarten, *Inorg. Chem.* **2008**, *47*, 6254–6261.
[54] H. Kunkely, V. Pawlowski, A. Vogler, *Inorg. Chem. Commun.* **2008**, *11*, 1003–1005.
[55] K. Matsuo, E. Yamaguchi, A. Itoh, *Asian J. Org. Chem.* **2018**, *7*, 2435–2438.
[56] S. K. Parida, T. Mandal, S. Das, S. K. Hota, S. De Sarkar, S. Murarka, *ACS Catal.* **2021**, *11*, 1640–1683.
[57] S. Gaillard, M. K. Elmkaddem, C. Fischmeister, C. M. Thomas, J. L. Renaud, *Tetrahedron Lett.* **2008**, *49*, 3471–3474.
[58] D. S. Patil, K. K. Sonigara, M. M. Jadhav, K. C. Avhad, S. Sharma, S. S. Soni, N. Sekar, *New J. Chem.* **2018**, *42*, 4361–4371.
[59] R. Marion, F. Sguerra, F. Di Meo, E. Sauvageot, J. F. Lohier, R. Daniellou, J. L. Renaud, M. Linares, M. Hamel, S. Gaillard, *Inorg. Chem.* **2014**, *53*, 9181–9191.
[60] X. Zhang, D. Qi, C. Jiao, X. Liu, G. Zhang, *Nat. Commun.* **2021**, *12*, 1–9.
[61] Z. Y. Song, C. L. Zhang, S. Ye, *Org. Biomol. Chem.* **2019**, *17*, 181–185.
[62] Y. Mao, W. Zhao, S. Lu, L. Yu, Y. Wang, Y. Liang, S. Ni, Y. Pan, *Chem. Sci.* **2020**, *11*, 4939–4947.
[63] M. A. Henriquez, S. Engl, P. Jaque, I. A. Gonzalez, M. Natali, O. Reiser, A. R. Cabrera, *Eur. J. Inorg. Chem.* **2021**, *2021*, 4020–4029.
[64] A. Sagadevan, A. Ragupathi, K. C. Hwang, *Angew. Chemie* **2015**, *127*,

14102–14107.
[65] A. Sagadevan, V. P. Charpe, A. Ragupathi, K. C. Hwang, *J. Am. Chem. Soc.* **2017**, *139*, 2896–2899.
[66] V. P. Charpe, A. Sagadevan, K. C. Hwang, *Green Chem.* **2020**, *22*, 4426–4432.
[67] A. Ragupathi, A. Sagadevan, C. C. Lin, J. R. Hwu, K. C. Hwang, *Chem. Commun.* **2016**, *52*, 11756–11759.
[68] A. Sagadevan, A. Ragupathi, C. C. Lin, J. R. Hwu, K. C. Hwang, *Green Chem.* **2015**, *17*, 1113–1119.
[69] A. Sagadevan, V. K. K. Pampana, K. C. Hwang, *Angew. Chemie - Int. Ed.* **2019**, *58*, 3838–3842.
[70] A. Ragupathi, A. Sagadevan, V. P. Charpe, C. C. Lin, J. R. Hwu, K. C. Hwang, *Chem. Commun.* **2019**, *55*, 5151–5154.
[71] A. Sagadevan, K. C. Hwang, *Adv. Synth. Catal.* **2012**, *354*, 3421–3427.
[72] A. Hazra, M. T. Lee, J. F. Chiu, G. Lalic, *Angew. Chemie - Int. Ed.* **2018**, *57*, 5492–5496.
[73] X. Li, M. Jiang, X. Zhu, X. Song, Q. Deng, J. Lv, D. Yang, *Org. Chem. Front.* **2022**, *9*, 386–393.
[74] J. Chen, B. Q. He, P. Z. Wang, X. Y. Yu, Q. Q. Zhao, J. R. Chen, W. J. Xiao, *Org. Lett.* **2019**, *21*, 4359–4364.
[75] Y. Zhang, D. Zhang, *J. Org. Chem.* **2020**, *85*, 3213–3223.
[76] Y. Zhang, Y. Sun, B. Chen, M. Xu, C. Li, D. Zhang, G. Zhang, *Org. Lett.* **2020**, *22*, 1490–1494.
[77] J. T. José, V. A. Fernandes, B. T. Matsuo, J. A. C. Delgado, W. C. De Souza, M. W. Paixão, *Chem. Commun.* **2020**, *56*, 503–514.
[78] M. Ociepa, J. Turkowska, D. Gryko, *ACS Catal.* **2018**, *8*, 11362–11367.
[79] Z. Ye, Y. M. Lin, L. Gong, *European J. Org. Chem.* **2021**, *2021*, 5545–5556.
[80] Z. Q. Song, Z. Liu, Q. C. Gan, T. Lei, C. H. Tung, L. Z. Wu, *Org. Lett.* **2020**, *22*, 832–836.
[81] S. M. Treacy, T. Rovis, *J. Am. Chem. Soc.* **2021**, *143*, 2729–2735.
[82] Y. W. Zheng, R. Narobe, K. Donabauer, S. Yakubov, B. König, *ACS Catal.* **2020**, *10*, 8582–8589.
[83] C. Wang, Y. Yu, W. L. Liu, W. L. Duan, *Org. Lett.* **2019**, *21*, 9147–9152.
[84] G. Zhang, H. Yi, G. Zhang, Y. Deng, R. Bai, H. Zhang, J. T. Miller, A. J. Kropf, E. E. Bunel, A. Lei, *J. Am. Chem. Soc.* **2014**, *136*, 924–926.
[85] R. Bai, G. Zhang, H. Yi, Z. Huang, X. Qi, C. Liu, J. T. Miller, A. J. Kropf, E. E. Bunel, Y. Lan, A. Lei, *J. Am. Chem. Soc.* **2014**, *136*, 16760–16763.
[86] D. Domyati, R. Latifi, L. Tahsini, *J. Organomet. Chem.* **2018**, *860*, 98–105.
[87] X. Y. Dong, Y. F. Zhang, C. L. Ma, Q. S. Gu, F. L. Wang, Z. L. Li, S. P. Jiang, X. Y. Liu, *Nat. Chem.* **2019**, *11*, 1158–1166.
[88] S. Engl, O. Reiser, *Chem. Soc. Rev.* **2022**, *3*, DOI 10.1039/d2cs00303a.
[89] G. Fumagalli, P. T. G. Rabet, S. Boyd, M. F. Greaney, *Angew. Chemie - Int. Ed.* **2015**, *54*, 11481–11484.

[90] H. Liu, Q. Guo, C. Chen, M. Wang, Z. Xu, *Org. Chem. Front.* **2018**, *5*, 1522–1526.
[91] J. He, C. Chen, G. C. Fu, J. C. Peters, *ACS Catal.* **2018**, *8*, 11741–11748.
[92] Z. Liu, H. Chen, Y. Lv, X. Tan, H. Shen, H. Z. Yu, C. Li, *J. Am. Chem. Soc.* **2018**, *140*, 6169–6175.
[93] Q. Guo, M. Wang, Q. Peng, Y. Huo, Q. Liu, R. Wang, Z. Xu, *ACS Catal.* **2019**, *9*, 4470–4476.
[94] J. Bariwal, E. Van Der Eycken, *Chem. Soc. Rev.* **2013**, *42*, 9283–9303.
[95] J. Luo, W. T. Wei, *Adv. Synth. Catal.* **2018**, *360*, 2076–2086.
[96] Y.-N. Zheng, H. Zheng, T. Li, W.-T. Wei, *ChemSusChem* **2021**, *14*, 5340–5358.
[97] S. E. Creutz, K. J. Lotito, G. C. Fu, J. C. Peters, *Science (80-.).* **2012**, *338*, 647–651.
[98] J. C. Peters, G. C. Fu, **2016**, *351*, 681–685.
[99] W. Zhao, R. P. Wurz, J. C. Peters, G. C. Fu, *J. Am. Chem. Soc.* **2017**, *139*, 12153–12156.
[100] Y. Xiong, G. Zhang, *Org. Lett.* **2019**, *21*, 7873–7877.
[101] H. Cho, H. Suematsu, P. H. Oyala, J. C. Peters, G. C. Fu, *J. Am. Chem. Soc.* **2022**, *144*, 4550–4558.
[102] G. N. Li, H. C. Li, Z. Lu, B. Yu, *Org. Biomol. Chem.* **2022**, 1–4.
[103] Y. Xiong, X. Ma, G. Zhang, *Org. Lett.* **2019**, *21*, 1699–1703.
[104] H. Narode, M. Gayke, G. Eppa, J. S. Yadav, *Org. Process Res. Dev.* **2021**, *25*, 1512–1523.
[105] J. F. Syu, B. Gopula, J. H. Jian, W. S. Li, T. S. Kuo, P. Y. Wu, J. P. Henschke, M. C. Hsieh, M. K. Tsai, H. L. Wu, *Org. Lett.* **2019**, *21*, 4614–4618.
[106] A. Jana, G. K. Zieliński, S. Czarnocka-Śniadała, K. Grudzień, D. Podwysocka, M. Szulc, A. Kajetanowicz, K. Grela, *ChemCatChem* **2019**, *11*, 5808–5813.
[107] C. D. Matier, J. Schwaben, J. C. Peters, G. C. Fu, *J. Am. Chem. Soc.* **2017**, *139*, 17707–17710.
[108] J. M. Ahn, T. S. Ratani, K. I. Hannoun, G. C. Fu, J. C. Peters, *J. Am. Chem. Soc.* **2017**, *139*, 12716–12723.
[109] H. Lee, J. M. Ahn, P. H. Oyala, C. Citek, H. Yin, G. C. Fu, J. C. Peters, *J. Am. Chem. Soc.* **2022**, *144*, 4114–4123.
[110] A. Bartoszewicz, C. D. Matier, G. C. Fu, *J. Am. Chem. Soc.* **2019**, *141*, 14560–14564.
[111] S. Q. Guo, H. Q. Yang, A. L. Wang, Y. Z. Jiang, G. Q. Xu, Y. C. Luo, Z. X. Chen, P. F. Xu, *Green Chem.* **2021**, *23*, 9571–9576.
[112] D. B. G. Williams, M. Lawton, *J. Org. Chem.* **2010**, *75*, 8351–8354.
[113] G. M. Sheldrick, *Acta Crystallogr. Sect. A Found. Crystallogr.* **2015**, *71*, 3–8.
[114] O. V. Dolomanov, L. J. Bourhis, R. J. Gildea, J. A. K. Howard, H. Puschmann, *J. Appl. Crystallogr.* **2009**, *42*, 339–341.
[115] G. M. Sheldrick, *Acta Crystallogr. Sect. C Struct. Chem.* **2015**, *71*, 3–8.

[116] G. F. Pauli, S. N. Chen, C. Simmler, D. C. Lankin, T. Gödecke, B. U. Jaki, J. B. Friesen, J. B. McAlpine, J. G. Napolitano, *J. Med. Chem.* **2014**, *57*, 9220–9231.

[117] M. J. Frisch, G. W. Trucks, H. B. Schlegel, G. E. Scuseria, M. a. Robb, J. R. Cheeseman, G. Scalmani, V. Barone, G. a. Petersson, H. Nakatsuji, X. Li, M. Caricato, a. V. Marenich, J. Bloino, B. G. Janesko, R. Gomperts, B. Mennucci, H. P. Hratchian, J. V. Ortiz, a. F. Izmaylov, J. L. Sonnenberg, Williams, F. Ding, F. Lipparini, F. Egidi, J. Goings, B. Peng, A. Petrone, T. Henderson, D. Ranasinghe, V. G. Zakrzewski, J. Gao, N. Rega, G. Zheng, W. Liang, M. Hada, M. Ehara, K. Toyota, R. Fukuda, J. Hasegawa, M. Ishida, T. Nakajima, Y. Honda, O. Kitao, H. Nakai, T. Vreven, K. Throssell, J. a. Montgomery Jr., J. E. Peralta, F. Ogliaro, M. J. Bearpark, J. J. Heyd, E. N. Brothers, K. N. Kudin, V. N. Staroverov, T. a. Keith, R. Kobayashi, J. Normand, K. Raghavachari, a. P. Rendell, J. C. Burant, S. S. Iyengar, J. Tomasi, M. Cossi, J. M. Millam, M. Klene, C. Adamo, R. Cammi, J. W. Ochterski, R. L. Martin, K. Morokuma, O. Farkas, J. B. Foresman, D. J. Fox, **2016**, Gaussian 16, Revision C.01, Gaussian, Inc., Wallin.

METHODOLOGY

11 METHODOLOGY

11.1 General Techniques

Ligands were synthesised using standard techniques such as Schlenk and reflux. In some cases, the anhydrous solvent and nitrogen atmosphere were used. Furthermore, these were purified using silica gel chromatographic techniques. Using anhydrous solvents, the complexes were synthesised using Schlenk techniques under an inert nitrogen atmosphere.

11.2 Drying of solvents and reagents

All solvents and reagents used were dried using the procedures described in the literature. [112]

11.3 Commercial Reagents

- The synthesis of ligands and complexes were developed using commercially available reagents or precursors.

11.4 Characterisation of ligands and complexes

Ligands and complexes were characterised by the following techniques and instruments:

- NMR: Bruker Advance 400 (^{1}H: 400 MHz, ^{13}C: 100 MHz, ^{19}F: 400 MHz, ^{11}B: 125 MHz, ^{31}P 161 MHz).
- FT-IR spectra were performed on a Bruker Vector-22 Spectrophotometer using KBr as a dispersant.
- HRMS-ESI-MS experiments were carried out using a Thermo Scientific Exactive Plus Orbitrap Spectrometer

- X-ray diffraction: X-ray crystallographic analyses were performed using an Agilent Technologies SuperNova, an Agilent Technologies Gemini R Ultra, an Agilent GV 50 or a Rigaku GV 50 diffractometer. Single source at offset/far, Atlas diffractometer. The crystal was kept at a steady T = 123.00(10) K during data collection. The structure was solved with the ShelXT[113] structure solution program using the dual solution method and by using Olex2[114] as the graphical interface. The model was refined with version 2018/3 of ShelXL[115] using Least Squares minimisation by the Central Analytic Department of the University of Regensburg.

11.5 Evaluation of optoelectronic properties

- Evaluation of electrochemical and photophysical properties of the synthesised complexes was performed at varying concentrations in solution and using CH_2Cl_2 or CH_3CN as a solvent

11.5.1 UV-visible spectroscopy: UV absorption spectra were recorded on a Jasco V-570 UV/Vis/NIR spectrophotometer

11.5.2 Emission spectroscopy: Photoluminescence spectra were taken on an Edinburgh Instrument spectrofluorimeter. Emission lifetimes were taken on a laser flash photolysis apparatus comprised of a Continuum Surelite II Nd: YAG laser (excitation at 355 nm, FWHM = 6-8 ns, was provided by THG from the 1064-nm fundamental). The light emitted by the sample was focused onto the entrance slit of a 300 mm focal length Acton SpectraPro 2300i triple grating, flat field, and double exit monochromator equipped with a photomultiplier detector (Hamamatsu R3896). Signals from the photomultiplier were processed by means of a TeledyneLeCroy 604Zi (400 MHz, 20 GS/s) digital oscilloscope. CH_2Cl_2 solutions of metal complexes **C1-4** were degassed by three freeze-pump-thaw cycles before steady-state and time-resolved

emission measurements

11.5.3 Voltammetry cyclic: The cyclic voltammograms were recorded using a PalmSens 3 Instruments Potentiostat. Using three electrodes: a platinum disc working electrode with an area of 0.02 cm^2, a saturated Ag/AgCl as a reference electrode and a platinum wire counter electrode. All electrochemical measurements were carried out in anhydrous dichloromethane solutions of Cu(I) complexes (1 mM) with tetrabutylammonium hexafluorophosphate ($TBAPF_6$) (0.1 M) as the supporting electrolyte at a scan rate of 0.1 V s^{-1}

11.6 Photocatalytic experimental set-up

11.6.1 Schlenk set-up

The evaluation of the photocatalytic activity for **C1-5** was carried out in a Schlenk set-up system (Figure 28), which was loaded with the substrates, catalyst, magnetic bar, solvent and a glass rod that allows contact between the LED light (1W: standard, 2W HP) over the glass stick with the reaction mixture.

- a) open Schlenk system b) close Schlenk system c) Schlenk for gram scale

- 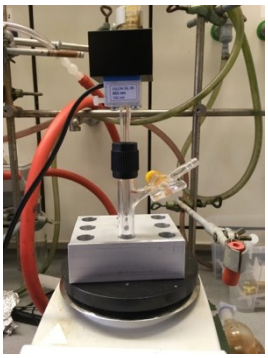

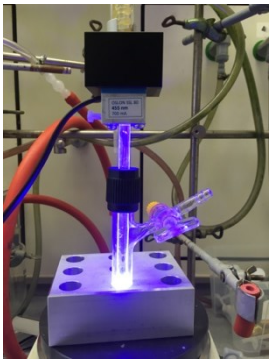

- d)Schlenk system light-off e) Schlenk system light-on

Figure 28. Schlenk set up system for photoreaction.

The photocatalytic activity of **C6-12** and the reactions of chapters II and III were evaluated in a plate system (Figure 29). The light comes from the outside (bottom), and the system has an aluminium block, which passes water inside as a cooling system to maintain the reactions from 20 °C to 25 °C. The reactions were carried out in a vial system, which was loaded with the substrates, photocatalyst, magnetic bar, solvent, and other components respectively. The vial is closed with a septum and purged for 10 -15 minutes with nitrogen. After purging is complete, the vial is left in the reactor to be exposed to light irradiation.

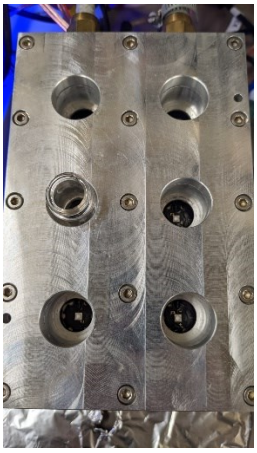

a) Light arrangement b) Aluminum block

c) Set-up ON

d) Vial and purge system

Figure 29. Plate set-up system for photoreaction.

A Kessil lamp (Figure 30) a commercial set-up was used to compare light source. the characteristics of the light source are described in Table 24.

Figure 30. Kessil lamp.

Table 24. Kessil lamp A360WE

Power Consumption	370nm (max 43W), 390nm (max 52W), 427nm & 440nm (max 45W), 456nm (max 50W), 467nm (max 44W), 525nm (max 44W)
Input Voltage	100-240 VAC

Operating Temperature	0 - 40°C / 32 - 104°F
Beam Angle	56°
Wavelength Options	370nm, 390nm, 427nm, 440nm, 456nm, 467nm, 525nm
Average Intensity of PR160 series	352mW/cm^2 (measured from 1 cm distance)
Dimensions (H x D)	4.49" x 2.48" / 11.4cm x 6.3cm

11.7 Synthesis of the compounds.

11.7.1 Synthesis of copper complexes

11.7.1.1 Synthesis of [Cu(dpa)(*P,P*)]BF_4 C1-5

The general synthetic procedure of complexes: dpa ligand (1.0 equiv) in CH_2Cl_2 was added dropwise to a solution of $[Cu(CH_3CN)_4]BF_4$ (1.0 equiv) in CH_2Cl_2 under a nitrogen atmosphere. The reaction mixture was stirred for 30 minutes at 20°C. After this time, a diphosphine ligand (1.0 equiv) solution in CH_2Cl_2 was added dropwise to the reaction mixture and stirred for additional 30 minutes. Finally, the solvent was removed under vacuum, and the crude product was purified by crystallization using a CH_2Cl_2/ Toluene mixture at – 20 °C.

11.7.1.2 Synthesis of [Cu(*N,N*)$_2$Cl]Cl C6-12

The general synthetic procedure of complexes: *N,N* ligand (2.0 equiv) and $CuCl_2$ (1.0 equiv) were dissolved in ethanol. The reaction mixture was stirred for 4 hours at room temperature (20 - 25 °C). After this time, the formed precipitate was filtered off and washed with ethanol. The solid was dried under a vacuum.

11.7.2 General procedures for photocatalytic studies.

11.7.2.1 General ATRA test reaction:

A 10.0 mL flame-dried Schlenk tube with a magnetic stirring bar was charged with CBr_4 (0.5 mmol), copper catalyst (1.0 mol%), and 3.0 mL of CH_3CN anhydrous solvent sealed with a screwcap and subsequently degassed by three consecutive freeze-pump-thaw cycles. Afterwards, alkene (0.5 mmol) was added under N_2, and the screwcap was replaced with a Teflon sealed inlet for a glass rod, through which irradiation with LED (455 nm) took place from above. At the same time, the reaction mixture was magnetically stirred at 20 °C for 24 h. The reaction was monitored by TLC. Then, the volatiles were removed, and the crude was concentrated. The residue was purified by flash chromatography on silica gel (eluent hexanes/ethyl acetate, 9:1).

Comment: For product determination using NMR, the crude concentrate was added an internal standard (1.3.5-trimethoxybenzene) and then dissolved in $CDCl_3$. The yield was determined according to the methods reported in the literature.[116]

For gram-scale reaction, the weight of the components was increased by a factor of ten, resulting in a 5.0 mmol scale of limiting substrate. The reaction was performed in a Schlenk tube (25.0 mL size: Figure 8c) with the same irradiation source.

11.7.2.2 Chlorosulfonylation reaction over alkene:

A 10.0 mL flame-dried Schlenk tube with a magnetic stirring bar was charged with TsCl (0.5 mmol), $[Cu(dpa)(S\text{-}BINAP)]BF_4$ (1 mol%), and 3 mL of CH_3CN: CH_2Cl_2 (1.5 mL: 1.5 mL) anhydrous solvent, sealed with a screwcap and subsequently degassed by three consecutive freeze-pump thaw cycles. Afterwards, alkene (0.5 mmol) was added under N_2, and the screwcap was replaced with a Teflon sealed inlet for a glass rod, through which irradiation

with LED (455 nm) took place from above. At the same time, the reaction mixture was magnetically stirred at 20 °C for 24 h. The reaction was monitored by TLC. Then, the volatiles were removed, and the crude was concentrated. The residue was purified by flash chromatography on silica gel (eluent hexanes/ethyl acetate, 9:1). For the evaluation of **C6-12**, the plate set-up system was used.

11.7.2.3 Chlorosulfonylation reaction over alkyne:

A 10.0 mL flame-dried Schlenk tube with magnetic stirring bar was charged with TsCl derivative (0.5 mmol), [Cu(dpa)(S-BINAP)]BF_4 (2.5 mol%), Na_2CO_3 (1.5 equiv), and 3 mL of CH_3CN:CH_2Cl_2 (1.5 mL: 1.5 mL) anhydrous solvent, sealed with a screwcap and subsequently degassed by three consecutive freeze-pump-thaw cycles. Afterwards, alkyne (0.5 mmol) was added under N_2, and the screwcap was replaced with a Teflon sealed inlet for a glass rod, through which irradiation with LED (455 nm) took place from above. At the same time, the reaction mixture was magnetically stirred at 20 °C for 24 h. The reaction was monitored by TLC. Then, the volatiles were removed, and the crude was concentrated. The residue was purified by flash chromatography on silica gel (eluent hexanes/ethyl acetate 5:1).

11.7.2.4 Appel-type reaction:

A 10.0 mL flame-dried Schlenk tube with a magnetic stirring bar was charged with tetrabromomethane (331.6 mg, 1.0 mmol, 2.0 equiv), sodium bromide (102.9 mg, 1.0 mmol, 2.0 equiv), [Cu(dpa)(S-BINAP)]BF_4 (2.0 mol%) and dissolved in anhydrous DMF (3.0 mL, 0.17 M), sealed with a screw-cap and subsequently degassed by three consecutive freeze- pump thaw cycles. Afterwards, 1-phenylethan-1-ol (8) (61.1 mg, 0.5 mmol, 1.0 equiv) was added under N_2, and the screwcap was replaced with a Teflon sealed inlet for a glass rod, through which irradiation with LED (455 nm) took place from above. At the

same time, the reaction mixture was magnetically stirred at 20 °C for 24 h. The reaction was monitored by TLC. Afterwards, the reaction mixture was quenched by adding water (10 mL) and diethyl ether (10 mL). The layers were separated, and the aqueous phase was extracted with diethyl ether (2×10 mL). The combined organic layers were washed with saturated $Na_2S_2O_3$ solution (10 mL), brine (10 mL), dried over anhydrous Na_2SO_4 and concentrated in a vacuum. The residue was purified on silica gel (hexanes) by flash column chromatography.

11.7.2.5 Decarboxylative coupling reaction:

A 10.0 mL flame-dried Schlenk tube with magnetic stirring bar was charged with 1,3- dioxoisoindolin-2-yl cyclohexanecarboxylate (136.6 mg, 0.5 mmol, 1.0 equiv), Hantzsch ester (190.0 mg, 0.75 mmol, 1.5 equiv), [Cu(dpa)(S-BINAP)]BF_4 (2.0 mol%) and dissolved in anhydrous THF (1.5 mL, 0.33 M), sealed with a screwcap and subsequently degassed by three consecutive freeze-pump-thaw cycles. Afterwards, diisopropylethylamine (129.3 mg, 1.0 mmol, 2.0 equiv) (bromoethynyl)benzene (135.8 mg, 0.75 mmol, 1.5 equiv) were added under N_2, and the screwcap was replaced with a Teflon sealed inlet for a glass rod, through which irradiation with LED (455 nm) took place from above. At the same time, the reaction mixture was magnetically stirred at 20 °C for 24 h. The reaction was monitored by TLC. Afterwards, the volatiles were removed, and the crude was concentrated. The residue was purified by flash chromatography on silica gel using as eluent hexanes.

11.8.2.6 Pinacol Type-Coupling reaction

A 10.0 mL flame-dried Schlenk tube with a magnetic stirring bar was charged with Hantzsch ester (190.0 mg, 1.0 mmol, 2.0 equiv), [Cu(dpa)(S-BINAP)]BF_4 (2.0 mol %) and dissolved in anhydrous THF (0.55 M), sealed with a screwcap,

and subsequently degassed by three consecutive freeze-pump-thaw cycles. Afterwards, dppa (5.0 mol %) and acetophenone (58.3 μL, 0.5 mmol, 1.0 equiv) were added under N_2, and the screwcap was replaced with a Teflon sealed inlet for a glass rod, through which irradiation with LED (455 nm) took place from above. At the same time, the reaction mixture was magnetically stirred at 20 °C for 24 h. The reaction was monitored by TLC. Afterwards, the volatiles were removed, and the crude was concentrated and analysed by ^{1}H-NMR.

11.7.2.7 Oxo-azidation reaction

A glass vial (5.0 mL size) equipped with a stirring bar was charged with **C6-12**, as corresponded (1.0 mol %). Then 2.0 mL CH_3CN was added followed by $TMSN_3$ (0.14 mL, 1.0 mmol, 2.0 equiv) and styrene (0.5 mmol, 1.0 equiv). Afterward, the vial was irradiated with a LED (455 nm) under air and the solution was stirred at room temperature of 25 °C for 24 h. Finally, the reaction mixture was concentrated in vacuo. The residue was purified by flash chromatography on silica gel using as eluent hexanes and ethyl acetate.

11.7.2.8 Synthesis of dpa ligand.

A 50.0 mL flame-dried Schlenk round bottom flask with a magnetic stirring bar was charged with pyridin-2-amine (470.6 mg, 5.0 mmol, 1.0 equiv), NaH (1.1 equiv), dissolved in anhydrous toluene (20 mL) and N_2-purged. Then, the reaction mixture was stirred for 30 min. Afterwards, 2-fluorpyridine (534.0 mg, 5.5 mmol, 1.1 equiv) was added under N_2, and the reaction mixture was magnetically stirred at 20 °C for 3.5 h. The reaction was monitored by TLC. Then, the volatiles were removed under vacuum. Finally, the residue was purified by flash chromatography on silica gel using petroleum ether / ethyl acetate as eluent (3:2), obtaining the dpa ligand in 81 % yield (693.3 mg, 4.05 mmol). The ^{1}H-RMN was in agreement with the data reported in literature.[58]

11.7.2.8.1 Synthesis of dpa ligand derivatives.

To develop the synthesis of dpa derivatives ligands, three different pathways were used (conditions a, b or c):

11.7.2.8.2 Synthesis of dpa ligand derivatives. Procedure A

The first step is the deprotonation of the corresponding substituted 2-aminopyridine for 1 hour with a base in a solvent such as toluene, or DMF, following the addition in situ of corresponding substituted 2-fluorpyridine, starting from room temperature to reflux. The reaction was monitored by TLC until the new compounds were observed.

11.8.2.8.3 Synthesis of dpa ligand derivatives. Procedure B

The corresponding substituted reagent (1.0 equiv) and base (1.2 equiv) were added to a microwave reaction flask using DMF as a solvent, and the reaction mixture was irradiated for 1 hour at 150 °C. The reactions were monitored by TLC until observing the consumption of the starting materials or apparition of a new compound.

11.7.2.8.4 Synthesis of dpa ligand derivatives. Procedure C

To a stirred solution of toluene, the corresponding derivative 2-aminopyridine was loaded (0.5 mmol), followed by the addition of base (1.4 equiv), and the corresponding 2-bromopyridine (1.0 equiv), then was loaded the phosphine (5.0 mol%) and Pd catalyst (5.0 mol%). The reaction mixture was stirred from 2-12 hours at 90 °C, monitored by TLC until observed consumption of the starting materials or apparition of a new compound.

11.7.2.9 Csp^3-Csp coupling

11.7.2.9.1 Propargyl reaction

Procedure A: A 10.0 mL flame-dried Schlenk tube with magnetic stirring bar was charged with 2-butoxyisoindoline-1,3-dione (54.81 mg, 0.25 mmol, 1.0 equiv), photocatalyst (10.0 mol%), L1 (20.0 mol%), K_2CO_3 (69.10 mg, 2.0 equiv) and dissolved in anhydrous DMF (2 mL), sealed with a screwcap, and subsequently degassed by three consecutive freeze-pump-thaw cycles. Afterwards, (0.25 mmol, 1.0 equiv) of phenylacetylene or (bromoethynyl)benzene was added under N_2, and the screwcap was replaced with a Teflon sealed inlet for a glass rod, through which irradiation with a LED (455 nm) took place from above. At the same time, the reaction mixture was magnetically stirred at 20 °C for 24 h. The reaction was monitored by TLC. Then, the volatiles were removed, and the crude was concentrated and analysed by ^{1}H-NMR using 1,3,5-trimethoxybenzene as an internal standard.

Procedure B: A 10.0 mL flame-dried Schlenk tube with a magnetic stirring bar was charged with 2-butoxyisoindoline-1,3-dione (54.81 mg, 0.25 mmol, 1.0 equiv), photocatalyst (2.5 mol%), HeH (75.98 mg, 0.3 mmol, 1.5 equiv) and dissolved in anhydrous DMF (2 mL), sealed with a screwcap, and subsequently degassed by three consecutive freeze-pump-thaw cycles. Afterwards, (0.25 mmol, 1.0 equiv) (bromoethynyl)benzene and DIPEA (86.9 μL, 2.0 equiv) were added under N_2, and the screwcap was replaced with a Teflon sealed inlet for a glass rod, through which irradiation with LED (455 nm) took place from above. At the same time, the reaction mixture was magnetically stirred at 20 °C for 24 h. The reaction was monitored by TLC. Then, the volatiles were removed, and the crude was concentrated and analysed by ^{1}H-NMR using 1,3,5-trimethoxybenzene as an internal standard.

11.7.2.9.2 C-C coupling via Katryzky salt

Procedure A: A 10.0 mL flame-dried Schlenk tube with a magnetic stirring bar was charged with cyclohexyl Katritzky salt (0.4 mmol, 2.0 equiv), photocatalyst (10.0 mol%), ligand (15.0 mol%) and anhydrous CH_3CN as solvent, sealed with a screwcap, and subsequently degassed by three consecutive freeze-pump-thaw cycles. Afterwards, phenylacetylene (0.2 mmol, 1.0 equiv), was added under N_2, and the screwcap was replaced with a Teflon sealed inlet for a glass rod, which irradiated with a LED (455 nm) took place from above. At the same time, the reaction mixture was magnetically stirred at 20 °C for 24 h. The reaction was monitored by TLC. Then, the volatiles were removed, and the crude was concentrated and analysed by ^{1}H-NMR using 1,3,5-trimethoxybenzene as an internal standard

Procedure B: A 10.0 mL flame-dried Schlenk tube with a magnetic stirring bar was charged with cyclohexyl Katritzky salt (0.4 mmol, 2.0 equiv), photocatalyst (2.0 mol %), HeH (1.5 equiv) and anhydrous THF as solvent (0.55 M), sealed with a screwcap, and subsequently degassed by three consecutive freeze-pump-thaw cycles. Afterwards, phenylacetylene (0.2 mmol, 1.0 equiv), and DIPEA (2.0 equiv) were added under N_2, and the screwcap was replaced with a Teflon sealed inlet for a glass rod, through which irradiation with a LED (455 nm) took place from above. At the same time, the reaction mixture was magnetically stirred at 20 °C for 24 h. The reaction was monitored by TLC. Afterwards, Then, the volatiles were removed, and the crude was concentrated and analysed by ^{1}H-NMR using 1,3,5-trimethoxybenzene as an internal standard

11.7.2.9.3 C-C coupling via HAT

A glass vial (5.0 mL size) equipped with a stirring bar was charged with catalyst

(10.0 mol%), ligand (20.0 mol%), and 3.0 mL CH_3CN as solvent. The reaction mixture was purged with N_2 followed by the addition of phenylacetylene (0.2 mmol, 1.0 equiv), cyclohexane (2.0 mmol, 10.0 equiv), DTBP (0.4 mmol, 2.0 equiv). Then, the vial was irradiated with a LED at 25 °C for 24 h. Finally, the reaction mixture concentrated in vacuo and analysed by ^{1}H-NMR using 1,1,2,2-tetrachloroethane as an internal standard.

11.7.2.9.4 C-C coupling via Dual photocatalysis pathway

A glass vial (5.0 mL size) equipped with a stirring bar was charged with **C6-12**, as corresponded (1.0 mol%). Then, 2.0 mL CH_3CN was added followed by $TMSN_3$ (0.14 mL, 1.0 mmol, 2.0 equiv), and styrene (0.5 mmol, 1.0 equiv). Afterwards, the vial was irradiated with a LED (455 nm) under air and the solution was stirred at 25 °C for 24 h. Finally, the reaction mixture is concentrated in vacuo. The residue was purified by flash chromatography on silica gel using eluent hexanes and ethyl acetate.

11.7.2.10 Aminosulfonylation of styrene

A glass vial (5.0 mL size) equipped with a stirring bar was charged with carbazole (50.16 mg, 0.3 mmol, 1.5 equiv), TsCl (57.20, 0.3 mmol, 1.5 equiv), Cu salt (10.0 mol%), base (1.5 equiv). Then 3.0 mL CH_3CN was added and purged with N2 for 10-15 min, followed by the addition of styrene (22.91 μL, 0.2 mmol, 1.0 equiv). Afterward, the vial was irradiated with a LED and the solution was stirred at room temperature of 25 °C for 24 h. Finally, the reaction mixture was concentrated in vacuo. The residue was purified by flash chromatography on silica gel using as eluent hexanes and ethyl acetate.

11.8 DFT Calculations

Fully relaxed geometry for all complexes in their ground states was carried out using the Grimme's dispersion corrected (D3) hybrid B3LYP functional (i.e., B3LYP-D3) combined with Def2SVPP double-ζ basis set. The implicit solvent effect was also taken into account in this procedure by the integral equation formalism of the polarizable continuum model (IEFPCM) using acetonitrile as solvent. All structures were confirmed as minima through the harmonic vibrational frequency calculations. The (IEFPCM)-B3LYPD3/Def2SVPP equilibrium structure has been used to compute vertical excited-states properties within the time-dependent density functional theory (TD-DFT) formalism at the level of theory. For purpose, a non-equilibrium protocol for solvation was employed to compute vertical excitation energies and oscillator strengths of electronic transitions. All calculations have been performed using Gaussian 09 suite of programs.[117]

Appendix

Synthesis and characterisation of [Cu(dpa)(*P,P*)]BF_4

General procedure:

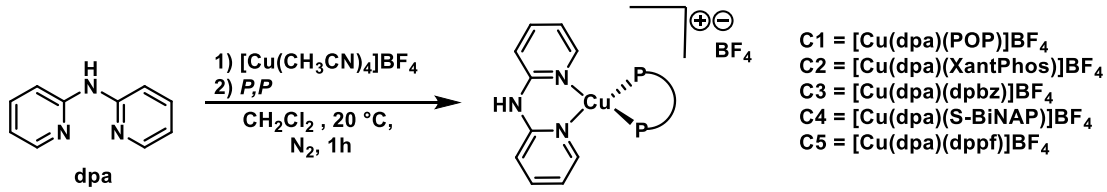

Dpa ligand (200 mg, 1.0 equiv) in CH_2Cl_2 was added dropwise to $Cu(CH_3CN)_4]BF_4$ (367.5 mg, 1.0 equiv) in CH_2Cl_2. The reaction mixture was stirred for 30 minutes at room temperature. Then, phosphine ligand (1 equiv) in CH_2Cl_2 was added dropwise to the reaction mixture and stirred for 30 minutes at room temperature. Finally, the volatiles were removed in vacuum and the crude product was purified by crystallization using CH_2Cl_2 / Toluene mixture at -20 °C.

[(di(pyridin-2-yl)amine)((Oxydi-2,1-phenylene)bis(diphenyl phosphine)) Cu^I]BF_4 (C1)

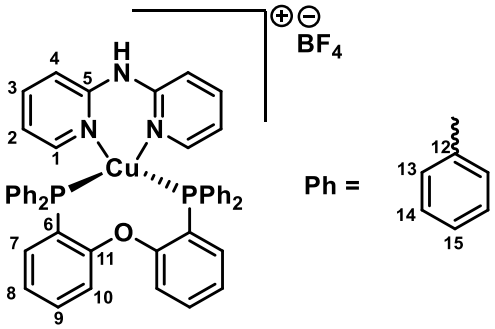

^{1}H-NMR (400 MHz, $CDCl_3$, 298 K): δ/ppm = 9.0 (s, 1H, N-H), 7.70 (dd, *J* = 5.7 Hz, 1.7 Hz, 2H, H4), 7.50 (ddd, *J* = 8.9 Hz, 7.2 Hz, 1.9 Hz, 2H, H2), 7.36 (d, *J*

= 8.3 Hz, 2H, H1), 7.34 – 7.26 (m, 6H, H15, H7), 7.23 (t, *J* = 7.5 Hz, 8H, H14), 7.13 (dt, *J* = 7.1 Hz, 5.0 Hz, 8H, H13), 7.06 – 6.98 (m, 4H, H8, H10), 6.91 – 6.85 (m, 2H, H9), 6.48 (t, *J* = 6.4 Hz, 2H, H3)

$^{13}C\{^{1}H\}$ NMR (100 MHz, $CDCl_3$, 298 K): δ/ppm = 157.8 (t, J^{C-P} = 6.2 Hz, C11), 153.8 (C5), 147.1 (C4), 138.7 (C2), 134.3 (C9), 133.2 (t, J^{C-P} = 8.2 Hz, C13), 131.7 (C7), 131.1 (t, J^{C-P} = 16.0 Hz, C6), 129.9 (C15), 128.7 (t, J^{C-P} = 4.7 Hz, C14), 125.0 (C8), 124.6 (t, J^{C-P} = 13.1 Hz, C12), 120.1 (C10), 116.8 (C3), 115.8 (C1)

^{1}H, ^{13}C-HMBC (400 MHz / 100 MHz, $CDCl_3$, 298 K) δ (^{1}H) / δ (^{13}C) =7.70 / 116.8 (H4)/(C3), 7.36 / 116.8 (H1)/(C3), 7.34 – 7.26 / 133.2 (H15)/(C13), 7.34 -7.26 / 125.0, 134.3 (H7)/(C8, C9), 7.13 / 129.9 (H13)/(C15), 7.06 – 6.98 / 120.1 (H8)/(C10), 7.06 – 6.98 / 125.0 (H10)/(C8), 6.91 – 6.85 / 131.7 (H9)/(C7), 6.48 / 115.8 (H3)/(C1)

^{1}H, ^{13}C -HSQC (400 MHz / 100 MHz, $CDCl_3$, 298 K): δ (^{1}H) / δ (^{13}C) = 7.70 / 147.1 (H4/C4), 7.50 / 138.7 (H2/C2), 7.36 / 115.8 (H1/C1), 7.23 / 128.7 (H14/C14), 7.13 / 133.2 (H13/C13), 7.06 – 6.98 / 125.0 (H8/C8), 7.06 -6.98 / 120.1 (H10/C10), 6.48 / 116.8 (H3/C3)

GCOSY (400 MHz / 400 MHz, $CDCl_3$, 298 K): δ (^{1}H) / δ (^{1}H) = (H4/H2), (H4/H3), (H2/H1), (H13/H14), (H8/H10)

^{19}F NMR (400 MHz, $CDCl_3$, 298 K): δ/ppm = -151.17 (s, BF_4)

^{11}B NMR (128 MHz, $CDCl_3$, 298 K): δ/ppm = -0.64 (s, BF_4)

$^{31}P\{1H\}$ NMR (160 MHz, $CDCl_3$, 298 K): δ/ppm = -13.37 (s, POP)

IR (KBr): n/cm^{-1} = 3384, 3055, 1635, 748, 649

HRMS(ESI): ($C_{46}H_{37}CuN_3OP_2$ $[M]^+$) = Calculated 772.1758, Found 772.1758.

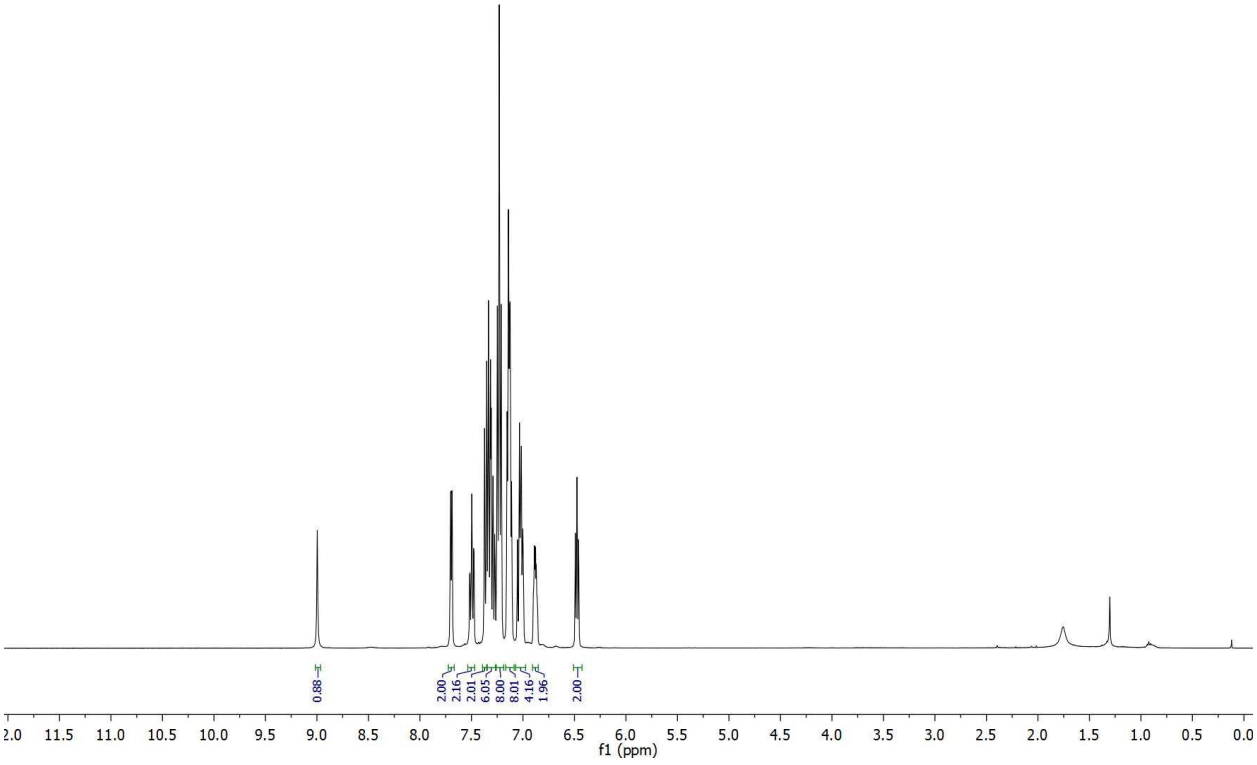

Figure A1**.** ^{1}H-NMR (400 MHz, $CDCl_3$, 298 K).of **C1**.

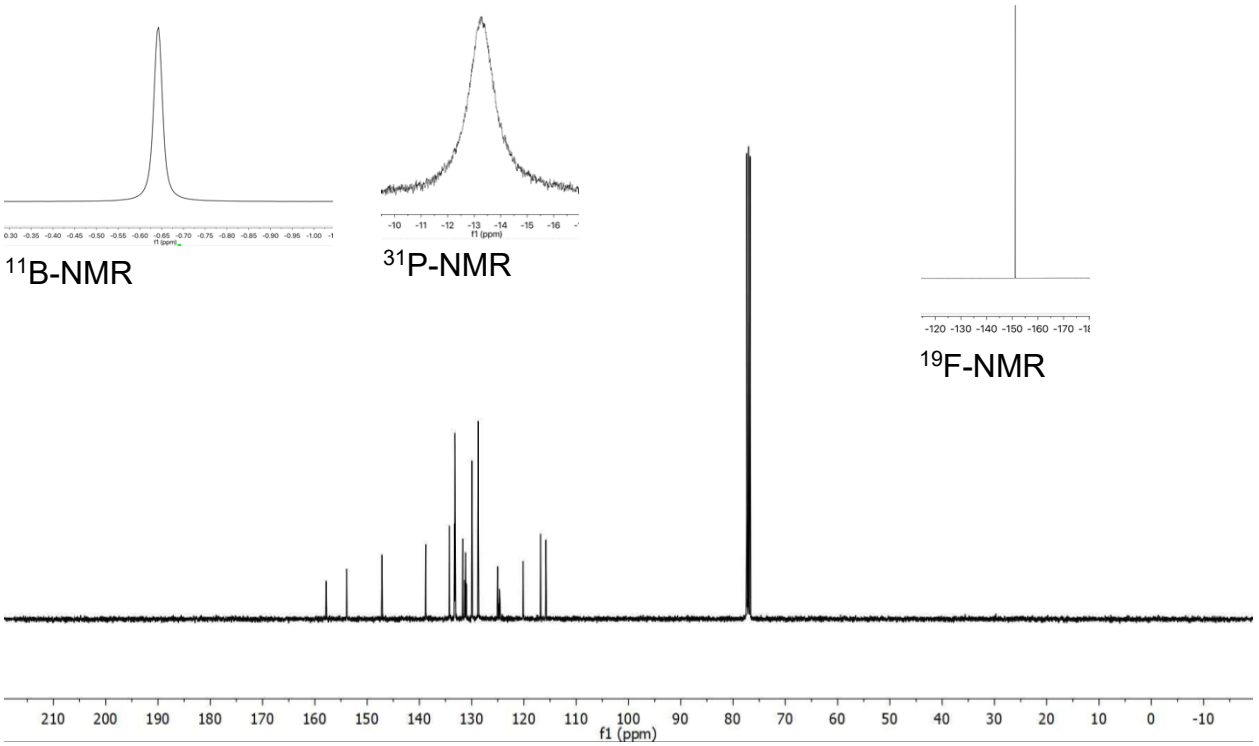

Figure A2. $^{13}C\{^{1}H\}$ NMR (100 MHz, $CDCl_3$, 298 K) and inserts of ^{19}F-NMR, ^{31}P-NMR, and ^{11}B-NMR of **C1**.

Table A1. X-ray information for **C1**.

Compound	**C1**
Formula	$C_{46}H_{37}BCuF_4N_3OP_2$
$D_{calc.}$/ g cm^{-3}	1.223
μ/mm^{-1}	1.733
Formula Weight	860.07
Colour	clear colourless
Shape	prism
Size/mm^3	0.18×0.10×0.09
T/K	123.00(10)
Crystal System	triclinic
Space Group	P-1
a/Å	12.3434(3)
b/Å	13.5815(3)
c/Å	15.3052(3)
α/°	80.808(2)
β/°	81.963(2)
γ/°	67.807(2)
V/Å^3	2336.32(10)
Z	2
Z'	1
Wavelength/Å	1.54184
Radiation type	Cu K_α
Θ_{min}/°	3.539
Θ_{max}/°	74.216

Measured Refl.	26620
Independent Refl.	9228
Reflections with I > 2(I)	8517
R_{int}	0.0207
Parameters	560
Restraints	58
Largest Peak	0.615
Deepest Hole	-0.457
GooF	0.997
wR_2 (all data)	0.0934
wR_2	0.0916
R_1 (all data)	0.0366
R_1	0.0340

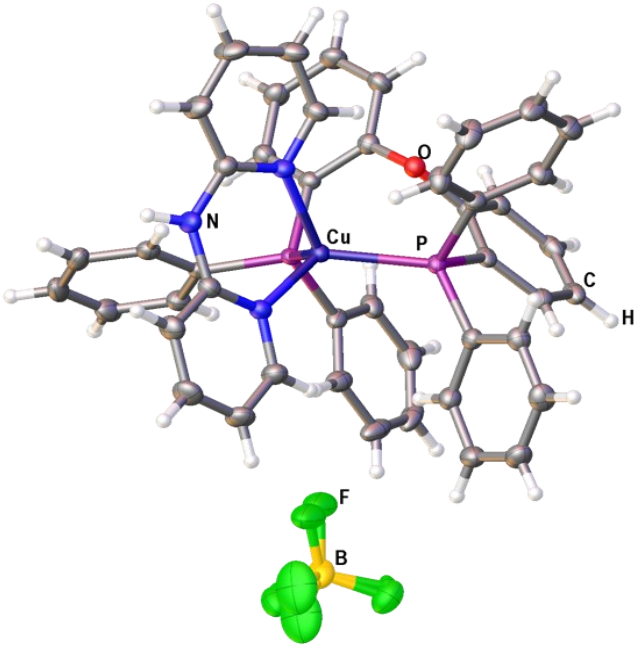

Figure A3. X-ray structure of **C1**

[(di(pyridin-2-yl)amine)((9,9-dimethyl-9H-xanthene-4,5-diyl)bis(diphenyl phosphane))Cu^{I}]BF_4 (C2)

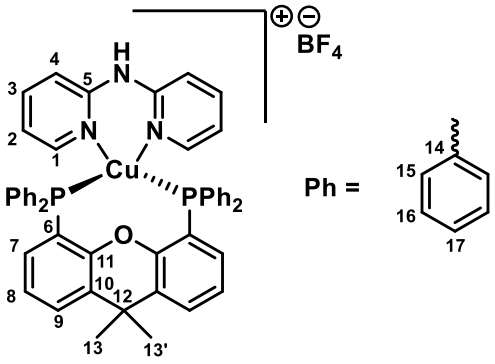

^{1}H-NMR (400 MHz, CD_2Cl_2, 298 K): δ/ppm = 8.85 (s, 1H, N-H), 7.65 (dd, *J* = 7.8 Hz, 1.4 Hz, 2H), 7.52 (ddd, *J* = 8.8 Hz, 7.2 Hz, 1.9 Hz, 2H), 7.42 (dd, *J* = 5.6 Hz, 1.2 Hz, 2H), 7.31 (t, *J* = 7.3 Hz, 4H), 7.24 (m, 4H), 7.17 (m, 20H), 6.55 (m, 2H), 6.42 (m, 2H), 1.76 (s, 6H).

^{13}C{^{1}H} NMR (100 MHz, $CDCl_3$, 298 K): δ/ppm = 155.3 (t, $J^{C\text{-}P}$= 6.3), 154.2, 147.5, 139.6, 138.5, 134.0 (t, $J^{C\text{-}P}$= 1.6), 133.64 (t, $J^{C\text{-}P}$= 8.1), 132.5 (t, $J^{C\text{-}P}$= 16.1), 131.55, 130.46, 129.5, 129.3 (t, $J^{C\text{-}P}$= 4.7), 128.72, 127.44, 125.8, 125.64 (t, $J^{C\text{-}P}$= 2.4), 121.14 (t, $J^{C\text{-}P}$= 12.8), 117.53, 116.10, 28.20.

Comment: Due to the overlap of the signals it was not possible to assign the protons using two-dimensional NMR

^{19}F NMR (400 MHz, $CDCl_3$, 298 K): δ/ppm = -150.61 (s, BF_4)

^{11}B NMR (128 MHz, $CDCl_3$, 298 K): δ/ppm = -0.79 (s, BF_4)

^{31}P{1H} NMR (160 MHz, $CDCl_3$, 298 K): δ/ppm = -13.15 (s, XantPhos)

IR (KBr): n/cm^{-1} = 3322, 3050, 1627, 748, 694

HRMS(ESI): ($C_{49}H_{41}CuN_3OP_2$ $[M]^+$) = Calculated 812.2021, Found 812.2075

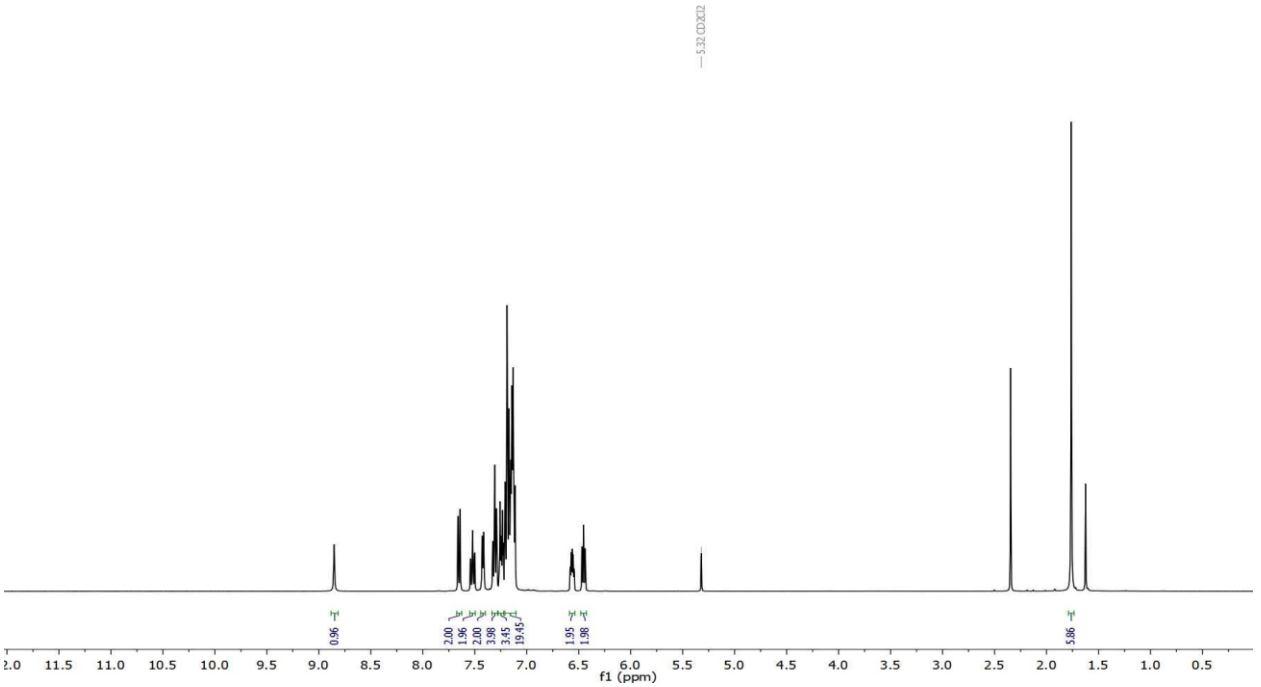

Figure A4. ^{1}H-NMR (400 MHz, CDCl3, 298 K) of **C2**.

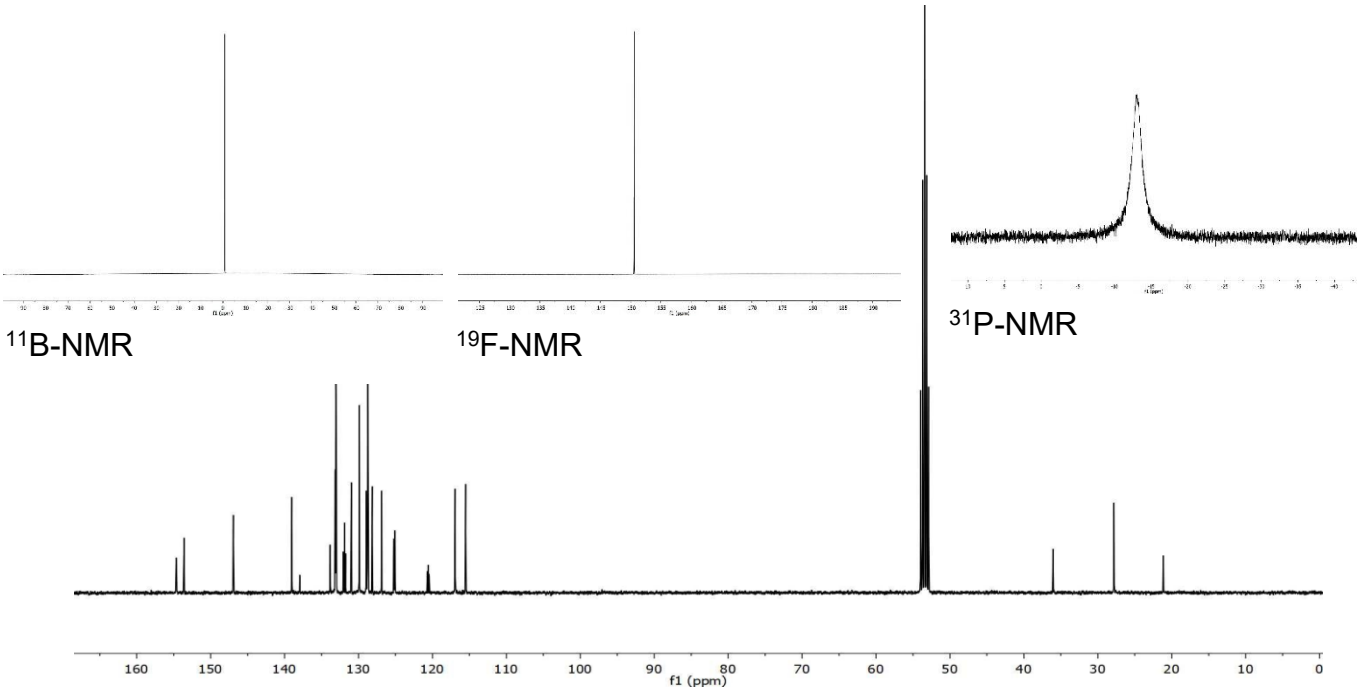

Figure A5. ^{13}C{^{1}H} NMR (100 MHz, $CDCl_3$, 298 K) and inserts of ^{19}F-NMR, ^{31}P-NMR and ^{11}B-NMR of **C2**.

Table A2. X-ray information for **C2**.

Compound	**C2**
Formula	$C_{56}H_{49}BCuF_4N_3OP_2$
$D_{calc.}$/ g cm^{-3}	1.352
μ/mm^{-1}	1.736
Formula Weight	992.27
Colour	clear colourless
Shape	prism
Size/mm^3	0.21×0.08×0.05
T/K	123.00(10)
Crystal System	monoclinic
Space Group	$P2_1/c$
a/Å	10.33629(14)
b/Å	14.5261(2)
c/Å	32.5477(4)
α/°	90
β/°	94.2593(12)
γ/°	90
V/Å^3	4873.40(11)
Z	4
Z'	1

Wavelength/Å	1.54184
Radiation type	CuK_α
$\Theta_{min}/^\circ$	4.084
$\Theta_{max}/^\circ$	74.782
Measured Refl.	29330
Independent Refl.	9581
Reflections with I > 2(I)	8831
R_{int}	0.0193
Parameters	718
Restraints	256
Largest Peak	0.420
Deepest Hole	-1.094
GooF	1.018
wR_2 (all data)	0.0943
wR_2	0.0915
R_1 (all data)	0.0381
R_1	0.0348
Creation Method	
Solution	Olex2 1.2-alpha
Refinement	(compiled 2018.07.26 svn.r3523 for OlexSys, GUI svn.r5532)

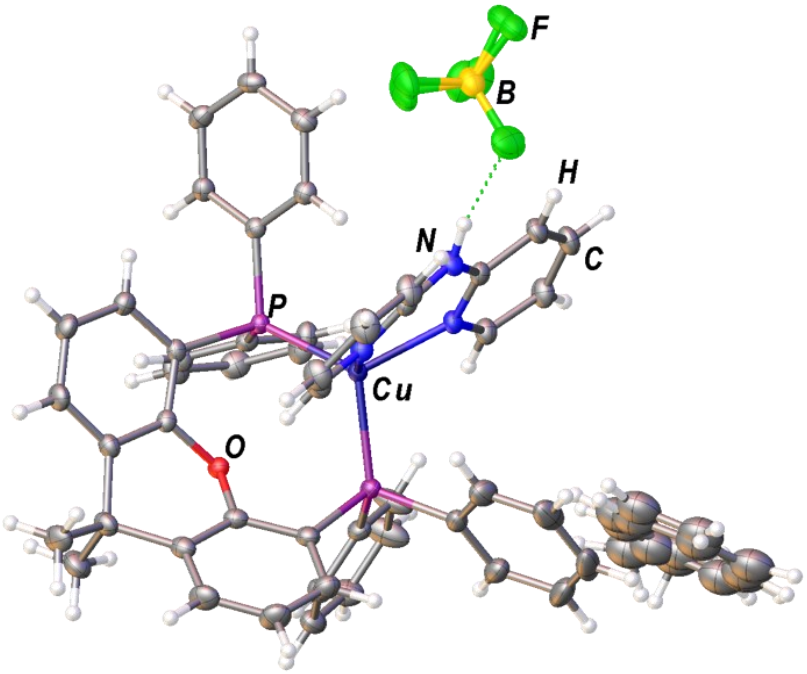

Figure A6. X-ray diffraction of **C2**

[(di(pyridin-2-yl)amine)(1,2-bis(diphenylphosphanyl)benzene))Cu^{I}]BF_4 (C3)

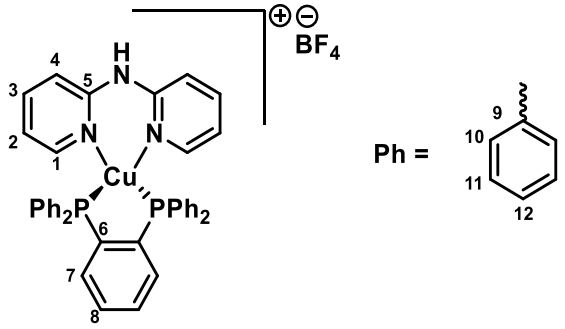

^{1}H-NMR (400 MHz, CD_2Cl_2, 298 K): δ/ppm =9.00 (s, 1H, N-H), 7.55 (m, 4H), 7.49 (m, 2H), 7.23 (m, 26H), 7.02 (m, 2H), 6.90 (m, 1H), 6.42 (m, 2H).
^{13}C{^{1}H} NMR (100 MHz, $CDCl_3$, 298 K): δ/ppm =153.7, 147.8, 141.6 (t, J^{C-P} = 33.6 Hz), 137.0, 135.0, 132.82 – 132.3, 131.2, 130.2, 129.9, 129.0 (t, J^{C-P} = 4.7 Hz), 116.4, 115.8.

Comment: Due to the overlap of the signals it was not possible to assign the protons using two-dimensional NMR

^{19}F NMR (400 MHz, $CDCl_3$, 298 K): δ/ppm = -151.25 (s, BF_4)
^{11}B NMR (128 MHz, $CDCl_3$, 298 K): δ/ppm = -0.67 (s, BF_4)
^{31}P{1H} NMR (160 MHz, $CDCl_3$, 298 K): δ/ppm = -7.06 (s, dpbz)
IR (KBr): n/cm^{-1} = 3340, 3055, 1581, 740, 694
HRMS(ESI): ($C_{49}H_{41}CuN_3OP_2$ $[M]^+$) = Calculated 680.1446, Found 680.1490.

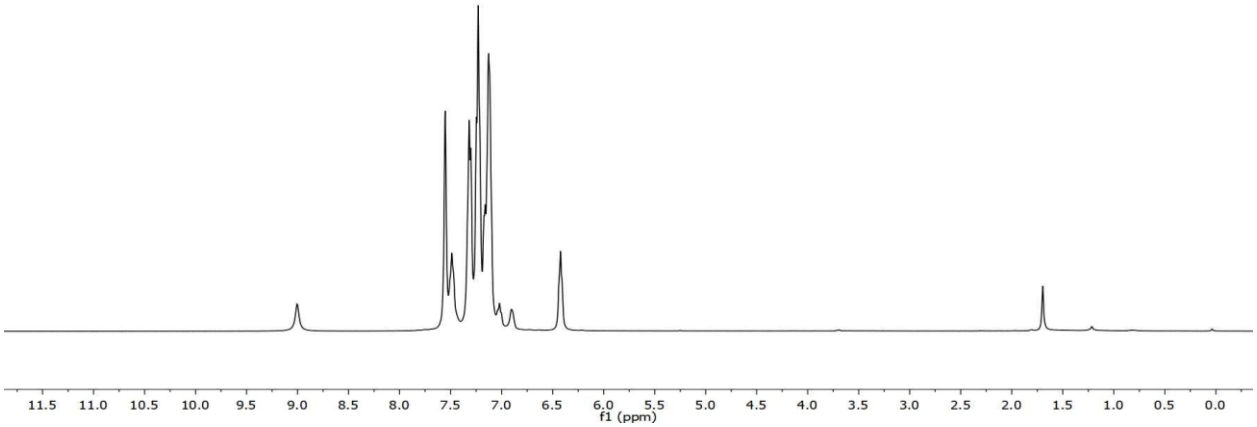

Figure A7**.** ^{1}HNMR (400 MHz, $CDCl_3$, 298 K) for **C3**.

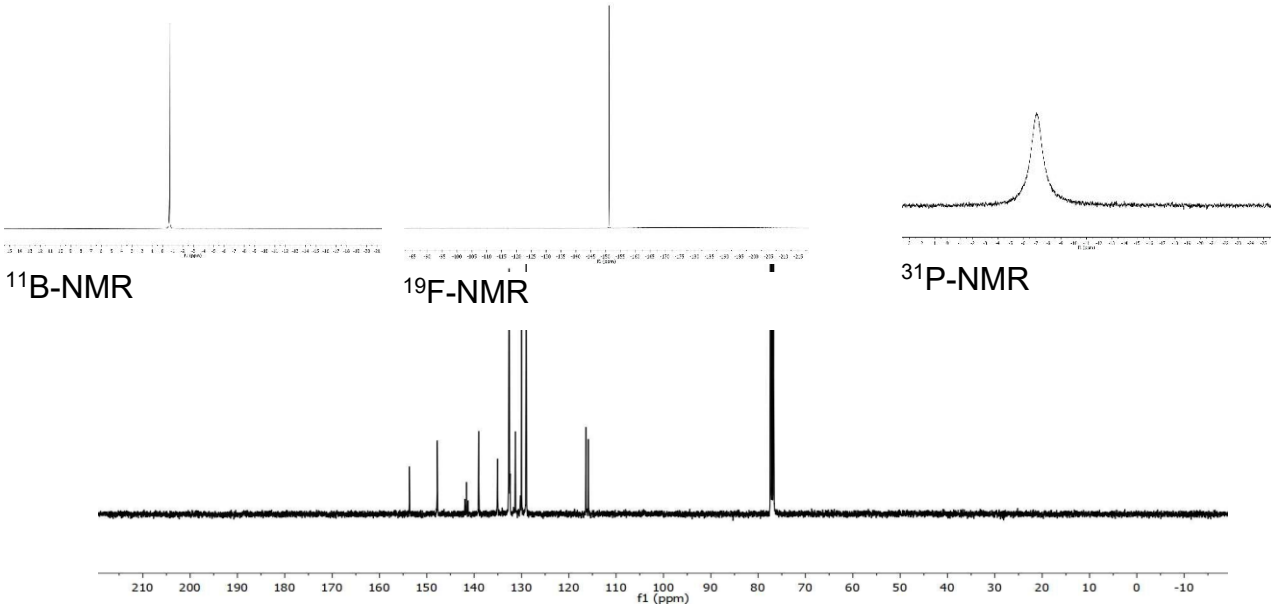

Figure A8. $^{13}C\{^{1}H\}$ NMR (100 MHz, $CDCl_3$, 298 K) and inserts of ^{19}F-NMR, ^{31}P-NMR, and ^{11}B-NMR for **C3**.

Table A3. X-ray information for **C3**.

Compound	**C3**
Formula	$C_{40}H_{33.5}BCuF_4N_3O_{0.25}P_2$
$D_{calc.}$/ g cm^{-3}	1.404
μ/mm^{-1}	2.132
Formula Weight	772.49
Colour	clear colourless
Shape	needle
Size/mm^3	0.24×0.09×0.08
T/K	123.00(10)
Crystal System	monoclinic
Space Group	$P2_1/c$
a/Å	10.5696(2)
b/Å	31.0454(9)
c/Å	11.3121(3)
α/°	90
β/°	100.141(2)
γ/°	90
V/Å^3	3653.95(16)
Z	4
Z'	1
Wavelength/Å	1.54184
Radiation type	CuK_α
Θ_{min}/°	4.218
Θ_{max}/°	74.329
Measured Refl.	20788
Independent Refl.	7190
Reflections with I > 2(I)	6893

R_{int}	0.0156
Parameters	632
Restraints	124
Largest Peak	0.363
Deepest Hole	-0.403
GooF	1.203
wR_2 (all data)	0.0860
wR_2	0.0854
R_1 (all data)	0.0408
R_1	0.0393
Creation Method	
Solution	Olex2 1.2-alpha
Refinement	(compiled 2018.07.26 svn.r3523 for OlexSys, GUI svn.r5532)

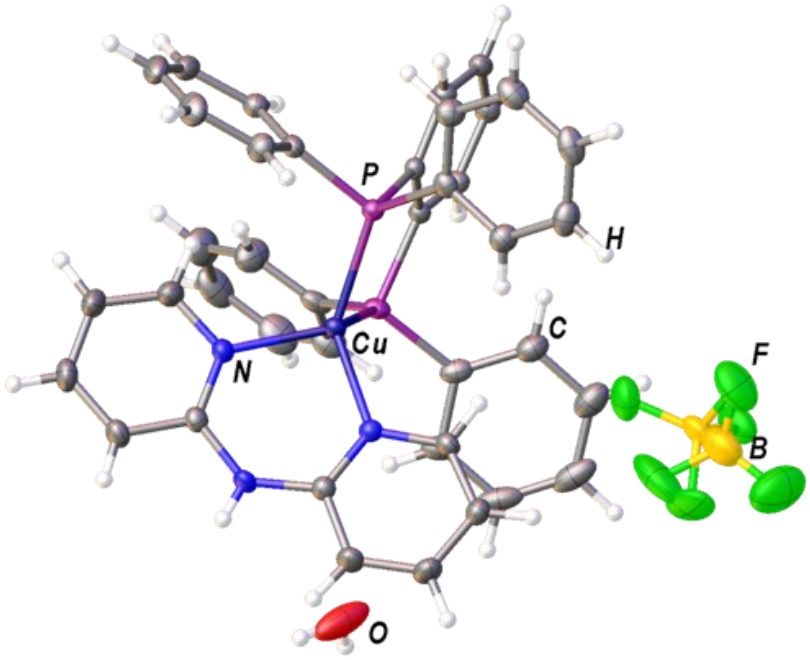

Figure A9. X-ray diffraction of **C3**.

[(di(pyridin-2-yl)amine)((*S*)-2,2'-bis(diphenylphosphanyl)-1,1'-binaphthalene)Cu^{I}]BF_4 (C4)

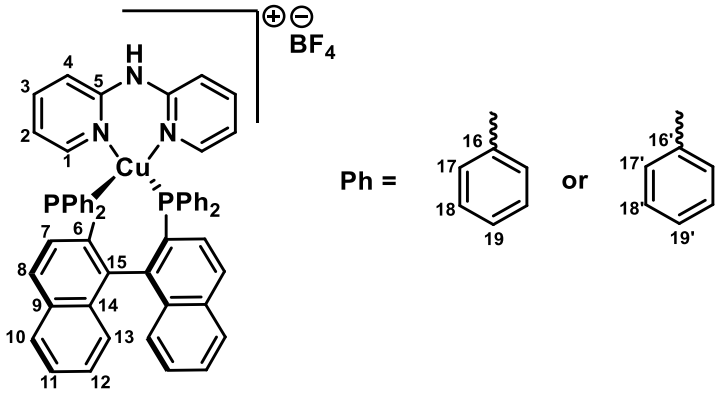

^{1}H-NMR (400 MHz, $CDCl_3$, 298 K): δ/ppm = 8.75 (s, 1H, N-H), 7.79 (dd, *J* = 5.5 Hz, 1.8 Hz, 2H, H4), 7.62 – 7.48 (m, 6H, H8, H2, H7), 7.45 – 7.40 (m, 4H, H17'), 7.35 – 7.27 (m, 6H, H10, H11,H1), 7.26 – 7.18 (m, 6H, H18', H19'), 6.91 (t, 2H, J = 7.7 Hz, H12), 6.82 – 6.75 (m, 4H, H17), 6.70 (t, 2H, *J* = 6.3 Hz, H3), 6.65 (t, 2H, *J* = 7.5 Hz, H19), 6.53 (d, 2H, *J* = 8.6 Hz, H13), 6.49 – 6.44 (m, 4H, H18)
^{13}C{^{1}H} NMR (100 MHz, $CDCl_3$, 298 K): δ/ppm = 154.8 (C5), 147.7 (C4), 139.5 (C15), 139.4 (C2), 134.4 (t, J^{C-P} = 9.7 Hz, C17'), 133.8 (t, J^{C-P} = 4.0 Hz, C14), 133.1, 132.9 (t, J^{C-P} = 8.7 Hz C17), 132.2 – 131.8 (C9, C6), 130.5 , 129,7, 129.3 – 129.1 (C19), 128.9 (C8), 127.9 (C7), 127.6 (t, J^{C-P} = 5.1 Hz, C18), 127.2 (C13), 126.8 (C18'), 126.7, 126.5 (C12), 117.5 (C3), 116.5 (C1)
^{1}H, ^{13}C-HMBC (400 MHz / 100 MHz, $CDCl_3$, 298 K) δ (^{1}H) / δ (^{13}C) = 7,79 / 117.5, 139.4, 154.8 (H4 / C3, C2, C5), 7.62 – 7.48 / 132.2 – 131.8 , 127.9 (H8/ C6, C7, C9), 7.62 – 7.48 / 154.8 (H2 / C5), 7.35 – 7.27/ 139.4, 117.5 (H1 / C2, C3), 6.91 / 133.8 (H12 / C14), 6.82 – 6.75 / 127.6 (H17 / C18), 6.70 / 116.5, 147.7 (H3 / C1, C4), 6.65 / 132.9, 127.6 (H19 / C17, C18), 6.53 / 139.5 (H13 / C15), 6.49 – 6.44 / 129.3 – 129.1 (H18 / C19)
^{1}H, ^{13}C -HSQC (400 MHz / 100 MHz, $CDCl_3$, 298 K): δ (^{1}H) / δ (^{13}C) = 8.48 / 132.7 (H4 / C4), 7.62 – 7.48 / 128.9 (H8/C8), 7.62 – 7.48 / 139.4 (H2/C2), 7.62 – 7.48 / 127.9 (H7/C7), 7.26 – 7.18 / 126.8 (H18'/C18'), 7.26 – 7.18 / 129.3 –

129.1 (H19'/C19'), 6.91 / 126.5 (H12/C12), 6.82 – 6.75 / 132.9 (H17/C17), 6.70 / 117.5 (H3/C3)

GCOSY (400 MHz / 400 MHz, $CDCl_3$, 298 K): δ (^1H) / δ (^1H) = 7.79 / 7.62 – 7.48 (H4/H2), 6.82 – 6.75 / 6.49 – 6.44 (H17/H18), 7.35 – 7.27 / 6.91 (H11/H12), 6.91 / 6.53 (H12/H13)

^{19}F NMR (400 MHz, $CDCl_3$, 298 K): δ/ppm = -151.13 (s, BF_4)

^{11}B NMR (128 MHz, $CDCl_3$, 298 K): δ/ppm = -0.70 (s, BF_4)

$^{31}P\{1H\}$ NMR (160 MHz, $CDCl_3$, 298 K): δ/ppm = -1.15 (s, S-BINAP)

IR (KBr): n/cm^{-1} = 3340, 3055, 1581, 740, 694

HRMS(ESI): ($C_{54}H_{41}CuN_3P_2$ [M]+) = Calculated 856.2066, Found 856.2133.

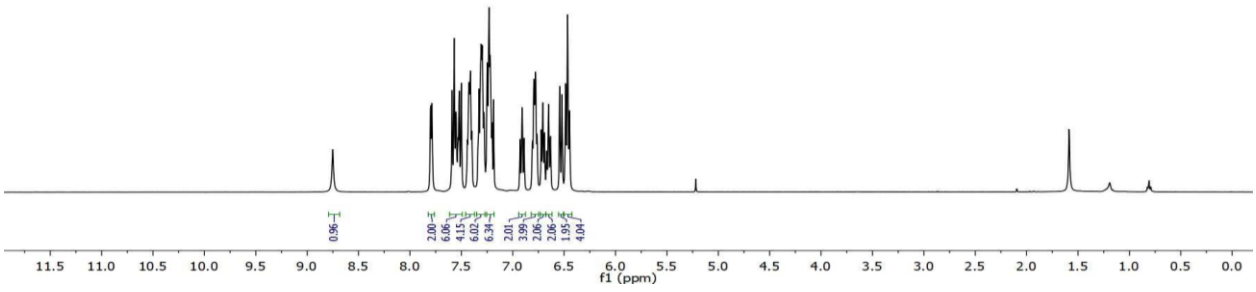

Figure A10. ^1H-NMR (400 MHz, CDCl3, 298 K) for **C4**.

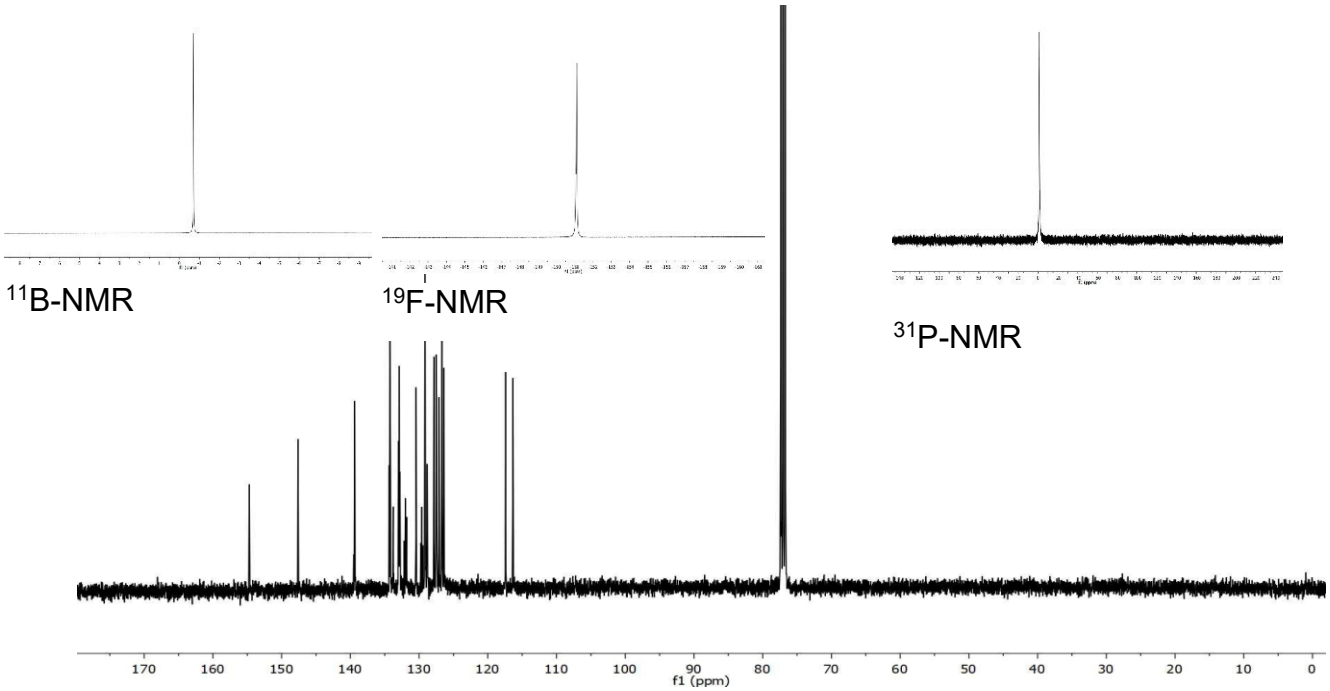

Figure A11. $^{13}C\{^{1}H\}$ NMR (100 MHz, $CDCl_3$, 298 K) and inserts of ^{19}F-NMR, ^{31}P-NMR and ^{11}B-NMR for **C4**.

Table A4. X-ray information for **C4**.

Compound	**C4**
Formula	$C_{54}H_{41}BCuF_4N_3P_2$
$D_{calc.}$/ g cm^{-3}	1.420
μ/mm^{-1}	1.872
Formula Weight	944.19
Colour	clear colourless
Shape	prism
Size/mm^3	0.18×0.13×0.12
T/K	123.00(10)
Crystal System	monoclinic
Flack Parameter	-0.004(8)
Hooft Parameter	0.002(4)
Space Group	$P2_1$
a/Å	11.99841(7)
b/Å	11.48163(7)
c/Å	16.15174(9)
α/°	90
β/°	97.0820(5)
γ/°	90
V/Å^3	2208.11(2)
Z	2
Z'	1
Wavelength/Å	1.54184
Radiation type	CuK_α
Θ_{min}/°	3.712
Θ_{max}/°	73.801
Measured Refl.	37540
Independent Refl.	8831

Reflections with I > 2(I)	8734
R_{int}	0.0309
Parameters	661
Restraints	146
Largest Peak	0.391
Deepest Hole	-0.339
GooF	1.027
wR_2 (all data)	0.0699
wR_2	0.0696
R_1 (all data)	0.0274
R_1	0.0270
Creation Method	
Solution	Olex2 1.2-alpha
Refinement	(compiled 2018.07.26 svn.r3523 for OlexSys, GUI svn.r5532)

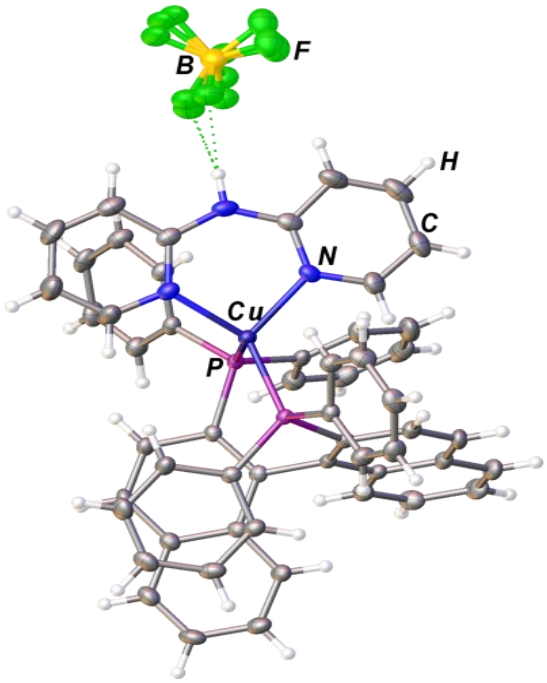

Figure A12. X-ray **C4**.

[(di(pyridin-2-yl)amine)(1,1′-Ferrocenediyl-bis(diphenylphosphine) Cu^{I}]BF_4 (C5)

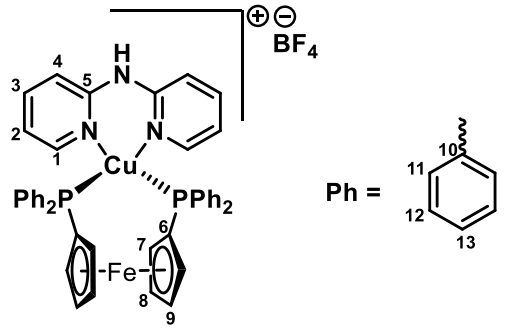

^{1}H-NMR (400 MHz, $CDCl_3$, 298 K): δ/ppm = 8.97 (s, 1H, N-H), 7.73 (dd, *J* = 5.6 Hz, 1.8 Hz, 2H, H4), 7.55 (t, *J* = 7.5 Hz, 2H, H2), 7.40 (m, 2H, H1), 7.38 – 7.2 (m, 20 H, H10, H11, H12), 6.61 (t, *J* = 6.3 Hz, 2H, H3), 4.52 (s, 4H, H8), 4.27 (s, 4H, H7)

^{13}C{^{1}H} NMR (100 MHz, $CDCl_3$, 298 K): δ/ppm = 154.5 (C5), 147.68 (C4), 139.16 (C2), 133.48, 133.33, 133.17, 133.09, 133.01, 130.16, 128.91, 128.86, 128.82, 117.22 (C3), 116.27 (C1), 76.31(t, *J* = 19.1 Hz, C6), 74.24 (C7), 72.30 (C8)

^{1}H, ^{13}C-HMBC (400 MHz / 100 MHz, $CDCl_3$, 298 K) δ (^{1}H) / δ (^{13}C) = 7.73 / 117.2, 139.16, 154.5 (H4 / C3, C2, C5), 7.55 / 147.68, 154.5 (H2 / C4, C5), 7.40 / 117.22 (H1 / C3), 6.61 / 116.27, 147.68 (H3 / C1, C4), 4.52 / 74.24, 76.31 (H8 / C7, C6), 4.27 / 72.30, 76.31 (H7 / C8, C6)

^{1}H, ^{13}C-HSQC (400 MHz / 100 MHz, $CDCl_3$, 298 K): δ (^{1}H) / δ (^{13}C) = 7.73 / 147.68 (H4 / C4), 7.55 / 139.16 (H2 / C2), 7.40 / 116.27 (H1 / C1), 6.61 / 117.22 (H3 / C3), 4.52 / 72.30 (H8 / C8), 4.27 / 74.24 (H7 / C7)

GCOSY (400 MHz / 400 MHz, $CDCl_3$, 298 K): δ (^{1}H) / δ (^{1}H) = 7.73 / 6.61 (H4/H3), 6.61 / 7.55 (H3/H2), 7.55/ 7.40 (H2/H1), 4.27 / 4.52 (H7/H8)

^{19}F NMR (400 MHz, $CDCl_3$, 298 K): δ/ppm = -151.34 (s, BF_4)

^{11}B NMR (128 MHz, $CDCl_3$, 298 K): δ/ppm = -0.96 (s, BF_4)

^{31}P{1H} NMR (160 MHz, $CDCl_3$, 298 K): δ/ppm = -13.87 (s, dppf)

HRMS(ESI): ($C_{44}H_{37}CuFeN_3P_2$ $[M]^+$) = Calculated 788.1108, Found 788.1164.

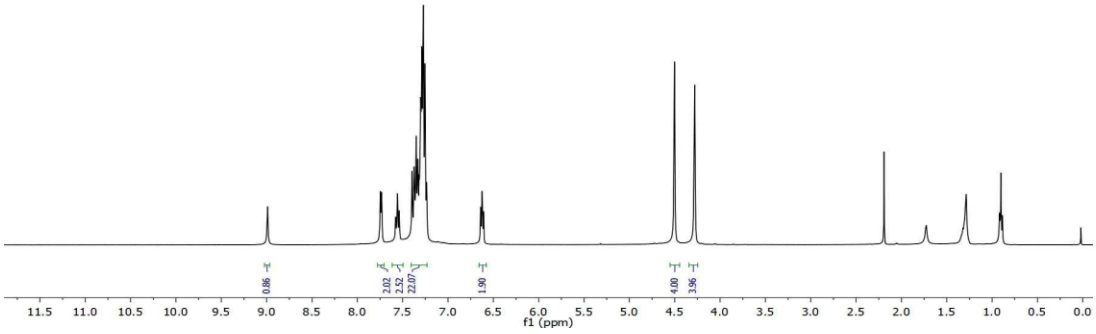

Figure A13**.** ^{1}H-NMR (400 MHz, CDCl3, 298 K) of **C5**.

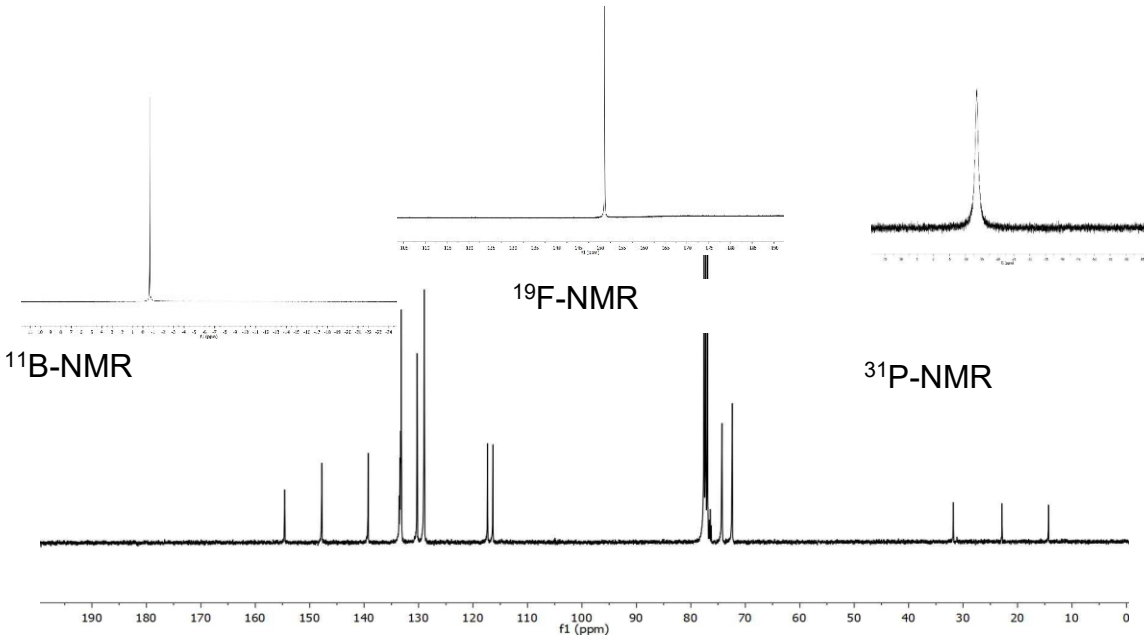

Figure A14**.** ^{13}C{^{1}H} NMR (100 MHz, $CDCl_3$, 298 K) and inserts of ^{19}F-NMR, ^{31}P-NMR and ^{11}B-NMR of **C5**.

Table A5. X-ray information of **C5**.

Compound	**C5**

Formula	$C_{51}H_{45}BCuF_4FeN_3P_2$
$D_{calc.}$/ g cm^{-3}	1.445
μ/mm^{-1}	4.350
Formula Weight	968.04
Colour	clear light yellow
Shape	prism
Size/mm^3	0.26×0.09×0.06
T/K	123.00(10)
Crystal System	monoclinic
Space Group	$I2/a$
a/Å	14.4035(3)
b/Å	19.6994(3)
c/Å	16.0607(4)
α/°	90
β/°	102.400(2)
γ/°	90
V/Å^3	4450.76(16)
Z	4
Z'	0.5
Wavelength/Å	1.54184
Radiation type	Cu K_α
Θ_{min}/°	3.602
Θ_{max}/°	76.204
Measured Refl.	20171
Independent Refl.	4595
Reflections with I > 2(I)	4464
R_{int}	0.0518
Parameters	377
Restraints	0

Largest Peak	0.790
Deepest Hole	-0.557
GooF	1.068
wR_2 (all data)	0.0958
wR_2	0.0947
R_1 (all data)	0.0338
R_1	0.0329

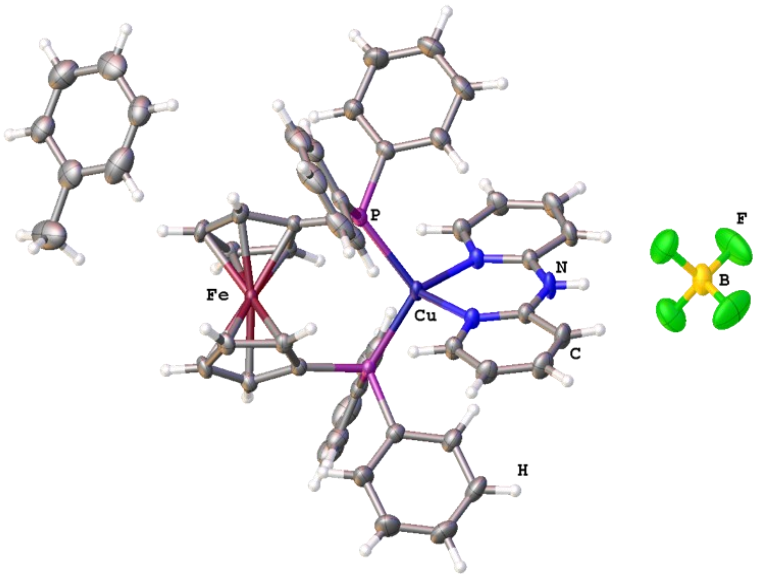

Figure A15. X-ray diffraction of **C5**.

Time-resolved emission decay of C1-5

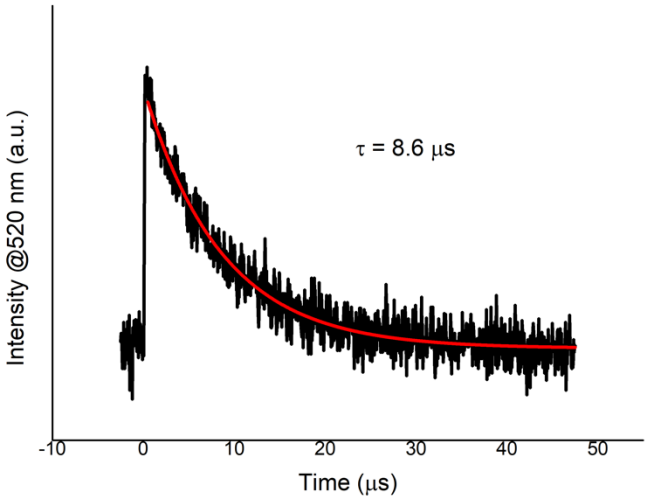

Figure A16. Time-resolved emission decay of **C1** in N_2-purged CH_2Cl_2 measured by laser flash photolysis (excitation at 355 nm, analysis at 520 nm).

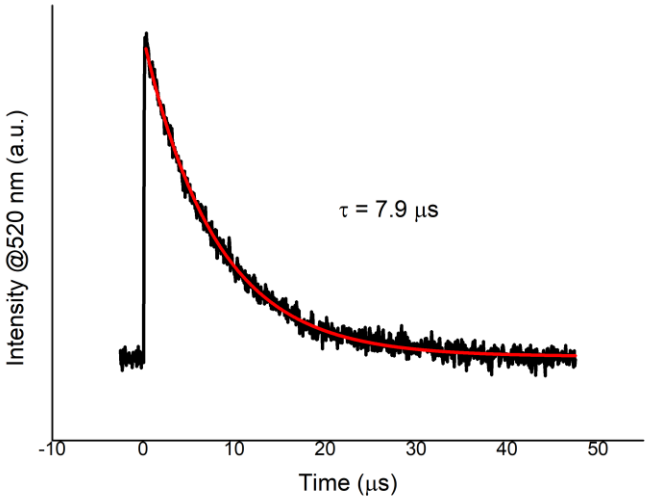

Figure A17. Time-resolved emission decay of **C2** in N_2-purged CH_2Cl_2 measured by laser flash photolysis (excitation at 355 nm, analysis at 520 nm).

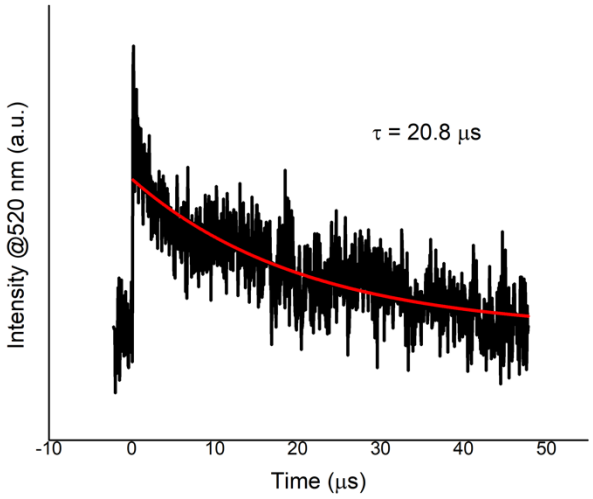

Figure A18. Time-resolved emission decay of **C4** in N_2-purged CH_2Cl_2 measured by laser flash photolysis (excitation at 355 nm, analysis at 520 nm).

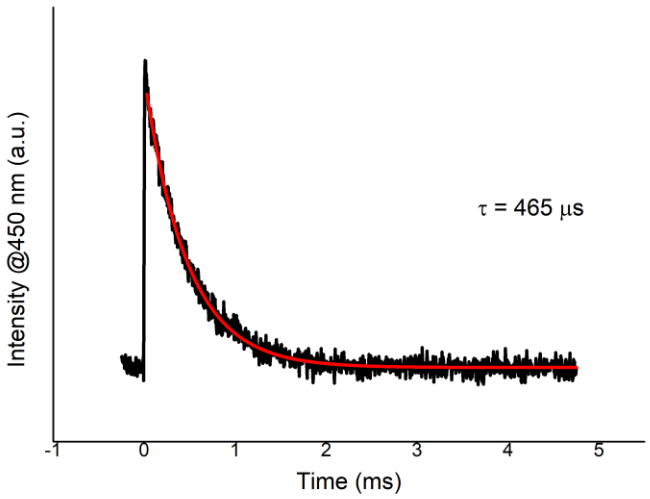

Figure A19. Time-resolved emission decay of **C1** in a 4/1 ethanol/methanol glassy matrix at 77 K measured by laser flash photolysis (excitation at 355 nm, analysis at 450 nm).

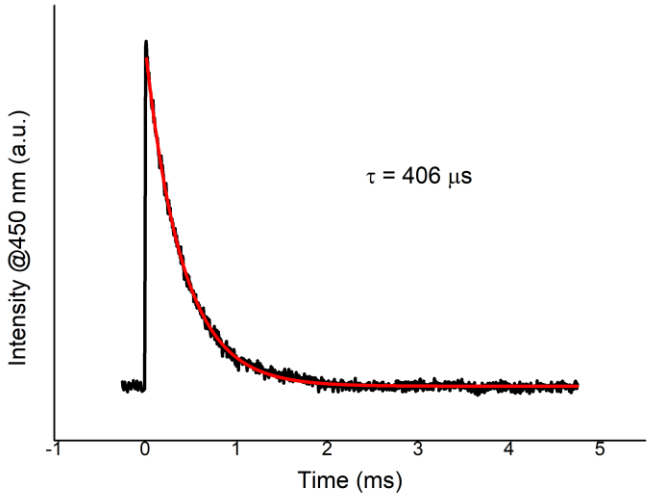

Figure A20. Time-resolved emission decay of **C2** in a 4/1 ethanol/methanol glassy matrix at 77 K measured by laser flash photolysis (excitation at 355 nm, analysis at 450 nm).

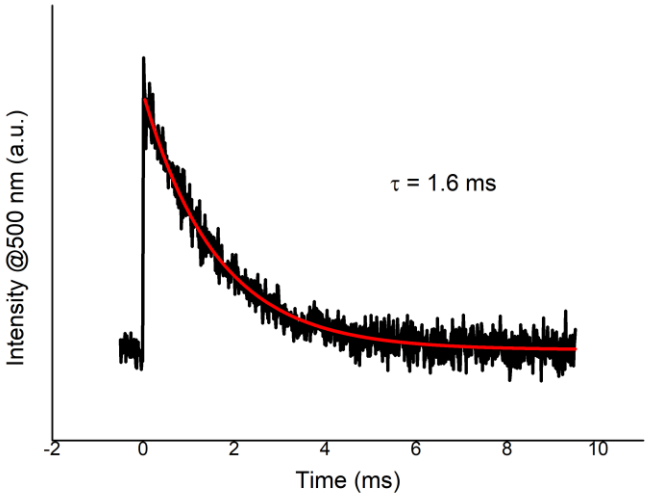

Figure A21. Time-resolved emission decay of **C3** in a 4/1 ethanol/methanol glassy matrix at 77 K measured by laser flash photolysis (excitation at 355 nm, analysis at 500 nm).

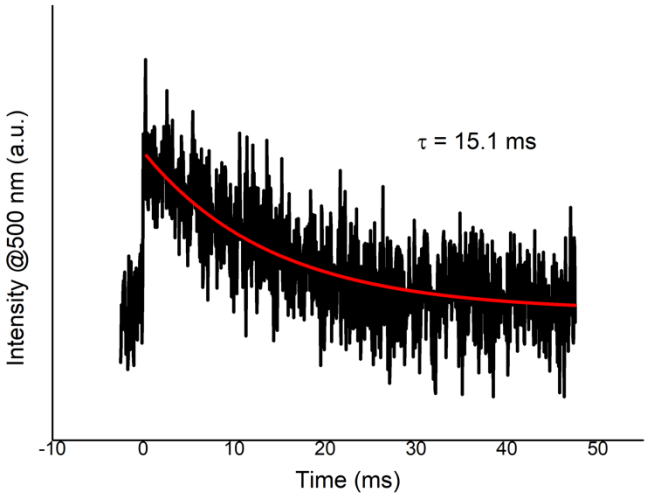

Figure A22. Time-resolved emission decay of **C4** in a 4/1 ethanol/methanol glassy matrix at 77 K measured by laser flash photolysis (excitation at 355 nm, analysis at 500 nm).

Theoretical Calculations

Table A6. Electronic transition energy (E), wavelength (λ), oscillator strength (*f*), main contributions and transition character for complexes **C1-5.**

Complex	E (eV)	λ (nm)	*f*	Contributions	Character
C1	4.28	290	0.0793	HOMO-3→LUMO (24 %) HOMO-1→LUMO+4 (11 %)	LC (dpa) LLCT (dpa→P,P)
	3.46	358	0.0526	HOMO→LUMO+1 (48 %)	MLCT (Cu^{I}→dpa)
C2	4.37	284	0.0789	HOMO→LUMO+8 (37 %) HOMO-2→LUMO+2 (4 %)	LLCT (dpa→P,P) LLCT (P,P→ dpa)
	3.50	354	0.0509	HOMO→LUMO+1 (47 %)	MLCT (Cu^{I}→dpa)
C3	4.24	293	0.1611	HOMO-2→LUMO (32 %) HOMO-1→LUMO+4 (4 %)	LC (dpa) LC (dpa)
	3.28	378	0.0456	HOMO→LUMO+1 (37 %) HOMO→LUMO+2 (12 %)	MLCT (Cu^{I}→dpa) MLCT (Cu^{I}→P,P)

C4	4.35	285	0.0912	HOMO→LUMO+12 (33 %) HOMO-3→LUMO+2 (8 %)	LLCT (dpa→P,P) LLCT (dpa→P,P)
	3.56	348	0.0528	HOMO→LUMO+3 (46 %)	MLCT (Cu^{I}→dpa)
	2.99	415	0.0308	HOMO→LUMO (49 %)	MLCT (dpaCu^{I}→P,P)
C5	4.36	284	0.0798	HOMO-5→LUMO (22 %) HOMO-3→LUMO+2 (13 %) HOMO-3→LUMO+4 (7 %)	LC (dpa) LLCT (dpa→P,P) LLCT (dpa→P,P)
	3.58	345	0.0233	HOMO→LUMO+1 (22 %)	MLCT (Cu^{I}→dpa)
	2.41	513	0.0005	HOMO-1→LUMO+8 (16 %) HOMO-2→LUMO+10 (6 %)	d-dπ^* d-dπ^*

Rehm Weller equation

Excited state reduction potential

The excited state potentials for **C1-5** ($E_{1/2}(C^*)$) were estimated via Rehm Weller equation (Equation 1) using the ground state electrochemical potential for the Cu^{2+}/Cu^{+} couple ($E_{1/2}(C)$) obtained by cyclic voltammetry experiments and the zero-zero spectroscopic energy of the excited state ($E_{0\text{-}0}$), calculated, on first approximation, from the maximum of the emission spectrum. The potential estimated can be employed to compare the energetics of our complexes with those of other photoredox catalysts.

$$E_{1/2}(C^*) = E_{1/2}(C) - E_{0-0} \qquad \text{Equation 1}$$

Table A7**.** Summary of optoelectronic properties of **C1-5** and comparison with other copper(I) photocatalysts.

Complex	λ_{abs}(nm)	λ_{emi}(nm)	τ (**µ**s)	$E_{1/2}$ (V)	$[Cu^{I}]^*/[Cu]^{II}$ (V)
C1	303	520	8.6	0.630	-1.75
C2	307	504	7.9	0.690	-1.77
C3	305	590	<0.01	0.620	-1.48
C4	310/367	567	14	0.550	-1.63
C5	325	449	<0.01	0.880	-1.88
$[Cu(dap)_2]Cl$	437	670	0.27 *	0.62	-1.43
$[Cu(dmp)(rac\text{-}BINAP)]PF_6$	390*	-	2.1 **		-1.6

* in CH_2Cl_2 solution, ** in $CHCl_3$ solution

Compounds

Compounds chapter I

(1,3,3,3-tetrabromopropyl)benzene (59a)

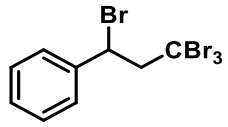

White crystalline solid

215 mg, 0.49 mmol, 99 % yield

Gram-scale 2.19 g, 3.52 mmol, 70 % yield

^{1}H-NMR (300 MHz, $CDCl_3$, 298 K): δ/ppm = 7.50 (m, 2H), 7.35 (m, 3H), 5.34 (dd, J = 7.6 Hz, 4.3 Hz, 1H), 4.14 (dd, *J* = 15.5, 4.3 Hz, 1H), 4.06 (dd, *J* = 15.6, 7.6 Hz, 1H).

^{13}C{^{1}H} NMR (75 MHz, $CDCl_3$, 298 K): δ/ppm = 140.80, 129.00, 128.93, 128.20, 66.46, 50.11, 35.10.

TLC (SiO_2): Rf= 0.7 (Petroleum ether: ethyl acetate, 9:1)

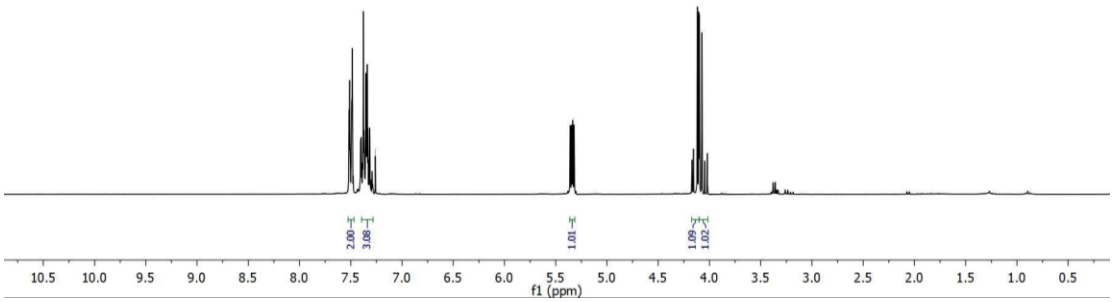

Figure A23. ^{1}H-NMR (300 MHz, $CDCl_3$, 298 K) of **59a**.

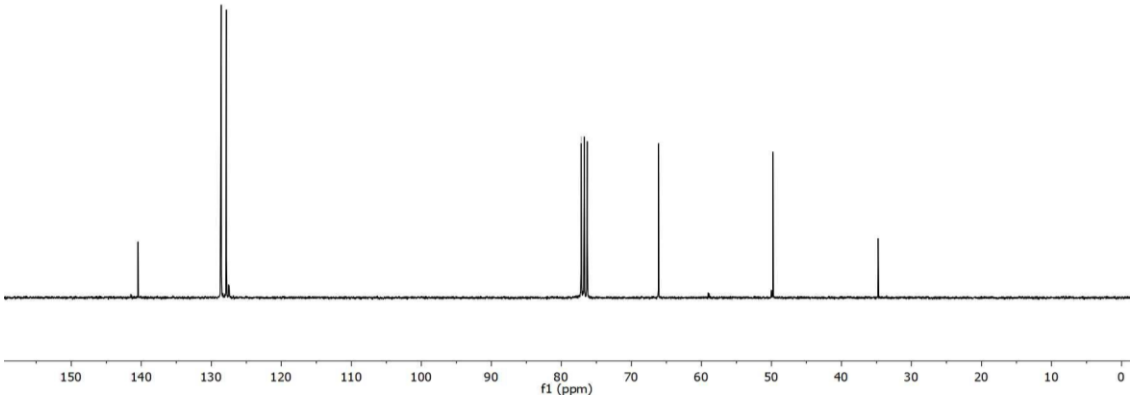

Figure A24. $^{13}C\{^{1}H\}$ NMR (75 MHz, $CDCl_3$, 298 K) of **59a**.

1-methyl-4-(1,3,3,3-tetrabromopropyl)benzene (59b)

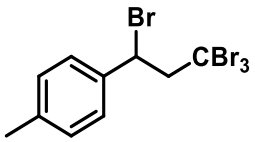

Colourless oil

54 mg, 0.12 mmol, 24 % yield

^{1}H-NMR (300 MHz, $CDCl_3$, 298 K): δ/ppm = 7.38 (d, J = 8.2 Hz, 2H), 7.17 (d, J = 7.6 Hz, 2H), 5.32 (m, 1H), 4.09 (m, 2H)

$^{13}C\{^{1}H\}$ NMR (75 MHz, $CDCl_3$, 298 K): δ/ppm = 139.03, 137.87, 129.59, 128.06, 66.44, 50.31, 35.21, 21.32.

TLC (SiO_2): Rf= 0.6 (Petroleum ether)

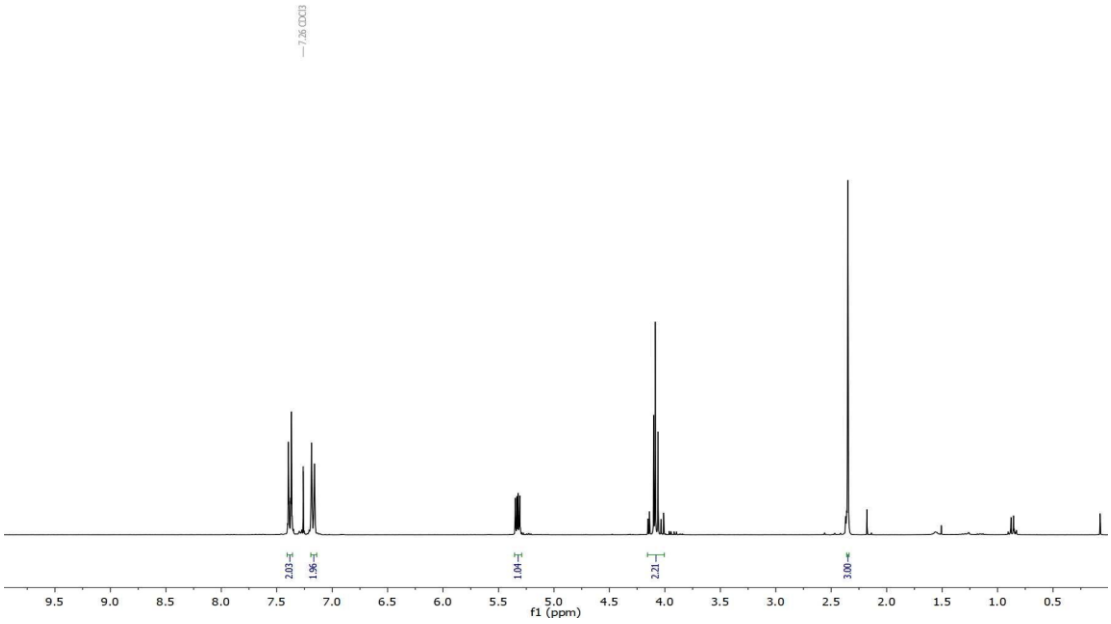

Figure A25. ^{1}H-NMR (300 MHz, $CDCl_3$, 298 K) of **59b**.

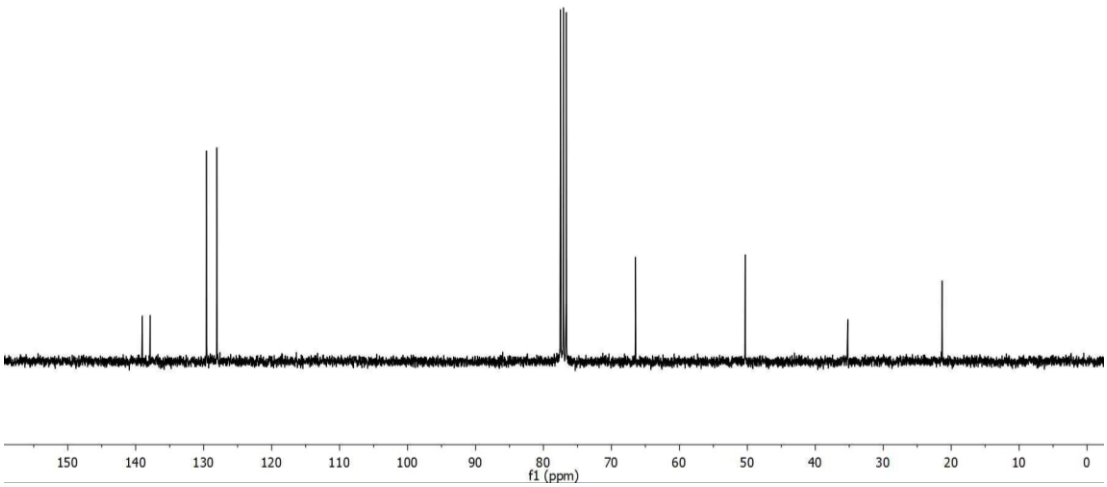

Figure A26. ^{13}C{^{1}H} NMR (75 MHz, $CDCl_3$, 298 K) of **59b**.

1-(tert-butyl)-4-(1,3,3,3-tetrabromopropyl)benzene (59c)

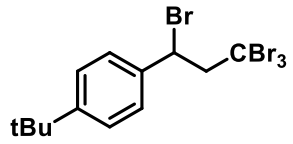

White crystalline solid

50 mg, 0.10 mmol, 20 % yield

^{1}H-NMR (300 MHz, $CDCl_3$, 298 K): δ/ppm = 7.39 (d, *J* = 8.0 Hz, 4H), 5.32 (dd, *J* = 7.2, 4.3 Hz, 1H), 4.18 – 3.98 (m, 2H), 1.32 (s, 9H)

^{13}C{^{1}H} NMR (75 MHz, $CDCl_3$, 298 K): δ/ppm = 152.20, 137.86, 127.73, 125.85, 66.58, 50.24, 35.30, 34.73, 31.30

TLC (SiO_2): Rf= 0.6 (Petroleum ether)

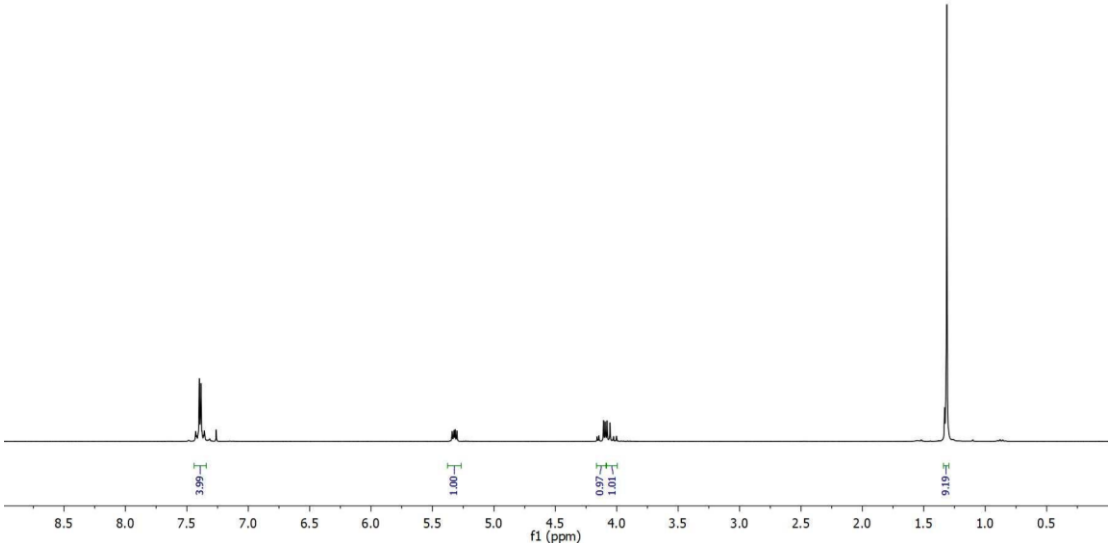

Figure A27. ^{1}H-NMR (300 MHz, $CDCl_3$, 298 K) of **59c**.

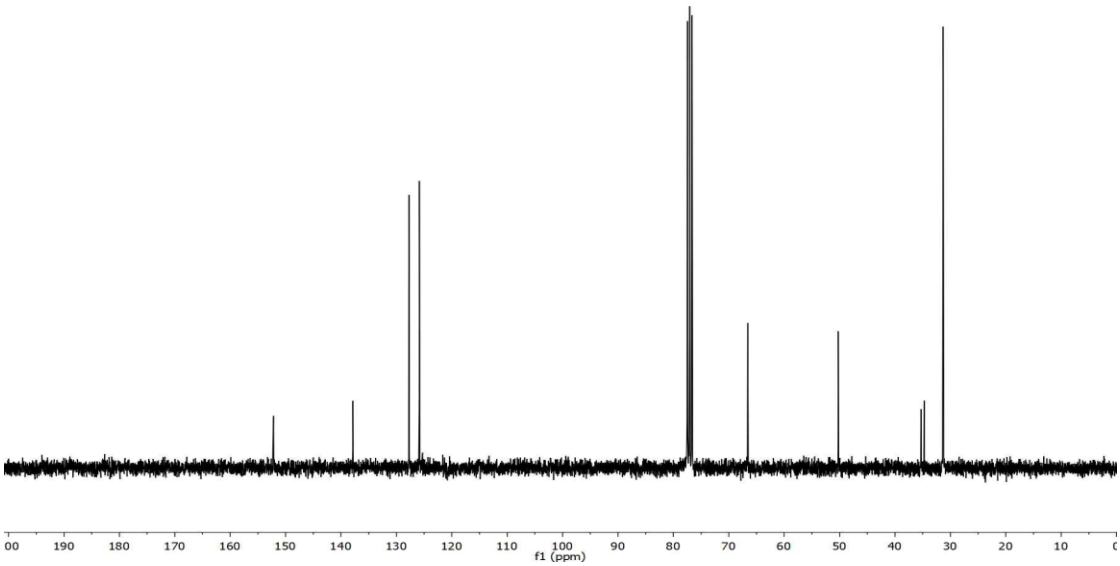

Figure A28. $^{13}C\{^{1}H\}$ NMR (75 MHz, $CDCl_3$, 298 K) of **59c**.

1-chloro-4-(1,3,3,3-tetrabromopropyl)benzene (59e)

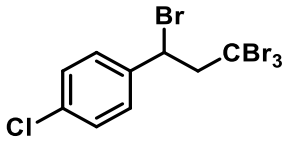

White crystalline solid

167 mg, 0.35 mmol, 71 %

^{1}H-NMR (300 MHz, $CDCl_3$, 298 K): δ/ppm = 7.42 (d, *J* = 6.3 Hz, 2H), 7.33 (d, *J* = 6.3 Hz, 2H), 5.30 (dd, *J* = 3.7 Hz, 8.6 Hz, 1H), 4.08 (dd, *J* = 3.7 Hz, 15.5 Hz, 1H), 4.01 (dd, *J* = 8.6 Hz, 15.5 Hz, 1H).

$^{13}C\{^{1}H\}$ NMR (75 MHz, $CDCl_3$, 298 K): δ/ppm = 139.2, 134.8, 129.5, 129.1, 66.2, 48.9, 34.6

TLC (SiO_2): Rf= 0.61(Petroleum ether)

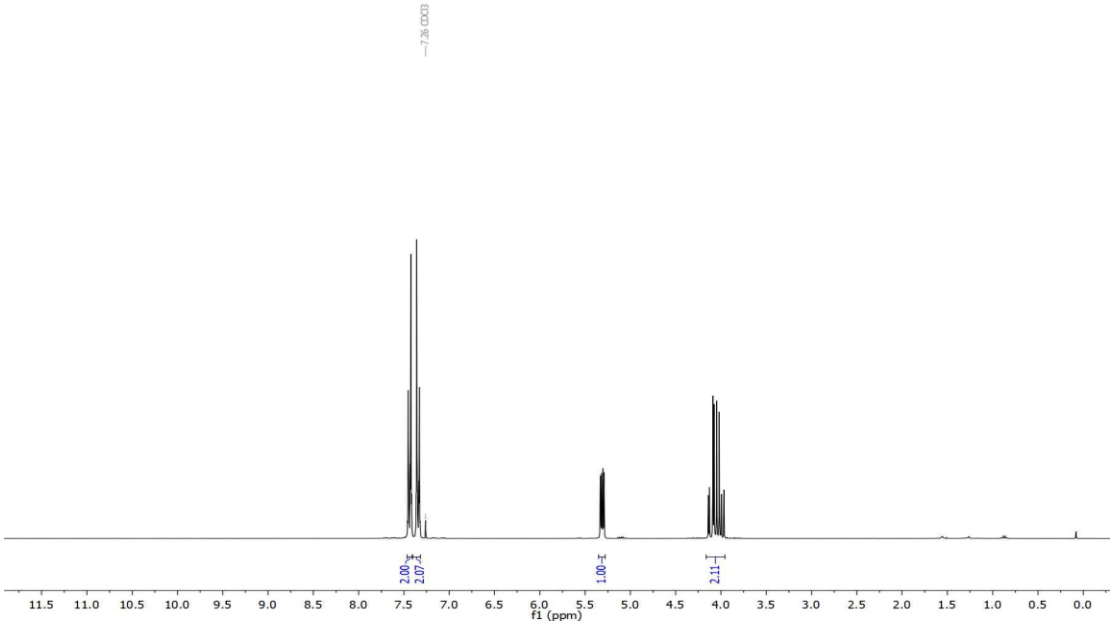

Figure A29. ^{1}H-NMR (300 MHz, $CDCl_3$, 298 K) of **59e**.

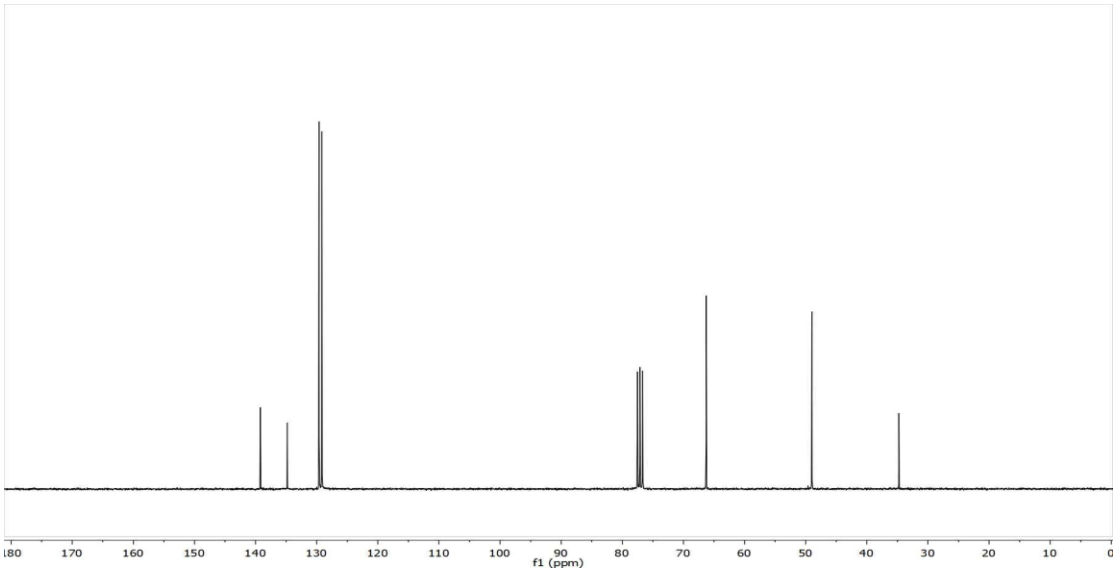

Figure A30. ^{13}C{^{1}H} NMR (75 MHz, $CDCl_3$, 298 K) of **59e**.

1-fluoro-4-(1,3,3,3-tetrabromopropyl)benzene (59f).

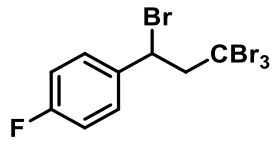

White crystalline solid

153 mg, 0.43 mmol, 68 % yield

^{1}H-NMR (300 MHz, $CDCl_3$, 298 K): δ/ppm = 7.48 (ddd, *J* = 8.6, 5.2, 1.1 Hz, 2H), 7.06 (td, *J* = 8.5, 1.1 Hz, 2H), 5.35 (dd, *J* = 8.2, 3.9 Hz, 1H), 4.12 (ddd, *J* = 15.6, 4.1, 1.0 Hz, 1H), 4.01 (ddd, *J* = 15.4, 8.3, 1.1 Hz, 1H)

^{13}C{^{1}H} NMR (75 MHz, $CDCl_3$, 298 K): δ/ppm = 164.48, 161.18, 136.64, 136.60, 130.22, 129.71, 116.15, 115.86, 66.49, 49.95, 34.92

TLC (SiO_2): Rf= 0.6 (hexanes)

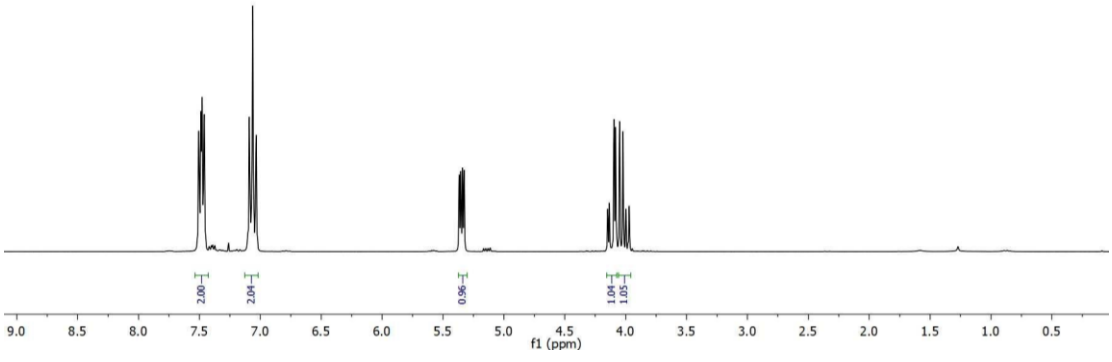

Figure A31. ^{1}H-NMR (300 MHz, $CDCl_3$, 298 K) of **59f**.

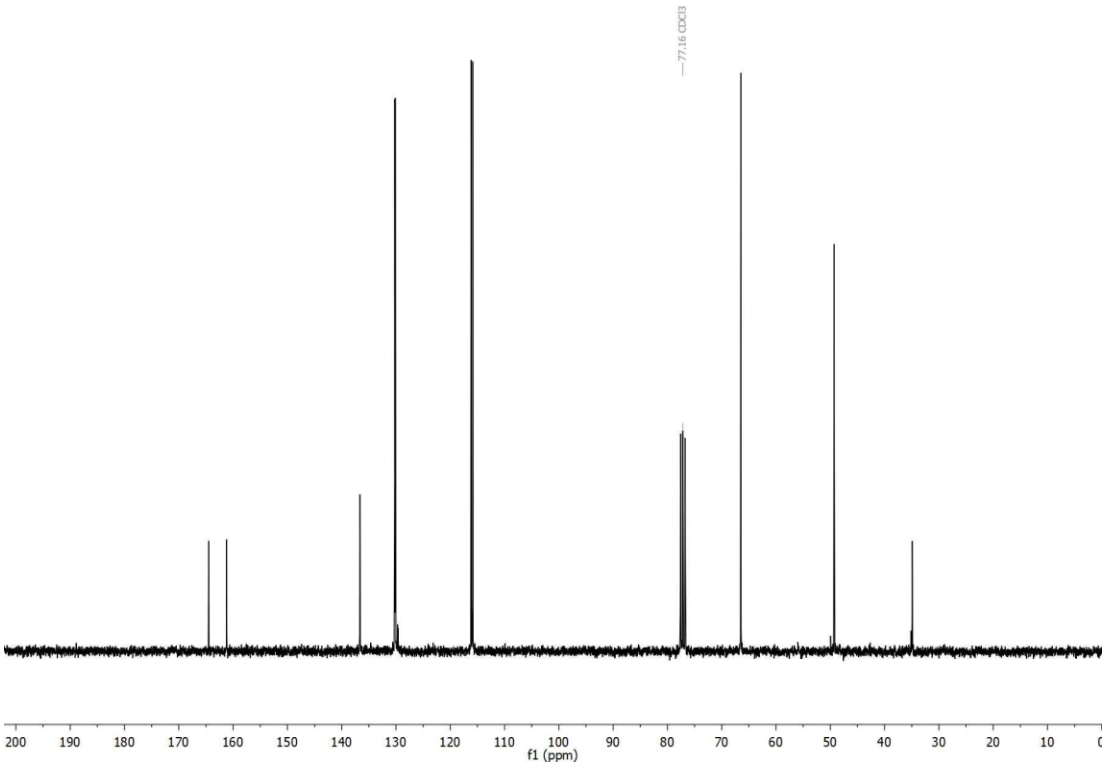

Figure A32. $^{13}C\{^{1}H\}$ NMR (75 MHz, $CDCl_3$, 298 K) of **59f**.

1-(1,3,3,3-tetrabromopropyl)-4-(trifluoromethyl)benzene (59g).

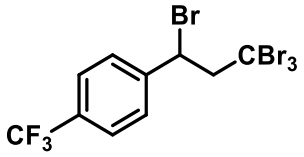

White crystalline solid

85 mg, 0.17 mmol, 34 % yield.

^{1}H-NMR (300 MHz, $CDCl_3$, 298 K): δ/ppm = 7.64 (s, 4H), 5.35 (dd, *J* = 8.0, 4.0 Hz, 1H), 4.15 (dd, *J* = 15.5, 4.0 Hz, 1H), 4.05 (dd, *J* = 15.6, 8.0 Hz, 1H)

$^{13}C\{^{1}H\}$ NMR (75 MHz, $CDCl_3$, 298 K): δ/ppm = 144.62, 131.24, 128.66, 125.98, 121.98, 66.20, 48.36, 34.50

TLC (SiO_2): Rf= 0.4 (hexanes)

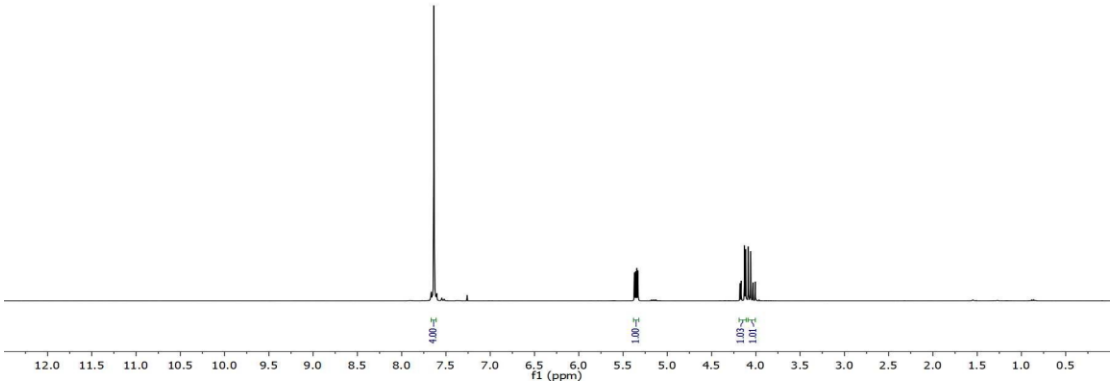

Figure A33. ^{1}H-NMR (300 MHz, $CDCl_3$, 298 K) of **59g**.

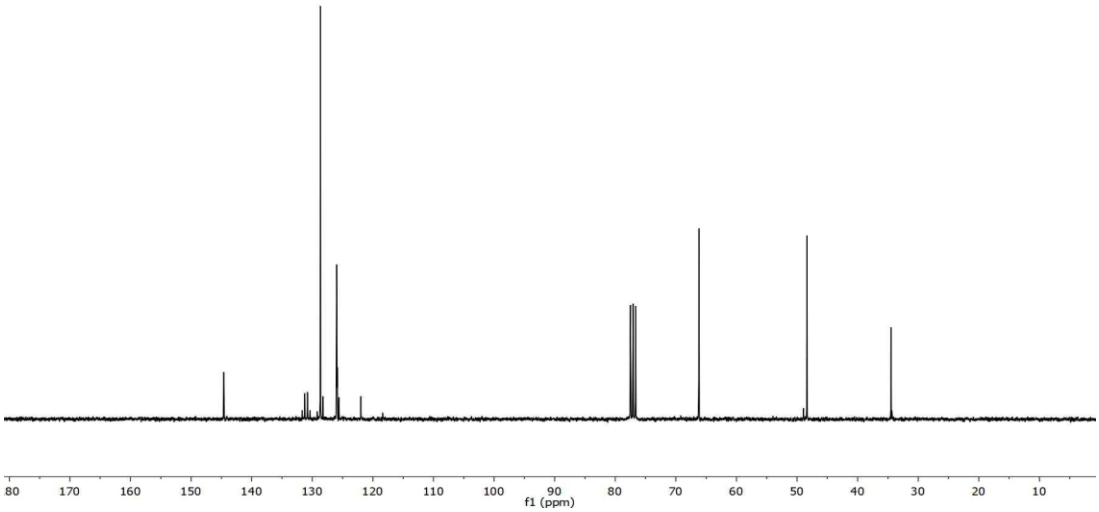

Figure A34. ^{13}C{^{1}H} NMR (75 MHz, $CDCl_3$, 298 K) of **59g**.

4-(1,3,3,3-tetrabromopropyl)benzonitrile (59h).

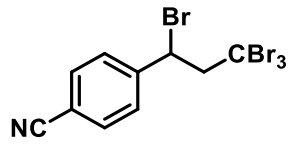

Colourless oil

163.58 mg, 0.355 mmol, 71 % yield.

^{1}H-NMR (300 MHz, $CDCl_3$, 298 K): δ/ppm = 7.69 – 7.55 (m, 4H), 5.31 (dd, *J* = 8.2, 3.9 Hz, 1H), 4.11 (dd, *J* = 15.5, 3.9 Hz, 1H), 4.00 (dd, *J* = 15.6, 8.3 Hz, 1H)

^{13}C{^{1}H} NMR (75 MHz, $CDCl_3$, 298 K): δ/ppm = 145.63, 132.73, 129.09, 118.25, 112.75, 65.89, 48.01, 34.26

TLC (SiO_2): Rf= 0.1 (hexanes)

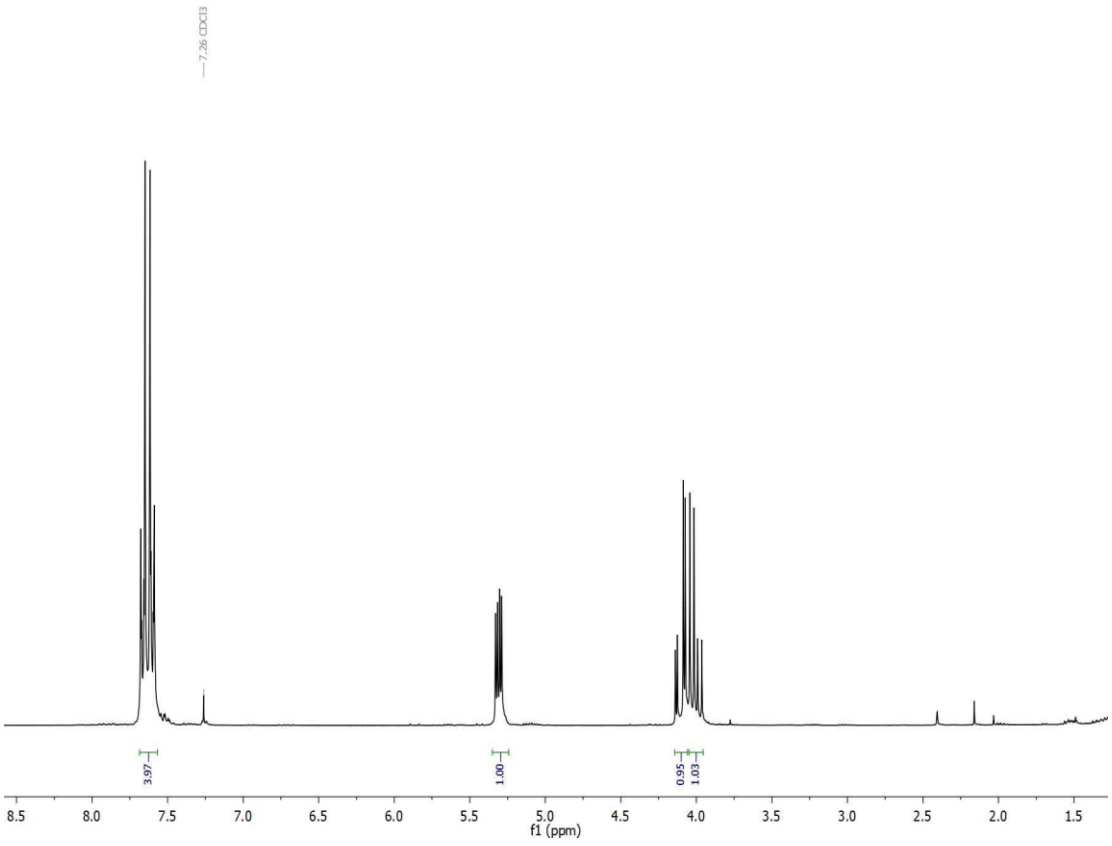

Figure A35. ^{1}H-NMR (300 MHz, $CDCl_3$, 298 K) of **59h**.

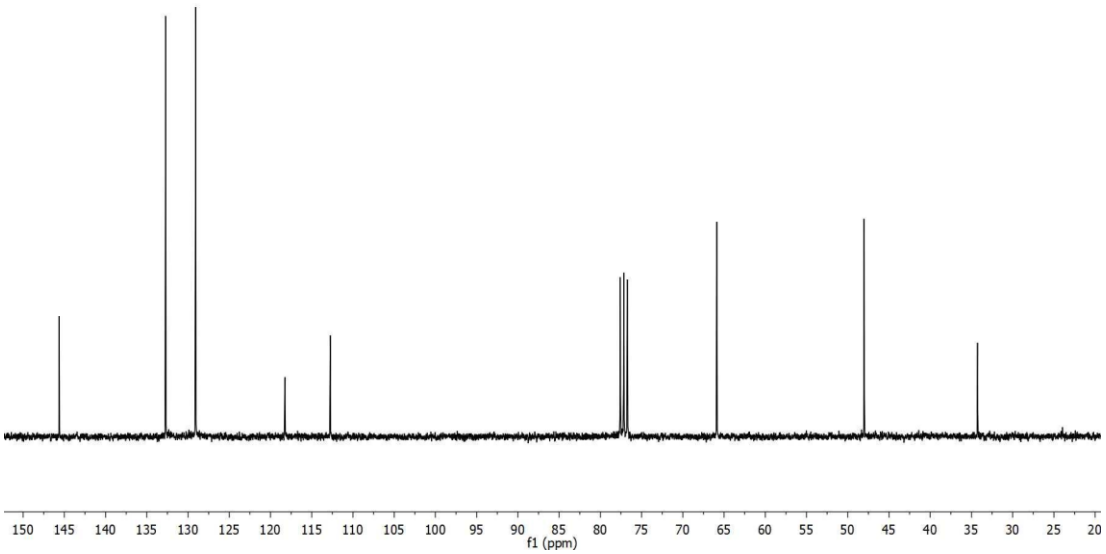

Figure A36. $^{13}C\{^{1}H\}$ NMR (75 MHz, $CDCl_3$, 298 K) of **59h**.

1,1,1,3-tetrabromononane (59j)

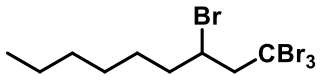

Colourless oil

44.38 mg, 0.100 mmol, 20 % yield.

^{1}H-NMR (300 MHz, $CDCl_3$, 298 K): δ/ppm = 4.20 (dq, *J* = 9.0, 4.5 Hz, 1H), 3.83 (dd, *J* = 16.1, 4.5 Hz, 1H), 3.54 (dd, *J* = 16.2, 4.9 Hz, 1H), 2.08 (dddd, *J* = 14.2, 10.1, 6.0, 4.2 Hz, 1H), 1.96 (ddt, *J* = 14.3, 9.3, 4.7 Hz, 1H), 1.68 – 1.45 (m, 2H), 1.42 – 1.23 (m, 6H), 0.95 – 0.86 (m, 3H)

$^{13}C\{^{1}H\}$ NMR (75 MHz, $CDCl_3$, 298 K): δ/ppm = 67.05, 52.22, 39.90, 36.51, 31.78, 28.57, 27.46, 22.72, 14.23.

TLC (SiO_2): Rf= 0.9 (hexanes)

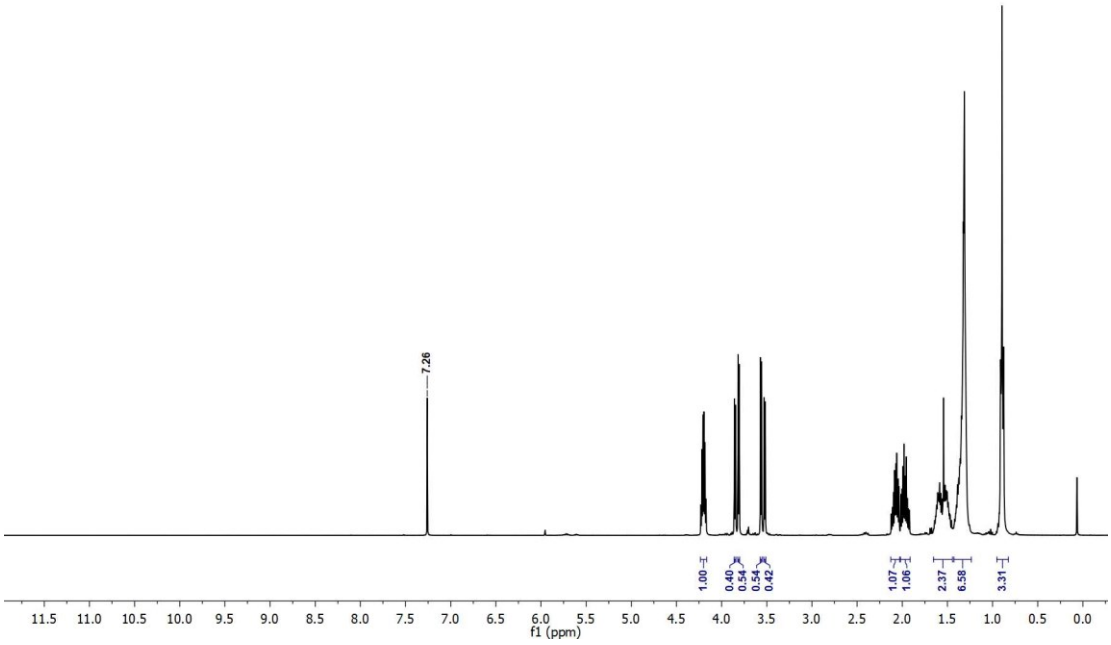

Figure A37. ^{1}H-NMR (300 MHz, $CDCl_3$, 298 K) of **59j**.

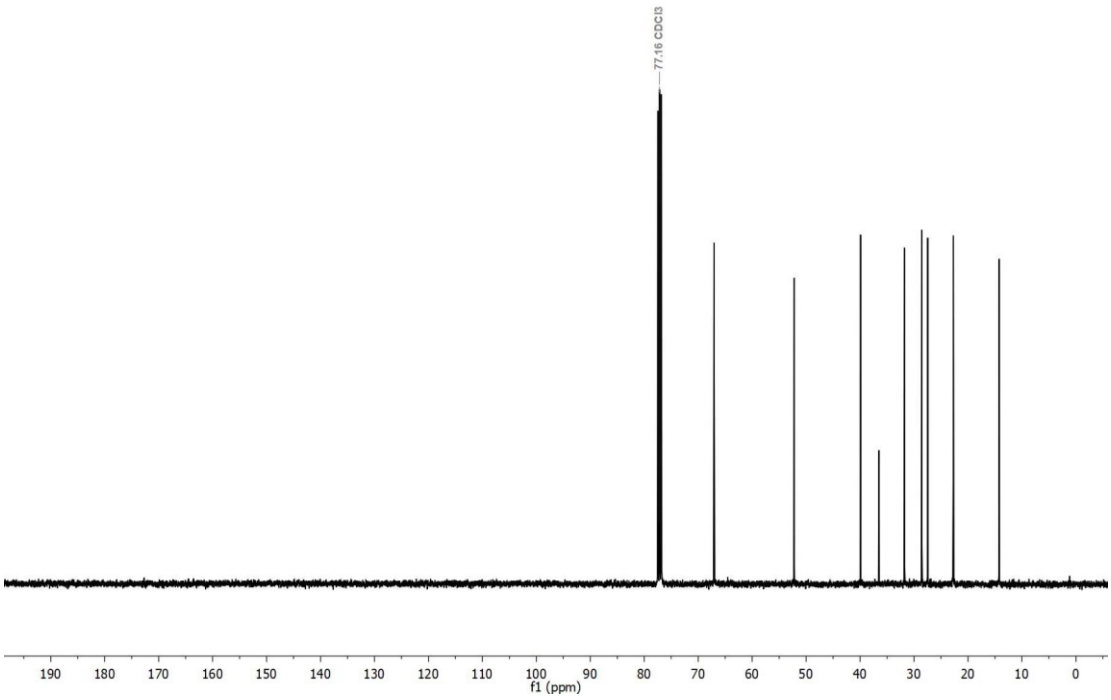

Figure A38. ^{13}C{^{1}H} NMR (75 MHz, $CDCl_3$, 298 K) of **59j**.

1-((2-chloro-2-phenylethyl)sulfonyl)-4-methylbenzene (61)

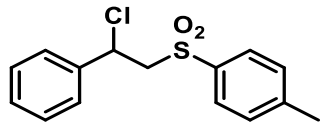

White crystalline solid

137.07 mg, 0.465 mmol, 93 % yield

Gram-scale 1.252 g, 3.52 mmol, 85 % yield

^{1}H-NMR (300 MHz, $CDCl_3$, 298 K): δ/ppm = 7.67 – 7.56 (m, 2H), 7.28 – 7.18 (m, 2H), 5.32 (t, *J* = 6.9 Hz, 1H), 3.94 (dd, *J* = 14.8, 6.9 Hz, 1H), 3.83 (dd, *J* = 14.8, 6.9 Hz, 1H), 2.40 (s, 3H)

^{13}C{^{1}H} NMR (75 MHz, $CDCl_3$, 298 K): δ/ppm = 145.0, 138.7, 136.3, 129.9, 129.2, 129.0, 128.3, 127.2, 64.2, 55.2, 21.8

TLC (SiO_2): Rf= 0.5 (Petroleum ether: ethyl acetate, 9:1)

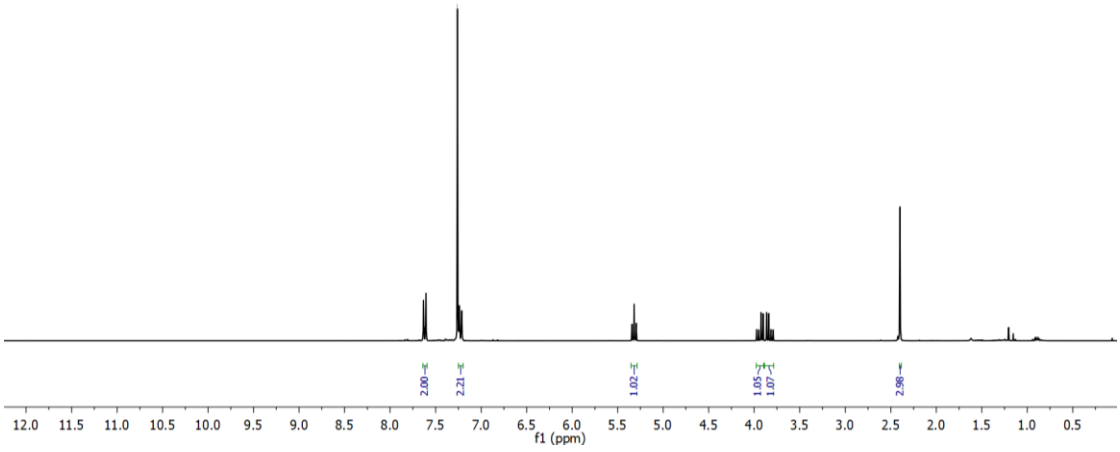

Figure A39. ^{1}H-NMR (300 MHz, $CDCl_3$, 298 K) of **61**.

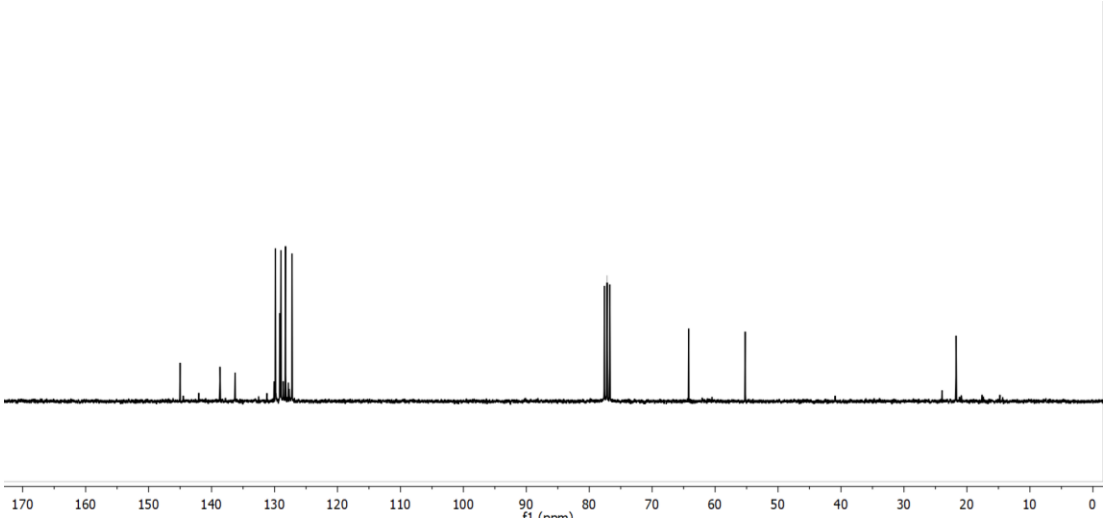

Figure A40. $^{13}C\{^{1}H\}$ NMR (75 MHz, $CDCl_3$, 298 K) of **61**.

(E)-1-((2-chloro-2-phenylvinyl)sulfonyl)-4-methylbenzene (62a)

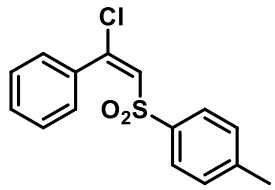

yellowish solid

90.75 mg, 0.31 mmol, 62 % yield

^{1}H-NMR (300 MHz, $CDCl_3$, 298 K): δ/ppm = 7.53 – 7.48 (m, 2H), 7.46 – 7.32 (m, 5H), 7.23 – 7.17 (m, 2H), 6.92 (s, 1H), 2.40 (s, 3H)

$^{13}C\{^{1}H\}$ NMR (75 MHz, $CDCl_3$, 298 K): δ/ppm = 148.0, 144.73, 137.7, 134.46, 131.10, 130.78, 129.76, 128.96, 128.12, 127.89, 21.75

TLC (SiO_2): Rf= 0.4 (Petroleum ether: ethyl acetate, 5:1)

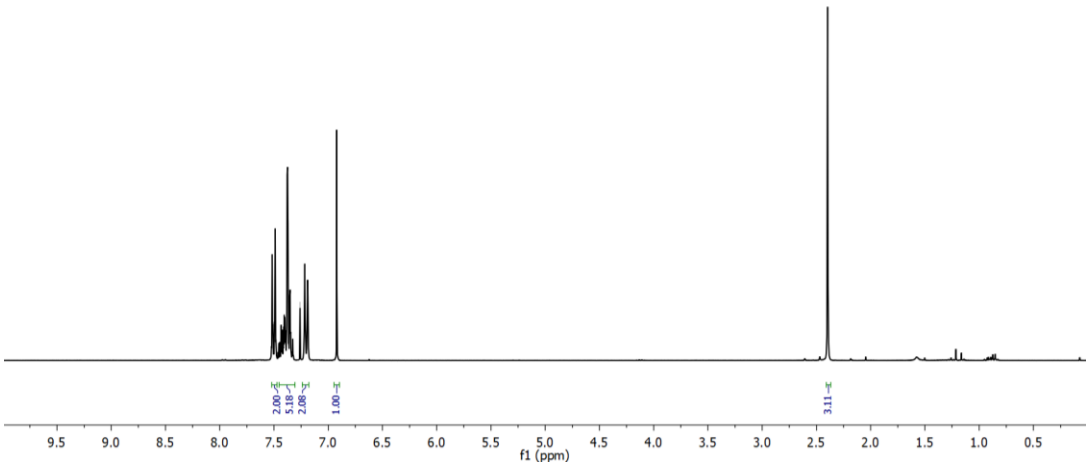

Figure A41. ^{1}H-NMR (300 MHz, $CDCl_3$, 298 K) of **62a**.

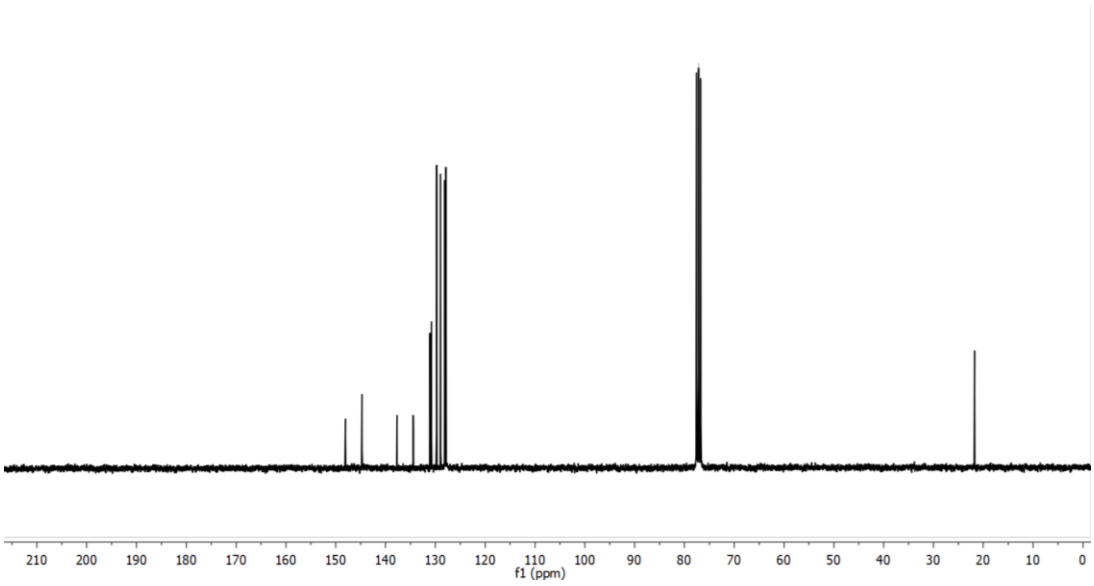

Figure A42. ^{13}C{^{1}H} NMR (75 MHz, $CDCl_3$, 298 K) of **62a**.

(*E*)-1-((2-chloro-2-phenylvinyl)sulfonyl)-4-methoxybenzene (62b)

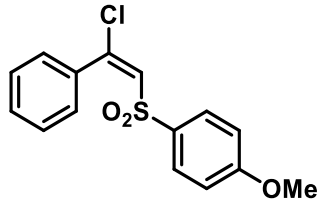

White solid

75.65 mg, 0.245 mmol, 49 % yield

^{1}H-NMR (300 MHz, $CDCl_3$, 298 K): δ/ppm = 7.53 (d, *J* = 8.9 Hz, 2H), 7.44 – 7.30 (m, 5H), 6.93 (s, 1H), 6.85 (d, *J* = 9.0 Hz, 2H), 3.84 (s, 3H)

^{13}C{^{1}H} NMR (75 MHz, $CDCl_3$, 298 K): δ/ppm = 163.74, 147.59, 134.50, 132.09, 131.49, 130.73, 130.09, 129.68, 128.96, 128.13, 114.83, 114.31, 55.81.

TLC (SiO_2): Rf= 0.4 (Petroleum ether: ethyl acetate, 5:1)

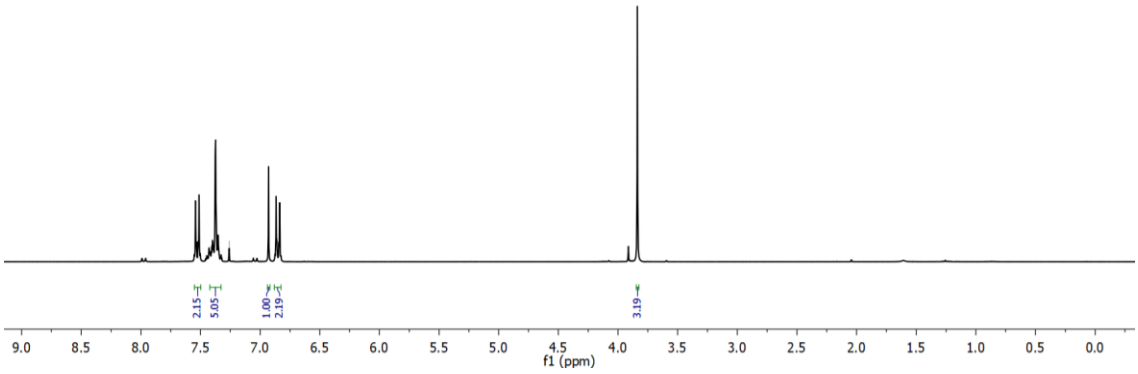

Figure A43. ^{1}H-NMR (300 MHz, $CDCl_3$, 298 K) of **62b**.

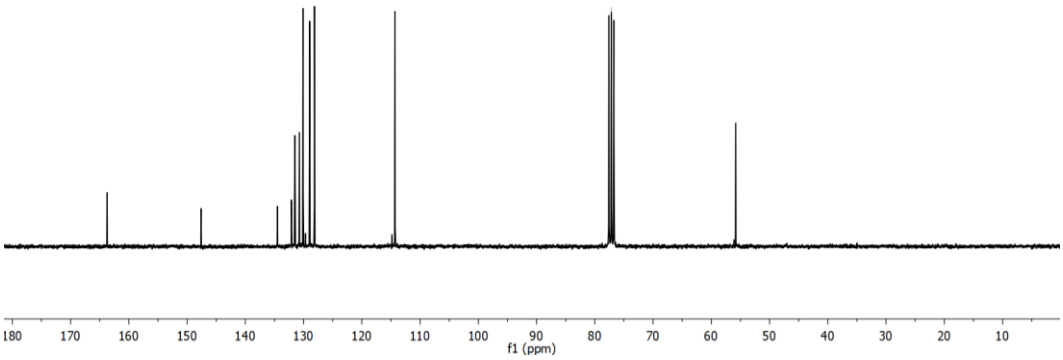

Figure A44. $^{13}C\{^{1}H\}$ NMR (75 MHz, $CDCl_3$, 298 K) of **62b**.

(*E*)-1-((2-chloro-2-phenylvinyl)sulfonyl)-4-fluorobenzene (62c)

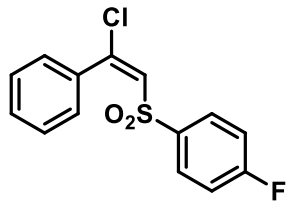

White solid

84.57 mg, 0.285 mmol, 57 % yield

^{1}H-NMR (300 MHz, $CDCl_3$, 298 K): δ/ppm = 7.62 – 7.55 (m, 2H), 7.48 – 7.39 (m, 1H), 7.37 – 7.33 (m, 4H), 7.10 – 7.00 (m, 2H), 6.95 (s, 1H)

$^{13}C\{^{1}H\}$ NMR (75 MHz, $CDCl_3$, 298 K): δ/ppm = 167.33, 163.93, 148.79, 136.46, 136.42, 134.19, 130.98, 130.87, 130.74, 130.61, 128.84, 128.16, 116.42, 116.12

^{19}F NMR (300 MHz, $CDCl_3$, 298 K): δ/ppm = -103.61

TLC (SiO_2): Rf= 0.5 (Petroleum ether: ethyl acetate, 5:1)

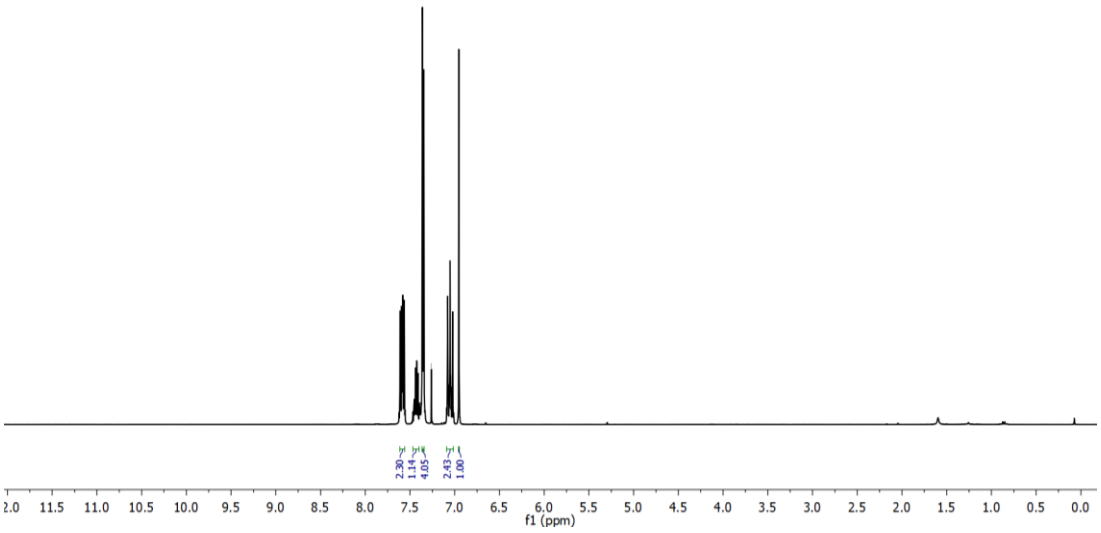

Figure A45. ^{1}H-NMR (300 MHz, $CDCl_3$, 298 K) of **62c**.

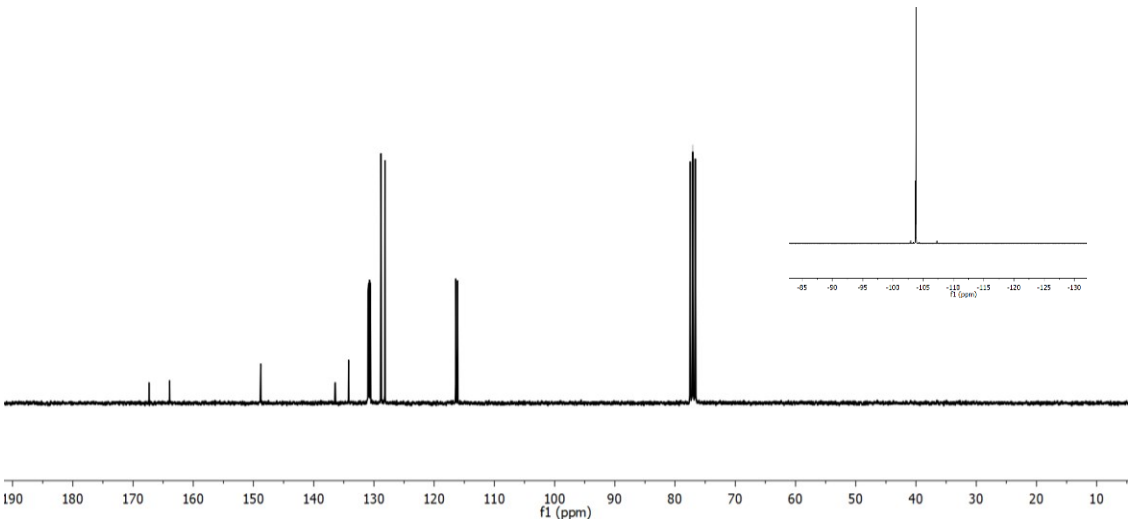

Figure A46. $^{13}C\{^{1}H\}$ NMR (75 MHz, $CDCl_3$, 298 K) and insert of ^{19}F-NMR of **62c**.

(1-bromoethyl)benzene (64)

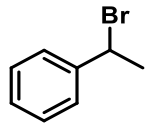

Colourless oil

51.81 mg, 0.280 mmol, 56 % yield

^{1}H-NMR (300 MHz, $CDCl_3$, 298 K): δ/ppm = 7.51 – 7.44 (m, 2H), 7.42 – 7.31 (m, 3H), 5.25 (q, *J* = 6.9 Hz, 1H), 2.09 (d, *J* = 6.9 Hz, 3H)

^{13}C{^{1}H} NMR (75 MHz, $CDCl_3$, 298 K): δ/ppm = 143.30, 128.76, 128.43, 126.89, 49.67, 26.91.

TLC (SiO_2): Rf= 0.6 (hexanes)

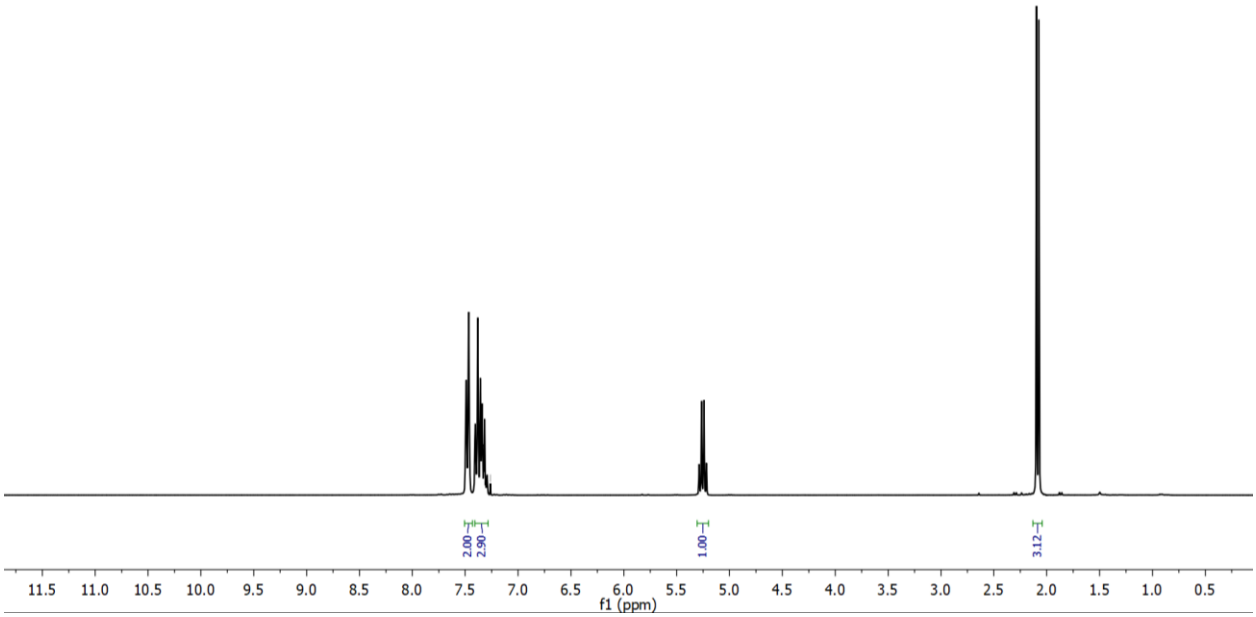

Figure A47. ^{1}H-NMR (300 MHz, $CDCl_3$, 298 K) of **64**.

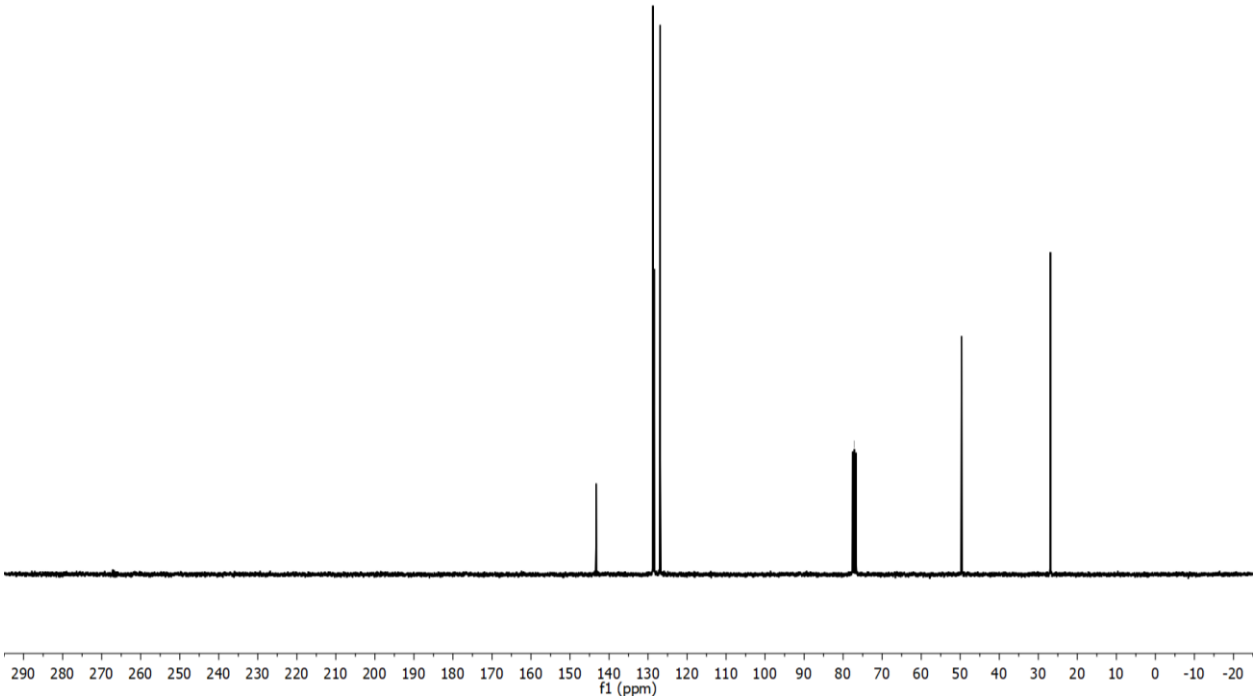

Figure A48. $^{13}C\{^{1}H\}$ NMR (75 MHz, $CDCl_3$, 298 K) of **64**.

(cyclohexylethynyl)benzene (35).

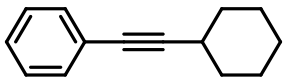

Colourless oil

47.91 mg, 0.260 mmol, 52 % yield

^{1}H-NMR (300 MHz, $CDCl_3$, 298 K): δ/ppm = 7.47 – 7.36 (m, 2H), 7.33 – 7.20 (m, 3H), 2.60 (tt, *J* = 9.3, 3.7 Hz, 1H), 1.90 (ddt, *J* = 12.4, 6.3, 3.2 Hz, 2H), 1.77 (dqt, *J* = 6.4, 4.5, 2.5 Hz, 2H), 1.55 (dq, *J* = 14.2, 5.8, 4.5 Hz, 2H), 1.37 (tdd, *J* = 10.0, 6.1, 3.0 Hz, 2H)

$^{13}C\{^{1}H\}$ NMR (75 MHz, $CDCl_3$, 298 K): δ/ppm = 145.0, 138.7, 136.3, 129.9, 129.2, 129.0, 128.3, 127.2, 64.2, 55.2, 21.8

TLC (SiO_2): Rf= 0.5 (hexanes)

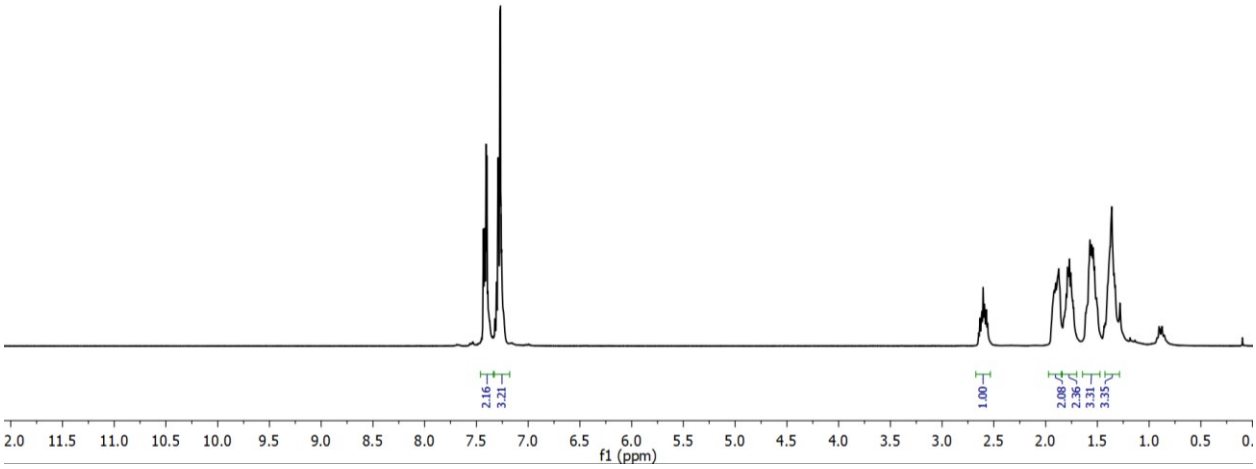

Figure A49. ^{1}H-NMR (300 MHz, $CDCl_3$, 298 K) of **35**.

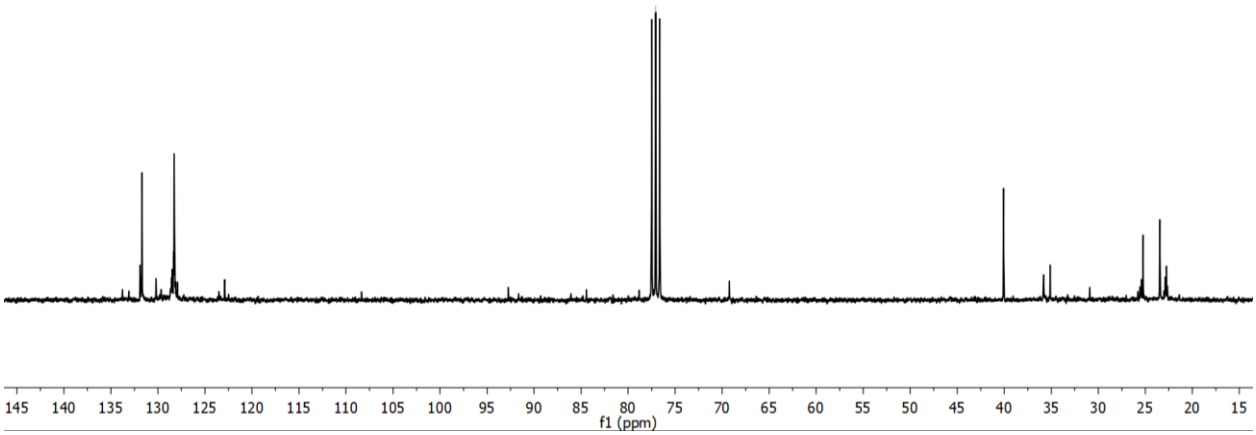

Figure A50. ^{13}C{^{1}H} NMR (75 MHz, $CDCl_3$, 298 K) of **35**.

Copper (II) complexes

[Cu(2,2'-bipyridine)$_2$Cl]Cl (C6)

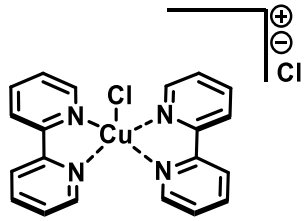

Blue, 212.15 mg, 0.481 mmol, 96 % yield.

[Cu(5,5'-dimethyl-2,2'-bipyridine)$_2$Cl]Cl (C7)

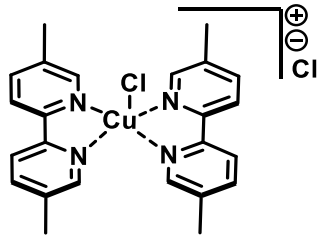

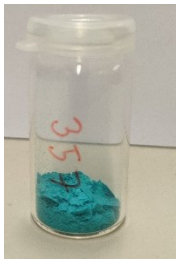

Sea green, 335.4 mg, 0.67 mmol, 67 %.yield.
HRMS(ESI): ($C_{30}H_{39}ClCuN_4O$ [M]+) = Calculated 466.0986, Found 466.0986

[Cu(4,4'-dimethyl-2,2'-bipyridine)$_2$Cl]Cl (C8)

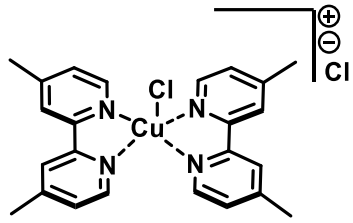

Blue, 259.1 mg, 0.52 mmol, 52 % yield.
HRMS(ESI): ($C_{30}H_{39}ClCuN_4O$ [M]+) = Calculated 466.0986, Found 466.0991

[Cu(4,4',5,5'-tetramethyl-2,2'-bipyridine)Cl]Cl (C9)

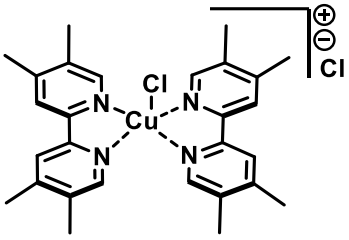


Pale green, 105.73 mg, 0.45 mmol, 90 % yield.
HRMS(ESI): ($C_{30}H_{39}ClCuN_4O$ [M]+) = Calculated 569.2108, Found 570.1624

[Cu(4,4'-di-tert-butyl-2,2'-bipyridine)Cl]Cl (C10)

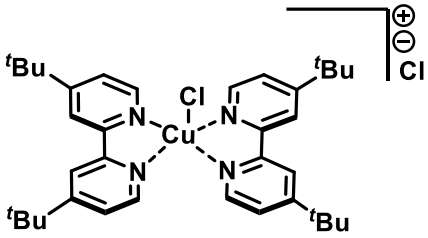


Turquoise blue, 307.3 mg, 0.46 mmol, 92 % yield.
HRMS(ESI): ($C_{36}H_{48}ClCuN_4$ [M]+) = Calculated 634.2864, Found 634.2884

[Cu(4,4'-diphenyl-2,2'-bipyridine)$_2$Cl]Cl (C11)

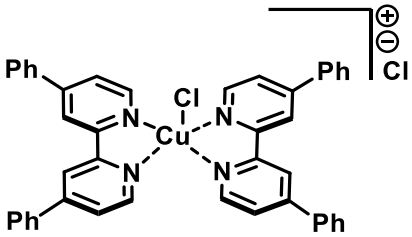


Dark green, 90.7 mg, 0.3 mmol, 60 % yield.
HRMS(ESI): ($C_{46}H_{38}ClCuN_4O$ [M]+) = Calculated 761.8330, Found 762.1362

[Cu(2,2'-biquinoline)$_2$Cl]Cl (C12)

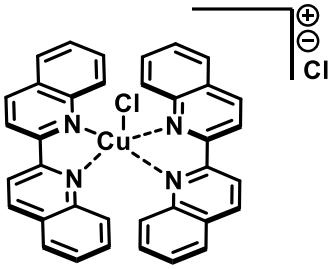

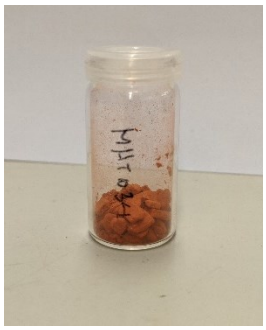

Red, 101.5 mg, 1.51 mmol, 76 % yield.
HRMS(ESI): ($C_{36}H_{24}CuN_4$ [M]+) = Calculated 575.1297, Found 575.1286.

Compounds chapter III

9-(1-phenyl-2-tosylethyl)-9H-carbazole (182)

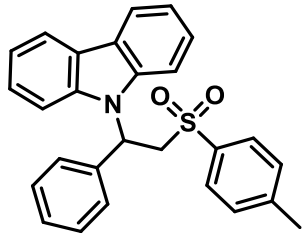

White solid

88.30 mg, 0.207 mmol, 83 % yield

^{1}H-NMR (300 MHz, $CDCl_3$, 298 K): δ/ppm = 7.85 (d, *J* = 7.81 Hz , 2H), 7.37 – 7.25 (m, 6H), 7.22 – 7.13 (m, 5H), 6.88 (d, *J* = 8.3 Hz, 2H), 6.54 (dd, *J* = 10.5, 3.2 Hz, 1H), 6.50 (d, *J* = 7.2 Hz, 2H), 4.73 (dd, *J* = 15.0, 10.5 Hz, 1H), 4.19 (dd, *J* = 15.1, 3.2 Hz, 1H), 2.12 (s, 3H)

^{13}C{^{1}H} NMR (75 MHz, $CDCl_3$, 298 K): δ/ppm = 143.64, 137.22, 134.08, 129.03, 128.54, 128.13, 126.17, 126.08, 125.69, 123.50, 119.93, 119.50, 110.09, 77.30, , 56.72, 52.41, 23.89, 21.42.

FT-IR (cm^{-1}): 3060, 2929, 1599, 1453, 1319, 1140

HRMS(ESI): ($C_{27}H_{23}NO_2S$ [M]+) = Calculated 425.1449, Found 426.1522.

TLC (SiO_2): Rf= 0.4 (Petroleum ether: ethyl acetate, 2:1)

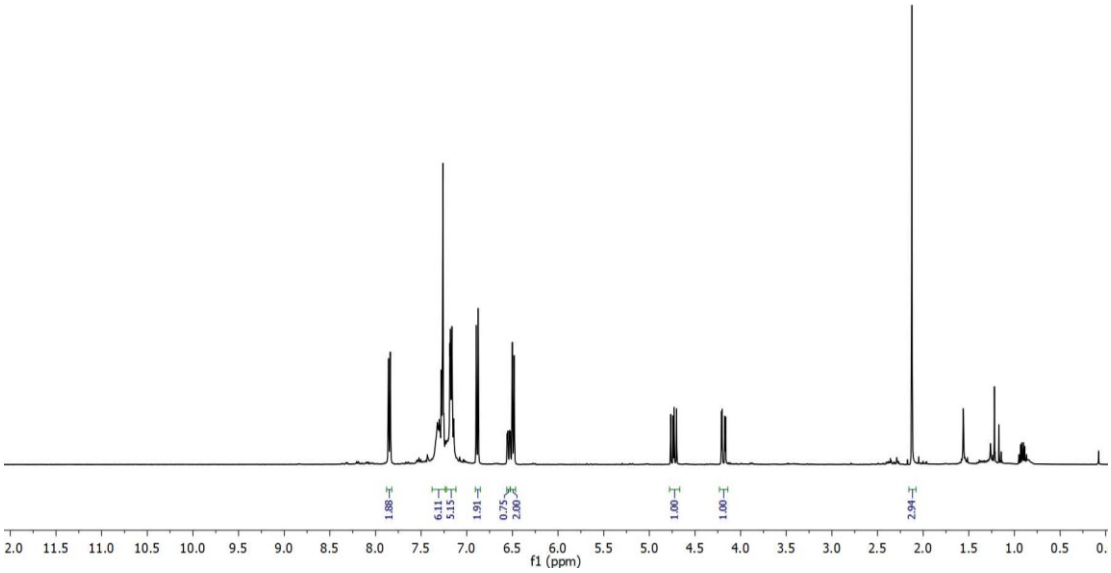

Figure A51. ^{1}H-NMR (300 MHz, $CDCl_3$, 298 K) of **182**.

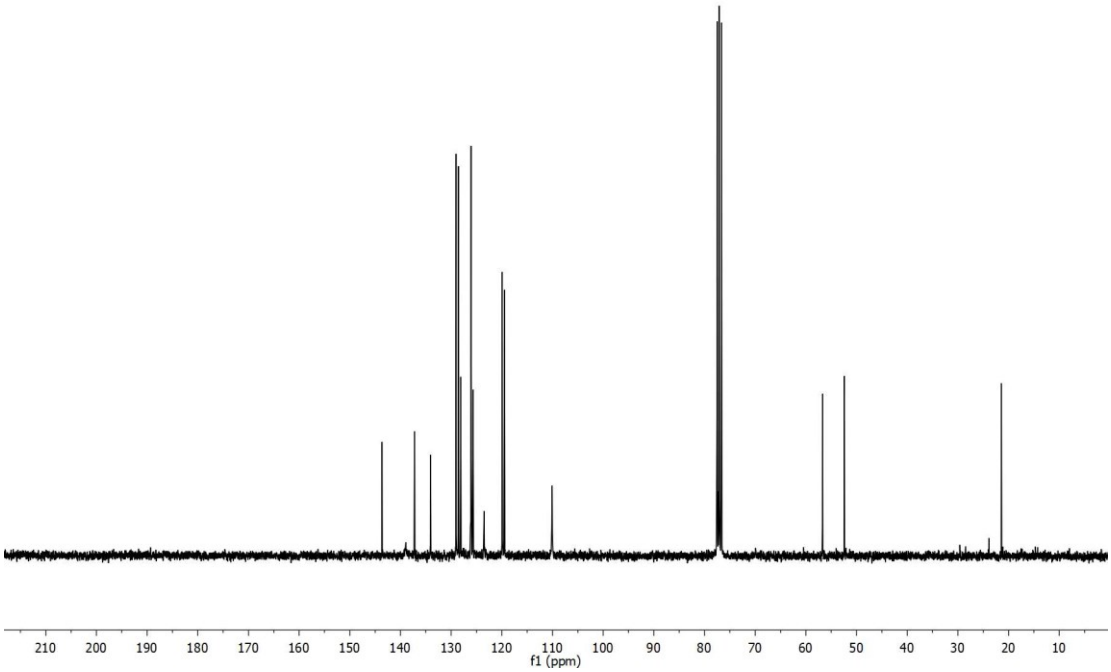

Figure A52. $^{13}C\{^{1}H\}$ NMR (75 MHz, $CDCl_3$, 298 K) of **182**.

Table A8. X-ray information for **182**.

Compound	**182**
Formula	$C_{27}H_{23}NO_2S$
$D_{calc.}$/ g cm^{-3}	1.315
μ/mm^{-1}	1.525
Formula Weight	425.555
Colour	clear yellow
Shape	prism-shaped
Size/mm^3	0.10×0.05×0.05
T/K	123.00(10)
Crystal System	orthorhombic
Space Group	*Pbca*
a/Å	10.6377(1)
b/Å	18.5499(1)
c/Å	43.5622(4)
α/°	90
β/°	90
γ/°	90
V/Å^3	8596.05(12)
Z	16
Z'	2
Wavelength/Å	1.54184
Radiation type	Cu K□
Θ_{min}/°	4.06
Θ_{max}/°	75.72
Measured Refl's.	63042
Indep't Refl's	8800
Refl's I≥2 σ(I)	7279

R_{int}	0.0309
Parameters	561
Restraints	0
Largest Peak	0.2757
Deepest Hole	-0.4823
GooF	1.0212
wR_2 (all data)	0.1002
wR_2	0.0939
R_1 (all data)	0.0478
R_1	0.0367

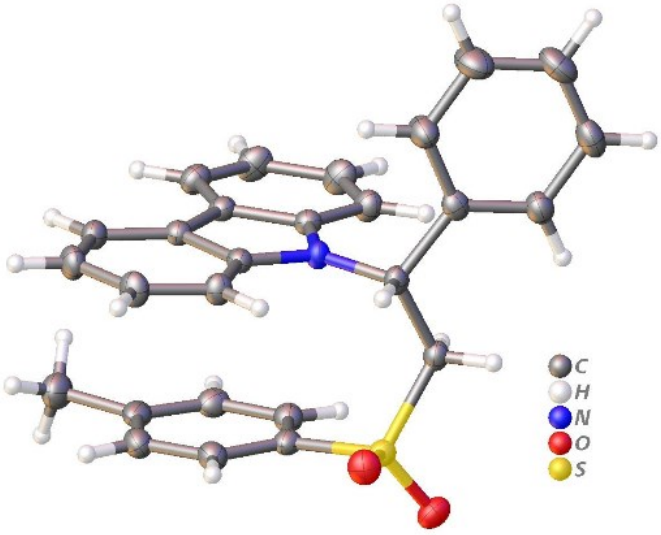

Figure A53. X-ray of **182**.

9-(1-(4-methoxyphenyl)-2-tosylethyl)-9H-carbazole (183)

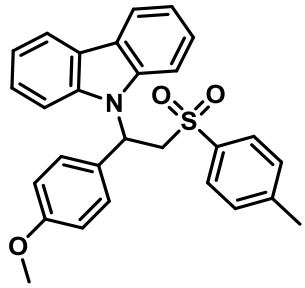

White solid

92.25 mg, 0.202 mmol, 81 % yield

^{1}H-NMR (300 MHz, $CDCl_3$, 298 K): δ/ppm = 7.86 (d, *J* = 7.6 Hz, 2H), 7.32 (t, *J* = 7.72 Hz, 2H), 7.16 (t, *J* = 6.81 Hz , 3H), 7.08 (d, *J* = 8.85 Hz, 2H), 6.88 (d, *J* = 8.26 Hz, 2H), 6.78 (d, *J* = 8.36 Hz , 2H), 6.49 (d, *J* = 7.35, 3H), 4.69 (dd, *J* = 4.41, 10.4 Hz), 4.16 (dd, J = 3.34, 11.7 Hz), 3.73 (s, 3H), 2.12 (s, 3H)

^{13}C{^{1}H} NMR (75 MHz, $CDCl_3$, 298 K): δ/ppm = 159.26, 143.60, 134.13, 130.35, 129.93, 129.10, 128.53, 127.61, 127.32, 126.17, 125.65, 123.47, 119.89, 119.42, 114.52, 114.30, 110.07, 56.79, 55.29, 51.95, 21.41.

FT-IR (cm^{-1}): 3052, 2933, 1599, 1513, 1453, 1315, 1140.

HRMS(ESI): ($C_{28}H_{25}NO_3S$ [M]+) = Calculated 455.1555, Found 456.1627.

TLC (SiO_2): Rf= 0.4 (Petroleum ether: ethyl acetate, 5:1).

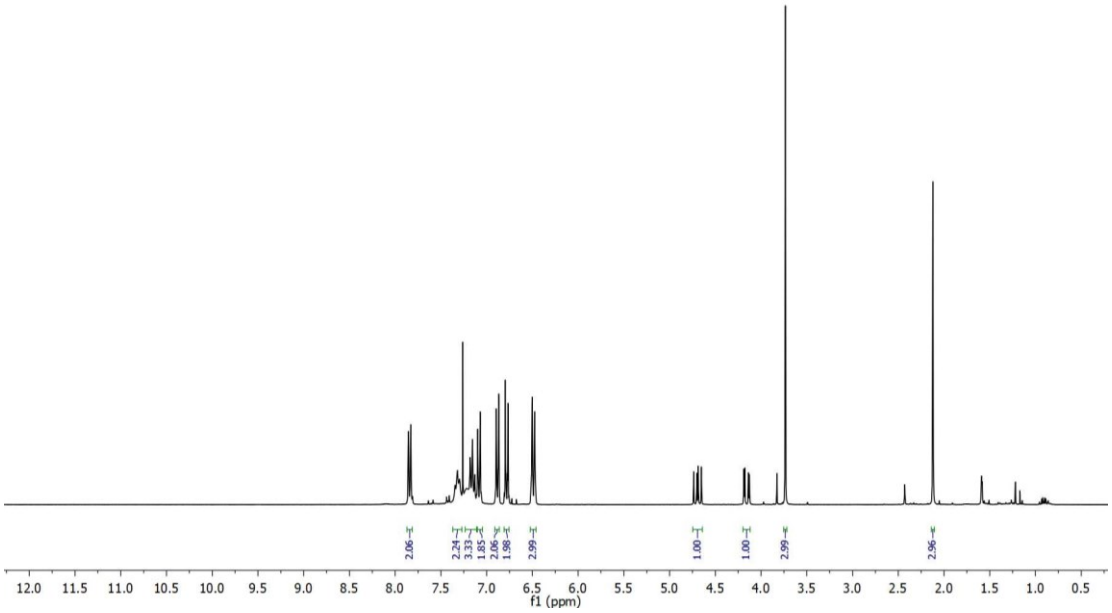

Figure A54. ^{1}H-NMR (300 MHz, $CDCl_3$, 298 K) of **183**.

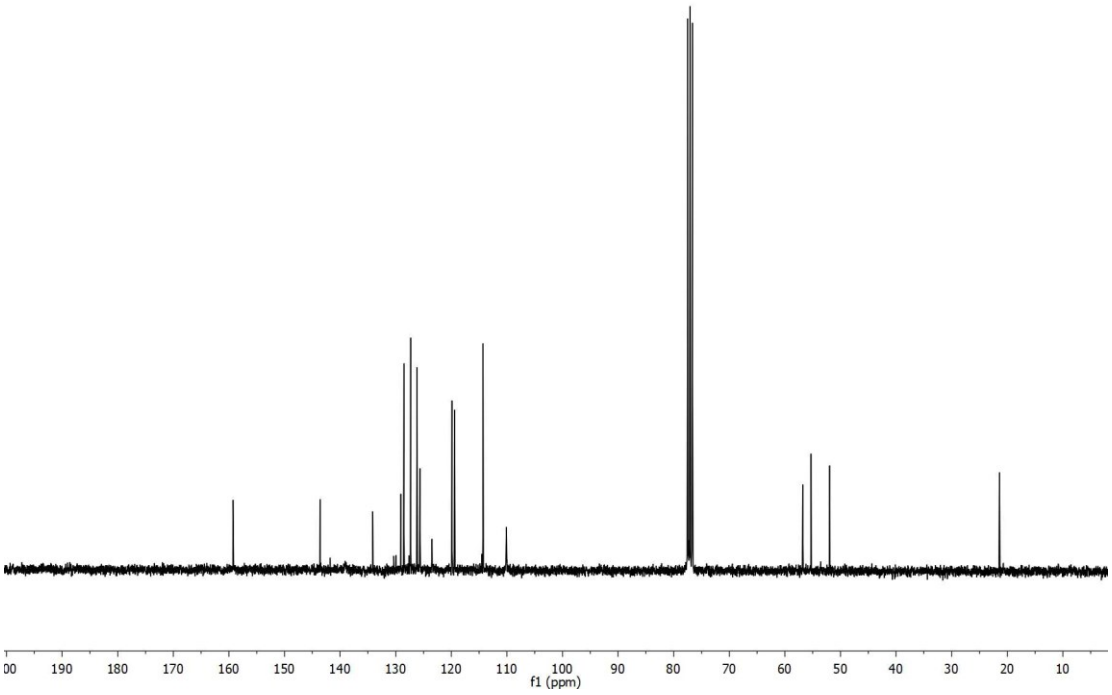

Figure A55. ^{13}C{^{1}H} NMR (75 MHz, $CDCl_3$, 298 K) of **183**.

9-(1-(4-chlorophenyl)-2-tosylethyl)-9H-carbazole (184)

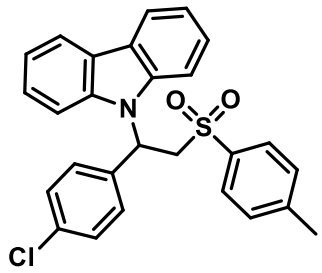

White solid

59.80 mg, 0.13 mmol, 52 % yield

^{1}H-NMR (300 MHz, $CDCl_3$, 298 K): δ/ppm = 7.87 (d, *J* = 7.59 Hz, 2H), 7.33 (t, *J* = 7.24 Hz, 2H), 7.24 (dd, *J* = 6.50, 2H), 7.17 (t, *J* = 6.79, 3H), 7.11 (d, *J* = 8.29, 2H), 4.67 (dd, *J* = 4.94, 8.60 Hz, 1H), 4.14 (dd, *J* = 3.66, 11.17 Hz, 1H), 2.10 (s, 3H)

^{13}C{^{1}H} NMR (75 MHz, $CDCl_3$, 298 K): δ/ppm = 143.83, 135.79, 134.12, 134.04, 129.61, 129.19, 127.56, 126.25, 125.80, 123.55, 120.04, 119.70, 109.94, 56.77, 51.93, 21.43.

FT-IR (cm^{-1}): 3056, 2929, 1599, 1490, 1453, 1140.

HRMS(ESI): ($C_{27}H_{22}ClNO_2S$ [M]+) = Calculated 459.1060, Found 460.1131.

TLC (SiO_2): Rf= 0.4 (Petroleum ether: ethyl acetate, 5:1).

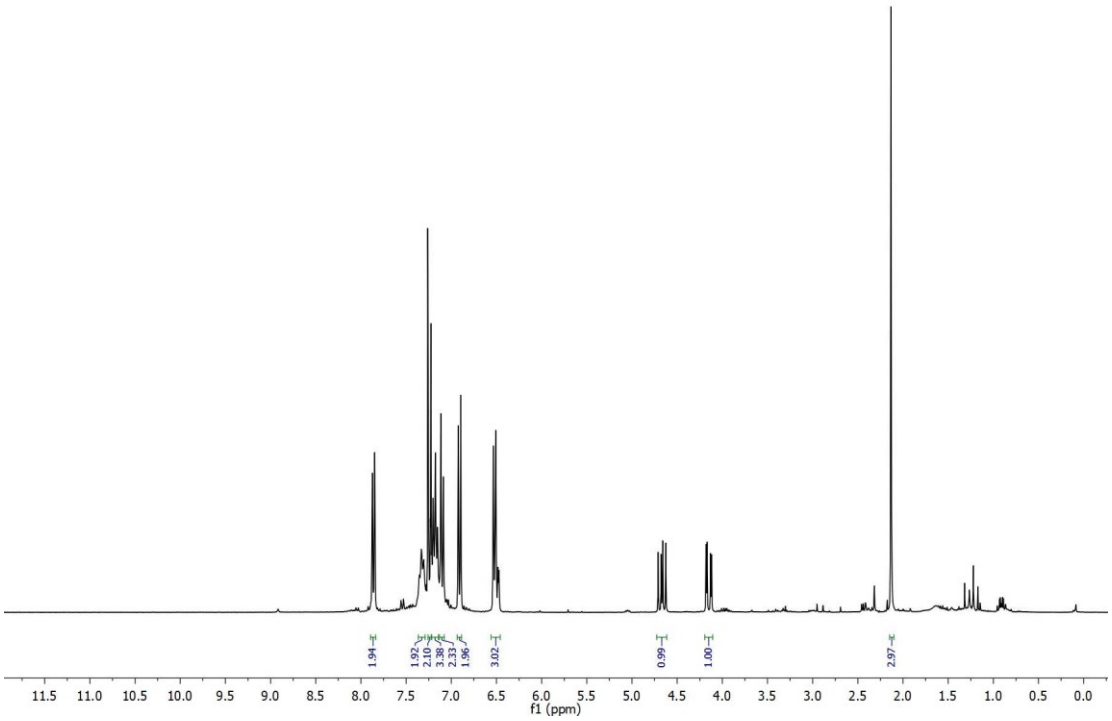

Figure A56. ^{1}H-NMR (300 MHz, $CDCl_3$, 298 K) of **184**.

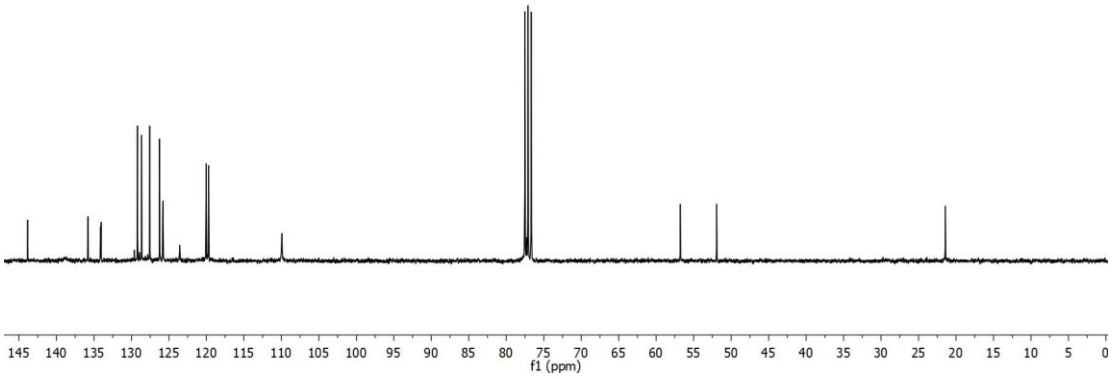

Figure A57. ^{13}C{^{1}H} NMR (75 MHz, $CDCl_3$, 298 K) of **184**.

CURRICULUM VITAE

Personal data:

Name:	Marco Antonio Henríquez Toro
Date and place of birth:	22.04.1993 Chile
Nationality:	Chilean
E-mail:	marco.henriqueztoro1@gmail.com

Work experiences:

Nov 2022 – at present: Research Scientist at Selvita (Pharma industry)

May 2022- Sep 2022: Research Scientist – Universidad Autónoma de Chile (Chile), “Synthesis of Rhenium complexes”. Supervisor: Patricia Toro.

March 2018 – Dec 2022: Ph.D. in chemistry - University of Regensburg (Germany) and Pontificia Universidad Católica de Chile (Chile)- Double degree. “*Synthesis of new photocatalysts and discovery of new reactions*”. Supervisors: Prof. Dr. Oliver Reiser and Dr. Alan Cabrera

July 2016 - March 2017: Research Scientist - Pontificia Universidad Católica de Chile (Chile). “*Synthesis of Al complexes and small molecules activation*”. Rojas group

Jan 2016 - July 2016: Chemist R&D – SIKA company

Dec 2014 – Dec 2015: Bachelor thesis – Pontificia Universidad Católica de Chile (Chile) "*Synthesis of nickel complexes and olefin polymerization"* Supervisor: Dr. René Rojas.

Academic Information

March 2018 – Dec 2022: Ph.D. in chemistry - University of Regensburg (Germany) and Pontificia Universidad Católica de Chile (Chile)- Double degree.

March 2011- Dec. 2015: Bachelor's degree, Pontificia Universidad Católica de Chile, Chile, 6.1/7.0

March 2011- Dec. 2015: Professional degree in Chemistry, Pontificia Universidad Católica de Chile, Chile, 6.1/7.0

Internships abroad

Dec 2020 – April 2022: Stay at University of Regensburg (Germany), second half of doctoral studies

April 2019 – June 2019: Short stay as a visiting PhD student at University of Regensburg (Germany) under supervision of Prof. Dr. Oliver Reiser, Photochemistry group.

Aug. 2014- Jan 2015: Erasmus exchange at Santiago de Compostela University, Spain

Publication record

”Iron(III)-light-induced homolysis: A dual photocatalytic approach for hydroacylation of alkenes using acyl radicals via direct HAT from aldehydes” .Anurag Chinchole, Marco Antonio Henriquez Toro, Diego Cortes-Arriagada, Alan R. Cabrera, Oliver Reiser. *ACS Catalysis* .**2022**, 12, 21, 13549–13554

” Influence of the thermal stability of ammonium perchlorate in presence of heteroleptic copper (I) complexes bearing ethane-1,2-diimine and biphosphines”. David Moreno da Costa, Marco A. Henriquez, Diego Gonzalez-Torres, César Zuñiga-Loyola, Iván Brito, Iván González, Alondra Villegas-Menares, Desmond MacLeod-Carey, Cesar Morales-Verdejo, Alan R. Cabrera. *Inorganica Chimica Acta*, 545, 2023,

“Phosphine Evaluation on a New Series of Heteroleptic Copper(I) Photocatalysts with dpa Ligand [Cu(dpa)(*P,P*)]BF_4” M. A. Henriquez, S. Engl, P. Jaque, I. A. Gonzalez, M. Natali, O. Reiser, A. R. Cabrera, *Eur. J. Inorg. Chem.***2021**, *2021*, 4020.

“Heteroleptic Cu(I) complexes bearing methoxycarbonyl-imidoylindazole and POP ligands – An experimental and theoretical study of their photophysical properties” - Iván A. Gonzalez, Marco A. Henríquez, Diego Cortés-Arriagada, Mirco Natali, Constantin G. Daniliuc, Paulina Dreyse, Jerónimo Maze, René S. Rojas, Cristian O. Salas and Alan R. Cabrera. *New J. Chem.*, **2018**, *42*, 12576 – 12586.

Articles in congresses

Heteroleptic copper complexes with dipyridylamine and diphosphines ligands as photoactive compounds for catalysis” Alan R. Cabrera, Marco Henriquez. XVIII Encuentro de Química Inorgánica, Olmué, Chile. Oral

Presentation, 16 al 19 de octubre, 2022.

Iron(III)-light induced homolysis: A dual photocalytic approach for hydroacylation of alkenes using acyl radicals via direct HAT from aldehydes. Anurag Chinchole, Marco Antonio Henriquez Toro, Diego Cortes-Arriagada, Alan R. Cabrera, Oliver Reiser EuChems Chemistry Congress, Lisbon, Portugal. Poster Presentation, 28 August – 1 September, 2022.

Design of heteroleptic [Cu(I)(N,N)(P,P)]BF_4 complexes as photoredox catalyst: Which phosphine is the best?. M. Henríquez, Sebastian Engl, Max I. Bayas, Mirco Natali, Oliver Reiser, Alan R. Cabrera. XXXIII Jornadas Chilenas de Química, Puerto Varas, Chile, Oral Presentation, 7 - 10 January, 2020.

New [Cu(N,N)(P,P)]BF_4 photoredox catalyst bearing 2,2-dipyridylamine ligand: Evaluation in chlorosulfonation reaction of alkenes. Marco Henríquez, Sebastian Engl, Max I. Bayas, Mirco Natali, Alan R. Cabrera and Oliver Reiser. 7th LATIN AMERICAN SYMPOSIUM ON COORDINATION AND ORGANOMETALLIC CHEMISTRY (SILQCOM7), Cartagena de Indias, Colombia. Poster Presentation, 27-30 August, 2019.

Synthesis, characterization and optoelectronic properties evaluation of heteroleptic Cu(I) complexes with *N,N,N*-Pincer ligand Alan R. Cabrera, Marco Henriquez, Jean-Luc G. Bertrand, Antonio Antiñolo. 7th LATIN AMERICAN SYMPOSIUM ON COORDINATION AND ORGANOMETALLIC CHEMISTRY (SILQCOM7), Cartagena de Indias, Colombia. Poster Presentation, 27-30 August 2019.

New [Cu(*N,N,N*)(*P*)BF_4] complexes as ATRA reaction catalysts using visible light: Synthesis, characterization and preliminary photocatalytic evaluation.

Marco Henriquez, Jean-Luc Bertrand, David Vera, Cristian O. Salas, Alan R. Cabrera. XVII Encuentro de Química Inorgánica (XVII EQI), Los Andes, Chile. Poster Presentation, 21-24 October 2018.

“Synthesis, structuralcharacterization and optoelectronics properties of new imidoylinzadoles- POP mixed ligand Cu(I) complexes with potential use as active material in LEEC devices”. Alan R. Cabrera, Ivan A. González, Marco Henríquez, Diego Cortés-Arriagada, Mirco Natali, Paulina Dreyse, Cristian O. Salas. 4th EuCheMS Inorganic Chemistry Conference (4th EICC), Copenhague, Dinamarca. Poster Presentation, 2 – 5 July 2017.

“Nuevos complejos de niquel con ligandos derivados de bases de Schiff - Potenciales catalizadores en polimerización de etileno”. Marco Henríquez, Alan R. Cabrera, Rene Rojas, Cristian O. Salas. XVI Encuentro de Química Inorgánica (XVI EQI), La Serena, Chile. Poster Presentation, 15 - 18 November 2016.

Scholarships, Awards and / or Distinctions

1) “Beca presidente de la Republica”; 2010-2015.
2) “Beca Complementaria UC”; scholarship awarded by the Pontificia Universidad Católica de Chile, 2010-2015.
3) “Beca Santander Universidades”; scholarship awarded by the Santander Bank (Academic Exchange Program).
4) Academic Exchange Scholarship, awarded by DRI UC
5) “Francisco Muñoz de la Rosa” Award for academic excellence in undergraduate chemistry, delivered by the Cloramon company (Chile), October 2017.
6) Beca Anid (PhD), scholarship awarded by the Chilean government, 2018-2022

Eidesstattliche Erklärung

Ich erkläre hiermit an Eides statt, dass ich die vorliegende Arbeit ohne unzulässige Hilfe Dritter und ohne Benutzung anderer als der angegebenen Hilfsmittel angefertigt habe; die aus anderen Quellen direkt oder indirekt übernommenen Daten und Konzepte sind unter Angabe des Literaturzitats gekennzeichnet.

Regensburg , 2023

Signature